






Universitat Autònoma de Barcelona

ADVERTIMENT. L'accés als continguts d'aquesta tesi queda condicionat a l'acceptació de les condicions d'ús establertes per la següent llicència Creative Commons:  http://cat.creativecommons.org/?page_id=184

ADVERTENCIA. El acceso a los contenidos de esta tesis queda condicionado a la aceptación de las condiciones de uso establecidas por la siguiente licencia Creative Commons:  <http://es.creativecommons.org/blog/licencias/>

WARNING. The access to the contents of this doctoral thesis it is limited to the acceptance of the use conditions set by the following Creative Commons license:  <https://creativecommons.org/licenses/?lang=en>



Universitat Autònoma de Barcelona

Departament d'Enginyeria Electrònica

Inkjet printing technology is driving the innovation of sensors for point-of-care Devices

by

Miguel Zea

Directores: Dr. Gemma Gabriel Buguña

and Dr. Eloi Ramon Garcia

Memoria de Tesis

Presentada para optar al título de

Doctor en Ingeniería Electrónica y de Telecomunicación

Julio 2021

Dr. Gemma Gabriel Buguña, Investigadora del Consejo Superior de Investigaciones Científicas y Dr. Eloi Ramon Garcia, Investigador del Consejo Superior de Investigaciones Científicas y Profesor Asociado del Departament d'Enginyeria Electrònica de la Universidad Autònoma de Barcelona,

Certifican |

que la Memoria de Tesis *Inkjet printing technology is driving the innovation of sensors for point-of-care Devices* presentada por Miguel Zea para optar al título de Doctor en Ingeniería Electrónica y de Telecomunicación se ha realizado bajo su dirección en el Institut de Microelectrònica de Barcelona (IMB-CNM) del Consejo Superior de Investigaciones Científicas (CSIC) y ha sido tutorizada en el Departament d'Enginyeria Electrònica de la Universitat Autònoma de Barcelona (UAB).

Directora | Dr. Gemma Gabriel Buguña

Director/tutor | Dr. Eloi Ramon Garcia

Bellaterra (Cerdanyola del Vallès), 02 de julio de 2021.

A Dios y mi familia.

I always like to look on the optimistic side of life,
but I am realistic enough to know
that life is a complex matter.

Walt Disney

Acknowledgements |

Desde muy joven cuando estaba por terminar el colegio siempre soñé con poder obtener un título de doctor. Este documento es una prueba, de que, si persigues tus sueños superando todas las adversidades, trabas, tristezas, inconvenientes, entre otros miles de obstáculos, estos sueños se vuelven realidad. Sin embargo, para llegar a este punto hay mucho que agradecer y a quien agradecer. Quisiera agradecer a cada una de las personas que me han ayudado, animado, retado e ilusionado a llegar a este punto, pero esta lista sería más larga que el propio documento. Aun así, tratare de agradecer a los que más influyeron directamente en este proceso, de antemano pido disculpas a aquellos que quedan excluidos del texto, pero créanme que en mi mente y corazón se los agradezco.

En primer lugar, quiero agradecer a mi directora, compañera, amiga e inclusive a veces le tocaba hacer de madre Gemma por ayudarme y dirigirme durante todo este camino, hasta finalmente poder llegar hasta aquí y poder culminar este documento. Gracias a ella conseguí la beca para este doctorado y juntos logramos todos los objetivos que nos propusimos. Sin el apoyo y ánimo de Gemma seguramente jamás hubiera podido optar a este título. También quiero agradecer a mi director y tutor Eloi por ayudarme a definir los objetivos de la tesis, dar los primeros pasos en la ejecución, introducirme a la tecnología inkjet printing y conciliación en la redacción de este documento. Adicionalmente quiero agradecer a Errachid que me acogió en su grupo de investigación como si fuera uno más de la familia, me enseñó a ver la investigación desde otro punto de vista y me acompañó en todo el proceso.

En la misma línea quiero agradecer a Ana Moya, por enseñarme, guiarme y educarme durante mis primeros pasos en el mundo de la ciencia. Siempre agradecido por su forma de ser y enseñar. Entre las muchas cosas que me enseñó, resalto que me haya enseñado a trabajar duro y exprimir cada proceso de fabricación al máximo. A mis compañeros de despacho ¡Eh JuanMa, que pasal, Raphaela, Fernando o Pedro, Marta, Daniel y Javier que siempre estuvieron apoyándome y dispuestos a ayudarme en cualquier momento, desde explicarme un tema científico o decorar la navidad. JuanMa que con su buena fe y actitud ante todo te contagia de alegría. Raphaela que con su novela te distraía y te daba ese respiro que en esos momentos necesitamos, además soy su mejor amigo. Fernando o Pedro que además de la sangre latina que nos unía, compartíamos un deseo de aprender y ayudarnos mutuamente. Marta que con su buena energía irradiaba paz y felicidad al despacho. A Daniel que, aunque fue poco lo que compartimos,

nos hicimos buenos amigos y vivimos grandes momentos. Y Javier, que con sus aficiones y responsabilidad nos centraba y nos educaba. Javier siempre está dispuesto a ayudar cuando lo necesitas.

Seguramente a la siguiente persona que tengo que agradecer es a mi tocayo de apellidos Aller Pellitero que si escribiera en todo lo que me ayudó y alcahuetó no terminaría nunca, excelente persona y amigo. Mención especial para Albertito, Josele, Javier del Campo y Xavi Muñoz sin su apoyo esto tampoco hubiera sido posible. A la gran jefa Rosa y a mis compañeros del grupo GAB, Eli, Mar, Xavi, Anton, Edu, Pau, Sergi, Denise, Ferran y Lucia, grandes compañeros siempre disponibles a ayudar. También a los compañeros del ISA Lyon: Hamdi, Imad, Fares, Francesca, Marie, Nadia, Fabien, Daiva y Alexandra, gracias por incluirme como uno más.

Como no quiero extenderme mucho más, quiero agradecer a mis amigos del ahora “Subidón volver al CNM Power”, que sin los cafés de la mañana, las comidas, las quedadas y las pastitas, esta experiencia en el CNM no hubiera sido tan enriquecedora y llevadera. Además, al otro grupo de “Comida viernes!!!” que sin esos Kebabs de Raja y charlas durante la comida no hubiera cerrado las semanas con broche de oro y sellos para reclamar kebabs. Tampoco puedo dejar de agradecer a mis compañeros de Inkjet Roger, Alba, Carme, Raquel y mi querida amiga ¡Che! Mijal.

Me gustaría agradecer a todas las personas del CNM, porque siempre me he sentido en familia con todos, siempre un cálido saludo y si en algún momento necesitaba de alguien podía recurrir a ellos sin ninguna objeción. De verdad les doy las gracias a todos (técnicos, mantenimiento, administración, personal investigador, Eli, etc, etc). También quiero agradecer a las chicas de la limpieza que siempre están dispuestas a darte una buena charla para animar el día. A los mecánicos que siempre me ayudaron con sus conocimientos y en la fabricación de moldes. Y a Paqui y Tomás pendientes de todo lo que pasa en el instituto y ayudándonos a recibir nuestros paquetes.

Finalmente, y no menos importante, inclusive siempre más importante en todos los aspectos de mi vida. Agradezco a toda mi familia. Especialmente a mi amada esposa Laura que siempre está a mi lado apoyándome y mostrándome el buen camino, a mi papá que en paz descansa por su apoyo incondicional y su amistad, a mi mamá siempre educándome, queriéndome y deseándome lo mejor, mi segundo papá que muestra el camino a seguir en base a trabajo y esfuerzo, además de su amor incondicional, a mi hermano con el siempre cuento para todo y a mi perrita SnowCity que sin su compañía esta cuarentena hubiera sido difícil.

La ciencia se compone de errores,
que a su vez son los pasos hacia la verdad

Jules Verne

Resumen |

La tecnología "Inkjet Printing" está llamada a liderar la próxima generación de electrónica flexible capaz de realizar funciones a las que sólo se podía acceder con tecnologías de microfabricación de última generación. Esto se puede explicar en parte gracias a la versatilidad que aportan las técnicas de impresión digital sin contacto, pero también debido a la inversión sustancial en investigación y desarrollo para el Inkjet Printing en el área de formulación de materiales funcionales en los últimos años. El Inkjet Printing es un método de fabricación aditiva que se basa en imprimir sin contacto microgotas de un material funcional con precisión micrométrica en el área del sustrato deseado, a través de un diseño digital. Además, es capaz de modificar el diseño de impresión en tiempo real. En consecuencia, se pueden introducir cambios de diseño sin ningún coste adicional, lo que permite crear diseños personalizados con características únicas. Hoy en día, el Inkjet Printing a nivel industrial ha alcanzado altos estándares de rendimiento, flexibilidad, robustez y confianza.

Se prevee que el Inkjet Printing facilitará la producción de productos electrónicos flexibles de forma rentable, en base a conceptos de economía circular y reduciendo el desperdicio, lo que permitirá el desarrollo de dispositivos portátiles y desechables no disponibles actualmente. Este es el punto en el que los dispositivos de Point-of-Care (PoC) entran en la ecuación debido a su importancia en las pruebas médicas. Estos dispositivos se definen como pruebas de diagnóstico médico en el paciente o cerca del mismo. Los dispositivos PoC se basan en una medición rápida y precisa basada en sensores que ofrecen al médico datos importantes para realizar un diagnóstico. Sin embargo, las principales limitaciones de estos dispositivos, incluso hoy en día, son el coste, la disponibilidad, la biodegradabilidad y la fiabilidad. El Inkjet Printing ofrece soluciones para abordar estos problemas donde sus grandes promesas son la fabricación rápida de prototipos, de bajo coste, usando una gran variedad de materiales y una amplia gama de sustratos. Además, la tecnología en los últimos 15 años ya ha demostrado su potencial en la fabricación de sensores cuantitativos y fiables que forman el componente esencial de los dispositivos PoC. Sin embargo, nuestra comprensión de la tecnología y sus capacidades permanece en una etapa prometedora o potencial, y es necesario adquirir más experiencia para facilitar el desarrollo de dispositivos PoC completos y totalmente impresos.

Identificando estos problemas y posibles soluciones, esta tesis se centra en mostrar el potencial del Inkjet Printing para desarrollar sensores sobre sustratos de plástico flexible y papel poroso, desafiando la tecnología hasta su límite actual. En una primera parte se aborda la formulación, impresión y caracterización de **nuevas**

tintas funcionales que permitan obtener nuevas tintas conductoras para ser usadas en el área del sensado de analitos de interés. Sobre plástico flexible, se han desarrollado dos sensores de pH potenciométricos. El primero muestra la importancia de la propiedad de rugosidad intrínseca de una nueva tinta de platino en base a nanopartículas para dotar de estabilidad mecánica al óxido de iridio, material sensible al pH, crecido electroquímicamente sobre él. Para este propósito, se desarrolló un sensor de pH en PEN utilizando la nueva tinta de Pt y se estudió la estabilidad a lo largo de un año de esta capa de óxido de iridio, que mostró una clara mejora de su rendimiento. El segundo sensor de pH va un paso más allá y es (hasta hoy) el primer sensor de pH totalmente impreso por Inkjet Printing. Para cumplir este objetivo, se formuló una nueva tinta polimérica compuesta de una mezcla de polipirrol y polianilina sensible al pH. Esta tinta se imprimió sobre un microelectrodo de oro, también previamente impreso, y para obtener finalmente un sensor de pH totalmente impreso se completó con una pseudo-referencia impresa de estado sólido de plata/cloruro de plata. En una segunda parte se abordó el reto de la impresión de un sensor sobre un sustrato más ecosostenible como es el papel, factor importante para los PoC desechables. Sobre el sustrato de papel, la dificultad en la impresión es más grande debido a sus propiedades de porosidad, delicadeza e hidrofobicidad. En un primer trabajo se abordó el desafío de imprimir tintas funcionales conductoras como el oro o la plata, y dieléctricas como el SU8 sobre el sustrato de manera eficiente y fácil de reproducir para la obtención de un sensor electroquímico. Se propone y se estudia la impresión de una nueva tinta hidrofóbica que permite bloquear selectivamente el área del papel donde se requerirá la impresión de las tintas conductoras que conforman el sensor electroquímico. Finalmente, en un segundo trabajo se implementó un inmunosensor de cortisol sobre estos sensores impresos sobre sustrato de papel y se caracterizó y comparó su respuesta respecto a otros sensores reportados, demostrando el buen rendimiento de esta tecnología en la detección de moléculas diana biológicas en muestras biológica.

Abstract |

The **'Inkjet printing'** technology is called to be the next generation of flexible electronics capable of performing functions that were only accessible with state-of-the-art microfabrication technologies. This is due, in part, to the versatility of digital, non-contact patterning techniques but also to the substantial investment in research and development for inkjet printing of functional materials in recent years. Inkjet printing is an additive manufacturing technology based on the contact-less deposition of micro-droplets of a functional material with micrometer precision on the desired substrate area, through a digital design. Moreover, inkjet printing is capable of modifying the printing pattern in real time. Consequently, design changes can be introduced without any additional costs, allowing to create personalized designs with unique features. Nowadays, industrial inkjet printing has reached high standards of flexible, robust, and reliable performances.

The consensus is that inkjet printing will facilitate the production of flexible electronics in a cost-effective, on circular-economy, and reducing waste manner, enabling the development of currently unavailable wearable and disposable devices. This is the point at which Point-of-Care testing devices (PoCT) enter in the equation due to their importance in medical trails. These devices are defined as medical diagnostic testing at or near the patient. PoCT devices rely on a fast and accurate measurement based on sensors that provide the physician with a set of important data to make a diagnosis. However, major limitations of state-of-the-art PoCT devices include cost, disposability, biodegradability, and reliability. Inkjet printing technology offers solutions to address these problems where its great promises are low-cost, non-contact, rapid prototyping, material varieties, and wide range of substrates. Moreover, in the last 15 years, this technology has already shown its potential in the fabrication of reliable and quantitative sensors which form the essential components of PoCT devices. However, our understanding of the technology and its capabilities are still in a promising or potential stage, and further expertise needs to be acquired to facilitate the development of complete fully printed PoCT devices.

Identifying these problems and possible solutions, this thesis focuses on showing the potential of inkjet printing to develop sensors on flexible plastic substrates and porous paper, challenging technology to its current limit. The first part addresses the formulation, printing, and characterization of new functional inks that allow us to obtain new conductive inks to be used in the area of sensing analytes of

interest. On flexible plastic, two potentiometric pH sensors have been developed. The first shows the importance of the intrinsic roughness property of a new platinum ink based on nanoparticles to provide mechanical stability to iridium oxide, a pH-sensitive material, grown electrochemically on it. For this purpose, a pH sensor was developed using the new Pt ink and the stability over a year of this iridium oxide layer was studied, which showed a clear improvement in its performance. The second pH sensor goes one step further and is, to date, the first pH sensor entirely fabricated by inkjet printing. To meet this objective, a new polymeric ink was formulated composed of a mixture of polypyrrole and pH-sensitive polyaniline. This ink was printed on a previously printed gold microelectrode and, to finally obtain a fully printed pH sensor, the fabrication was completed with a printed silver/silver chloride pseudo-reference electrode. The second part addresses the challenge of printing a sensor on a more eco-sustainable substrate such as paper, an important factor for disposable PoCs. On any paper substrate, the difficulty in printing is greater due to the porosity, delicacy and hydrophilicity of this material. In a first work, the challenge of printing conductive functional inks such as gold or silver, and dielectric inks such as SU8 on the substrate in an efficient and easy-to-reproduce way to obtain an electrochemical sensor is addressed. The printing of a new hydrophobic ink that allows to selectively block the area of the paper where the printing of the conductive inks that make up the electrochemical sensor will be required is proposed and studied. Finally, in a second work, a cortisol immunosensor was implemented on these sensors printed on a paper substrate and its response was characterized and compared with other reported sensors, demonstrating the good performance of this technology in the detection of biological target molecules in biological samples.

Contents

Acknowledgements	9
Resumen	13
Abstract	15
Chapter 1 Dissertation Summary	29
1.1. Motivation of this Work	30
1.2. Main Contribution of this Thesis	31
1.2.1. Objectives of the Thesis	32
1.2.2. List of publications	33
1.2.3. Thesis outline	34
1.3. Thesis Framework	35
Chapter 2 Introduction to Inkjet Printing Technology and new developments	36
2.1. Overview of Inkjet Printing Technology	37
2.1.1. The inkjet printing technology	38
2.1.2. DoD technology	40
2.1.3. Piezoelectric actuator working principle	42
2.2. DoD inkjet printer	43

2.3.	Printable materials	45
2.4.	Substrates for Inkjet printing	46
2.5.	Inkjet printing focused on sensors	48
2.5.1.	Electrochemical sensors	50
2.5.2.	Electrochemical sensors fabricated by inkjet printing	58
Chapter 3	Printable Materials for sensing	63
3.1.	Printable inks	64
3.1.1.	Conductive inks	65
3.1.2.	Semiconductive inks	70
3.1.3.	Dielectrics inks	71
3.2.	Inks requirement for printing an electrochemical sensor	71
3.2.1.	Drop deposition	73
3.2.2.	Ink jettability	74
3.2.3.	Drop spacing (DS)	77
3.3.	Printed pH sensors	78
3.3.1.	Publication I: Enhanced performance stability of iridium oxide based pH sensors fabricated on rough inkjet-printed platinum	80
3.3.2.	Publication II: Specially designed polyaniline/polypyrrole ink for a fully printed high sensitive pH microsensor.	105
Chapter 4	Inkjet printed PoC devices	127

4.1.	Overview of PoC	128
4.2.	Overview of inkjet printed PoC devices	130
4.3.	Paper-based PoC devices	132
4.3.1.	Cellulose substrate composition and applications	132
4.3.2.	Electrochemical detection on paper	135
4.3.3.	Paper-based PoC devices	137
4.3.4.	Publication III: Inkjet-printed Paper-based Electrochemical Sensors: Tuning Active Area through Surface Modification	140
4.4.	Cortisol sensing	161
4.4.1.	Publication IV: Electrochemical sensors for cortisol detections: almost there	161
4.4.2.	Publication V: A Fully Paper-Based Electrochemical Sensor Made by Inkjet Printing for Saliva Cortisol Detection	181
Chapter 5	Conclusion and further work	199
5.1.	Concluding remarks	200
Listed PhD outcomes		204
Chapter 6	Supplementary of published Articles	207
6.1.	Supplementary of Publication I	208
6.2.	Supplementary of Publication II	215
6.3.	Supplementary of Publication III	225
6.4.	Supplementary of Publication V	231

List of Figures

Figure 2.1. Lord Rayleigh’s idea of instability jets.....	39
Figure 2.2. Inkjet printing operation modes.....	40
Figure 2.3. Waveform phases.....	43
Figure 2.4. Dimatix printer and cartridge.....	44
Figure 2.5. Schematic of sintering process of nanoparticles inks.....	45
Figure 2.6. Schematic representation of the path that electrochemical sensor is following.....	50
Figure 2.7. Electrochemical sensor publication in the past seven years.....	51
Figure 2.8. ISEs types.....	55
Figure 2.9. EIS setup cells.....	57
Figure 2.10. Representation of the fabrication of an electrochemical sensor by ink jet.....	59
Figure 2.11. Schematic and photography of Nilsson et al. sensor.....	60
Figure 2.12. Fully inkjet printed electrochemical sensors.....	61
Figure 3.1. Parameters of metallic inks.....	68
Figure 3.2. Coffee ring formation of evaporation patterns.....	74
Figure 3.3. Drop spacing pattern.....	77
Figure 3.4. Printed pH sensing film.....	80
Figure 3.5. Inkjet Pt electrode fabrication process.....	88

Figure 3.6. Printing characterization of Pt ink.....	92
Figure 3.7. Electrical characterization Pt ink.	94
Figure 3.8. Electrochemical characterization Pt patterns.	96
Figure 3.9. EIROF pH sensor calibration.....	99
Figure 3.10. Impedance comparisson of printed Pt and evaporated Pt.....	101
Figure 3.11. Stability studio of EIROF coating.	102
Figure 3.12. Fully inkjet printed pH sensor.	110
Figure 3.13. PANI and PPy ink characterization.....	113
Figure 3.14. Printing characterization of polymeric inks.....	115
Figure 3.15. pH calibration of PANI and PPy printed films.....	117
Figure 3.16. Interferences study for PANI:PSS/PPy:PSS sensor.	119
Figure 3.17. Chemical schematic illustration of AuNp ink and polymers.	121
Figure 3.18. PANI:PSS/PPy:PSS pH calibration curves.....	122
Figure 3.19. Tritration and stability study of PANI:PSS/PPy:PSS pH sensor.....	124
Figure 4.1. Overview of PoC devices for healthcare applications.....	128
Figure 4.2. Analytical Capabilites of paper-based PoC.....	134
Figure 4.3. Multiplexed EPAD for detection of glucose and protein in urine.	136
Figure 4.4. Schematic representation of the inkjet printed multianalyte device.....	138
Figure 4.5. Schematic illustration of inkjet printed three-electrode platform.....	139

Figure 4.6. Fabrication process of a paper-based inkjet printed sensor.	146
Figure 4.7. Water contact angle study on treated paper.	149
Figure 4.8. SEM images of paper treatments.	150
Figure 4.9. Electrical characterization of metallic inks on paper.	154
Figure 4.10. Optical characterization of inkjet printed patterns on paper.	155
Figure 4.11. Electrochemical characterization of three-electrode cell on paper.	157
Figure 4.12. Cortisol secretion pathway in humans.	166
Figure 4.13. Schematic example of functionalization process of an electrode.	170
Figure 4.14. Number of published articles about electrochemical cortisol detection.	171
Figure 4.15. Fabrication process of cortisol immunosensor.	188
Figure 4.16. Biofunctionalization of an inkjet printed electrode.	189
Figure 4.17. Electrochemical characterization of biofunctionalization.	191
Figure 4.18. Detection of cortisol in standard solution.	193
Figure 4.19. Cortisol detection in artificial saliva.	194
Figure 4.20. Cortisol detection in human saliva.	195
Figure 5.1 Developed sensors in this thesis.	200
Figure 5.2. Summarized conclusion of the thesis.	201

List of Tables

Table 2-1. Electrochemical measurements techniques.....	52
Table 3-1. Summary of Physical Properties and Dimensionless Numbers for Each Fluid.....	76
Table 3-2. Pt ink main properties	90
Table 3-3. CPs-based pH sensors on the literature.	123
Table 4-1. Electrochemical results of printed electrodes on paper.	159
Table 4-2. Cortisol usual levels in human fluids.	165
Table 4-3. Published works of electrochemical cortisol detection.	176
Table 4-4. Comparisson of published similar cortisol immunosensors.	197

List of Acronyms

counter electrode

(CE), 56

Drop spacing

(DS), 77

drop-on-demand

(DoD), 38

electrical impedance spectroscopy

(EIS), 55

electrochemical paper-based devices

(EPAD), 136

ion selective electrode

(ISE), 53

Point-of-care testing

(PoCT), 128

Polyethylene naphthalate

(PEN), 81

polyethylene terephthalate

(PET), 62

polyimide film

(Kapton), 61

reference electrode

(RE), 53

working electrode

(WE), 56

working sensing electrode

(WSE), 57

Chapter 1 | Dissertation Summary

This chapter describes the study overview of this thesis, where the most pertinent aspects are briefly introduced.

1.1. Motivation of this Work

Inkjet printing technology is currently at the foot of its own S-curve¹, more or less at the point where screen printing was 20 years ago². The technology has become an attractive alternative to be used in several patterning applications³. The advantages of this low-cost technique include reduction of complexity of fabrication steps, compatibility with various substrates, reduction of wasted material and having no requirement for mask patterning^{4,5}, consequently the technology reduce cost and it is more eco-friendly. Direct write attribute of inkjet printing allows for deposition of versatile thin films, the designs of which can be changed with ease from batch to batch⁴. In contrast to standard mask-based microfabrication it is capable of testing new materials and designs in a rapid prototyping approach. As such, it has the potential to play a powerful role in the development of customized devices⁶. It is clear that inkjet printing technology is in a young stage of development meaning there is a lot of work to do.

Sensors play an important role in several application fields, nowadays you can find sensors almost everywhere from an old fridge to a complex satellite in orbit. In the healthcare field sensors has been earning attention for several years, however despite the increased interest in this area, a significant gap remains between the existing sensors and the requirements of healthcare field. Additionally, one major challenge of the world for last decades has been the continuous elderly population increase in the developed countries⁷, already in Europe older persons (aged 65 or over) had a 20.3% share of entire population (newborn and over)⁸. Hence the need of delivering quality care to this elderly population, we need solutions to enable people to stay healthy without hospitals intervention-based, hospital cares are expensive and hospital saturation has to be avoid⁹. Therefore, accurate real-time monitoring of physiologically relevant parameters is crucial not only in critical hospital settings¹⁰, but also during routine daily activities¹¹. Continuous vital information can aware the person or patient about a symptom leading to precautionary steps or early diagnostics¹², wherefore reducing hospital expenses and attendance. Modern technology has allowed to be surrounded of sensors near, on, and around the body, in clothing, jewelry, and many other accessories to measure movement, physiology, environment, and even mood/emotion⁹. Most of them are known as “wearable” devices. The importance of these wearable sensors is known already, but the field has experienced unbalanced advances in research and development, most widely wearable sensors track the user’s physical activities and vital signs. However, continuous, rapid, and accurate monitoring of chemical parameters is crucial to obtain complete information about user’s health, performance, or stress at the molecular level¹³.

Chemical sensors in the healthcare field is exponentially growing¹⁴. The bibliography seems to have a natural division between chemical and physical sensors. However, there are some that cannot be classified easily, like relative humidity sensors, a chemical sensor traditionally lumped with physical sensors¹⁵. However, biosensors are defined as sensors that use biomolecules and/or structures to measure something with biological significance or bioactivity, this measure is sent out as an energy signal, be it thermal, electrical, acoustic, or optical. Chemical sensors include electrical, acoustic, and optical readings, the approach of the last two is qualitative. And, as it is pointed out above, quantitative (electrical approaches) electrochemical biosensors for healthcare field and wearable need to be addressed. These healthcare devices are most known as point-of-care (PoC) devices. Basically, they are medical tests that do not involve the use of laboratory staff and facilities to provide the final result. PoC devices target analytes with biological significance such as proteins, nucleic acids, metabolites, drugs, dissolved ions and gases, human cells, and microbes. Samples are blood, saliva, urine, or other bodily fluids or (semi)solids¹⁶. Whether used “near-patient” in a hospital, clinic, or doctor’s office, or administered at home to maintain health, manage disease, or monitor therapy, these devices accept a sample with little or no pre-preparation and provide a result, the “answer”, from seconds to hours¹⁷. These PoC devices are formed usually of four parts: the biosensor itself, the reading equipment (usually a potentiostat), the battery, and a display.

Recent challenges in healthcare mentioned above demand a new diagnostic solution worldwide^{18–20}. It is expected that PoC devices will offer considerable advantage to address these challenges^{21–23}. However, to achieve a worldwide solution according to global needs these devices must enter in circular-economy^{24,25}, in simple words they need to be low-cost, reduce-waste, reusable or bio-degradable, and with low-grade raw materials. Here is where inkjet printing technology and the development of PoC devices converge and offer a solution to nowadays healthcare challenges. It is in this sense that the motivation of this thesis appears for offering technological advantages in the development of PoC devices through inkjet printing technology.

1.2. Main Contribution of this Thesis

Obtaining quantitative, reliable, and accurate results is the main goal of a PoC device, and this can be accomplished with a mature developed sensor. For this reason, this thesis is focused on the development of functional and reliable sensors and biosensors made with a technology in accordance to circular-

economy trends. In a first stage, it has been developed two pH sensors using inkjet printing technology with two novel synthesized inks (home-made) on to a flexible plastic reusable substrate and, in a second stage, it has been engaged the challenge to incorporate for the first time a fully inkjet printed biosensor on paper porous substrate. To achieve this, a fully characterization of printed arrays on paper and different printing approaches were studied. Additionally, the paper-based biosensor was biofunctionalized to detect such an interesting human hormone as cortisol.

Following are described the main and the specific objectives of this thesis to obtain the final goal. After this, it is presented the list of publications that comprise this work in which Miguel Zea is the first author of all of them. The section finishes with the outline of this dissertation, presenting each chapter of this thesis.

1.2.1. Objectives of the Thesis

The ambition of this thesis deals with the development of low-cost sensor/biosensor for PoC devices. In general terms, the goal is to develop functional, reliable, and low-cost sensor/biosensors to be easily to incorporate in PoC systems. These developed sensors need to be designed allowing their integration with portable potentiostat. Inkjet printing technique has been employed during this work, using two different substrates. For this reason, the three main objectives are:

- **Demonstrate the potential of inkjet printing technology to develop novel potentiometric pH sensors on flexible plastic substrate with low sintering temperature inks.** To achieve this objective some specific sub-objectives are proposed:
 - ❖ To synthesize a novel metallic low sintering temperature Pt ink.
 - ❖ To print a novel pH sensitive polymeric ink.
 - ❖ To characterize and set-up printed parameters of these novel inks to evaluate their printability, morphology, and electrochemical properties that have not been reported before.
 - ❖ To develop a fully printed pH sensor on a flexible plastic substrate.
- **To develop a fully printed electrochemical cell on a paper porous biodegradable substrate.** To achieve this objective, the following sub-objectives have been addressed:
 - ❖ To characterize different conductive and insulating inks to develop inkjet-printed electrochemical sensors in order to assess their printability on paper substrate.

- ❖ To study different strategies to print the inks on the paper substrate.
 - ❖ To develop a complete electrochemical cell platform by inkjet printing on paper substrate and to study their functionality and electrochemical response.
 - ❖ To validate the electrochemical active area of the printed microelectrode and its tuning capability.
- **To develop a cortisol sensor on paper substrate by using inkjet printing technology.** To achieve this objective, the subsequent sub-objectives have been given:
 - ❖ To develop and characterize a cortisol sensor platform on paper substrate.
 - ❖ To validate the sensor performance detecting cortisol hormone in standard solution.
 - ❖ To develop and characterize a complete electrochemical platform formed by an array of four integrated working electrodes, two counter and two reference electrodes in a single area using paper substrate for detecting cortisol.
 - ❖ To evaluate its reproducibility and repeatability.
 - ❖ To validate the cortisol sensing platform with physiological samples, concretely, with artificial saliva and real saliva samples, detecting cortisol in complex matrix of interferences.

1.2.2. List of publications

The publications included in this list shall be considered for the evaluation of this thesis dissertation. A reproduction of each publication can be found on the indicated chapter summarized below.

1.2.2.1 Accepted publications. A copy of each publication listed below can be found in the manuscript.

Publication I. Miguel Zea, Ana Moya, Marco Fritsch, Eloi Ramon, Rosa Villa, and Gemma Gabriel. Enhanced performance stability of iridium oxide based pH sensors fabricated on rough inkjet-printed platinum. *ACS Applied Materials & Interfaces*, Mar. 2019, doi: 10.1021/acsami.9b03085. (Q1, IF: 8.758).

Publication II. Miguel Zea, Robert Texido, Rosa Villa, Salvador Borrós, and Gemma Gabriel. Specially designed polyaniline/polypyrrole ink for a fully printed high sensitive pH microsensor. *ACS Applied Materials & Interfaces*, May. 2021, (Q1, IF: 8.758).

Publication IV. Miguel Zea, Francesca G. Bellagambi, Hamdi Ben Halima, Nadia Zine, Nicole Jaffrezic-Renault, Rosa Villa, Gemma Gabriel, and Abdelhamid Errachid. Electrochemical sensors for cortisol detections: Almost there. *TrAC Trends in Analytical Chemistry*, vol. 132, p. 116058, Nov. 2020, doi: 10.1016/j.trac.2020.116058. (Q1, IF:9.801)

1.2.2.2 Submitted publications. A copy of each publication listed below can be found in the manuscript [Capítulo 6](#).

Submission III. Miguel Zea, Ana Moya, Rosa Villa, and Gemma Gabriel. Inkjet-printed Paper-based Electrochemical Sensors: Tuning Active Area through Surface Modification. The article has been SUBMITTED to *Advanced Materials Technologies* in June 2021. (Q1, IF: 7.39)

Submission V. Miguel Zea, Hamdi Ben-Halima, Ana Moya, Rosa Villa, Nadia Zine, Abdelhamid Errachid, and Gemma Gabriel. A Fully Paper-Based Electrochemical Sensor Made by Inkjet Printing for Saliva Cortisol Detection. The article has been SUBMITTED *ACS Applied Materials & Interfaces* in June 2021. (Q1, IF: 8.758).

1.2.3. Thesis outline

With regards to the objectives that guided this thesis and the publications pointed out in the previous section ([Section 1.2.2](#)), the dissertation is organized in 6 chapters which are summarized below.

Chapter 1 entitled “Dissertation Summary” presents the dissertation overview, where the most relevant aspects and publications of this thesis are briefly introduced.

Chapter 2 entitled “Introduction to Inkjet Printing Technology and some applications” presents the technology used for the development of the sensors presented in this thesis. This chapter has a short introduction about printed electronics and inkjet printing technology. Following, the importance of the development of novel inks for the fastest adoption of this young technology. Next, it is demonstrated the potential of inkjet printing technology as additive non-contact technology and its capability to developed sensors and electrochemical sensors, additionally a small overview of electrochemical measurements is described.

Chapter 3 entitled “Printable materials for sensing” A small overview about the inks for the development of electrochemical sensors, follow but their requirements for fabricate sensors. Finally, the development of pH inkjet printed sensors on plastic substrate are show.

Chapter 4 entitled “Inkjet printed PoC devices” presents the PoC devices, their importance in the healthcare field and their recognition methods. Next, a short review of PoC devices develop using inkjet printing technology. Follow by the use of inkjet printing for the development of paper-based PoC devices. In the end of this chapter, the develop of a paper-based cortisol biosensor using inkjet printing.

Chapter 5 entitled “Conclusion and further work” summarizes the main conclusions of this thesis, as well as conclusions that are made from the research.

1.3. Thesis Framework

The main part of this thesis has been carried out in the facilities of the Institut de Microelectrònica de Barcelona (IMB-CNM) del Consejo Superior de Investigacions científicas (CSIC).

Miguel Zea has received a pre-doctoral scholarship granted by Fundación Ceiba and Gobernación de Bolívar, Colombia. Miguel Zea spent 4 months (February to June 2019) in the Université de Lyon, Institut des Sciences Analytiques, under the supervision of prof. Abdelhamid Errachid. Two articles of the five presented articles that compose this thesis and several contributions to scientific conferences have been carried out with the collaboration of both groups.

Chapter 2 | Introduction to Inkjet Printing Technology and new developments

This chapter includes a brief explanation and description of the inkjet printing technology and its implementation. Followed by the need to develop new inks and its importance in the future of this technology. Finally, the interest of print on alternative substrates, following by the development of a complete three-array electrochemical cell on paper porous substrate.

2.1. Overview of Inkjet Printing Technology

Inkjet printing is a contact less, accurate and reproducible manufacturing technique, which relies on the formation of individual droplets that are ejected from a nozzle thus allowing the maskless deposition of different functional materials on a wide range of substrates. It is based on digitally controlled ejection of fluid drops from a small aperture, named nozzle, directly to a pre-specified position²⁶. The original idea of the Inkjet printing technology is attributed to Lord Rayleigh back in 1878, who proposed a liquid jet of constant radius able to fall vertically under gravity²⁷. Today, it is widely use, from newspapers to food packaging, from magazines to roadside advertising, we live in a world of printed materials. However, scientific community has shown a growing interest in developing low-cost flexible electronics by exploiting innovative materials and printing technologies²⁸. This interest is driven by several reasons:

- The need for low-cost mass-production processes such as, RFID tags, antennas, keyboards, displays, and flexible sensors^{29,30}.
- New applications requiring shapeable and reusable/disposable devices where low-cost and flexible sensors can be suitable used³¹.
- The demand for the fast fabrication of electronics and sensors³².

Inkjet printing technology allows rapidly developing of inexpensive devices and sensors, which is why it has got so much attention from the scientific community. As a digital printing process, it enables variable printing since no printing plate or mask is needed, and thus it can correct in-line for distortion. It is a suitable technology for a wide range of production scales, with a lower initial investment than other printing techniques. The ink consumption and material wastage are minimal and it can produce patterned thin films³³. Inkjet printing printhead developers have continued to improve with finer and finer printheads and incrementing nozzles numbers, which are starting to enable features of few μm and faster printing processes. Also, the implementation of multi-head printers has been substantially improved allowing multi-materials process with smoother workflow. Lately inkjet printing have been considered as a “high resolution” technology^{34,35}. The above-mentioned properties and advantages makes the inkjet printing technology a technology of high scientifically and world’s concern interest.

2.1.1. The inkjet printing technology

Already ubiquitous in the small office and home environment, inkjet printing is likely to take an increasingly important share of the commercial printing market soon and to become more widely used for decorative products, packaging, general industrial applications, and textile printing as well³⁶. The global inkjet printers market size was valued at USD 34.24 billion in 2019 and is expected to expand at a compound annual growth rate of 5.3% from 2020 to 2027³⁷.

Additionally, as inkjet print quality increases, more opportunities become available for printing, gaining attention to the technology, and attracting more market and investment. Because printed patterns by inkjet are defined digitally from digital data files and never as physical master templates, they can be easily changed, therefore the setup costs and times for inkjet printing are low. Lately, the technology has increased in reliability and robustness, hence, applications at which inkjet competes with more conventional processes in terms of cost have also increased.

As it is mentioned in previous section 2.1, the original idea of the technology was conceived by Lord Rayleigh²⁷, who proposed a liquid jet of constant radius able to fall vertically under gravity. As the liquid length increases and reaches a critical value, the jet loses its cylindrical shape and decomposes into a stream of droplets as shown in Figure 2.1, for this reason it is necessary an accurate control of printing parameters. This principle allows to progressively build up patterns directly on to the substrate by the non-contact deposition of a large number of individuals, tiny drops of ink. Each small droplet, typically 10–100 μm in diameter, is created and deposited under digital control, so that each pattern printed in a sequence by the same machine can just be a mass production of the same pattern or be a personalized pattern for each user or device. This has led to two main modes of operation, continuous and drop-on-demand (DoD) printing technologies.

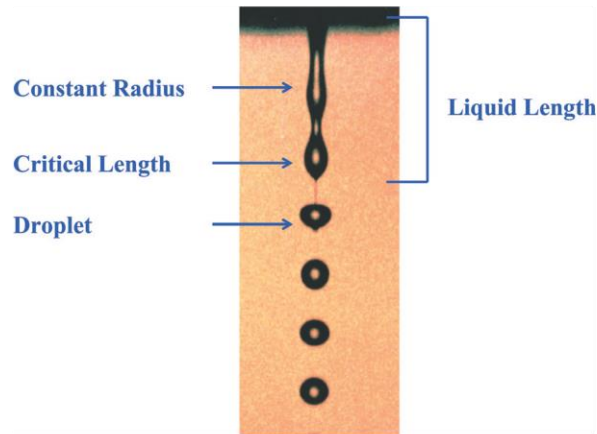


Figure 2.1. Lord Rayleigh's idea of instability jets.

Source ²⁷. Copyright 2001 Society of Photo Optical Instrumentation Engineers.

In both continuous and DoD methods, the liquid ink is jet through a nozzle (small hole in the print head). Main difference between both methods lies in the essence of drop departure to substrate. In continuous, as the name implies, drop ejection is non-stop, while DoD generates drop by request.

Continuous inkjet was the first existing inkjet technology³⁸. It relies on a continuous ink ejection, where the stream is adapted into volume-controlled droplets generated by acoustic pressure waves as it is sketched in Figure 2.2(a) (section 2.1.2 below). The ink droplets are subjected to an electrostatic field created by a charging electrode. The charged droplets pass through another electrostatic field and are deflected by electrostatic deflection plates to land at the right place on the substrate³⁹, allowed to undeflected droplets goes into a gutter for recirculation. In this manner, a stream of deflected drops from a single nozzle, in combination with a moving substrate or/and printhead, can be used to print a digital pattern. In this method only a small fraction of the droplets is used to print, the majority are being recycled. This inkjet technique is used for very low-cost system where no need of high resolution is necessary. Multi-nozzle configuration can be used in continuous printing method, with each drop addressing one pixel position through printed pattern. The printed pattern is created by a cluster of correctly jett drops on to a substrate.

The resulting evolution of continuous inkjet technique leads to the DoD inkjet technique, where a single drop is ejected by the cartridge nozzles only when is required to achieve the printed pattern. Applications of inkjet printing in the commercial world have been developed rapidly, predominating the use of DoD

technology. DoD technology is the selected technique used in the development of this work and it will be further explained in section 2.1.2.

2.1.2. DoD technology

In DoD drops are not deflected, on the contrary drops are generate by request. This on-demand drop can be pressure-pulse ejected from the nozzle drive by a thermal pulse (Figure 2.2(b)) or by a piezoelectric actuator (Figure 2.2(c)). Generally, in DoD, liquid ink is contained on nozzle's exit-channel by surface tension and when pressure pulse is strong enough, an ink column emerges from the nozzle with surface tension leading to a stream of ink to form the drop. This stream of ink lead by the main droplet which eventually detaches from the nozzle (at the top of Figure 2.1), while, at the same time becoming thinner ideally conforming the main droplet, but more often forming a series of "satellite drops" that can form the droplet on the fly. The final shape of the droplet before placing on the substrate can be a spherical drop (ideal case) or a main drop followed by one or more "satellite" drops. Clearly "satellite" drops need to be avoided and various strategies are employed such as adjusting pressure-pulse parameters, ink formulation, printing temperature, modifying surface tension's head, among others.

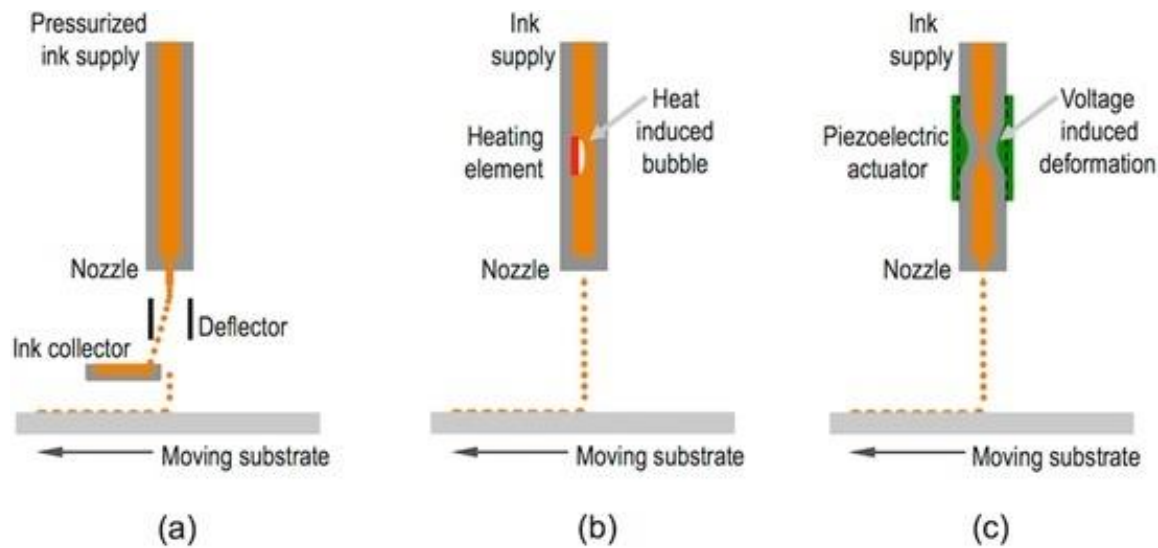


Figure 2.2. Inkjet printing operation modes.

Schematic representation of (a) continuous inkjet (CIJ) and Drop on demand (DOD) inkjet printing systems using (b) thermal and (c) piezoelectric technology. Adapted from ⁴⁰.

2.1.2.1 Thermal DoD

This printing method was invented and developed in the late 1970s and early 1980s by Canon and Hewlett Packard⁴¹ independently but concurrently. This method is still the most used in home and office printers. In nozzle's exit-channel it is placed a small resistive heater in thermal contact with the ink. An electric current pulse is injected on the heater causing a rapid heating (within a few micro-seconds and up to 400 °C)

and vaporization, creating bubbles from adjacent ink as show in Figure 2.2(b). These bubbles quickly expand, producing a pressure force to push out the ink in form of a droplet. Once the drop is ejected, the heater then cools down collapsing the bubble, getting in fresh ink in the exit-channel, and the cycle is ready to start again.

One advantage of this printing method is the simplicity of heater fabrication, resistive track can be fabricated in a several numbers of simple ways, most of them suitable for large-quantity manufacture. On the other hand, nozzles typically suffer from a short-lifespan due to residue build-up on the resistive heater, and some types of inks are restricted due to the need to be able to support and withstand the heating and vaporization process, constraining the types of solvent which can be used. However, as only very thin layer of ink is heated and vaporized, the bulk of the ink maintain room temperature allowing the use heat-sensitive material such as biomolecules and living cells⁴². But another functional materials such as e.g. metal nanoparticles can be sintered on the heater due to the heat, resulting in the deposition of a metal thin layer on the heater causing malfunction and shortener its lifespan.

2.1.2.2 Piezoelectric DoD

In this printing method a piezoelectric actuator is placed in the exit-channel to control ink ejection. A voltage pulse is applied to the piezoelectric plate causing a deflection, creating pressure in the channel, and ejecting a droplet as show in Figure 2.2(c). Unlike thermal actuator, piezoelectric allows low-pressure pulses, by deflecting it negatively increases exit-channel volume. This property is used to improve ejection performance and drop shape. Additionally, it allows the use of inks with low viscosity and low surface tension.

Due to the fast actuator of the piezoelectric plate (in the range of μs), this method is faster than thermal type limited by the extra time need to cool the resistive plate. The resolution in the inkjet printing

technology is defined by ejected drop volume. Nowadays technology allows the fabrication of 1 pL nozzle's chamber, which generates drop of the same volume (in ideal case). These 1 pL drops create spots around 15 μm or higher in diameter on the substrate, highly depending on contact angle, flying time, surface tension, among others condition of the substrate and ink. Creating a printed pattern is restricted by the serial characteristics of nozzle ejection, where droplets are generated one after another. To overcome this limitation, industrial inkjet printheads utilizes hundreds to thousands of nozzles to enhance printing performance via parallelization.

2.1.3. Piezoelectric actuator working principle

The printer used in this thesis is based on piezoelectric system. Deflection of the piezoelectric is controlled by a voltage pulse, named waveform, that is responsible for the jetting performance of the nozzle. The typical basic waveform is divided into four segments as show in Figure 2.3. Each segment has three main properties: duration (time), level, and slew rate of the applied voltage waveform.

The level value in phase 'Start' and phase 1 have the most impact on the jetting process. Changing the duration of phase 'Start' and slew rate and/or duration of phase 1 has a strong influence on drop formation. The applied voltage relates directly to the volume of the pumping chamber. Faster ('duration') changes in voltage modifies the volume faster, bigger amplitudes in voltage level cause bigger volume changes. And the slew rate determines how fast the volume changes. Published works demonstrate a clearly dependance between waveform characteristics and drop formation process and ejection⁴³⁻⁴⁵.

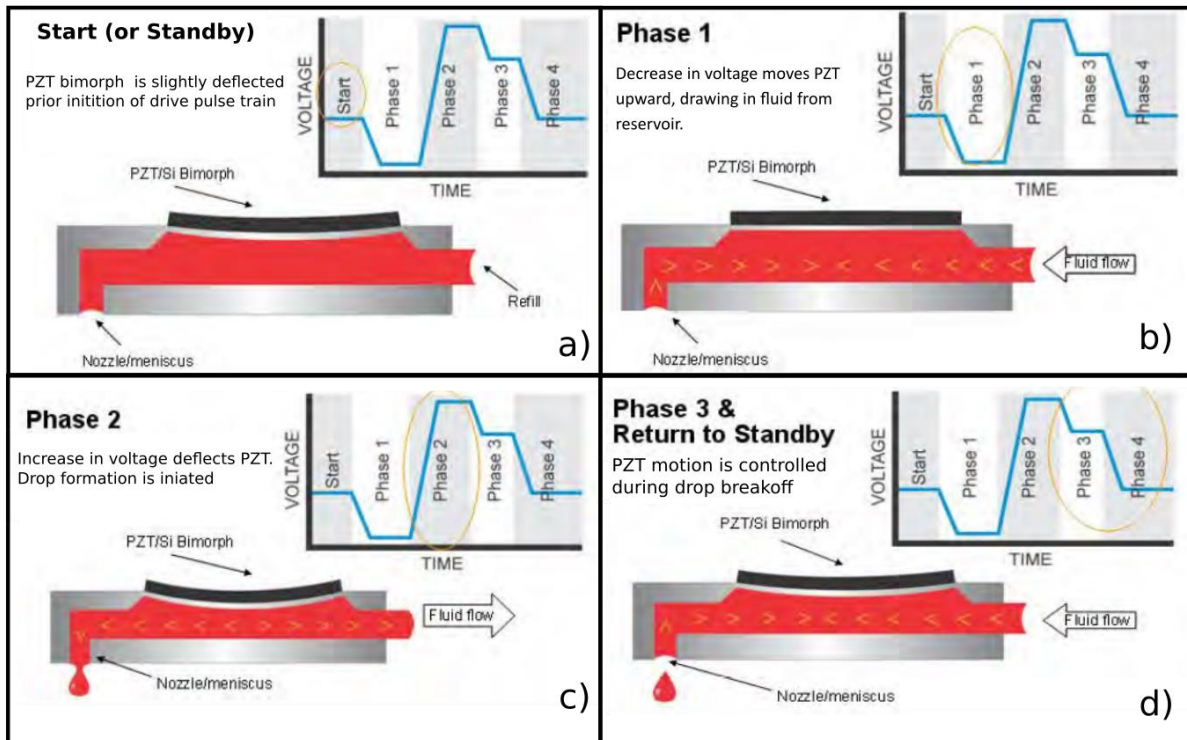


Figure 2.3. Waveform phases.

Waveform steps for drop ejection controlling piezoelectric deflection, a) Start, b) Phase 1, c) phase 2, and d) phase 3. Source from ⁴⁶.

Few microseconds of rise and fall times are needed for jet formation. Figure 2.3 shows a drop formation in the printhead. In detail, 'start' phase brings the piezoelectric to a relaxed position with the chamber at its 'normal' volume capacity (Phase 'start'). Immediately a decreased voltage is applied to retract the piezoelectric drawing fluid into the pumping chamber and followed by a settling time (Phase 1). In this phase the fluid is pulled into the chamber through the inlet. The end of phase 1 need to be aligned with the beginning of the next one to deflect the piezoelectric precisely at the center of the pumping chamber to push out a droplet with its maximum energy (Phase 2). During the last phase (phase 3), the piezoelectric retracts slightly breaking the droplet from the chamber and the voltage returns to the 'standby/start' state. Nevertheless, waveform generation is highly dependent to the ink properties, and its ejection. Ink viscosity, density and surface tension are crucial for Inkjet printing⁴⁷.

2.2. DoD inkjet printer

The printer used in this thesis is the piezoelectric Dimatix Material Printer (DMP-2831 from FUJIFILM Dimatix, Inc, USA) model shown in Figure 2.4(a). It is a versatile system for inkjet printing development

mainly used in research area to evaluate the use of inkjet technology for new manufacturing and analytical processes. It is a self-contained system that allows the deposition of materials on substrates up to A4 size and utilizes disposable piezoelectric cartridges with a featuring 16 nozzles printhead (Figure 2.4 (b)). It is designed to be convenient and easy to use to carry out “proof of concept” and development work using inkjet technology. It does have extensive capabilities to allow increased experimental sophistication to optimize process parameters for the user’s applications⁴⁶.

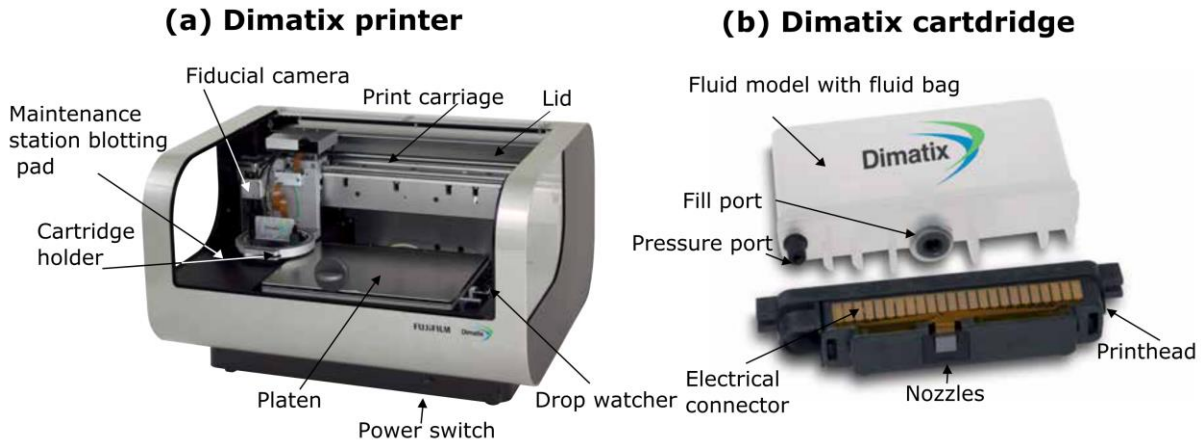


Figure 2.4. Dimatix printer and cartridge
 (a) Dimatix material printer and (b) Printhead and cartridge.

The Dimatix printer incorporates two cameras: a drop watcher system and a fiducial camera for alignment and pattern inspection. The drop watcher function is to characterize and develop the ink droplet, examining the drop formation and progression from each of the printhead’s nozzles. It offers a simultaneous and real-time control over the electronics driving signals supplied to the printhead thus allowing to explore fluid jetting properties, understand its suitability for inkjet deposition, and establish conditions for printing process. A reticule enables observe and measure drop quality, trajectory and drop speed. Figure 2.4(a) and (b) detail different parts of the printer and cartridge.

Printed patterns can be created using the editor program in-software or importing files to create complex structures. The substrate platen can be heated up to 60 °C. The use of substrate heating can be used to slightly enhance the drop drying in order to improve the film formation. It can also slightly modify substrate/ink surface tension to enhance drop deposition. However, the substrate heating may raise the nozzle temperature and degrade the jetting process. It is important to study carefully the optimum applied temperature to the substrate to obtain the desire result.

Fujifilm Dimatix supplies two kind of printhead, one for general purposes with 16 nozzles delivering a drop volume of 10 pL and another for special patterns or inks of 1 pL also with 16 nozzles. These smaller nozzles are hard to handle and narrow the materials that can be used. In the Dimatix printer, a drop velocity of between 6 and 10 m/s is desired; therefore, an ink with a viscosity below 15 mPa.s and surface tension between 28 and 33 mN/m is recommended to obtain stable jetting.

2.3. Printable materials

High number of inks have been used from early stages of inkjet printing technology. At the beginning, inkjet printing inks were colorants (pigments or dyes) for graphic art. With the advancement of the technology, Inkjet printing has been used to deposit a very wide range of materials, including metals, ceramics, polymers, and biological materials for many different applications³⁸. The most inherent restriction for a printable material is that the substance being printed must be in liquid form (or be a nano size material suspended in a liquid medium), additionally it must have proper rheological properties to go through the nozzle and to be handled by the printhead actuator. The material which is printed do not need to be the same as the final developed material; post-processing steps (e.g., of sintering process is show in Figure 2.5), or a print a precursor material followed by other steps can allow achieving a final material different than the jetted one. The most common materials when printing electronic devices by inkjet printing technology are classified in three groups conductive, semiconductive, and dielectrics⁴⁸.

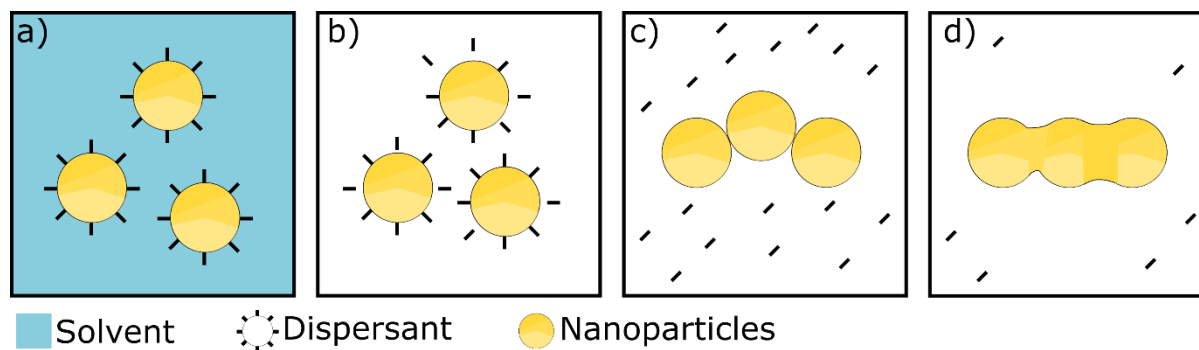


Figure 2.5. Schematic of sintering process of nanoparticle inks.

Representation of sintering process of a nanoparticle-based ink; a) Nanoparticle dispersed in solvent as it is printed, b) Solvent evaporation and beginning of degradation, usually due to heating, c) Evaporation of other additive and beginning of sintering process, and d) Sintering of nanoparticles, usually by nanoparticles fusion.

Conductive inks

Electrical conductive inks usually comprise colloidal suspensions of metal nanoparticles, nanowires, carbon nanotubes, organometallic compounds in solution or dispersed conductive polymers⁴⁹⁻⁵². Conductive inks have been developed to fulfill the demand of printing technology to develop electronics, sensors, batteries, and connections among components. Generally, conductive metal inks based on nanoparticles or precursor are commonly employed as conductive or transducer element due its reliable and stable conductivity⁵³. Selection of conductive ink is strongly dependent of their application. Silver ink is the most common printable metal conductor, it is available in almost all additive technologies such as screen, flexo, gravure and inkjet.

Semiconductive inks

The development of a wide variety of materials represent the key element for mature a technology⁵⁴. Semiconductive ink development has different alternatives to meet the electrical requirements and the material restriction. A semiconductor resistivity falls as its temperature rises, against metal behavior; and its resistivity value as its name implies is between a conductor and dielectric. Inorganic semiconductor generally shows better electrical performance and stability, while organic semiconductors generally ensure cost-effectiveness, easier synthesis development, and higher mechanical bending strength.

Dielectrics

Dielectric materials are non-conductive which are used and/or necessary in many types of devices. Various dielectrics materials are solution processable and can be formulated to use in inkjet printing. Dielectrics play an important role in device performance. They have diverse useful functions, spanning from avoiding short-circuits, enhancing capacitance in electronic devices (capacitors or transistor), multi-layer antennas, define electrode active area, among others⁵⁵⁻⁵⁷. Printable dielectric materials can be classified in inorganics, polymers, organics, and hybrid materials⁵⁸.

2.4. Substrates for Inkjet printing

The process of inkjet printing involves the deposition of a pattern on a substrate, widely used to represent text or/and images, however in the past decades printed electronics, sensor fabrication, and other applications have been gaining the attention of global market. These new applications require a new variety of substrates that need to be conscientiously analyzed their characteristics and restrictions

are challenging. Nowadays the global market is looking for a technology which can fit circular economy that's target efficiency, reduction, eco-design, recovery, and recycling⁵⁹. And here is where substrates for inkjet printing technology can play a crucial role because substrate represent usually more than the 80% of the composition of a printed system.

Inkjet printed devices target the use of flexible and potentially low-cost substrates to enable large area and robust products enabling a higher freedom of design. Substrates vary widely depending on the application requirements. In general, glass and metal are still the only substrates readily available with intrinsically high and reliable barrier properties; a key requirement for many applications⁴⁸. Plastic substrates have received much interest due to their intrinsic characteristics (transparency, strength, cost, etc). Nevertheless, its low transition glass temperature and the large thermal expansion coefficient constitute their main drawbacks due to the high sintering temperatures of some metallic inks. Surface modification with planarization, hard coats or other modifiers is also a common approach for plastic substrates. During the last decade, has started a growing interest in paper in medical and other industrial applications. Paper is a disposable and biodegradable material made from renewable resources which has unique properties and compatibility with chemicals and biochemicals. While some simple devices can be made on standard paper, special coated papers like paper microfluidics are also available, and some standard packaging papers appear to be promising as well. Microfluidic paper-based analytical devices (PADs) devices are targeting healthcare-related diagnostics, where the impact of cost reduction and simplicity is deemed to be highest. In other fields of applications, such as environmental monitoring, explosives detection, or screening for food the use of paper is growing⁶⁰.

The inkjet printing technology is a non-contact method, the only forces which are applied to the substrate result from the impact of very small liquid drops. Thus, fragile substrates can be processed which would not survive other conventional printing methods. Nonetheless, it is important to evaluate the properties of the substrate, such as, the service temperature, its barrier properties against humidity, and its electrical, optical, mechanical, and chemical properties. But equally important is to consider the receptivity of the ink by the substrate or with previously printed layers, in the case where a different ink has been used. The droplet size can vary depending on the interactions between the ink and the substrate⁶¹. Also, sometimes substrate surfaces are hydrophobic in nature, so to increase the adhesive property of the substrate, it needs some surface modifications⁶¹. Thereby, during the manufacturing step,

the printed pattern characteristics are dependent on the materials (ink and substrate) and their interaction.

It is important to remark that for the advance of the inkjet printing technology a huge effort must be done in the analysis and the use of new substrates for printed devices in applications such as PoC devices. Specifically, the emergence of the PoC devices is demanding the use of paper as a substrate⁶². Using paper substrate has enhanced the advantages of inkjet printing because paper is eco-friendly and an extremely low-cost material.

2.5. Inkjet printing focused on sensors

Inkjet printing technology offers the possibility of combining the performances of functional inks and flexible substrates with a wide range of applications, thus creating the conditions for the fast development of sensors and electronic components^{32,63-67}. This technology with its unique features allows to design a sensor and almost immediately fabricate a prototype to test and, eventually, easily produce a batch of sensors to validate them. Today, the technology is ready for mass production to hit the market. Ink jet printing introduces huge innovation in sensor developments and flexible electronics. These innovations are driven by the use of new materials (inks and substrates) and cost efficiency. By exploiting and applying these features to a new field or application, both development and production can be substantially improved.

The continuous pursuing of global market of cost saving, is also applying to sensor development. These features have led to great innovation in this field, allowing an affordable price for the fabrication of sensor platforms and sensing devices. Unquestionably, other requirements such as sensitivity, response, and size are also addressed and huge advances have been achieved, however it has become progressively more crucial to introduce low-cost, fast, reliable, biodegradable/disposable materials and portable sensing solutions to the market⁶⁸. Inkjet printing technology can tackle the current demands for sensing solutions due to its advantages already explained in above sections.

Nowadays sensors have a wide range of applications from construction, aerospace industry, health services, to domestic appliances and military defense equipment. Sensors contributed to achieve substantial accuracy and control in automation and industrial processes⁶⁹. Additionally, health sensors have been a reliable companion of health tracker since new technologies allow the fabrication of portable

and low-cost sensing devices (e.g., Holter monitors). Sensor advancements are the spearhead of vehicle auto-pilots, space missions, and satellite. Advances in signal processing and computer algorithms have opened opportunities to have sensor in/on almost every place of our lives.

So, what is a sensor? According to the ANSI, a sensor is a device which provides a readable output in response to a specific measure⁷⁰, instrumentation engineering limit this definition to a device used for measurement purpose. Moreover, sensor and transducer term are frequently used, however there are differences. Basically, the transducer is just the input block that transform the signal and the sensor include all the array of elements or circuitry parts to obtain the readable signal.

Flexible sensors or sensors with bent tolerance are an increasing area of research and development due to the huge demand for chemical, biological, force, health, and deformation sensors, along with many others. The classical method of fabrication of these sensor are photolithography, spin-coating, and vacuum deposition⁷¹⁻⁷³. Nevertheless, these classical methods, even with recent modernization applied to flexible substrates, show some drawbacks for the high demand of innovation and low-cost production. When using conventional production technologies, the fabrication of these sensors involve a high number of fabrication steps, high processing temperatures, produce toxic waste, mask expenses, poor tolerance to design changes, and a huge quantity of equipment is needed⁷⁴. So, deposition printing techniques such as inkjet printing and screen printing have received attention for the implementation of these sensors⁷⁵.

Inkjet printing allow a more versatile fabrication process, it does not require mask and has good alignment in the case of multilayer fabrication, on the contrary of screen printing. Although, screen printing is widely used for industrial mass-production when low resolution patterns are required, and the sensor design is almost stable. Another important advantage of inkjet printing is that it is a non-contact method, thus reducing the risk of contamination and substrate damage, particularly important in the fabrication of chemical, electrochemical, and biological sensors^{74,76,77}, inkjet printing allows precise deposition and control of the layer thickness and the quantity of ink, as it does not need being in contact with the substrate and just the need of a camera and proximity sensors; resulting in a critical factor for the fabrication of flexible electronic and sensors⁷⁸. Inkjet printing also offers the required performance to print with high reproducibility and large-scale production demands.

With this in mind, inkjet printing technology is therefore taking its first steps thanks to its great potential in sensors fabrication. Furthermore, new materials are in development or have been recently developed opening the range of application that ink jet printing can reach. It is therefore clear that this technology is well suited for the production of sensors and can be expanded to novel sensors or applications through new materials (ink and substrates mainly), new printing designs and printing processes.

2.5.1. Electrochemical sensors

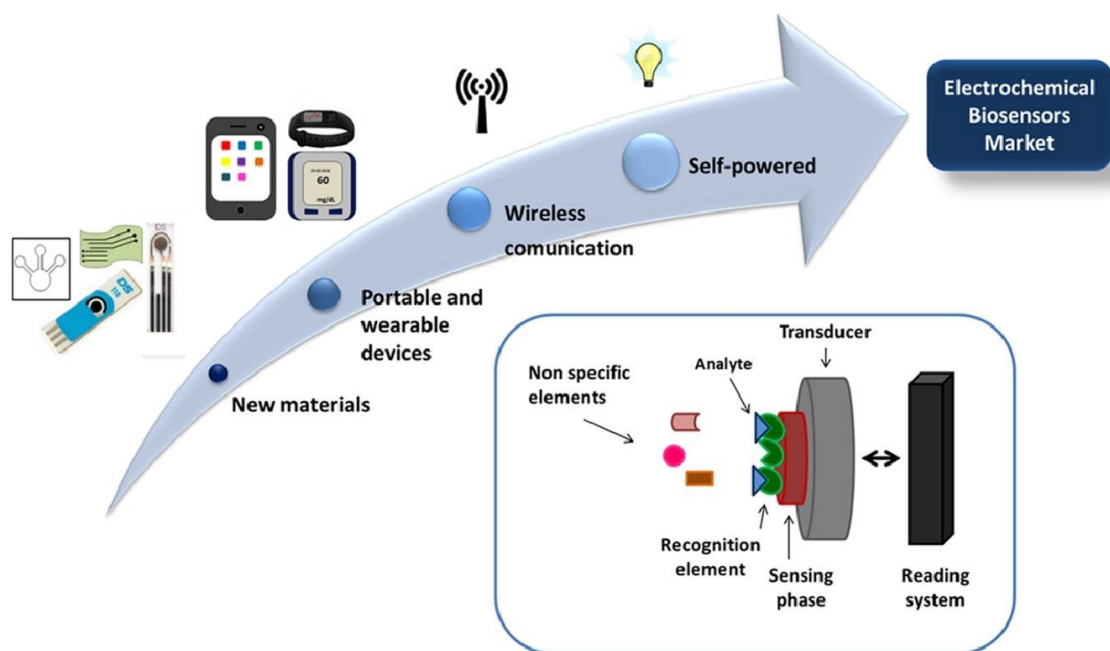


Figure 2.6. Schematic representation of the path that electrochemical sensor is following. The path that electrochemical sensors are following to reach the market. Source ⁶⁸.

Electrochemical sensors are devices capable of providing quantitative or semi-quantitative analytical information with an electrochemical transducer⁷⁹. They are especially attractive for research and innovation because of their remarkable detectability, experimental simplicity, integrity and low-cost. Additionally, they do not need sophisticated instrumentation since the sensor directly converts chemical information into an electrical signal⁸⁰. Nowadays the interest in electrochemical sensor continues growing as show in Figure 2.7. According to Scopus website 5007 articles were published last year (2020)

that it is more than the double that were published in 2013, showing the substantial research effort ongoing in this field. All this effort research is stimulated by the wide range of application where they can be used and provide a solution, Figure 2.6 inset shows a schematic of electrochemical biosensor. Off course, they have the goal of follow the electrochemical sensing response that have reached the commercial ones. Figure 2.6 shows the path that electrochemical sensors are following in conditions of market trends.

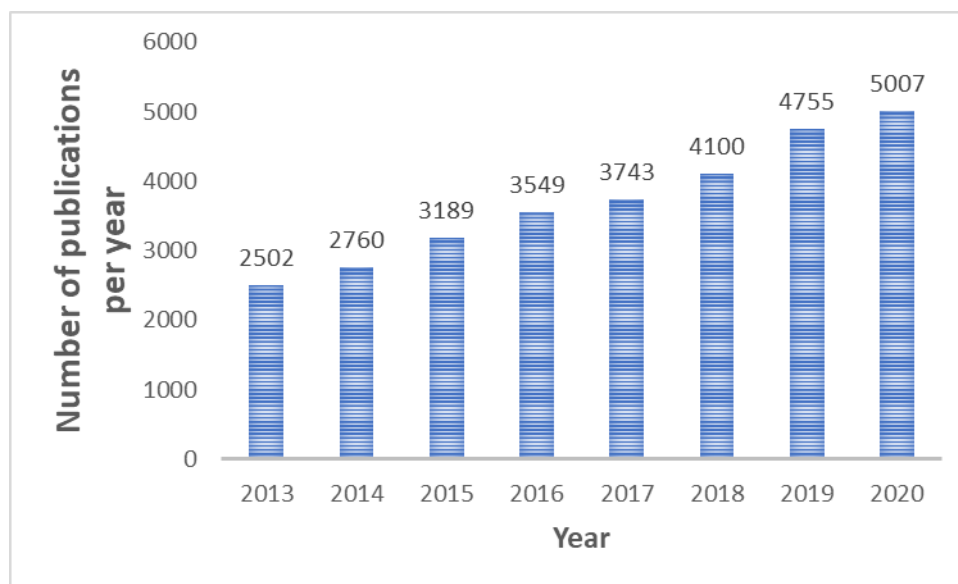


Figure 2.7. Electrochemical sensor publication in the past seven years.

Number of publications per year from 2013 to 2020 according to Scopus website, searching for “Electrochemical AND Sensor”.

Sensors along this thesis are based on electrochemical sensing, where the transduction mechanism it is based in a noble metal that it is coated with the necessary material to sense the desire analyte. This detection method is ideally suitable for the integration in portable, small, miniaturized systems due to its reliability and durability⁸¹. Electrochemical detection techniques are amperometry, potentiometry or impedance, and field effect⁸². Table 2-1 shows the electrochemical sensors classification according to its detection technique, and its often-used types of measurement.

In the following section, it is described the working principle of the electrochemical techniques used in this thesis work. Now, just a brief summary about potentiometric and impedimetric technique, a fully description of both techniques is widely described in the literature^{83,84}.

Table 2-1. Electrochemical measurements techniques.

Electrochemical sensors classified type of measurements, with corresponding common transducer type and the usual measured analytes. Source ⁷⁹.

<i>Measurement type</i>	<i>Transducer</i>	<i>Transducer analyte</i>
<i>Potentiometry</i>	ion-selective electrode (ISE)	K ⁺ , Cl ⁻ , Ca ²⁺ , F ⁻
	glass electrode	H ⁺ , Na ⁺ ...
	gas electrode	CO ₂ , NH ₃
	metal electrode	redox species
<i>Impedance</i>	interdigitated electrodes, metal electrode	urea, charged species, oligonucleotides...
<i>Amperometry</i>	chemically modified electrodes (CME)	sugars, alcohols, phenols,
	metal or carbon electrode	oligonucleotides...
		O ₂ , sugars, alcohols..
<i>Field Effect</i>	ion-sensitive field effect transistor (ISFET), enzyme FET (ENFET)	H ⁺ , K ⁺ ...

2.5.1.1 Potentiometric technique

Potentiometric technique is suitable for the analysis of substances which the electrochemical equilibrium is established at a suitable indicator electrode at zero current⁸³. In this technique the analytical information is obtained by converting the recognition process into a potential signal, which is logarithmically proportional to the activity of species generated or consumed in the recognition event⁴⁸. According to Nernst equation (2.1), the measured potential E_{cell} is logarithmically related to the relative activities of the redox species of interest:

$$E_{cell} = E^0 - \frac{RT}{zF} \ln \frac{a_0}{a_R} \quad (2.1)$$

where E^0 is the standard half-cell reduction potential and a_0 and a_R are the activities of the oxidized and reduced species, R is the universal gas constant; T is the absolute temperature; F is the Faraday constant; z is the number of moles of electrons exchanged in the electrochemical reaction.

This implies a poorer accuracy and sensitivity of the measurements in comparison with other analysis techniques where limiting the current or a current of a maximum is determined, but it also implies that the accuracy does not only depend on the absolute value of the concentration being measured. In this technique, the relative error does not increase drastically with decreasing concentration and decreasing faradaic current. However, a small error in determining the potential E_{cell} produces an error of 4 times of the determined potential for $z = 1$ and 12 times for $z = 3$. Nonetheless, potentiometry technique can be used over a much wider range of solution concentrations than the voltametric methods⁸³. Additionally, it has high selectivity; the potential of the electrode should response only to the examined analyte. For this reason, potentiometric sensors have been highly used almost a century ago, due to their easy-use, simplicity, and cost.

In practice, a potentiometric sensor usually has a two-electrode structure, where one electrode is the indicator (sometimes miscalled working electrode) and the other is the reference electrode (RE). Normally, the transduction and measurement of the potential relies to zero current. Potentiometric measurements involve determination of the potential difference between either the indicator and the RE, or two REs separated by a permselective membrane, when there is no significant current flowing between them. This potential differences between the indicator and the REs are proportional to the logarithm of the ion activity or gas fugacity as it has been explained before.

The setup of a potentiometric sensor is usually simple, also the electronic equipment (potentiostat) for its operation and data acquisition is not usually electronically complex. Potentiometric sensors provide real time information for process control, and signal (electrode potential) are obtained directly in-situ. The need for maintenance and calibration is low. Despite their simplicity the potential measurement requires an improved knowledge of the measuring conditions such as temperature, ion-strength, and others, which determine the restrictions of the measurement. For long-term measurements, the stability of the potentiometric sensor is determined by the potential stability of the RE.

On the development of the potentiometric sensors the key element is the indicator electrode. Depending on the construction of this electrode there are different types of potentiometric devices, such as ion selective electrode (ISE), glass electrode, gas electrode, and metal oxide electrodes. For the purpose of this thesis just ISEs potentiometric method will be briefly explained.

ISEs are the most common potentiometric devices, these types of sensors convert the activity of a target ion into an electrical potential as a measurable signal. The electrical response of an ISEs is provided by the RE and the potential signal is generated by a charge separation at the interface between the ion-selective membrane and the solution due to selective partitioning of the ionic species between these two phases⁸⁵. First ISEs were based in glass ion selective membrane, where the metal electrode is inside. The first developed ISE was a pH sensor and it was made by M. Cremer in 1906⁸⁶. Then, around 1970's the concept of liquid ion selective membrane is introduced, this type of ISEs are based on water immiscible liquid substance produced in a polymeric membrane⁸⁷. From the development of this polymeric membrane emerges the first ionosphere based solvent polymeric membrane based in polyvinyl chloride (PVC)⁸⁸, and almost 60 years later, this matrix is still widely used. This liquid junction membranes allow researchers to miniaturize potentiometric sensors and the large developed variations in ionosphere-based membrane made possible to use ISEs in various routine analysis including environmental and healthcare analysis^{89,90}. The systems are based on the junction-liquid set-up, where the back side of ISE is in contact with a well-known electrolyte to obtain stable potentials as show Figure 2.8a.

However, parallel to these developments, solid-state ISEs were developed. Solid-state ISEs do not need a liquid junction as show Figure 2.8b, which allows a much simpler fabrication, but years ago they have not sufficient potential stability to use in applications⁹¹. This promising fabrication process of ISEs is currently a solution for ISE sensors^{92,93}. They are usually applied to portable, small, and low-cost devices, granted by ISEs miniaturization. This required miniaturization can be develop just in solid-state ISEs due to replacing the liquid junction with a solid element. In solid-state ISEs a solid contact is formed between the sensing membrane and an electron-conducting substrate (Figure 2.8b), serving as an ion-to-electron transfer.

The ion-to-electron membranes for solid contact ISEs are required for their construction and their potential stability. In this type of ISEs, the ion-to-electron membrane is coated with a conventional ion-selective membrane and the ion selectivity is determined mainly by the ion-selective membrane. However, as it has been stated above, the stability and reproducibility of the measurement is provided by the RE potential. For this reason, huge efforts have been done to obtain solid state reference (no liquid junction), however the major challenges of miniaturized REs still remain⁹⁴. Nonetheless, in the past years major advances have been done⁹⁵, where a stable solid state RE has been achieved by depositing a protecting membrane on the metal electrode. Usually, this membrane not only protects the

outer surface of the RE but also allows the ionic contact between the solution and the phase boundary acting as a liquid junction bridge.

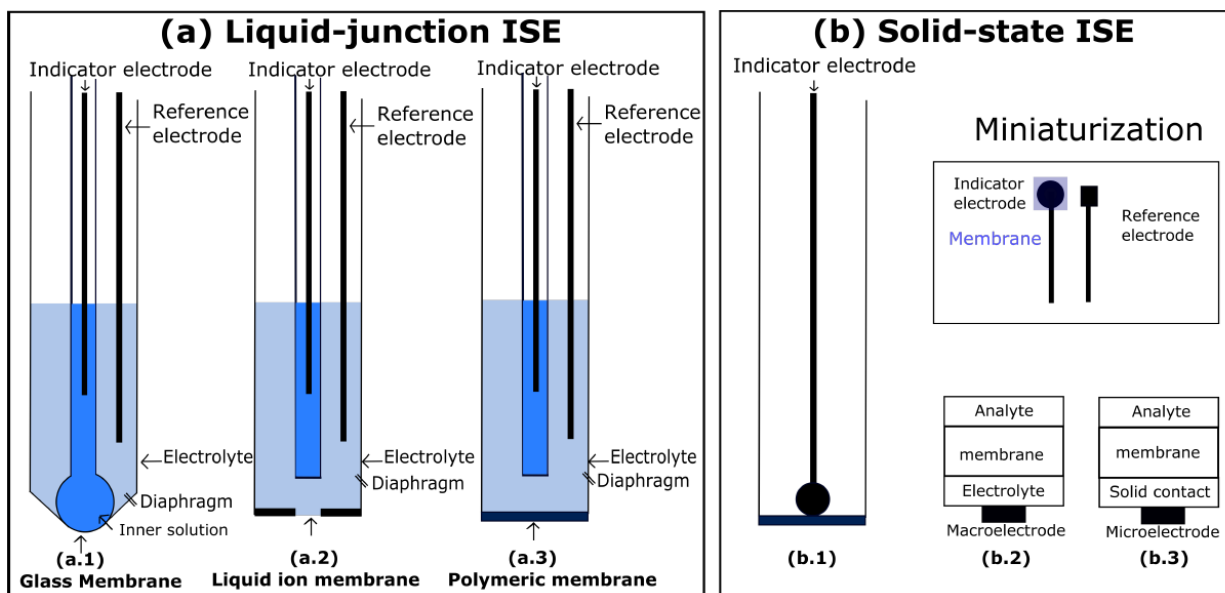


Figure 2.8. ISEs types.

(a) Liquid-junction potentiometric ISE in a combination (a.1) glass membrane, (a.2) liquid ion membrane, and (a.3) polymeric membrane, (b) Solid-state potentiometric ISE, (b.1) in a macroelectrode construction, (b.2) Scheme of liquid-junction construction and (b.3) Scheme of miniaturize system replacing the electrolyte with a solid contact membrane. Source ⁴⁸.

Solid contact ISEs have nowadays similar performance characteristics to conventional liquid junction ISEs and with the recent advances in the RE they are the future solution for ion-selective potentiometric sensors. The potentiometric sensors developed in this thesis are based in this solid state ISE construction approach.

2.5.1.2 Impedimetric technique

Impedance is a useful and attractive methodology that can be implemented in a wide range of applications such as human body analysis, characterization of solid electrolytes, pathogen detections, neuronal activity and hormones detection, among others⁹⁶. This technique is also known as spectroscopy (EIS) In 1894 the EIS methodology was reported by W. Nerst, when he measured the dielectric constant of aqueous electrolytes and other organic fluids⁹⁷. However, it was almost a century after (mid 1980's) with the advancement in computer controlling digital instruments, which allowed fast and easy measurements along with complex mass data processing and analysis that a huge interest in EIS really

grew significantly. Even today according to Scopus website the published articles on EIS technique grow around 10% each year, showing that is a technology completely active.

The principle of this type of transducer is based on the technique of electrical impedance EIS which is in proportion and dependent with the concentration of analyte and application of the sensor. The most common used, it is based on the application of a sinusoidal variation in voltage with a fixed amplitude in the order of millivolts between the working electrode (WE) and RE or/and working sensing electrode; and measuring the current generated between the working and the counter electrode (CE) as a function of frequency⁸³. This variation in time function of the input potential $E(t)$ is of the form of the equation (2.2, where V_m is Voltage amplitude, ω is the pulsation measured ($2\pi f$), f is the frequency, and t is the time.

$$E(t) = V_m \sin(\omega t) \quad (2.2)$$

And the measuring sinusoidal induced response signal as a current time function and accompanied by a phase shift is show in equation (2.3), where ϕ is phase shift between the two signals and it depends on the electrical element presented in the system.

$$I(t) = I_m \sin(\omega t + \phi) \quad (2.3)$$

The impedance value as frequency function ($Z(\omega)$) is determined by $E(t)$ over $I(t)$ as show equation (2.4).

$$Z(\omega) = \frac{E(t)}{I(t)} = \frac{V_m \sin(\omega t)}{I_m \sin(\omega t + \phi)} = Z_o \frac{\sin(\omega t)}{\sin(\omega t + \phi)} = |Z| e^{-j\phi} \quad (2.4)$$

$$Z(\omega) = |Z| e^{-j\phi} \quad (2.5)$$

$$Z(\omega) = Z'(\omega) + jZ''(\omega), j = \sqrt{-1} \quad (2.6)$$

The impedance $Z(\omega)$ is a complex quantity so it can be written in its equivalent algebraic (Equation (2.5)) and exponential (Equation (2.6)) forms.

EIS makes possible to differentiate the different phenomena that can take place in an electrochemical cell as a function of frequency. Thus, rapid phenomena such as electron transfer occurs at high frequency, while slow phenomena such as mass transfers and diffusion occurs at low frequencies⁹⁸.

EIS measurements can be made with a different number of electrodes in different configurations, among which the most common ones (usually called two-, three- and four-electrode cell) are shown in Figure

2.9. All three configurations are detailed in the literature^{84,96}. The Figure 2.9a shows the simplest cell that consists in two electrodes WE and CE, where the stimulus is applied, and the measurement is done using the same two electrodes and $jZ''(\omega)$ includes contributions due to the sample interface at both electrodes. To reduce the influence of the sample interface a third electrode is added the RE as show Figure 2.9b, where usually the test signal is applied in the first two electrodes and the current is measured in the third added one. While in the four electrode cell (Figure 2.9c) the measured impedance is independent of the electrode sample interface because current is applied between the first two electrodes WE and CE, while the voltage with no current is measured in the two added ones, CE and working sensing electrode (WSE). The use of a higher number of electrodes makes the measurements more complex but also more precise; thus, a trade-off is in order with the optimum solution depending on the constraint of any specific application.

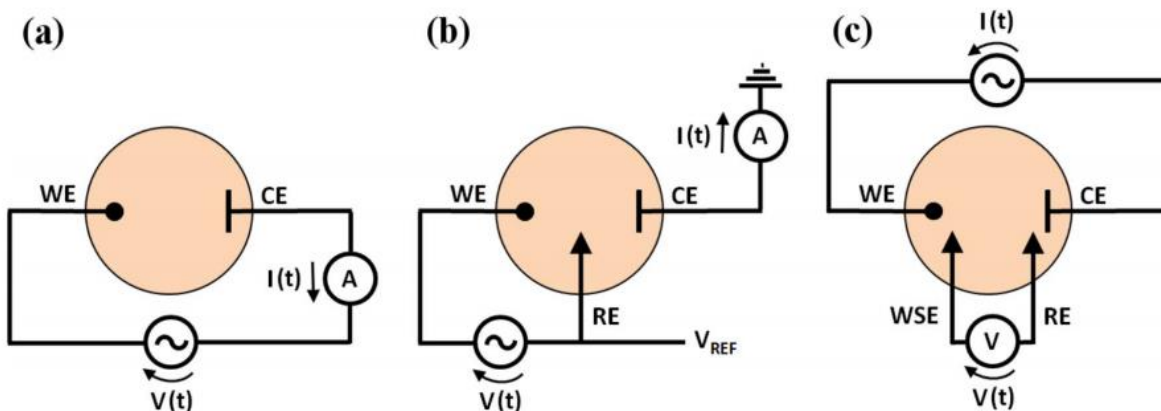


Figure 2.9. EIS setup cells.

Measurement setup cells used in EIS featuring (a) two electrodes, (b) three electrodes and (c) four electrodes. Source⁹⁶.

The data are normally interpreted using equivalent circuits, made of resistors and capacitors, while more complex elements (such as constant phase elements or Warburg impedances) can also be added. Data fitting using these models and extraction of the circuit parameters is a computer assisted process carried out by specific software packages. The use of electrical quantities allows a kinetic study, which makes it possible to dissociate the couplings between the various elementary phenomena.

For the purpose of this thesis an impedance biosensor has been developed. The typical experimental setup used in impedance biosensors (electrochemical cells) is a three-electrode configuration, where the test signal is applied between WE and RE, while the current is measured at CE⁹⁶. Impedance biosensing

is a sensitive technique usually used for simultaneous, label-free detection of antigen–antibody binding called impedimetric immunosensor. In this application antibodies are immobilized on the WEs, and they have attracted great interest in recent years because of their promising applications in various areas. Antibodies and antigens are bound to each other and thus an immunocomplex is formed and the electrode is coated with a blocking layer. As a result of that, electron transfer changes. After antigens binding to the antibodies, the access of the redox probes is hindered to a higher degree than in the absence of antigens. Since the Faradic reaction of a redox couple obstructs increasingly, the electron transfer resistance will increase and the capacitance will decrease⁹⁹.

2.5.2. Electrochemical sensors fabricated by inkjet printing

Thousands of new electrochemical sensors are reported in the scientific literature every year (Figure 2.7). However, most of these developed sensors stay where they were developed and just some of them achieve to be used outside the research lab, and less hit the market². Manufacturing is a complicated process, and the lack of reproducibility is what condemn these new developments to remain just in the literature database. The inkjet printing technology offers an alternative low-cost, easy manufacture, and with high reproducibility rate to manufacture electrochemical sensors and can be used outside the research laboratory. The last year (2020), 543 articles were published according to Scopus website (Keywords: Electrochemical AND Sensors AND inkjet-printing), this represents an increase of 2.2-fold in comparison of published in 2015. It means that a lot of effort has been put in the development of electrochemical sensor with inkjet printing technology.

The construction or fabrication of electrochemical sensors by inkjet printing is similar to other additive techniques, where layers of conductive, dielectric or semiconductive materials are patterned and deposited on the substrate. As it is discussed before, this technology has the advantage of not using masks and it is entirely digital, meaning that an alteration in the design does not suppose any additional cost (mask, calibration, etc.). Another improvement in comparison with other additive techniques such as microfabrication or screen printing is that inkjet printing just deposits the necessary material to print a pattern, and the remaining ink stays in the printhead and it can be employed in the next pattern or another job, it is almost zero waste except when it executed nozzles cleaning process. Figure 2.10 shows a representation of the fabrication of an electrochemical sensor by inkjet printing technology.

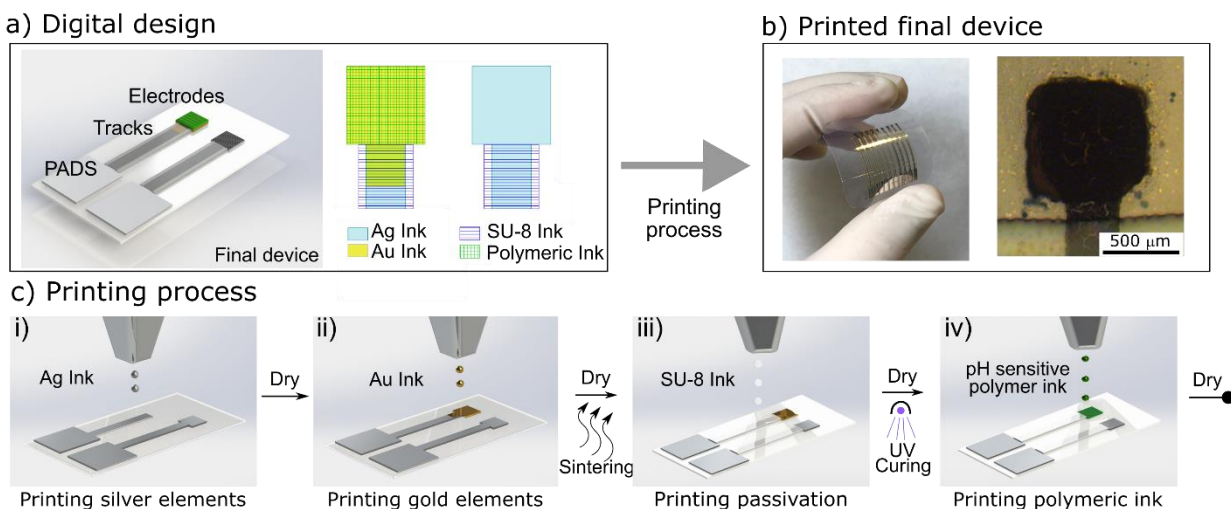


Figure 2.10. Representation of the fabrication of an electrochemical sensor by ink jet.

Representation of the fabrication of electrochemical sensors by inkjet printing (A fully printed polymer-based pH sensor is shown as an example). a) Digital design of multilayer configuration, b) photographic images of the final printed device, after the printing process c) A minimum of two inks are required to produce the transducers i) and ii), and an additional ink is often needed to improve sensor performance such as iii) passivation and/or iv) polymer ink.

Inkjet printing technology does not require the pre-fabrication of a stencil or template. Instead, the digital pattern is designed using a bitmap software and sent directly to the printer which is able to precisely deposit the ink pixel by pixel to recreate the digital design. Some examples of the versatility of the technology have been shown, where desktop/home printers were modified to be used with custom ink for development of electrochemical sensors^{100,101}. On the other hand, when better precision and control are necessary, industrial or for research printers are available on the market that allow for precise adjustment of ink droplet volume, ejection speed, and spacing¹⁰². Additionally, the high-end printers even come with post processing accessories such as heated beds to allow better control over ink dry times, UV lamps for curing photosensitive inks, and laser curing, among others. As an example, the Ceradrop CeraPrinter F-Serie Printer is a very capable inkjet printer machine that enables incredible control over the printing process, it incorporates three printheads to allow multi-material development, up to 3 post-treatment, and auto-inspection of droplets during printing¹⁰³.

Given these advantages, inkjet printing has been used by many researchers to fabricate electrochemical sensors. One of the first inkjet printed electrochemical sensor was developed by Nilsson et al.¹⁰⁴ in 2002, where they described a transducer concept based on an organic electrochemical transistor to measure air humidity. It was based on conducting polymer PEDOT:PSS and operates at low voltages, around 1 V. The device was realized on plastic foils and on ordinary coated fine paper substrates. As it is shown

in Figure 2.11a) to obtain the organic transistor the conducting polymer is patterned into the T-shaped and square-shaped geometries, defining the transistor channel (area a), drain (D) and source (S) together with the gate CE (area b) and the gate contacts (G1 and G2). As the next step the spacer is added including an opening into which the Nafion proton conductor is solution-casted. A photography of the device is shown in Figure 2.11b).

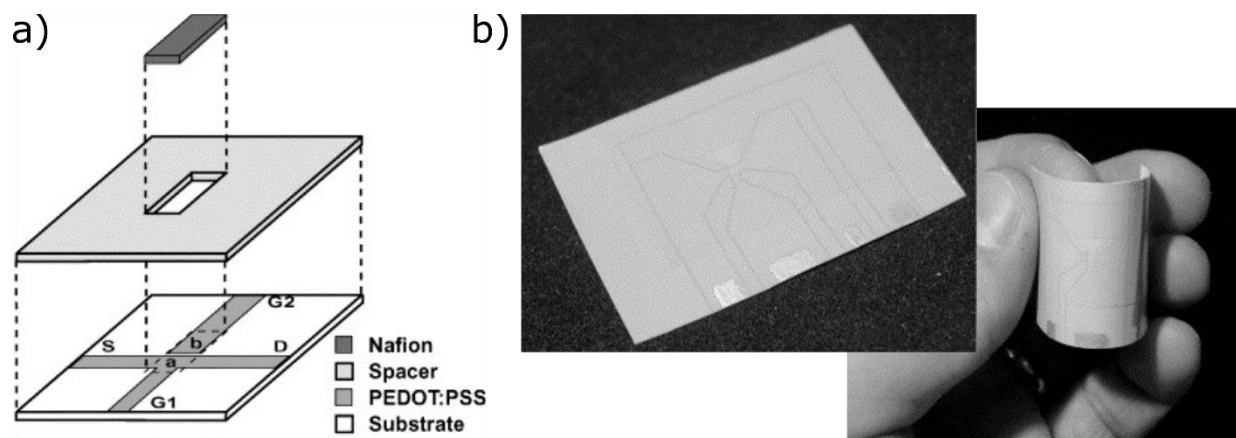


Figure 2.11. Schematic and photography of Nilsson et al. sensor.

The schematic diagram and photography of the inkjet-printed electrochemical sensor developed by Nilsson et al. a) Schematic structure of the Nafion–organic electrochemical transistor sensor, and b) Photography of the printed sensor realized on a polyethylene coated fine paper and its flexibility is show. Source ¹⁰⁴.

Another excellent demonstration of printed electrochemical sensors was presented by Lee et al. ¹⁰⁵ in the earlies 2000’s. They presented a printed humidity-sensitive membrane made of ionene oligomer. The humidity-sensitive characteristics of the sensor obtained by ink-jet printing technique were compared with the dip-coating method. Printed humidity sensor showed a decrease in impedance as the relative humidity increase and their impedance characteristics are in a close agreement with dip-coating method. These two above works have something in common, both use another technique to complement the inkjet printing technology or vice versa. Even today fully inkjet-printed electrochemical sensors are rather rare due to difficulties to print all components of the sensor. As it is discussed before, inkjet printing conductive tracks and/or transducer is well stablished, however the sensing material or even pads connection sometimes cannot be inkjet printed, and other techniques can overcome and complement this technology such as electrodeposition, drop casting, hand-painting, or gravure printing^{106–108}. Though, Da Costa et al. ¹⁰⁰ in 2015 introduces the first fully printed electrochemical sensor. They reported a sensor which consists of carbon nanotube-printed WE, RE, and CE . The carbon

nanotube electrodes showed a reasonable low sheet resistance, and they demonstrated the applicability of the sensor to measure iron (Fe^{2+}) and dopamine (DA) in concentrations as low as $10\ \mu\text{M}$. Figure 2.12a) shows Da Costa et al. electrochemical sensors. Recently (2020), Pandhi T et al.¹⁰⁹ demonstrate a consistent fabrication process to control the sheet resistance of inkjet printed graphene electrodes, thereby accomplishing repeatable electrochemical performance. The electrochemical sensor was inkjet printed on flexible polyimide film (Kapton) substrates, as shown in Figure 2.12b). They used silver ink for the electrical contacts, SU-8 for isolation of the tracks, and graphene flakes as sensing layer. Additionally, they inkjet printed a RE, and CE made of silver/silver chloride and Pt respectively, in order to obtain a three-electrode electrochemical cell. Cyclic voltammetry was used to analyze the electrochemical reversibility of a fully inkjet-printed graphene electrode and a fully inkjet-printed three-electrode device using the ferri/ferrocyanide $[\text{Fe}(\text{CN})_6]^{-3/-4}$ redox couple as the analyte. The electrodes showed quasi-reversibility with a low peak to peak potential separation and fast electron-transfer kinetics. This work enables a deeper understanding of how the combination of ink rheology and additive electronics manufacturing can enable the scalable manufacturing of flexible biosensors.

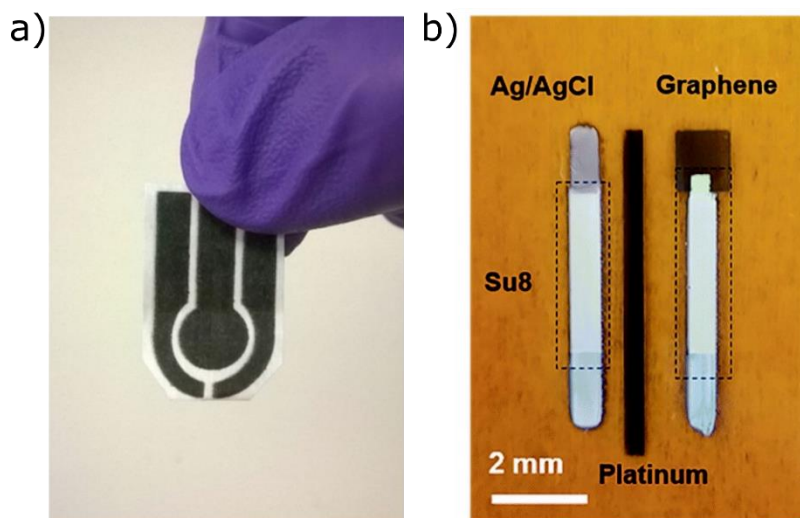


Figure 2.12. Fully inkjet printed electrochemical sensors.

Photographies of fully printed electrochemical sensor devices. a) Da Costa et al. carbon nanotube sensor, b) Pandhi et al. graphene electrochemical (Ag/AgCl as the RE platinum as the CE, and graphene as the WE). Adapted from ^{100,109}

Even several years after inkjet printing is in the focus of research a restricted limited types of inks and substrates have been used. The most common reported inks are silver, gold, carbon nanomaterials, poly(3,4 ethylene dioxythiophene)-poly(styrenesulfonate) (PEDOT:PSS), polyaniline (PANI), poly(amic

acid), and SU-8^{2,100,106,107,107,110–112,112,113,113–124}. These inks are basically divided in three groups, conducting materials mostly used for electrodes/transducer, carbon nanomaterials usually used for detection interface, and dielectric materials commonly used to isolate conductive tracks and to define the electrochemical active area of the electrodes. The list of substrates is more limited, the most reported ones are PEN, polyethylene terephthalate (PET), Kapton®, and paper^{111,113,114,122,125} due to its flexibility and low-cost attributes. However, sensor can relatively easily be printed onto other substrates such as silicon, metal, glass or 3D complex structures^{110,123,126,127}. In applications such as RFID and electric connections printing technologies are becoming the standard low-cost solution for these rigid substrates^{128,129} but for electrochemical sensors is just becoming a real viable solution.

The success of inkjet technology in sensor manufacturing strongly depends on the availability of functional materials and suitable post-processing techniques². Inkjet printing is particularly well suited for handling flexible substrates, but the substrates that are more interesting from a cost point of view are incompatible with sintering temperatures above 130 °C, which are required by most functional inks nowadays¹³⁰. This is an open discussion and for the purpose of this thesis this topic will be further treated in the next chapter.

Chapter 3 | Printable Materials for sensing

A brief overview of printable inks for the fabrication of electrochemical sensors is presented. Followed by the ink requirements for a printing process. Next, a short review of the printed pH sensor presented in the literature. And finally, two novel inkjet printed pH sensors are presented.

3.1. Printable inks

Global market has shown a growing interest in developing electronic devices according to circular economy strategies by exploiting innovative materials and printing technologies. The success of inkjet technology in sensor manufacturing strongly depends on the availability of functional materials and suitable post-processing techniques. One of the main challenges is the development of low sintering temperature metallic inks for inkjet printing technologies in order to handle a wide range of flexible substrates. The majority of these substrates have a glass-transition temperature below 130 °C¹³⁰. However, in the last years a huge effort have be done to obtain conductive polymer inks that can overcome this limitation. These inks are a current alternative to develop inkjet printed sensors. They are usually water based and showing low curing temperatures¹³¹.

To achieve the objectives of this thesis, the development of novel and/or low sintering inks is required to allow the fabrication of electrochemical sensors on flexible substrates with low glass-transition temperatures. Usually, apart from the ink raw materials, the main ink components are the solvent and additives in order to improve stability, suspension, and rheological properties of the ink. These components need to be removed through a post processing step in order to obtain the final functional layer. Generally, the post processing process is an evaporation step of the solvent and additives, but more complex processes can be required such as polymerization and sintering. Moreover, and depending on the application, ink properties, printing effects, or chemical reactions, it is important to cure almost immediately after printing the patterns. Today, the main challenge for inkjet printing technology is imposed by the restricted availability of functional materials, especially in the sensing material for the fabrication of electrochemical sensors.

During inkjet printing fabrication process, the liquid phase of a material dissolved in solvents is deposited onto the substrate with high accuracy and without any extra waste of material. Hence, it is crucial to understand the fluid dynamic properties of the materials to prepare a printable ink. It is also essential to comprehend the different aspects of droplet formation, impact as well as spreading of the ink on each substrate after ejection^{132,133}. A complete fluid dynamics study of inks will contribute to the selection of proper solvents as well as functional materials and surfactants for ink preparation. After printing on the substrate, the interaction of the ink with the substrate and the post processing affects the device performance and morphological behavior of the printed pattern⁵⁵. Such types of morphological changes

are already known such as coffee ring effect and material crackdown^{55,134}, therefore it is required to understand the mechanism of such changes as well as the methodology to overcome them during the fabrication of devices.

As already discussed in section 2.5.1, for the development of electrochemical sensors two or three electrodes are needed to obtain a common electrical transducer. For the fabrication of a WE and RE, a sensor requires at least of two conductive inks. Additionally, and in order to obtain a fully printed sensor, a third ink is required for the sensing application. This ink is usually made by a conductive material polymer, oxide, enzymes, or antibodies, among others. Furthermore, to easy connect the sensor with the measuring equipment, tracks and pads must be printed, usually by the same conductive material of electrodes but in the case of using a material with poor electrical properties for electrodes, a high conductivity ink must be used. Following the approach of fabricating a fully printed sensor, these tracks must be isolated by using an insulator ink to avoid short circuits and define electrode area to reduce crosstalk. In conclusion at least four functional inks are required in order to obtain a fully inkjet printed electrochemical sensor.

As it has been stated, a lot of effort have to be done in order to develop novel inks to increase exponentially the applications of this young technology. Currently available inks for inkjet printing consists of organic polymers, metal nanoparticles and carbon materials such as graphene and carbon nanotubes. For the effectiveness of the printing process, the fluid dynamic parameters such as viscosity and surface tension, must fulfill technology restrictions. In the next sections, three main types of ink will be discussed focusing on conductive, semiconductive and dielectric inks.

3.1.1. Conductive inks

Conductive patterns are required in almost all inkjet printed applications on various rigid or flexible substrates, such as paper or polymeric substrates^{135,136}. Many types of conducting inks have been developed by researchers with different types of active materials such as metal nanoparticles, conducting polymers, graphene, and carbon nanotubes, among others^{137–139}. However, all the active materials have their own advantages and limitations for its use in inkjet printing technology. Usually, polymeric inks shows low conductivities and poor electrical properties, however they can be used as sensing or protecting membrane with high selectivity and proper coating properties, as well as they are most of them water-based with low curing temperatures making them suitable for polymer and delicate

substrates. Leaving out of the equation the substrate restrictions, metal nanoparticles have mainly two drawbacks: the high cost and oxidation. As an example, silver ink possesses high electrical conductivity among various metals and relatively low cost with respect to gold. Even though, copper inks are cheaper than silver and possesses high electrical conductivity too, but they easily oxidize. On another hand, Ag nanoparticles are stable without forming any oxide. Gold and platinum are biocompatible and do not form oxide due to their chemical nobility but they are costly than silver that has antibacterial properties making it suitable for medical applications also¹⁴⁰. Graphene inks have many interesting properties as printable material such as good electrical conductivity, optical transparency, mechanical strength, and simple preparation method of the ink¹⁴¹⁻¹⁴³. However, graphene is currently hard to obtain in large quantities, making it difficult to use for many applications. Finally, another reported ink is carbon nanotube based ink showing unique properties due to its physical and chemical properties such as good thermal conductivity, high mechanical strength, and conductive and semiconductive properties¹⁴⁴. On the other hand, as well as graphene, the obtention of printable carbon nanotubes is complex and large production method are limited. Despite of this fact, both carbon-based inks have shown very promising applications for ink jet printing technology.

For the purpose of this thesis, this section will briefly describe different aspects of preparation or synthesis, printing, and post processing of metal nanoparticles and polymer-based inks. These two types of conductive inks were used for the development of the sensors and devices that will be presented in this thesis.

3.1.1.1 Metal nanoparticles inks

Nanoparticle-based materials possess many remarkable properties which are different from the bulk¹⁴⁵. Understanding and predicting the nanoparticle thermodynamics is a key when developing functional materials for printable inks. Owing to the change of the properties, the fabrication of nanomaterials and nanodevices with unique properties in atomic scale has become an emerging interdisciplinary field involving solid-state chemistry, biology, physics, and materials science¹⁴⁶. The most noticeable example of the change in properties is the depression of the melting point with nanometallic species in comparison with conventional bulk. This property is known as thermodynamic size effect, it reduces the melting point of nanoparticles compared to the bulk material¹⁴⁷. The property is useful to obtain highly conductive printed patterns, which facilitate the fabrication of sensor and conductive electrodes thus allowing the use of substrate with lower glass-transition temperatures.

In the earliest 1900, P Pawlow¹⁴⁸ established a relation between melting temperature and the radius of nanoparticles, however 50 years before M Takagi reported¹⁴⁹ lower melting points of Pb, Sn and Bi thin films (10 to 1000 Å). A large research has been done since then in this topic due to its high applicability¹⁵⁰⁻¹⁵³. These works concluded that a significant decrease in melting temperature is observed in isolated nanoparticles and substrate-supported nanoparticles with relatively free surfaces, in comparison with their corresponding bulk materials. Very briefly, this phenomenon occurs by physical origin where the ratio of the number of surface-to-volume atoms is enormous, and the liquid/vapor interface energy is generally lower than the average solid/vapor interface energy¹⁵². Meaning, as the particle size decreases, its surface-to-volume atom ratio increases and the melting temperature decreases as a consequence of the improved free energy at the particle surface¹⁴⁷. This physical phenomenon is one of the major attractive properties when using nanoparticle-based inks in inkjet printing.

In consequence, the researchers are working to obtain smaller nanoparticles to obtain higher conductivities without the need of high temperatures. Nevertheless, the particle itself cannot be inkjet printed directly thus a proper ink formulation is necessary to obtain a printable material. Rheological restriction for inkjet printing will be discussed in the next section, but certain parameters must have into account in order to obtain a stable nano dispersion of a metallic material for its use. As an example, the uniformity of the nanoparticles dispersion and the smaller size of nanoparticles are key due to the fact that the nozzle diameter plays a critical role in drop formation and ejection. Stabilizing agents and organic additives are used to prevent agglomeration in order to obtain an uniform dispersion¹⁵⁴, although its use affects the conductivity of the printed patterns causing a need for a post-process treatment to remove the stabilizing agent, usually by heat. These stabilizing agents need to be correctly selected because the interaction between atoms play an important role on dispersion function. A trick or treat between both define the ideal stabilizing agent. Then, the desired printed conductive pattern will consist of metallic nanoparticles after removing the stabilizing agents and organic additives. Therefore, metallic nanoparticles composition largely determines the mechanical, electrical, and morphological properties of the printed patterns.

For instance, the parameters of metallic nanoparticle inks can be categorized into metallic nanoparticles and liquid medium as show Figure 3.1. The liquid medium can be classified according to the carriers, dispersants, and additives. And, metallic nanoparticles can be further classified according to their material compositions, particle size, particle shape, and particle concentration¹³⁷.

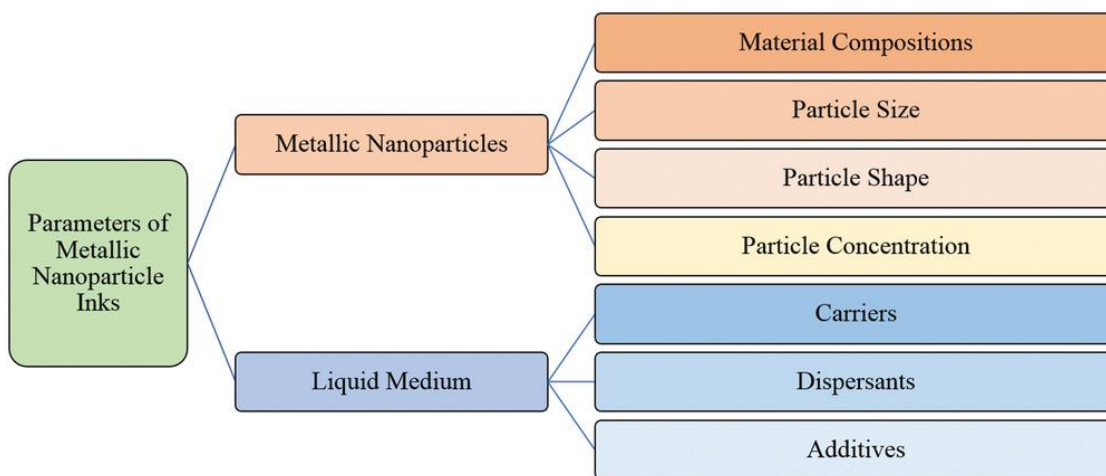


Figure 3.1. Parameters of metallic inks.
Nanoparticles metallic inks parameters. Source ¹³⁷

The selection of the metallic nanoparticle ink is not obviously, for example the first thought could be select the best conductor. However, other factors have to be consider, as has been discussed before, such as oxidation, cost, and electrical and magnetic properties.

3.1.1.2 Polymeric conductive inks

Conductive polymers offer many advantages in terms of processability, flexibility and conductivity. They attract a great deal of interest for a large range of applications. Additionally, they are easily processable in thin conductive films ¹⁵⁵. One of most reported conducting polymers is poly(3,4-ethylenedioxy)-thiophene-poly(styrene sulfonate) (PEDOT:PSS). PEDOT:PSS has been prepared by standard oxidative chemical or electrochemical polymerization methods since several years¹⁵⁶⁻¹⁵⁹. However, the processability of PEDOT:PSS is very poor because it is an insoluble polymer and the method to mitigate this drawback is by polymerizing it with water soluble polyelectrolyte¹⁶⁰. These drawbacks pushed researchers to develop and search novels conductive polymers. Additionally, some polymers also contribute with special characteristics such as ion selective property, protective membrane, and others⁹⁵.

Conducting polymers offer great prospects for practical applications especially in stretchable electronics due to their level of conductivity, low cost and ease of synthesis. Furthermore, electro-materials are highly suited for biological systems because of their structural similarity to present compounds in human body such as proteins, carbohydrates and nucleic acids ¹⁶¹. Despite polymers advantages, their application on flexible and stretchable substrates is a difficult due to the young modulus mismatch between the

polymer and the substrates¹⁶². Its poor solubility in common solvents due to their conjugated structure, induces a strong rigidity to the macromolecular backbone^{163–165} and the inter-macromolecular hydrogen bonds thus hindering the correct solvent penetration into polymeric chains and limiting the solvation¹⁶⁶.

To solve these shortcomings and obtain functional inks or solutions, a wide range of methods have been developed such as the modification of their intrinsic properties altering their molecular structure by chemical synthesis, and producing composite materials made from blending of conducting polymers particles^{167–171}.

In order to obtain a suitable conductive polymer ink for inkjet printing, the ink must fulfill printing requirements (viscosity, surface tension, particles size restriction, etc). To accomplish the technology constraints, conducting polymers must be presented in a homogeneous and stable water solution ideally. Using water as a solvent provides a cost-effective and environment-friendly media while a non-biocompatible toxic solvent is avoided. Currently, even though conducting polymers ink implementation is still challenging and each new polymer must be considered individually in terms of suspension and preparation, conducting polymers processing main issues have been solved thanks to the control provided by recent methods for nano-suspension. Nano-suspension is a submicron colloidal dispersion of dispersed particles¹⁷². A polymeric nano-suspension is defined as very finely colloid, biphasic, dispersed solid polymer particles in an aqueous vehicle, with a size below 1 μm , stabilized by surfactants and stabilizing agents prepared by suitable methods for polymeric-based applications^{173–176}. Nano-suspension have revealed their potential to solve the problem associated with the delivery of poorly water soluble and poorly water and lipid soluble polymers¹⁷⁷.

However, nowadays there is still a need to develop a simple approach for synthesizing water-soluble conducting polymers suspensions due to the drawbacks of conventional methods. Additionally, most suspensions have large size distributions and precipitate in water when the suspension is left without agitation or interaction for minutes or hours¹⁷⁸. Novel methodologies, such as enzyme-catalyzed synthesis of PANI generates good electrical and good particle stability at small size distribution performance, but it is a costly process compared with other approaches^{179,180}. Interfacial polymerization also forms a stable colloid in water media. However, the formed films obtained with this methods presents lower conductivity values¹⁸¹. The two most innovative methodologies for the development of inks are electrostatic interaction nano-suspension and emulsion polymerization^{182, 183}.

Electrostatic interaction nano-suspensions are based on the use of electrostatic forces between a monomer and a stabilizer molecule (usually a polyelectrolyte). These electrostatic forces allow the physical trapping of polymeric chains with the polyelectrolyte when the monomer starts growing. The polyelectrolyte isolates the monomer during radical polymerization and control the size distribution. The **emulsion polymerization method** main strategy is to develop a polyaniline suspension, consisting of using a surfactant (dodecylbenzenesulfonic) to obtain micelle structures in the polymerization media. Micelles allow, during the radical polymerization, anilinium cations to reside on a specific and controlled position. The polymeric nano-suspensions made by these two methods are suitable for the development of inkjet printing inks thus allowing the deposition of thin polymeric films on a variety of substrates including flexible substrates. Inkjet printing technology is one of the most promising technologies for conducting polymer depositions nowadays, allowing the fabrication of devices with new applications ¹⁸⁴.

3.1.2. Semiconductive inks

Semiconducting materials are crucial for the performances of transistor, organic light emitting diodes (OLED), solar cells, etc. Therefore, from the beginning of the 2000's researcher were focused on the design and synthesis of new materials and different types of organic semiconductors enabling flexible and low-cost manufacturing ^{185,186}. Conjugated polymers have been interesting candidates for electronic devices due to their semiconducting properties ¹⁸⁷. They can be tailored to optimize the final device properties, for instance by adding side chains to the polymer backbone for an improved electron affinity or solubility. However, semiconducting polymers shows low electrical conductivity and poor electrical and thermal stabilities, limiting their application ¹⁸⁸. Nonetheless, taking into account their structure, molecular weight, solvent, and concentration, they allow ink formulation with tuned rheological properties.

Polythiophenes are one of the most important classes of semiconducting polymers currently known ¹⁵⁶. In combination with fluorene bithiophene (F8T2) impressive progress have be done in the develop of polymer-based inks, either conductive and semiconductive ¹⁸⁶. Most polythiophenes-based inks studied in the literature exhibited non-Newtonian behavior with stable printing process, fulfilling printability conditions, furthermore, they also show fast drying behavior.

Many organic semiconductors show a robust performance response to materials in their ambient. The mechanisms for this behavior are diverse, and include doping of the semiconductor by the analyte,

swelling of the semiconductor upon absorption of the analyte, distortion of grain boundaries due to accumulation of the analyte, and various steric effects within the semiconductor upon analyte exposure¹⁸⁹. On the other hand, inks containing dispersions of semiconducting nanoparticles, can form nanocomposite materials with unique electronic properties when cured¹⁹⁰. For example, Nam et al.¹⁹¹ demonstrated that printing semiconducting metal oxide nanoparticles enhanced a photovoltaic solar cell system. Several works have demonstrated the promising results of semiconducting metal oxide nanoparticles formulated as inks^{192,193}.

In conclusion, many semiconductive inks can be synthesized and their application have been demonstrated during last decade. As it was stated above, semiconductor inks can be based on polymers and nanoparticles. Generally, the use of the semiconductive inks is destined to transistor and displays, a topic that it is far from the objective of this work.

3.1.3. Dielectrics inks

Dielectric layers are mostly used in the field of printed transistors for the development of the isolating film separating the gate electrode from the semiconductor or more generally for the fabrication of passivation layers used to protect the transistors and other circuits elements such as tracks, pads, and others from short circuits and the environment^{194,195}. Specifically in sensor development, insulator inks are used to define the active electrode area and additionally to obtain a fully printed device with a protective passivation on the connective tracks and pads. Most dielectric inks reported in the literature are based in polymer solutions. They are an ideal material due to its solubility in a wide variety of solvents, and the dielectric constant can be relative easily tuned by inserting ceramic or metallic nanoparticles into the matrix^{196–199}. In order to obtain stable and reliable isolating films, the dielectric inks are limited by the requirements of the technology and its rheology. The deposition of dielectric passivating layers is rarely done by inkjet printing.

3.2. Inks requirement for printing an electrochemical sensor

Inks have many different properties that collectively influence in the jettable process. Many of these properties depend on operating conditions and the nature of the fluid molecules. Two key properties have the most influence of printing an ink: viscosity and surface tension.

The most crucial part of inkjet printing technology is probably the ink and its physical properties, in particular the viscosity and surface tension. The viscosity should be suitably low, typically below 20 mPa.s⁴⁷ and surface tension should be intermediate lower than water's surface tension value (72.8 mN/m). The development of novel inks play an important role in the future of inkjet printing technology, reason why a huge amount of effort is put in the development of new inks. However, the design and preparation of this ink are not often very simple, as it is mentioned above inks must have physiochemical properties that allow an appropriate printing process. As the aim of this work is the development of PoC devices, special attention in the selection and development of biocompatible low sintering temperature conductive and dielectric inks is required.

- **Viscosity**

Viscosity is the fluid property that defines its resistance to shear deformation or flow²⁰⁰. The viscosity depends on the attractive force between molecules and the momentum interchange between molecules in adjacent layers of fluid as they move relative to one to another. In a liquid, molecular cohesion forces dominate the viscosity, and these cohesive forces depend on temperature. As the temperature increases, molecules in a liquid become more energetic and separated. Thus, the cohesive force decreases, and so does viscosity^{201,202}.

- **Surface tension**

The surface tensions of liquids cover a wide range of values, and most decrease slightly with increasing temperature²⁰³. The molecules of a liquid exhibit adhesion as well as cohesion. The adhesive force, attractive force between unlike molecules, enables a liquid to adhere to another body. When a liquid is placed on a substrate, the shape it takes depends on the relative strengths of these forces. If the cohesive force dominates, the liquid will tend to “bead up” on the surface. If the adhesive force dominates, the liquid will be pulled onto (wet) the substrate^{202,204}.

Printhead has a specific range of viscosity and surface tension, which enable proper jetting. As is mentioned in section 2.2 for the Dimatix printer these parameters are set in below 15 mPa.s for viscosity and between 28 and 33 mN/m for surface tension. Ink preparation is a complex process, usually it conveys a compromise of right amount of solvent, dispersant, and desired material. Such selection affect viscosity, surface tension, particle size, particle suspension, and so on. It also affects printing quality,

drop formation, clogging, jettable continuity and final application performance. These are the reasons why the implementation of inkjet printing technology will not be possible without huge research efforts in the area of printable material inks.

3.2.1. Drop deposition

The dynamics of a fluid drop impacting on a solid nonporous surface is a classical subject of interfacial hydrodynamics, which occurs in many industrial and environmental situations such as coating, rapid spray cooling of hot surfaces, quenching of aluminum alloys and steels, motor jet, rain drop, pesticides, and inkjet printing²⁰⁵. The impact of liquid drops on dry surfaces creates various flow patterns depending on the properties of the liquid and the surface. The velocity and the volume of a droplet also have a significant influence on the resulting behaviors. For common inks and conditions of inkjet with droplets diameter of tens of microns impacting with speeds of few meters per second, gravitational effects can be neglected, and splashing is not expected to happen. The drop initially spreads just after impact being this behavior controlled by inertial forces (impact driven regime). The kinetic energy of the drop is transformed into surface energy by spreading over the dry substrate. After the spreading there is a surface tension driven retraction of the extended drop followed by oscillations of the droplet in which energy is dissipated by viscous forces taking importance the capillary forces (capillary driven regime) until the deposited drop reaches the stationary shape that is dictated by surface energy forces²⁰⁶. Finally, the pattern resolution relies on the size of the ejected drop and the equilibrium contact angle of the ink on the substrate.

At the end of the impacting drop sequence, the drop remains with an equilibrium shape on the substrate, which follows Young's angle²⁰⁷. At this stage, evaporation of the drop occurs, and the drop will vanish, and a solid residual layer remains on the substrate. Drying time depends on the ambient/platen temperature and humidity, on the droplet size and on the ink solvents. The drying phase is followed by the sintering/curing process. This step is performance to make functional the printed ink. The required temperature for the sintering of the nanoparticles is determined by the size of the particles, solvent, and the encapsulant/dispersant. The processing temperature needs to be below the glass-transition temperature of the substrate materials to avoid deformation and/or melting. The sintering/curing temperature is another item that need to be also taken into the equation of the ink preparation in order to use low-cost substrates, usually with low glass-transition temperature.

Another variable of the drying process is the coffee ring effect, and it was firstly explained by Deegan et al.²⁰⁸. A coffee ring can easily be obtained when the jetted drop completely wets the surface leading to an excess of solute at the edges, as shown in Figure 3.2. This is due to higher evaporation at the outer edges of the deposited drop, causing an outward convective flow to replenish the lost solvent thus resulting in the accumulation of solute at the edges. The coffee ring effect can be reduced using several methods: e.g., changing substrate temperature, incorporation of a solvent system with a higher boiling point and a lower surface tension to suppress coffee ring²⁰⁹, and others. Due to higher evaporation at the outer edges, the solvent composition at the outer edges becomes mainly the solvent with high boiling point. As a result, the solvent at the edges has a lower surface tension than in the center, resulting in a surface tension gradient, then a surface-tension driven Marangoni flow occurs to carry the solute inward to the center (Figure 3.2 b))²¹⁰.

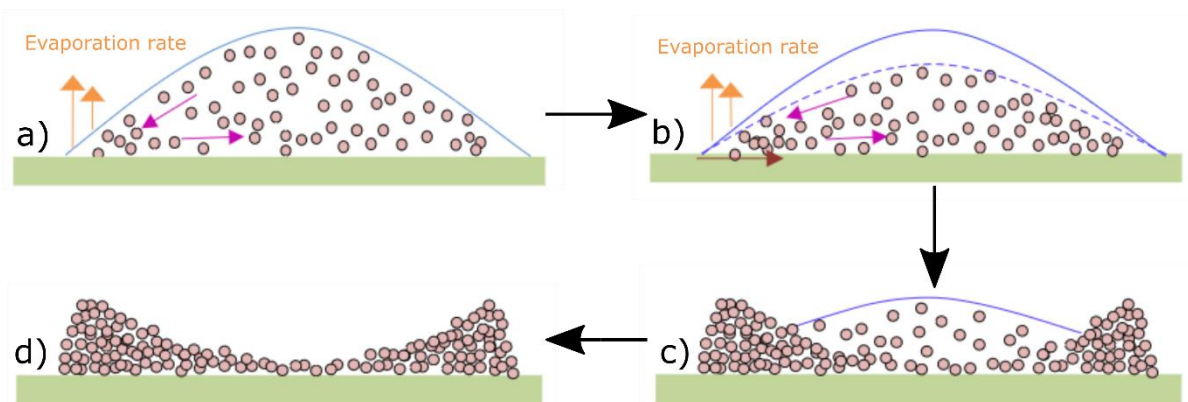


Figure 3.2. Coffee ring formation of evaporation patterns

Formation mechanism of evaporation patterns a) Higher contact angle cause low evaporation rate, b) recycling flow is constructed, c) in the later stages of evaporation, many particles remain in the dispersion, and d) coffee ring deposition. Adapted from¹³⁴.

3.2.2. Ink jettability

Appropriate functional ink materials are limited in availability. An inappropriate ink will lead to unstable ink-jetting in which long-lived filaments form, connecting the ejected droplet to the nozzle²¹¹. An microscopical ink understanding of inkjet dynamics is recently emerging, and fluid dynamics implicated in the technology have been studied²¹²⁻²¹⁷. The important physical parameters of printing fluids are viscosity and surface tension. These fluid properties influence the drop formation mechanism and subsequent drop size at a given voltage. Fromm²¹⁸ obtained an approximate solution to the Navier–Stokes equations for the case of droplet ejection²¹⁹. He used characteristic dimensionless

numbers representing fluid physical properties. The Reynolds number (N_{Re}) is the ratio of inertial to viscous forces, and the Weber number (N_{We}) is the balance between inertial and capillary forces²²⁰:

$$N_{Re} = \frac{va\rho}{\eta} \quad (3-1)$$

$$N_{We} = \frac{v^2a\rho}{\gamma} \quad (3-2)$$

Equations (3-1) and (3-2) show the calculation of N_{Re} and N_{We} respectively, where v is the average travel velocity, ρ is the density, a is the radius of printing orifice, γ is surface tension and η is viscosity. Another dimensionless number is the inverse (Z) of the Ohnesorge number (Oh), which is defined as the ratio between the Reynolds number and a square root of the Weber number, and is independent of fluid velocity (Equation (3-3)):

$$Z = \frac{(a\rho\gamma)^{1/2}}{\eta} = \frac{N_{Re}}{N_{We}^{1/2}} \quad (3-3)$$

Based on mathematical analysis using complete complex flow equations, stable drop formation in the DoD printable inks is determined by the value of Z . Fromm predicted that stable drop formation is permitted only when $Z > 2$. With lower values of Z , the viscosity does not allow drop ejection, while higher values make the uncontrollable and with a large number of satellites drops. But different experimental results give different values of Z for printable inks due to printer properties, printhead differences, applied voltage, ink reservoir pressure, and availability of cleaning cycle, among others.

However, Jang et al.²²¹ make a remarkable study of different mixtures of fluids usually used as solvent in printable inks. The physical properties and dimensionless numbers for each fluid are summarized in Table 3-1. Finally, according to Jang et al (using their printer: lab-made) the results shows that the printability range of Z is within the limit $4 \leq Z \leq 14$ and for fluids with $Z \leq 4$, the droplet filament is long and the time for droplet generation is also long. Similarly for a fluid for which the value of $Z > 14$, there is no formation of single droplets.

Table 3-1. Summary of Physical Properties and Dimensionless Numbers for Each Fluid.
 Jang et al. study of Z number for common solvents used in printable inks. Source: ²²¹

<i>Solvent</i>	ρ	η	γ	N_{Re}	N_{We}	Z
ethylene glycol (0.15) + water (0.85)	1059	3.11	54.8	51.08	8.69	17.32
ethylene glycol (0.25) + water (0.75)	1068	3.69	47.8	43.42	10.07	13.68
ethyl alcohol (0.75) + ethylene glycol (0.25)	866	4.83	28.9	26.89	13.47	7.32
ethylene glycol (0.5) + water (0.5)	1094	7.61	45.8	21.56	10.76	6.57
ethylene glycol (0.75) + water (0.25)	1106	12.3	45.6	13.49	10.91	4.08
glycerol (0.66) + Water (0.33)	1172	16.05	56.2	10.95	9.37	3.57
diethylene glycol (0.5) + water (0.5)	1111	22.0	41.4	7.58	12.08	2.17
diethylene glycol	1118	35.1	44.8	4.78	11.23	1.43

ρ : density (Kg/m^3); η is viscosity ($mPa\cdot s$); γ is surface tension (mN/m)

Following Lang study, Liu and Derby in 2019 ²²². They have studied the limiting value N_{We} and the value of Z when printing inks with the Dimatix material printer (DMP2831/2850). They found that the limiting value of is $2 < N_{We} < 25$, whereas for practical ink design they mentioned the limit of Z to be $2 < Z < 20$. The higher limit of N_{We} is the instability of tail formation during drop injection with the onset of many satellites drops, and the lower limit signifies the limit of the capillary force that should be overcome for drop formation. They conclude that the dimensionless parameters Z and N_{We} are crucial for determine the printability of a fluid with known (Newtonian) physical properties. Stating that the use of Z is justified because it does not contain a velocity term and the N_{We} is determined using the velocity of the fluid prior to drop formation.

The jetting availability of an ink suitable for use with an inkjet printer is defined by the ability to eject a well-formed single drop without the formation of satellite drops, therefore is necessary to study rheological characteristics of the inks before the printing process to avoid wasting time and supplies. Here Z and N_{We} dimensionless numbers are introduced which can help to know if an ink is viable for inkjet printing. However, it is clear that each printer has if own restriction to print an ink. A conscious study must be done to create suitable a fluid for inkjet printing technology.

3.2.3. Drop spacing (DS)

Inkjet printing main purpose is not printing isolated dots. Functional devices need continuous printed tracks or areas so individual droplets must be overlapped and the resultant features should be stable to maintain their shape and functionality. When drops of ink are deposited next to each other, each overlapping with the previously deposited one, they coalesce into a single liquid bead. A rich phenomenology is observed when varying the distance between sequentially ejected drops that is common for many other sets of inks and substrates. As shown in Figure 3.3, for large distances between drops, such that they do not interact on spreading, the individual printed appear as individual drops. As the distance between printed dots becomes smaller, drop coalescence takes place, forming a line with a rounded contour, this phenomenon is known as scalloped lines. If drop spacing (DS) is further decreased, the wavy contact lines disappear and a transition to parallel side edges is observed conforming uniform lines. If spacing decreases even more, line widening can occur however eventually a bulging instability with regions that outflow the line and other where the line remains uniform might appear, called bulging lines.

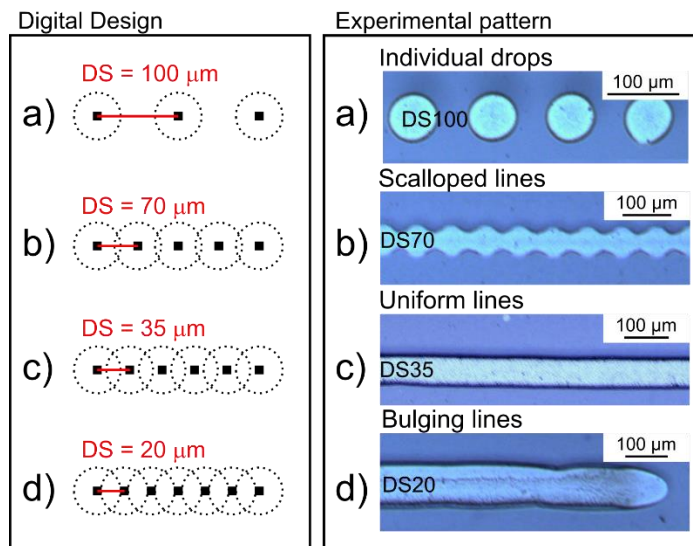


Figure 3.3. Drop spacing pattern

Droplets deposition along same axis using different DS showing different behaviors. a) Larger DS causes individual drops, b) no close enough DS causes scalloped lines, c) right DS generate uniform lines, and d) too close DS causes bulging lines.

In words, the DS is the center-to-center distance in X and Y of two consecutive drops. For the Dimatix printer the DS is adjustable between 5 and 254 μm in five-micron increments. For example, with a DS50

(DS of 50 μm), the pattern generator place drops 50 μm apart in X and 50 μm apart in Y to fill in the pattern. So, for a 100 μm x 10 mm (x,y) rectangle pattern, the system places 3 drops in the X direction (one for the first edge, another at 50 μm , and another at 100 μm for the next edge) by 2001 drops tall. The DS, therefore, determines resolution or density in the X direction and Y direction. The amount of jetted ink per area depends on the selected DS.

For the aim of this thesis each ink was first characterize using a line pattern design⁵⁵. It consists in an array of lines with different DS from a high DS (140 μm) to a small DS (5 μm). From the analysis of the line pattern can be extracted very important information for printed patterns such as resolution, DS to obtain uniform lines, drop dimensions, thickness, width, and coffee ring effect, among others.

3.3. Printed pH sensors

pH sensors are particularly important as the pH levels influence most chemical and biological reactions in materials, life and environmental sciences²²³. pH sensors have received considerable attention for monitoring human healthcare due to their versatility, possibility of real-time measurements, and quantitative results²²⁴. Possible areas of interest can be found in the continuous monitoring of blood^{225,226} and sweat^{227,228}, and the determination of the pH of tumors²²⁹ as the chemo-dynamic therapy heavily depends on acidic chemical environment pH measurements that can determine the effectiveness of this treatment. Even though the pH sensor is a broadly studied one, for all the above mentioned applications, integrated pH sensors must fulfill strict requirements that are technologically unresolved to date. The most relevant points where the technology still faces important challenges to be accomplished are²³⁰ 1) flexibility, to be adapted to body tissues; 2) the need for miniaturized pH sensors that are minimally invasive; 3) good performance such as good stability, sensitivity and response time, to allow monitoring for definite time; and 4) accuracy at neutral pH, especially interesting for physiological measurements.

Conventional glass pH electrodes are not proper for new applications such as wearables and portables devices due to the fact that glass can easily crack during user movement and their lack of bending capability²³¹. Additionally, glass electrode are considerable big in size, and due to its liquid-junction functionality they are hard to be miniaturized, and regular refill of the liquid is needed²³². Therefore, solid-state pH sensors have gained a lot of attention in the last two decades²²⁷. They offer the possibility of miniaturization, flexibility if they are fabricated on a flexible substrate, moreover they have another attractive features such as faster response, wider pH sensing range, excellent sensitivity, simple

electronics, biocompatibility, low cost of fabrication, and the possibility of integration on different substrates (polymer, plastic, textiles, paper, etc.)²²³. Generally, the electrochemical measurement of pH is done by potentiometric, conductimetric/chemi-resistors or ion sensitive field effect transistors, etc.^{92,233–240}. In respect of the pH sensors fabricated by inkjet printing reported to date, due to simplicity and the possibility of miniaturization, all those reported are electrochemical sensors based on potentiometric technique²⁴¹. For the purpose of this thesis, we will discuss just about the potentiometric pH sensor made by inkjet printing.

Potentiometric pH sensors offer stable high sensitivity, performance, low power, less interference, easiness in wireless system, long lifetime and fast response compared to other type of pH sensors²²³. Currently there is no pH sensor entirely made from inkjet technology. All pH sensors are rendered combining inkjet and screen printing technology, depositing the transducer layer electrochemically or by drop casting. Until the one presented in this thesis. However, in 2016 Qin et al.¹¹⁶ presented a work where functionalized single-wall carbon nanotubes were inkjet printed with a double purpose, both conductive and pH sensitive layer. This work supposed the basis for the development of a fully inkjet printed pH sensor, because they fabricated the tracks and isolation with a painted Ag paste and drop casted PDMS solution respectively, as it is shown in Figure 3.4. Another example is the work presented by Määttä et al.²⁴² where they printed the metal electrodes (gold and silver) and electropolymerize polyaniline film for pH sensing. The pH sensitivity of polyaniline on the printed WE was verified by comparing its performance with the sensitivity of a bare gold electrode. The sensitivity of the polyaniline-functionalized electrode was 65 mV/pH after correcting for the Cl⁻ buffer.

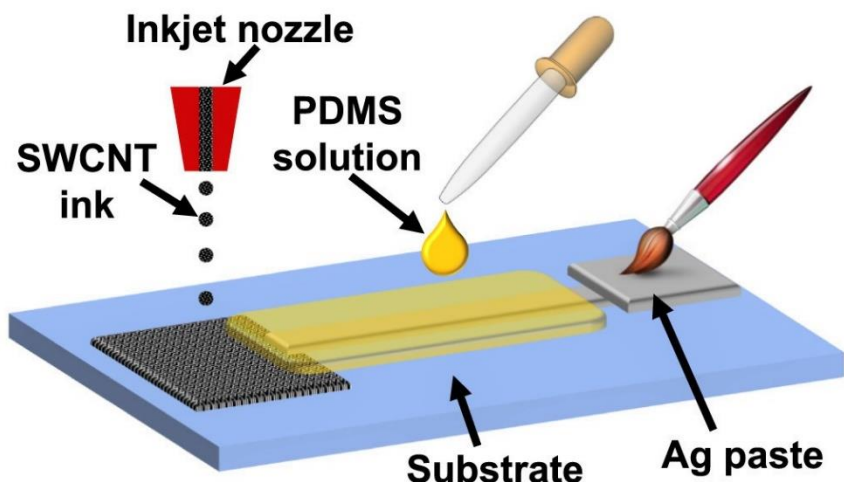


Figure 3.4. Printed pH sensing film.

Schematic of the fabrication process of a carbon nanotube-based pH sensing electrode. Source

116

Also, Qin et al.¹²³ presented an inkjet printing process for depositing palladium thin films. To demonstrate the electrochemical pH sensing application, the surfaces of the printed palladium was oxidized by oxygen in air during the thermolysis at 200 °C for ion-to-electron transduction and the underlying layer is left for electron conduction. These potentiometric sensors have sensitivities of 60.6 ± 0.1 and 57 ± 0.6 mV/pH. Additionally, Xu et al.¹¹³ developed a multiparametric inkjet printed platform on Kapton film for water quality monitoring system. Where, one of the inkjet printed sensor was used for pH sensing. The indicator electrode was made of Au ink, the reference is silver ink, and the isolation was made of Poly (amic acid) ink. The WE was functionalized by electroplated Iridium Oxide using cyclic voltammetry. The sensitivity of the printed pH sensor was measured to be 67.5 mV/pH, which was slightly lower than the 70 mV/pH achieved by non-printing methods. However, the result is still within the theoretical 60–80 mV/pH range. These results indicate that the facile and cost-effective inkjet printing and integration techniques may be applied in fabricating future electrochemical pH monitoring systems for environmental parameters and human health conditions.

3.3.1. Publication I: Enhanced performance stability of iridium oxide based pH sensors fabricated on rough inkjet-printed platinum

The first paper presented in this Chapter, **Publication I**, is a published article about the development of a novel Pt ink and its applications as pH sensor. The article is focused in the complete characterization

of the functional Pt ink that can be processed and sintered at low temperature (180 °C) in comparison with traditional methods, this novel ink was printed on to Polyethylene naphthalate (PEN) substrate. The printed Pt ink shows a high rough surface that enhance the adhesion of the Iridium Oxide, allowing pH sensing during a year. The sensitivity results were compared with evaporate Pt electrodes also coated with the same oxide.

This article has been edited from the version published in ACS Applied Materials & Interfaces (edition consist in formatting and numbering figures, references, tables, and equations in accordance with the thesis manuscript, however acronym corresponds to the article):

Miguel Zea, Ana Moya, Marco Fritsch, Eloi Ramon, Rosa Villa, and Gemma Gabriel, **Enhanced performance stability of iridium oxide based pH sensors fabricated on rough inkjet-printed platinum**. 2019, 11, 16, 15160–15169, <https://doi-org.ue.uab.cat/10.1021/acsami.9b03085>.

This work has been also presented in different conferences with their corresponding Proceedings:

- ❖ Conference **Ibersensor – TMSB2018**: M. Zea, A. Moya, M. Fritsch, E. Ramon, R. Villa, and G. Gabriel. ENHANCED PH SENSOR PERFORMANCE ON ROUGH INKJET-PRINTED PLATINUM. Oral presentation.
- ❖ Conference **SPIE2017**: A.Moya, M. Zea, E. Sowade, R. Villa, E. Ramon, R.R. Baumann, G. Gabriel. Inkjet-Printed Dissolved Oxygen and pH Sensors on Flexible Plastic Substrates. Oral presentation. Proceedings Volume 10246, Smart Sensors, Actuators, and MEMS VIII; 102460F (2017); doi: 10.1117/12.2264912.
- ❖ Conference **jPHD2017**: M. Zea, A. Moya, I. Gimenez, R. Villa, and G. Gabriel. Miniaturized multi-sensing platform for pH and Dissolved Oxygen monitoring in Organ-On-a-Chip systems. Poster presentation.
- ❖ Conference **FLEX MEMS & SENSORS2020**: Miguel Zea, Ana Moya, Eloi Ramon, Gemma Gabriel. Development of inkjet printed biosensors on flexible and porous substrates. Oral Presentation.

Enhanced performance stability of iridium oxide based pH sensors fabricated on rough inkjet-printed platinum

Miguel Zea^{†,‡,k} Ana Moya^{†,‡,k} Marco Fritsch,[§] Eloi Ramon,[†] Rosa Villa,^{†,¶} and Gemma Gabriel^{†,¶,}*

[†]Instituto de Microelectrónica de Barcelona IMB-CNM (CSIC), Campus Universitat Autònoma de Barcelona, 08193 Cerdanyola del Vallès, Barcelona, Spain

[‡]PhD in Electrical and Telecommunication Engineering, Universitat Autònoma de Barcelona (UAB)

[¶]CIBER de Bioingeniería, Biomateriales y Nanomedicina (CIBER-BBN)

[§]Fraunhofer IKTS Institute, Winterbergstrasse 28, 01277 Dresden, Germany

^kThese authors contributed equally to this work

Corresponding Author

*E-mail: gemma.gabriel@imb-cnm.csic.es

*Note: The supplementary information of this article can be found in section 6.1 (Figures and tables number with S of prefix are inserted there)

Abstract

Today, electrochemical sensors are used for a broad range of applications. A fundamental challenge is still the achievement of long-term sensor stability by ensuring a good adhesion between the deposited sensing layer and the substrate material, e.g. a metal electrode. Until now, the most applied strategy to overcome this problem is to increase the surface roughness of the metal layer by mechanical etching or by electroplating of additional material layers, which both imply an increase in manufacturing steps and thus the final cost of the overall device. Alternatively, to overcome these adhesion problems we propose the direct printing of a novel platinum nanoparticle ink, which is compatible with low-cost additive digital inkjet and with flexible low-cost substrates. This water based platinum ink has two unique features: it leads to highly rough surfaces, which promotes the adhesion of deposited sensing material and it is a highly low-temperature curing ink, compatible with polymeric substrates that cannot withstand high temperatures. Based on this concept, we report about a long-term stable and highly sensitive solid-state pH sensor functionalized by anodic electrodeposited iridium oxide on rough nanostructured platinum printed layer. The sensors showed an excellent reproducibility with a linear super-Nernstian response (71.3 ± 0.3 mV/pH unit) in a wide pH range (pH 2 to 11). Long-term stability tests for over 1 year of application demonstrate an excellent mechanical sensor layer stability, which is correlated to the distinct roughness of the printed platinum layer. This novel approach is useful to simplify the fabrication process and with that the sensor costs.

Keywords

Inkjet Printing, IrOx, platinum ink, pH sensor, adhesion, rough platinum, printed electronics.

3.3.1.1 Introduction

Inkjet Printing (IJP) is an additive manufacturing, digital and non-contact approach that allows the maskless deposition of functional materials in small drop volumes on a wide range of substrates. IJP should not be considered as a replacement for conventional silicon fabrication techniques, but in certain applications, such as environment, food safety and biomedical, low-cost disposable IJP devices are key for obtaining reliable sensors with real applicability in the future.² However, the implementation of this technology will not be possible without research efforts in the area of printable material inks and process compatible substrates.

Electrical conductive inks usually comprise colloidal suspensions of metal nanoparticles, nanowires, carbon nanotubes, organometallic compounds in solution or dispersed conductive polymers.^{50–52,243} Even if there are plenty of suitable materials available for IJP techniques, there is still a need to develop new conductive materials with low sintering temperatures suitable for the fabrication on temperature sensitive substrates like polymers or paper. Several metallic inks have been reported,^{52,244} but only a few of them are commercially available. Silver (Ag) is one of the most reported metals for conductive inks and a few gold (Au) inks can also be found. Great effort is also being made in the synthesis of nonnoble metal nanoparticle inks (e.g., Cu, Al, Ni), however they face issues in terms of oxidation stability during ink storage and printed film stability.

Platinum (Pt) is a singular noble metal and possess unique properties like chemical and oxidative stability, suitable for sensing applications. Usually, Pt layers are costly deposited by thin film technologies, but to date, no IJP Pt ink has been reported that achieves the required high conductivity at low sintering temperature. Recently Lesch²⁴⁵ reported a useful strategy to obtain catalytic layers for the use as electrodes for energy research purposes. A developed chloroplatinic acid ink was used to prepare a thin printed Pt precursor film, which was finally exposed to a short pulse light from an Xe flash lamp, to be converted into a Pt nanoparticle film. Additionally, Özkan *et al.*²⁴⁶ reported the deposition by IJP of a chloroplatinic acid hydrate solution, which is also a Pt precursor solution, for use as a counter electrode (CE) for dye-sensitized solar cells. In this case, the Pt layers were sintered at 385 °C to complete the thermal decomposition of the layer and to obtain a good catalytic activity. Chatziiona *et al.*²⁴⁷ published the printing of a catalyst solution of 0.1 wt.-% Pt/Al₂O₃, which possess an excellent activity on the selective reduction of NO by H₂.

Following these studies, in this work, we report about a novel nanoparticle IJP Pt ink, which gets electrically conductive at low-temperatures starting from 180 °C. As far as we know, this is the lowest curing temperature ever reported for a Pt ink, and it paves the way to develop sensing devices based printing of functionalized Pt films on a broad variety of low-cost substrates such as plastic or paper. The Pt ink properties were achieved by controlling the particle synthesis as well as the type of chemical surfactant layer on the particle surface during ink preparation. During heating of the printed film, the organic dispersant decomposes and leaves the particles surface. The particle packing density increases along with direct particle-particle contacts, which leads to an overall film conductivity. The IJP process for this Pt ink was optimized to obtain low-resistive layers with good adhesion on plastic substrates. The

applicability is demonstrated by a potentiometric solid-state pH sensor, where we modified the printed Pt layer with electrodeposited iridium oxide (IrOx) as pH sensing material.²⁴⁸

pH sensors are of interest for a wide range of applications and numerous strategies can be found in the literature for their fabrication. Metal oxide based pH sensors have commonly been used, where especially IrOx shows the most promising approach to achieve good sensor stability over a broad pH range, a fast response along with an excellent biocompatibility.²⁴⁹ There are several procedures published that allow the preparation of hydrated or anhydrous iridium oxide films (IROF) and their pH response depends strongly on the degree of film hydration.²⁵⁰ Surprisingly all the procedures related with the preparation of anhydrous IrOx are not compatible with the use of plastic substrates, due to the high temperature processing.^{251–253} The most effective way to obtain hydrated IROF is via the electrodeposition of iridium salts in aqueous solutions, resulting in an electrodeposited IrOx (EIROF).^{254–256} These are amorphous thin films that show a super-Nernstian behavior, that depends on the oxidation of the IROF.²⁵⁷ Although these sensors have been fully characterized in terms of sensitivity, response time and reproducibility, only a few results are concerning sensor stability in terms of sensitivity over extended periods and mechanical stability of IrOx film. Here we present a sensor concept, which is stable for more than one year. This was achieved by an excellent adhesion of the deposited IrOx layer on a printed Pt electrode, which shows an inherent high surface roughness. We demonstrate one of the most stable, reproducible and sensitive pH sensors based on IrOx reported till today, which can be manufactured by digital additive IJP based on a novel Pt nanoparticle ink.

3.3.1.2 Experimental

3.3.1.2.1 Materials and chemicals

A commercially available Ag nanoparticle ink (DGP-40LT-15C from ANP, Korea) and a dielectric photoresist SU-8 ink (SU-8 2002 from MicroChem, USA) were used for the fabrication of the microelectrodes. For the synthesis of Pt ink, Pt powder (Pt 100-03, Heraeus), hydrochloric acid (HCl), nitric acid (HNO₃, 99.9 %), hydrazine monohydrate (N₂H₄·H₂O, 65.0 %) and ethylene glycol per analysis (all reagents from Sigma-Aldrich) were used. Phosphate-buffered saline (PBS, pH 7.4) was used for characterization of the printed electrodes. Hydrochloric acid (HCl, 0.1 M) was used for the chlorination of the printed Ag electrode, and potassium chloride (KCl, 0.1 M) for testing the pseudo-reference electrode (pRE). Iridium trichloride trihydrate (IrCl₃·3H₂O, 99.9 %), oxalic acid (H₂C₂O₄·H₂O, 99 %) and potassium carbonate (K₂CO₃, 99 %) were used for the development of IrOx based pH sensor (all

reagents from Sigma-Aldrich). Commercial buffer solutions of pH 2 to 11 (Panreac), and also HCl and sodium hydroxide (NaOH) were used for the pH calibration and the study of response time.

3.3.1.2.2 Pt ink synthesis

The Pt ink was prepared by chemical precipitation of Pt nanoparticles followed by the formulation of the inkjet ink. Pt powder was solved in nitrohydrochloric acid to form H_2PtCl_6 as a precursor dissolved in deionized water. By adding $N_2H_4 \cdot H_2O$ Pt nanoparticles precipitate in the presence of a dispersant (copolymer with pigment affine groups). A particle fraction with a size below 200 nm was separated by centrifugation (Heraeus Multifuge X3FR from Thermofisher Scientific) and re-dispersed in a water/ethylene glycol mixture (2:1 vol.-%) to form a 20 wt.-% Pt ink.

3.3.1.2.3 Characterization of the Pt ink

The Pt solid content of the ink was characterized by measurement of the ink weight loss after heating an ink quantity of 100 mg with a Bunsen burner in a small alumina crucible. This heat treatment burns off the solvent and organic ink components, leaving behind pure Pt in the crucible. The ink density was measured by weighting a predefined ink volume of 1 mL with a micropipette. For these measurements, a special accuracy-weighing machine was used (Sartorius LA230S). The surface tension was measured by a drop shape analyzer (Krüss, DSA100), using the Young-Laplace method by characterization the outline of 5 individual ink droplets of 7 μ l at 20 °C. The ink viscosity was measured in a rheometer (Haake Rheo Stress RS 150) with cone and plate geometry at 10/sec and 100/sec, with 100 measurement points within 15 min respectively, at 22 °C. The Pt ink showed a Newtonian fluid behavior, where the viscosity is independent on the shearing rate. The particle size distribution and sedimentation of the Pt ink was characterized by an analytical centrifuge (LUMiSizer®, LUM GmbH) that instantaneously measures the extinction (space- and time-resolved) of the transmitted light across the entire length of an ink filled cuvette with 400 μ l. For characterization of the particle size, the ink was diluted by 1:499 wt.-% with ink solvent (water/ethylene glycol (2:1 vol.-%)) and measured two times at 7 °C. The ink sedimentation was characterized based on the original Pt ink with solid concentration of 20 wt.-%. The calculation of the sedimentation rate is based on the measurement of the time depended change of the ink interphase (sedimentation of particles) at 4000 rpm (2325 g, enforced sedimentation) for 50 min (threshold value of 10 % transmission). Due to a linear dependence between sedimentation rate and

rotation speed (g number), described by Stokes' s law, a re-calculation of the sedimentation speed to 1 g was done in normal storing conditions.

3.3.1.2.4 Fabrication of solid-state pH sensor

The pH sensor structure was fabricated using IJP technology with a drop-on-demand Dimatix Material Printer (DMP 2831 Fujifilm Dimatix, Inc., USA). The printer operates with 10 pL nominal drop volume piezoelectric printheads, which have 16 individually addressable nozzles, each with a diameter of 21.5 μm . Printing patterns were designed using CleWin 5 software, which were imported with the Dimatix Bitmap editor. The printing process was carried out in a standard laboratory environment at ambient conditions, without non-particle filtered enclosure systems and without precise control of temperature or humidity. Microelectrodes were printed on a 125 μm thick planar polyethylene naphthalate substrate (PEN, Teonex®Q65HA DuPont Teijin Films). The printer has a vacuum temperature controllable plate, where the substrate is placed, and the temperature was set to 40 °C in order to obtain uniform printing pattern. The waveform was generated and optimized for each ink to achieve a stable droplet ejection. The whole fabrication of the pH sensor can be understood as two steps: the printing processes of the two microelectrodes and the post-treatments of these electrodes to turn them functional. In the first step (Figure 3.5a) a series of successive printing processes of the materials are performed, to obtain the necessary elements for the electrochemical sensor. The Pt ink was first printed (a.i) to obtain a 300 x 300 μm^2 (a geometric surface area (GSA) of 0.09 mm^2) wide indicator electrode (IE). To evaluate a suitable drop spacing (DS) for printing, systematic test patterns with a variation of DS from 5 to 140 μm were prepared and analyzed (see discussion section 3.2). Finally, the Pt ink was printed with a resolution of 847 dpi (dots per inch), which means a DS of 30 μm . As the printed ink films contain different solvents, the substrate was put on a hot-plate at 80 °C for 15 min for drying. Then, Ag elements were printed (a.ii): the pRE of 600 x 600 μm^2 , connections and pads. The DS selected for the Ag ink was 40 μm (635 dpi), as it was optimized in²⁰. The same drying treatment, as for Pt ink, was applied for the printed Ag films. Pt and Ag films were finally sintered (a.iii) on a hot-plate at 180 °C for 30 min, which leads to sufficient electrical conductivity. Afterwards, in order to isolate tracks and define the active electrode area and connection pads, the dielectric SU-8 ink was printed (a.iv) over the Ag tracks with a DS of 15 μm (1693 dpi). The curing (a.v) was done in two steps as described in⁵⁵. First a soft bake on hot plate at 100 °C for 5 min followed by an UV treatment for 15 sec to polymerize this layer by polymer

cross-linking. The final cost of materials (PET substrate and inks) for a single IJP sensor is estimated around 0.072 € as calculated in Table S1.

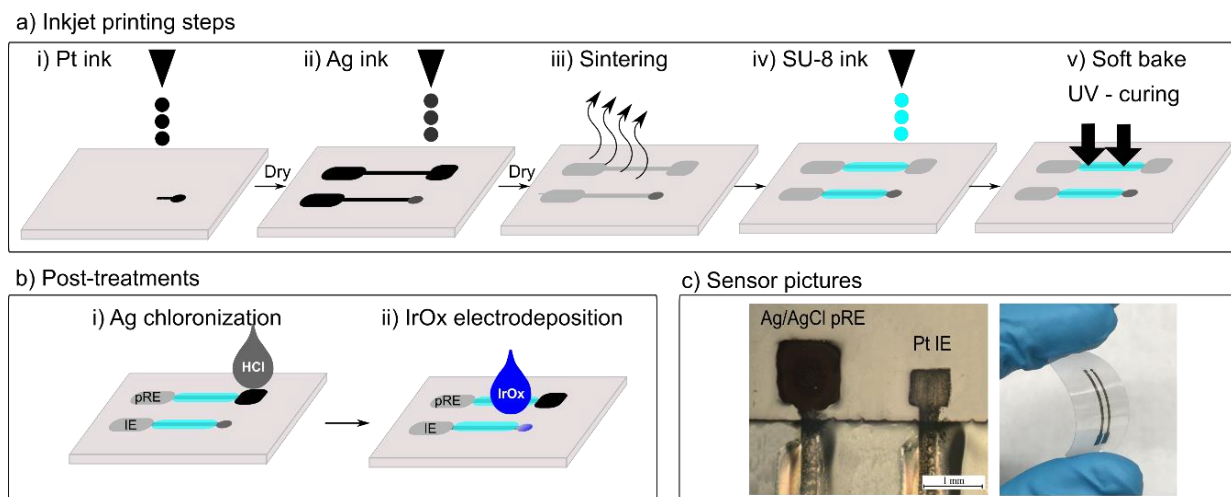


Figure 3.5. Inkjet Pt electrode fabrication process.

Illustration of the overall pH sensor fabrication process. a) IJP of the Pt IE (i), IJP of the Ag pRE, connections and pads (ii), sintering of Pt and Ag patterns (iii), IJP of the passivation layer SU-8 (iv), soft bake and UV curing of SU-8 (v). b) Post-treatments: chlorination of the RE (i), IrOx electrodeposition of the IE (ii). c) Left, microscope image that shows in detail the Ag/AgCl pRE (left) and the Pt IE (right); Right, picture of the final pH sensor illustrating sensor flexibility.

A second step (Figure 3.5b) involves the required post-treatments to make the electrodes functional for the pH sensing. The chlorination of the printed Ag electrode (b.i) was achieved by a cyclic voltammetry (CV) in HCl (0.1 M) (detailed in Figure S1a), from 0 V to 0.2 V at 20 mV/s,²⁵⁸ and allowed to obtain a stable Ag/AgCl pRE (detailed in Figure S1b). The electrodeposition of the IrOx on the Pt electrode (b.ii) was done in a solution made from 0.2 mM of $\text{IrCl}_3 \cdot 3\text{H}_2\text{O}$, 1 mM of $\text{H}_2\text{C}_2\text{O}_4 \cdot 2\text{H}_2\text{O}$ and 5 mM of K_2CO_3 dissolved in a total amount of 50 mL deionized water. These materials were mixed step by step, with stirring for half an hour between. The final solution was aged four days at 37 °C.^{259,260} EIROF were obtained by a dynamic potential sweep method consisting of 50 potential sweeps between 0 V and 0.65 V at scan rate of 10 mV/s,^{261,262} (detailed in Figure S2a). Figure 1c shows two images of the printed sensor on the flexible PEN substrate.

3.3.1.2.5 Morphological and electrical characterization

The printed layers were analyzed using an atomic force microscope (AFM, Nanoscope IV controller and Dimension 3100 head from Veeco), an optical microscope (DM4000M LEICA, Germany), a

profilometer (KLA Tencor P-15, USA) and a scanning electron microscopy (SEM, Auriga40 from Carl Zeiss, Germany). The electrical conductivity was evaluated using a semiconductor parameter analyzer (HP4155 Hewlett Packard, USA) connected to a manual probe station (Karl Suss PA200, Germany). Sample cross-sections were prepared by Focused Ion Beam (FIB, Zeiss 1560XB Cross Beam, Germany).

3.3.1.2.6 Electrochemical characterization

The electrochemical characterization of the printed electrodes was done by CV and electrochemical impedance spectroscopy (EIS). CVs were recorded with an 8-channel potentiostat (CHI1030A CH Instruments, USA). A standard three-electrode cell arrangement was used with printed Pt microelectrodes as IE, a commercial Pt electrode (Radiometer Analytical, France) as CE and Ag/AgCl (3 M KCl) (Metrohm, Germany) electrode as RE. EIS measurements were conducted in PBS (15.5 mS/cm) in the range of 10 Hz to 1 MHz, against a commercial Pt plate electrode, by using SI1287 Electrochemical Interface and SI1260 Impedance/Gain-Phase Analyser (Solartron, United Kingdom).

3.3.1.2.7 pH measurements

The open-circuit potential (OCP) of the inkjet-printed electrodes was measured by a μ AutolabIII/FRA2 (Metrohm, Germany). Measurements were carried out in various commercial pH buffer solutions ranging from pH 2 to 11. The pH change was induced by switching the sensor from one pH buffer solution to another. The response time was studied in KCl (0.1 M) buffer solution and the pH was modified by addition of NaOH (1 M) or HCl (1 M), while it was magnetically stirred. Also pH value was recorded in parallel using a commercial pH-meter (GLP22, Crison).

3.3.1.3 Results and discussion

3.3.1.3.1 Conductive Pt ink formulation and properties

Due to the wide range of printed electronics and sensor applications that can be potentially developed on low-cost polymer substrates, there is great demand for materials and inks with very low curing temperatures below 200 °C. The Pt ink developed in this study was based on our experiences with Ag and Au inks,²⁶³ which showed that the organic surfactant layer around the metal particles dominates the sintering temperature. By varying the length of the hydrocarbon backbone or the functional group of the surfactant in the synthesis, it is possible to influence the curing temperature of the Pt ink. Thereby, the chemical composition of the dispersant strongly influences not only the nanoparticle stabilization,

but also the thermal dispersant stability.²⁶³ After a systematic investigation and screening of various dispersants, we found that copolymers with pigment affine groups showed the best trade-off between particle stabilization and low-temperature stability (debinding of dispersant). During curing, the dispersant leaves the Pt particle surface and the printed ink layer shrinks, which increases the particle packing density and leads to several particle-particle contacts, resulting in an increase of electronic film conductivity.

Beside the need for low-temperature sintering, water based inks are advantageous in terms of ink handling and are more environmental friendly (e.g. cleaning, disposal of waste) and for these reasons we developed a water based particle and ink synthesis. To avoid a fast drying of the ink on the inkjet nozzle plate, especially when heat radiation due to substrate heating by small distance between substrate and printhead occurs, we used a mixture of water with ethylene glycol, which has a lower vapor pressure. Furthermore, we observed a significant lower coffee-ring effect during wet film drying by using a solvent mixture of water/ethylene glycol with 2:1 vol.-%. Table 3-2 summarizes the main Pt ink properties (data shown in Figure S3). Surface tension, viscosity and particle size values meet the general requirements for the compatibility with piezo inkjet printheads, such as the Dimatix DMP-printer (e.g. 28-42 mNm, 8-14 mPas, filtration < 0.2 μm).

Table 3-2. Pt ink main properties

Property	Value
Pt solid content	20.5 wt.-%
Ink density	1.23 g/cm ³
Surface tension	34 \pm 0.5 mNm @ 20 °C
Viscosity	14.8 \pm 0.4 mPas @ 10/sec and 22 °C
	14.1 \pm 0.2 mPas @ 100/sec and 22 °C
Pt particle sizes	d ₁₀ =30 nm, d ₅₀ =47 nm, d ₉₀ =81 nm
Sedimentation rate	0.007 mm/day

The main particle sizes are distributed in the range of 25 nm to approximately 100 nm with a very small tail of particles above 100 nm to 250 nm being visible. Overall, the results of particle size correlate well with the centrifugation step during ink synthesis, which was set to cut off all particles above 200 nm. This procedure ensures a stable ink jetting process and avoids nozzle clogging due to large particles in the ink. Figure S3e shows a SEM image of the Pt ink after drying on a sample holder at 80 °C for 10 min. The visible size of the particles correlates well with the measured particle size distribution. The Pt particle precipitation generated rounded particles in a narrow size distribution. One of the biggest issues

for particle based inks is their stability against particle sedimentation, which usually limits the ink shelf life. The sedimentation speed of the developed Pt ink was characterized to be 0.007 mm/day. This value is very low, meaning that in an ink batch the biggest particles sediment only 2.5 mm per year. From our experience, this type of Pt ink stored in laboratory conditions, protected from light and at room temperature have a shelf life of more than 1 year, which is comparable or even superior to other commercial inkjet inks.

3.3.1.3.2 Printing process of Pt ink

To create the fluid flow for ejecting, several printing parameters need to be optimized depending on the IJP mode. The optimum waveform and parameters, which were found for the reliable printing of the developed Pt ink with stable droplet ejection and avoiding of satellite droplets, are shown in Figure S4. The ink-substrate interaction affects the spreading of the ink on the substrate surface (wettability). Additionally, the selection of the DS and the platen temperature influences the quality of the printed pattern on a specific substrate. The DS is the drop-to-drop distance in X and Y axis of two consecutive drops, which determines the resolution and density in both directions. Also, platen temperature plays an important role in inkjet processes because it is directly related to the coffee-ring effect, resistance (conductive ink), line formation and pattern definition.²⁶⁴ In order to evaluate an optimum DS to achieve a continuous and homogeneous printed line, a line pattern test with systematic variation of the DS from 5 μm to 140 μm described in⁵⁵ was used.

The printed lines (Figure 3.6a) were analyzed to characterize their thickness and width. As can be observed, for DS 80 μm or higher the pattern resulted in isolated drops, which did not merge to form continuous lines. When droplets are inkjet-printed closer to each other, continuous lines are formed upon drop coalescence; however, different behaviors were observed. When the chosen DS was too small (less than 30 μm) bulging effects appeared due to an excess of deposited material, whereas a DS between 60 and 70 μm resulted in scalloped, but continuous lines. Only when the DS is optimized, homogeneous and continuous lines are obtained: for the Pt ink studied, the optimal DS is between 20 and 40 μm . The complete information of the printed lines patterns is shown in Figure S5. Despite the DS, the substrate temperature (controlled by the platen temperature) has significant influence on the film quality. Figure 3.6b shows that with increasing temperature, which means a rapid ink solvent evaporation, the line width can be decreased at a given DS. However, for all DS tests a distinct coffee-ring effect was observed. This effect was studied using a profilometer for characterization of the thickness homogeneity after film

drying. As shown in Figure 3.6c, the Pt ink exhibits a coffee-ring effect for continuous lines under all tested conditions as well as for single printed droplets. This may be attributed to a limited substrate wetting (rather high contact angle) and a rather fast evaporation of Pt ink solvent, which hinders a complete levelling of the inks. A platen temperature of 40 °C was finally chosen, as a compromise to get the most homogeneous lines, narrow line width along a limited coffee-ring effect. With a platen temperature of 40 °C and a DS of 30 μm , the printed lines with an $85 \pm 1.17 \mu\text{m}$ width and $0.075 \pm 0.03 \mu\text{m}$ height were prepared.

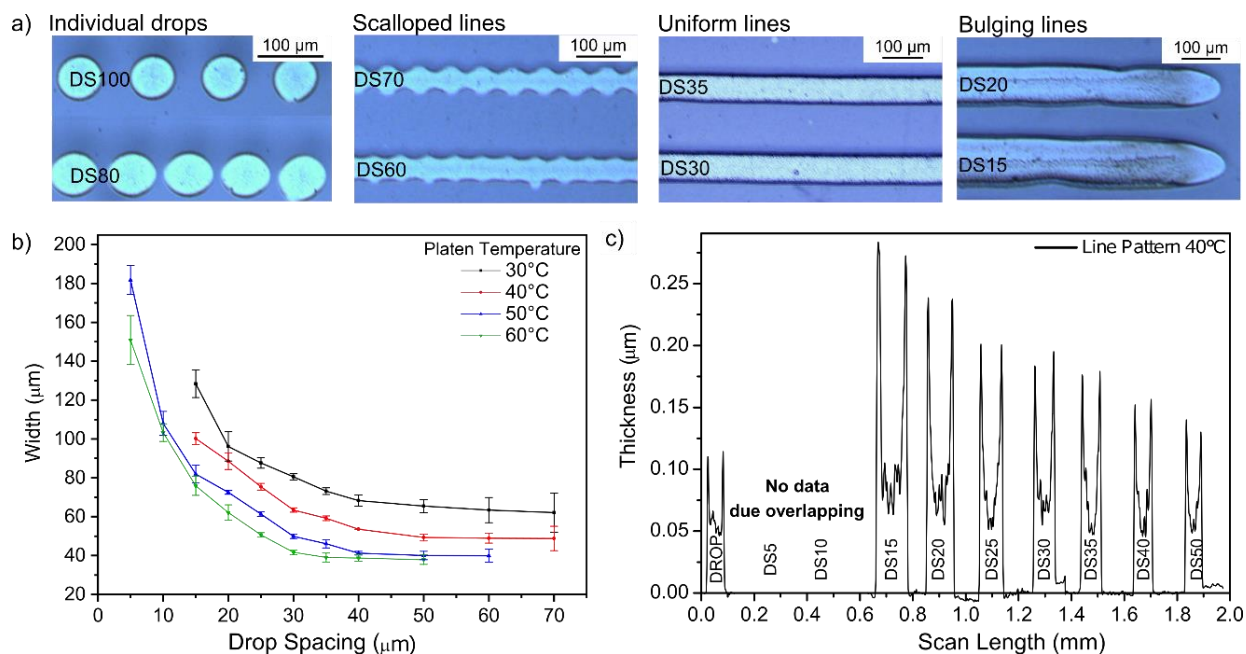


Figure 3.6. Printing characterization of Pt ink.

a) Morphologies of IJP line pattern for Pt ink at different DS: individual droplets, scalloped, homogeneous and bulging lines. b) Dependence of the Pt line width on the DS at several platen temperatures on PEN film. The error bars are the standard deviation of six different width measurements along the lines of the line pattern test. c) Characterization of the printed Pt film thickness in relation to DS at platen temperature of 40 °C.

3.3.1.3.3 Electrical resistivity and morphological characterization of printed Pt thin films

For using IJP technology the optimum printing conditions must be evaluated for each ink material and substrate type individually. Especially a low electrical resistance of printed electrodes is a necessary requirement for any electrochemical sensor. Van der Pauw structures were used to study the electrical behavior of the printed and sintered Pt ink films.²⁶⁵ These structures were dried at 80 °C for 15 min followed by a sintering with variation of temperature and time. Taking into account that the PEN

substrate has a polymer glass transition temperature of 200 °C, above that substrate warpage is likely, the selected sintering temperatures were set to 150, 180 and 200 °C for 15, 30 and 60 min. Figure 3.7a shows the measured sheet resistance versus several sintering temperatures and times for the Pt ink films. Starting at 150 °C and at 15 min, the Pt ink exhibited reasonably low resistance ($9.0 \pm 1.0 \Omega \cdot \text{sq}^{-1}$). Increasing the temperature to 180 °C, the sheet resistance decreased considerably to around $6.7 \pm 0.3 \Omega \cdot \text{sq}^{-1}$. A sintering at 200 °C leads to a further reduction in film resistance, the difference to 180 °C was about $\sim 10 \%$, and prolonged sintering times lead also to lower resistance values. Time increased up to 30 min the corresponding sheet resistance decreased by 17.5 %, 5.7 % and 2.2 % for 150, 180 and 200 °C respectively; and a further increase of the sintering time to 60 min, led to a further decrease in sheet resistance of 1.2 %, 0.5 % and 3.4 % for each sintering temperature respectively. The lowest sheet resistance of $5.6 \pm 0.1 \Omega \cdot \text{sq}^{-1}$ was reached with 200 °C and 60 min holding time.

However, taking into account that at 200 °C for prolonged holding times the PEN substrate begins to warp and deform, the small improvement of film conductivity is not relevant. Although low-temperatures achieve good sheet resistances, all results exhibit higher deviation at 150 °C than at 180 °C, demonstrating that reproducibility is improved by increasing the sintering temperature. Therefore, the selected sintering temperature for the sensor fabrication was set to 180 °C for 30 min, resulting in a sheet resistance of $6.3 \pm 0.3 \Omega \cdot \text{sq}^{-1}$, which equals to a film conductivity of $1.58 \cdot 10^6 \text{ S/m}$ (16 % of bulk Pt). However, it must be pointed out that the final election of a sheet resistance threshold depends on the required application and the final sintering parameters must be chosen looking for a good device performance.

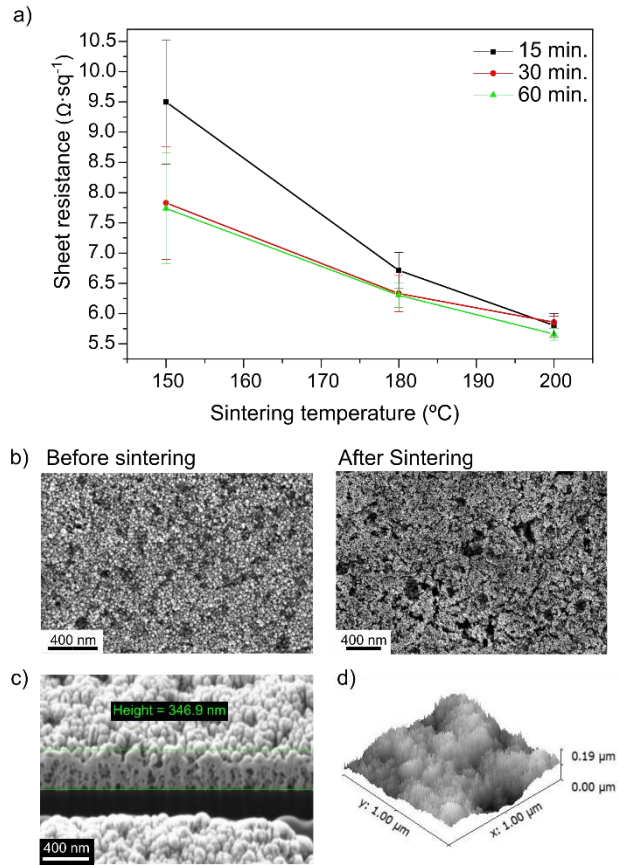


Figure 3.7. Electrical characterization Pt ink.

a) Sheet resistance measured by printed Van der Pauw structures with variation in sintering parameters of time and temperature. The error bars correspond to the standard deviation on the average values obtained by performing 3 independent measurements. b) Surface SEM images of IJP Pt film before and after sintering. c) A cross-section image of the sintered Pt film. d) AFM image of the sintered Pt film.

To study the underlying sintering process, topography and cross-section morphology of the sintered films were imaged with AFM and SEM techniques. Figure 3.7b shows SEM images of the inkjet-printed Pt ink before and after the sintering process. The removal of organic surfactants from the surface of the nanoparticles plays a significant role in enhancing the conductivity of the printed films. These images show that after the sintering process, the particles were agglomerated and structurally very porous; however, changes in particle morphology before and after the sintering process were hard to observe from top view. For a detailed study of the morphological microstructure, a cross-section of the sintered Pt layer prepared by FIB cut, was analyzed in SEM (Figure 3.7c). The film cross-section shows that after the sintering step still a porous morphology exists, but that the initial individual nanoparticles were successfully transformed into larger clusters and hence to a continuous network of Pt particles. From

these results we do not see a distinct Pt particle sintering, like particle-particle neck building as known from typical metal powder sintering. However, the final Pt microstructure with particle contacts and its increased particle density after sintering are the main parameter that influences the film resistivity. The thickness of one layer of Pt ink was determined to approximately 350 nm. The film surface was also studied by AFM technique as shown in Figure 3.7d. The image reveals an overall rough surface with larger hills and valleys superimposed on a smaller close packed particle landscape. The root-mean-square (RMS) roughness of the Pt surface was determined to about 25 nm, confirming a rough nanostructured electrode surface suitable for further fabrication of electrochemical sensors. In fact, this roughness value of sintered Pt ink is still higher than other previously published values for Ag ink (9.3 nm) and Au ink (16.4 nm).⁵⁵

3.3.1.3.4 Electrochemical characterization of printed Pt and EIROF microelectrodes

CVs obtained in PBS of printed Pt microelectrodes and EIROF over these microelectrodes are compared in Figure 4a. In this study, we have included the results of our previous reported smooth Pt²⁶⁶ microelectrode as a reference, which has an identically sized geometry (300 x 300 μm^2) prepared by evaporation. The same EIROF coating was deposited on this evaporated Pt microelectrode for comparison purposes and to illustrate the advantage of the printed Pt ink in this study.

The voltammograms for the evaporated and the printed Pt film (Figure 4a, continuous lines) show approximate rectangular shapes, which is expected for electrodes exhibiting only double-layer capacitance, suggesting a capacitive behavior. The significantly higher charge storage capacity (CSC_c), calculated from the time integral of the cathodic current over a potential sweep, obtained with printed Pt electrode rather than the evaporated one is reflected in the CV. The evaporated Pt microelectrodes show a far lower surface roughness of RMS = 5.0 nm,²⁶⁶ and can be considered to be almost completely smooth. Figure 4b shows direct comparison of both Pt electrodes, whereas the evaporated Pt surface is bright, the printed Pt is completely dark. Although the evaporated Pt is thinner than the printed Pt (200 nm thick vs. 350 nm of the printed Pt), the significantly higher load capacitance of the printed Pt electrodes can be explained by the high porosity and roughness morphology as discussed in the previous section.

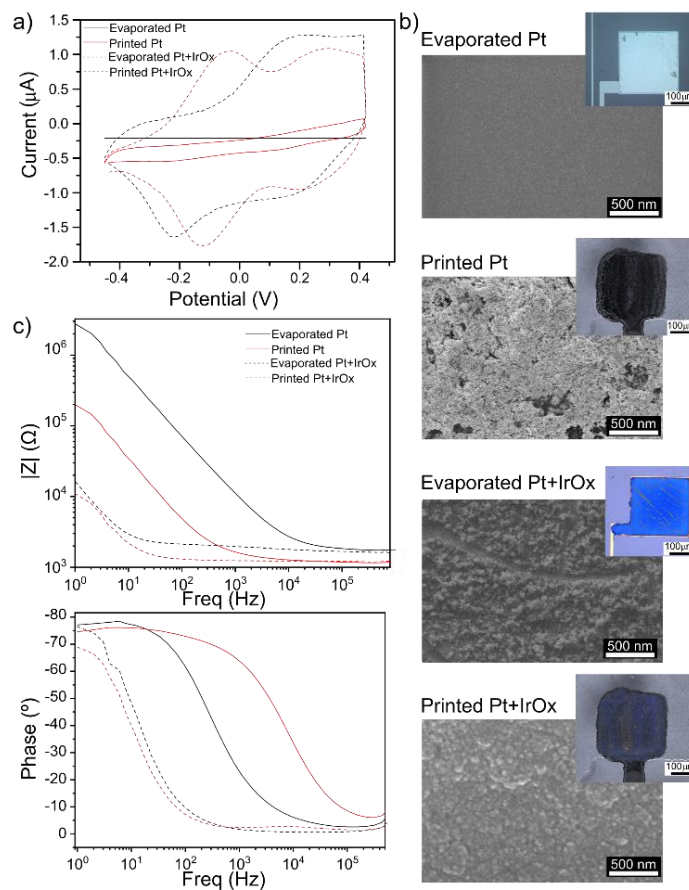


Figure 3.8. Electrochemical characterization Pt patterns.

a) Comparison of CVs recorded of smooth evaporated Pt, printed Pt ink and EIROF over both Pt microelectrodes (GSA of 0.09 mm²) in PBS and scan rate of 20 mV/s. b) Microscope and SEM images of evaporated and printed Pt microelectrode surfaces and their corresponding ones modified with EIROF. c) EIS measurements of evaporated and printed Pt and their corresponding EIROF coatings. CV and impedance data are representative of 6 samples in each group.

The measured CVs of EIROF microelectrodes, obtained by electrodeposition on both Pt electrode types (Figure 3.8a, dashed lines), correspond well to typical hydrated EIROF that exhibit distinct peaks associated with the oxidation and reduction of IrOx (Ir(III)/Ir(IV)),^{267,268} independent from the underlying Pt type. Although the EIROF is only ≈ 150 nm thick (determined from SEM image in Figure S2b), it has more than 31 and 5.5 times the available charge for the same evaporated and printed Pt microelectrodes. The CSC_c of the electrodes in Figure 3.8a are 1.44, 8.52, 45.7 and 46.6 mC/cm² for evaporated and printed Pt, and EIROF coating for evaporated and printed Pt, respectively. These values are in good agreement with previously reported results.^{249,250} The hydrated IrOx exhibited a characteristic blue color²⁵ over both platinum microelectrodes of its oxidized form and an amorphous microstructure, as can be seen in the optical microscope and SEM images in Figure 3.8b.

EIS can be used to investigate electrode-electrolyte properties. The benefit of high CSCc coatings to reduce the charge-transfer resistance of electrodes is also observed in the Bode plots in Figure 3.8c for evaporated and printed Pt, and EIROF microelectrodes. All electrodes exhibited the same high-frequency impedance, whereas a marked reduction in low-frequency impedance was observed with the porous coatings of printed Pt and EIROF coatings. For printed Pt, over a frequency range of 10^3 – 10^6 Hz, the porous film exhibited a near-resistive phase angle (approaching 0°) and an impedance modulus ($|Z|$) that was almost entirely solution resistance. A similar response was obtained for EIROF coated Pt microelectrodes for which resistive behavior was observed in almost the complete frequency range of 1– 10^6 . In the low-frequency region, the effective surface area is a significant feature as the impedance value depends on active surface area of the electrode in the electrolyte. A large surface area allows more charge to pass and consequently reduces impedance in low-frequencies. As the roughness of the material also changes the overall active area, the inkjet-printed Pt electrodes show, as expected, a lower impedance than the photolithographic evaporated ones. The impedance response is in good accordance with the roughness and porosity data presented before and with their CSCc values. EIROF coatings lead to an impedance improvement of approximately 150-fold and 15-fold reduction (at 1 Hz) with respect to the initial bare evaporated and printed Pt electrode impedance values, and their final impedance values are similar according to their electrochemical capacitance above mentioned.

3.3.1.4 pH sensor performance of EIROF on printed Pt

3.3.1.4.1 Sensitivity

Although the pH sensing mechanism for IrOx films is well known, it is still not fully understood and several models have been suggested.^{250,269} However, it is clear that the potential response of the EIROF involves an equilibrium between the oxidized and the reduced forms of IrOx,²⁵⁷ and as they exist in several possible states, super-Nernstian sensitivities ranging from 60 to 80 mV/s can be expected depending on each hydrated IrOx layer grown. It is generally accepted that such great discrepancies come from differences in fabrication conditions, which lead to differences in the oxidation state, the extent of hydration and the thickness of the final layers.

The potentiometric pH measurements were carried out by measuring the OCP at room temperature of the EIROF modified printed Pt in the range of pH 2-11 using an external RE. Each sensor was tested three times in the same solution in order to demonstrate the super-Nernstian response and repeatability of the prepared electrodes. Figure 3.9a shows the potential response, obtaining sensitivities of -71.6, -

71.2 and -71.1 mV/pH with high correlation coefficient r^2 values between 0.9991 and 0.998. This super-Nernstian response illustrates the applicability of such hydrated IrOx and is in good agreement with other reported sensitivities.^{250,270–273}

Commercial Ag/AgCl RE are usually voluminous electrodes. In this study we propose the integration of a miniaturized built-in Ag/AgCl pRE printed on the same sensor chip. The pH measurements with the integrated pRE were validated in the range of pH 3-10, as the pRE is not stable out of this pH range.²⁷⁴ As expected, the sensitivity obtained was 69.89 mV/pH, in good agreement with the use of a commercial RE. The intercepts at pH = 0 indicate that E^0 is 795 ± 0.3 mV for the external Ag/AgCl RE and shifts slightly to 767 ± 0.8 mV due to the use of the integrated Ag/AgCl pRE. The pH sensors proposed herein show a good linearity and sensitivity response validating the use of the printed Pt on a polymer as a sensor microelectrode. Furthermore, the high sensitivity values obtained indicate that the grown EIROF has a high porous surface with the presence of highly oxidized IrOx and oxyhydroxides^{257,275} that possess a high number of hydrophilic sites, which are responsible for the proton and electron transfer during redox processes inside the oxide film.

3.3.1.4.2 Reproducibility

The complete evaluation of the pH sensing characteristics requires a reproducibility study of the EIROF grown on top of the printed Pt film. Three EIROFs microelectrodes, made from the same fabrication batch, were used for the potential-pH dependence (vs Ag/AgCl commercial RE) and the acid-to-base and base-to-acid direction response was studied repeatedly as shown in Figure 3.9b. Sequential immersion in freshly buffer solutions was followed by a cleaning step with deionized water to avoid cross-contamination. As can be observed, the potential responses for the microelectrodes almost overlap, indicating an excellent reproducibility. The average sensitivity obtained for the 3 electrodes was 70.91 mV/pH with a relative standard deviation (RSD) of 0.899 % for the acid-to-base direction (b1) and 71.48 with an RSD of 0.892 % for the base-to-acid direction (b2), confirming the excellent reproducibility of the grown EIROF on printed Pt film with a correlation coefficient larger than 0.998 for all measurements. The electrochemical potentials slightly differ in the same pH levels, commonly known as hysteresis. This effect is well known for IrOx and even other metal oxide films.^{257,276}

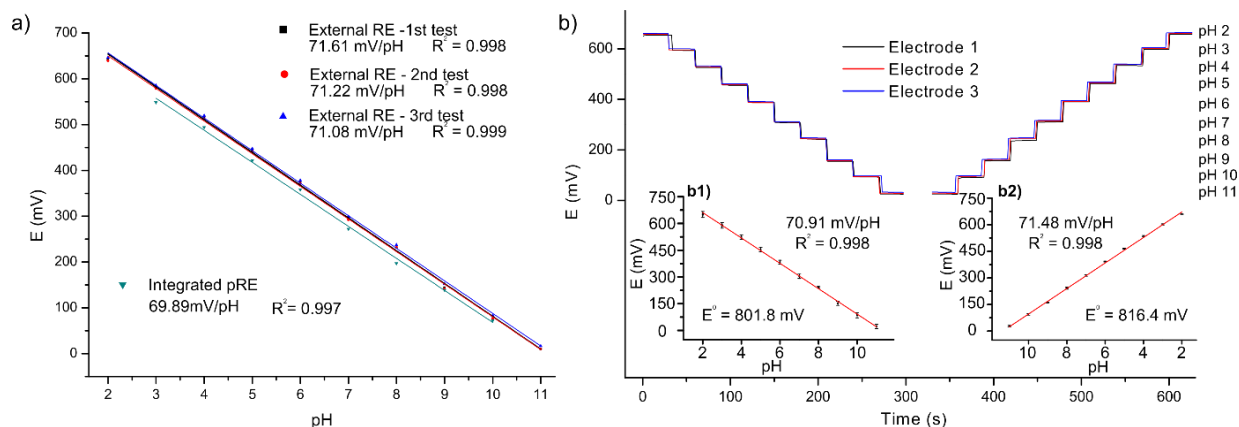


Figure 3.9. EIROF pH sensor calibration.

a) Sensor sensitivity of grown EIROF on printed Pt films in the pH range of 2-11 using an external RE and 3-10 using the integrated pRE. b) Reproducibility of the electrode at different pH values from 2 to 11 Inset: plots represent the average potential for b1) acid-to-base and b2) base-to-acid direction versus pH.

3.3.1.4.3 Response time

The response time, calculated as the time needed to reach 90 % transition of the total potential step, was studied in acid and alkaline environments as shown in Figure S6a. In an acid medium a pH step of 5 to 4.25 and vice versa was applied by adding desired HCl or KOH, and the response time in both directions was less than 6 seconds. In alkaline conditions (pH step of 9 to 10 and vice versa) it was found that a longer time was needed to reach equilibrium; however, the sensor still shows a quick response, as in both directions less than 8 seconds was needed. This difference in response time can be explained from the concentration of hydrogen ions in alkaline medium being lower than in acid medium, which leads to a little bit slower ion exchange inside the EIROF.

3.3.1.4.4 Stability

It is known that the electrodeposition yield of IrOx film is rather poor due to adhesion problems.²⁷⁷ Specifically for pH sensors, the delamination, crack formation and low adhesion of IrOx layers to the underlying substrates is an issue that can become severe, when the microelectrodes are exposed for long times in liquid media (needed to maintain them hydrated). To overcome this Marzouk *et al.*, in their search for a pH sensor integrated in a flow injection analysis (FIA) system, proposed an acid-

etched titanium treatment to increase the electrode roughness to improve electrodeposited IrOx adhesion.²⁷⁸ Other publications suppose the heat-treatment of the IROF²⁷⁶, where first a sol-gel layer of IrOx is deposited, for being then thermally oxidized at 300 °C for 5h. For this reason, the pH sensors stability of such sensors is not commonly reported, as it is one of the weak points for such IrOx layers, especially the hydrated ones. However, stability can be understood in two correlated ways. The first one is the mechanical stability, which refers in this study to the adhesion of the EIROF to the Pt electrode. The second one is the stability of the EIROF by itself, as the sensing material, and is related with the intrinsic aging of this material.

EIROF mechanical stability

To study the mechanical stability of the IrOx coatings in terms of adhesion, a batch of electrochemical IrOx layers were prepared over the above presented section evaporated (smooth) Pt²⁶⁶ and over the printed (rough) Pt microelectrodes. The devices were stored in PBS at room temperature without any other specific treatment and their interface changes were monitored in time by following their impedance (Figure 3.10). The impedance of EIROF over evaporated Pt (Figure 3.10a) increases gradually and almost in 15 days the interface impedance value restores the bare Pt one. It is important to note that the impedance value at 15 days corresponds to a deactivated Pt microelectrode. This data, representative of the six tested microelectrodes, corresponds to the three optical images where the IrOx detachment is clearly highlighted. The progressive detachment of the iridium that initially recovers homogeneously the entire electrode, leads to the almost exposure of the initial bare Pt. While the IrOx is easily delaminated from the evaporated Pt in 15 days, over the printed Pt presents just slight changes in the same period of time (Figure 3.10b). One year later the impedance increased, however, the optical images revealed that the oxide does not detach from the surface. The colored appearance of this one year old EIROF microelectrode suggests that this increase in impedance can be explained by an aging effect which, as discussed later, can be explained by a change in the oxidation state of the IrOx. As the loss of IrOx on the evaporated Pt is only affected by a wet storage in PBS solution, despite the similar electrochemical characteristics of the described EIROF, it can be assumed that the main weakness of the EIROF over the evaporated Pt is its lack of adhesion to the electrode, which compromises its mechanical stability and indicates the poor adhesion to the substrate.

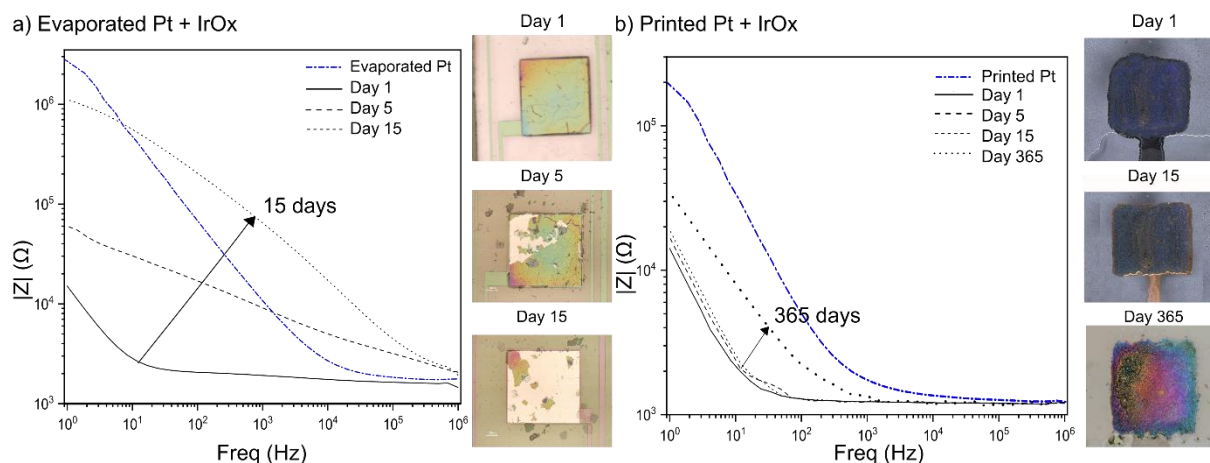


Figure 3.10. Impedance comparison of printed Pt and evaporated Pt.

Impedance changes of evaporated Pt (a) and printed Pt (b) microelectrodes coated with EIROF over time for devices being immersed in PBS solution at room temperature. Representative impedance and microelectrode microscope images ($n=6$) at different times to observe the EIROF coating over the Pt substrate.

EIROF aging

The stability of the IrOx in terms of device reliability was studied on the printed Pt as it showed the best long-term stable adhesion by measuring the sensitivity of two batches of three sensors for one year. Some of these sensors were stored in dry conditions and others in PBS solution at room temperature (Figure 3.11a). The dried sensors were exposed to a rehydration followed by a dehydration process each time when they were measured. Both storage conditions showed aging effects of the EIROF grown on the printed Pt, probably due to an unstable hydrated redox state of the grown oxide. The changes in color shown in the image of the microelectrode (Figure 3.10b) stored for one year corroborate this. This known effect in highly hydrated oxides provokes a loss of sensitivity, in our case 19 % (wet storage) and 23% (dry storage) of the initial sensitivity in the first 50 days, which finally stabilizes in 54.1 ± 0.9 mV/pH. Therefore, for the first 50 days the sensors must be checked and, if necessary, calibrated daily before using them. While this makes long-term studies difficult, punctual pH measurements, with an established procedure for calibrating the sensors, ensure the effectiveness and sensibility of each sensor, as can be seen from the excellent reproducibility. Drift studies (Figure S6b) made in buffer solution at pH 7 show that a microelectrode stored in dry conditions for 9 months needs 4 hours of conditioning. After this conditioning step, the potential drift during continuous measurement over 14 h is 0.2 mV/h, thus providing reliable pH read-outs for mid-term measurements.

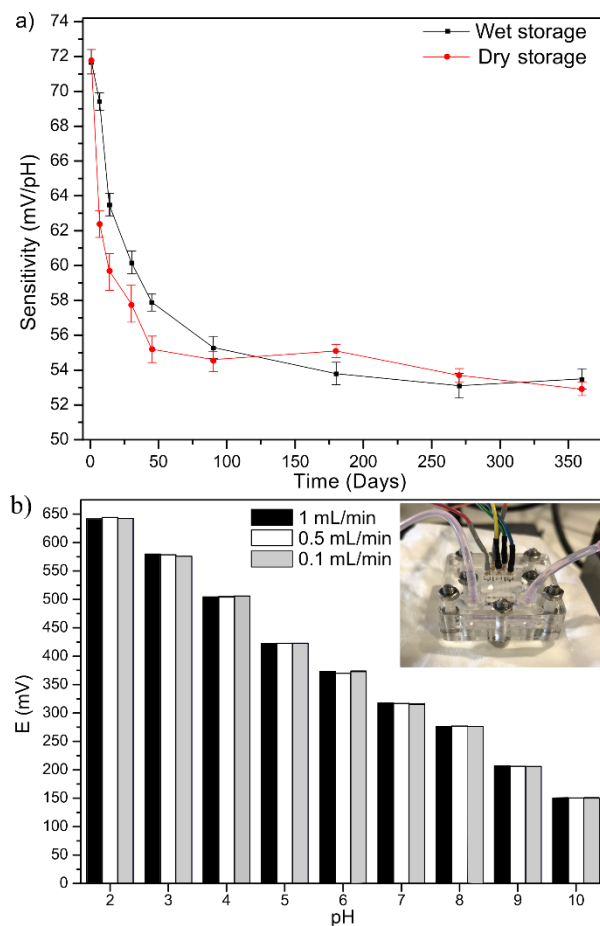


Figure 3.11. Stability studio of EIROF coating.

a) Sensitivities of the pH EIROF Pt sensors measured for one year in two different storage conditions, dried and wet (PBS solution). b) Potential recordings of a one month aged sensor in the pH range 2 to 10 under different flow rates of 0.1, 0.5 and 1 mL/min. The inset in top right corner shows the sample holder fabricated for the microfluidic pH calibrations.

EIROF stability under flow conditions

To further test the adhesion of the prepared EIROF of this work, sample of one month exposure was chosen and pH calibrations were performed under flow conditions. A sample holder (inset image in Figure 3.11b) with a microfluidic channel was specifically designed, as described in Figure S7. Three flow rates (FR) of 0.1, 0.5 and 1 mL/min were applied and liquid buffer solutions, in the range of pH 2-10, were consecutively tested. Figure 7b shows that the recorded potential with various FR are highly stable, the sensor shows a response of 60.83 ± 0.07 mV/pH unit, which indicate a good performance of the EIROF as well a good long time adhesion of this layer on top of the rough printed Pt film. These results were confirmed by testing pH sensors of various ages, which all showed sensitivities according to the aged situation (values shown in Figure 3.11a) and high stability under various flow conditions.

In summary, this study shows that printed Pt particle ink can be used as a microelectrode for obtaining a highly stable pH sensor, whereas the EIROF sensitive material shows a very good adhesion to it. The results illustrate the benefit of a nanostructured film, which shows a far higher surface roughness in comparison to traditional films, which serves as a mechanical adhesion promoter for the metal oxide film grown on top of it. This concept maybe interesting for further research for several other potential types of sensors as numerous examples in the literature can be found, apart from pH sensing, which look for strategies to increase the adhesion.^{278,279} For example, this feature has been especially studied in neuroscience applications, where materials such as IrOx or other conducting polymers are required to produce very stable layers for both recording and stimulating activities.^{279,280} Also, solid-state ion-selective electrodes are devices, where the ion selective membrane needs a highly rough intermediate layer, such as a conducting polymer coating on metal²⁸¹ or carbon nanotubes²⁸², which leads to a stronger adhesion in comparison to results achieved with flat Au, Pt or carbon electrodes. The high observed roughness of the printed Pt film can also be useful in applications where low impedance requirements are needed, as for example, in applications such as neural recordings.^{283,284} Our results illustrate the further need to explore the applicability of particle printing inks, because they allow a simplification of the sensor fabrication process and especially the advantage in film adhesion will enable to achieve long-term stable sensors in the future. We suppose that this approach can be extended to a large variety of particle material inks and sensor types.

3.3.1.4.5 Conclusions

We present a novel approach for fabricating a stable pH sensor by using a highly rough printed Pt ink as a substrate metal electrode. The proposed fabrication method by additive digital IJP is highly interesting under cost aspects; it is compatible with any electrode design in the micrometer range, at low-cost and on a wide range of substrates. Our developed pH sensor is based on a nanostructured EIROF sensing layer on such a printed rough Pt electrode, which has been demonstrated to have an excellent adhesion to the Pt. The pH sensors exhibit a linear super-Nernstian response in a wide pH range, with an excellent reproducibility and a rapid response time. The high mechanical stability for the EIROF coating over the printed Pt can be attributed to the high roughness of the Pt layer, after its comparison with a smooth evaporated Pt. This improved adhesion of the EIROF layer is also demonstrated by the evaluation of the sensor over 1 year, which stabilizes in a sensitivity of 54.1 ± 0.9 mV/pH, and by the test under flow conditions, where fluxes ranging from 0.1 to 1 mL/min do not alter the pH sensor

response. The presented approach, of directly printed rough metal films, could lead to the manufacture of electrochemical sensors on a variety of substrates, which are cost-efficient and long-term stable. Such Pt ink is a promising material that can be directly printed on a substrate to form rough metal layers, which is an interesting alternative to other established and expensive methods and can suppose a further improvement of a wide range of sensors.

Acknowledgements

M. Zea would like to acknowledge his financial support covered by Fundación Centro de Estudios Interdisciplinarios Básicos y Aplicados (CEIBA)-Gobernacion de Bolivar (Colombia). This work was supported by the Spanish government funded project by Ministerio de Economía y Competitividad CTQ2015-69802-C2-1-R (MINECO/FEDER, EU) and DPI2015-65401-C3-3-R (MINECO/FEDER, EU). Authors also want to thank the support of the Generalitat de Catalunya to 2017-SGR-988, and the SU-8 Unit of the CIBER in Bioengineering, Biomaterials and Nanomedicine (CIBER-BBN) at the IMB-CNM (CSIC) of ICTS "NANBIOSIS". This work has also made use of the Spanish ICTS Network MICRONANOFABS partially supported by MEINCOM.

Supplementary Information (section 6.1).

Cost analysis of the IJP pH sensor; pseudo-reference electrode chlorination and stability characterization; iridium oxide electrodeposition and characterization; Pt ink rheological properties and SEM image; Inkjet printing waveform of Pt ink; Pt line pattern test; EIROF pH sensor response time and stability; Microfluidic chamber fabrication.

3.3.2. Publication II: Specially designed polyaniline/polypyrrole ink for a fully printed high sensitive pH microsensor.

The first paper presented in this Chapter, **Publication II**, is an accepted article about the development of a novel Polyaniline and Polypyrrole based ink for pH sensing, it also presents the development of the first fully inkjet printed pH sensor on flexible PEN substrate. The proposed ink displayed a good linearity for the range of pH 3 to pH 10, solving the common conductive polymers drawback.

This article has been edited from the version accepted in ACS Applied Materials & Interfaces, with permission from ACS (edition consist in formatting and numbering figures, references, tables, and equations in accordance with the thesis manuscript, however acronym corresponds to the article):

Miguel Zea, Robert Texido, Rosa Villa, Salvador Borrós and Gemma Gabriel. **Specially designed polyaniline/polypyrrole ink for a fully printed high sensitive pH microsensor**. Accepted on 22/06/2021.

This work has been also presented in different conferences with their corresponding Proceedings:

- ❖ Conference **FLEX MEMS & SENSORS2020**: Miguel Zea, Ana Moya, Eloi Ramon, Gemma Gabriel. Development of inkjet printed biosensors on flexible and porous substrates. Oral Presentation.

Specially designed polyaniline/polypyrrole ink for a fully printed high sensitive pH microsensor.

Miguel Zea^{1,2,‡}, Robert Texido^{3,‡}, Rosa Villa^{1,4}, Salvador Borrós³ and Gemma Gabriel^{1,4,}.*

¹ Instituto de Microelectrónica de Barcelona IMB-CNM (CSIC), Campus Universitat Autònoma de Barcelona, 08193 Cerdanyola del Vallès, Barcelona, Spain

² PhD in Electrical and Telecommunication Engineering, Universitat Autònoma de Barcelona (UAB)

³ Grup d'Enginyeria de Materials, Institut Químic de Sarrià-Universitat Ramon Llull, via Augusta 390, 08017 Barcelona, Spain

⁴ CIBER de Bioingeniería, Biomateriales y Nanomedicina (CIBER-BBN)

KEYWORDS: pH sensor; polymeric ink; polyaniline; polypyrrole; inkjet printing,

*Note: The supplementary information of this article can be found in section 6.2 (Figures and tables number with S of prefix are inserted there)

ABSTRACT: pH sensing for healthcare applications requires sensors with mechanically stable materials of high-sensitivity, high reproducibility combined with low-cost fabrication technologies. This work proposes a fully printed pH sensor based on a specially formulated conducting polymer deposited on a microelectrode in a flexible substrate. A formulation, which combined polyaniline (PANI) and polypyrrole (PPy) with integrated polyelectrolyte poly(sodium 4-styrenesulfonate) (PSS), was specially prepared to be printed by Inkjet Printing (IJP). The sensor has good sensitivity in the physiological region (pH 7-7.5) key for the healthcare biosensor. This mixture printed over a commercial gold ink, which has a singular chemical functionalization with phthalocyanine (Pc), increased the sensor sensitivity, showing an excellent reproducibility with a linear super-Nernstian response (81.2 ± 0.5 mV/pH unit) in a wide pH range (pH 3 to 10). This new ink together with the IJP low-cost technique opens new opportunities for pH sensing in the healthcare field with a single device, which is disposable, highly sensitive, and stable in the whole pH range.

3.3.2.1 Introduction

pH is a key indicator for many biochemical processes and for this reason, pH sensors have received considerable attention for monitoring human healthcare due to their versatility, possibility of real-time measurements, and quantitative results²²⁴. Possible areas of interest can be found in the continuous monitoring of blood^{225,226} and sweat^{227,228}, and the determination of the pH of tumors²²⁹ as the chemodynamic therapy heavily depends on acidic chemical environment pH measurements that can determine the effectiveness of this treatment. Even though the pH sensor is a broadly studied one, for all the above mentioned applications, integrated pH sensors must fulfill strict requirements that are technologically unresolved to date. The most relevant points where the technology still faces important challenges to be accomplished are²³⁰ 1) flexibility, to be adapted to body tissues; 2) the need for miniaturized pH sensors that are minimally invasive; 3) good performance such as good stability, sensitivity and response time, to allow monitoring for definite time; and 4) accuracy at neutral pH, especially interesting for physiological measurements.

Most of these pH sensors are designed for single use and for this reason, their fabrication technology must be easy to allow scaling up and production of a wide range of devices and at a reasonable cost. In particular, the healthcare field is growing towards a promising platform for personal wearable electronic and flexible biochemical sensors, which are envisaged to replace bulky and costly medical instruments for healthcare monitoring or at least, to complement the laboratory-based devices, expanding the areas

of application. One of the most important digital fabrication techniques in flexible electronics for the fabrication of sensors is inkjet printing (IJP). In the last few years, flexible electronics has grown exponentially in application fields such as healthcare and industry, and the market is expected to reach USD 87.21 billion by 2024²⁸⁵. It is an additive manufacturing and non-contact approach that allows the maskless deposition of functional materials in small drop volumes on a wide range of substrates²⁸⁶. These singular features are of significant interest for the fabrication of biochemical sensors due to their simple implementation and scalability to high-volume manufacturing. Although IJP cannot be considered as a replacement for conventional silicon fabrication techniques, it is a reliable technique for the development of sensors with the above mentioned requirements, namely, low cost, disposable, robust and miniaturized²⁸⁷ in novel low-cost flexible substrates such as a broad range of plastics and even paper with real applicability in the future²⁸⁸.

In respect of the pH sensors fabricated by IJP reported to date, due to simplicity and the possibility of miniaturization, all those reported have been electrochemical sensors based on potentiometric technique²⁴¹. The printed metallic electrodes have been functionalized by depositing or growing some of the most representative pH sensitive materials, usually oxides, polymers, and biomolecules. The sensing materials that have a pH-dependent potential over printed metallic inks proved until now are those electrochemically grown iridium oxide^{113,289}, grown palladium oxide over a printed palladium ink (Pd/PdO)^{113,123} and electropolymerized PANI polymers²⁴².

Conducting polymers (CP) are ideally suited for pH sensing applications^{290,291} because they not only exhibit high conductivity and electroactivity but they can also be used as a general matrix and can be further modified with other compounds in order to increase the pH range²⁹². Although many polymers have been studied²⁹³, the most popular polymer-film-coated electrodes reported are the ones using electropolymerized pyrrole and aniline^{294,295}. For this work, CPs have been considered as the optimal candidate among all the range of materials used for pH sensors because they allow the formulation of a suitable ink with adequate rheological properties to be printed by the IJP technique.

In this work, we propose a printable pH sensitive CP that allows the first fully printed polymer-based pH sensor reported until now. We develop a new water based ink formulation based on a mixture of PANI:PSS/PPy:PSS that gives a high stability and super-Nernstian sensitivity (81 mV/pH) to the final performance of the pH sensor. This mixture of polymers pays special attention to neutral pH (pH values 7 – 7.5), key for the healthcare biosensor and monitoring applications. To obtain physiological

measurements in this pH interval is still a challenge due to the high precision and resolution required in this narrow range as well as the difficulty to obtain a stable measure without pronounced potential drifts. The proposed ink displayed a good linearity for the range of pH 3 to pH 10, solving the common CP drawback of a good performance at physiological range of pH. Therefore, the inks and the fabrication approach herein described can open new ways for the mass production of miniaturized pH sensors for healthcare applications fully compatible with large-scale production methods.

3.3.2.2 Experimental section

3.3.2.2.1 Materials and Chemicals.

For the development of the microelectrodes, we used three commercially available inks. A low-curing gold colloidal ink (Au-Pc) (DryCure Au-J 1010B from Colloidal Ink Co., Ltd, Japan), low-curing gold nanoparticle ink (Au-Np) (Au-LT-20 from Fraunhofer IKTS, Germany), silver nanoparticle ink (Dupont-PE410, USA), and SU-8 ink (2002 from MicroChem, USA). All the ink formulations were printed with a drop-on-demand Dimatix Materials Printer. Hydrochloric acid (HCl, 0.1 M) was used for the chlorination of the printed Ag electrode, and potassium chloride (KCl, 0.1 M) for testing the pseudo-reference electrode (pRE). Polyethylene naphthalate of 125 μm (PEN, TeonexQ65HA DuPont Teijin Films) was used as substrate to print the microelectrodes. Commercial buffer solutions of pH 3 to 10 (Panreac), and HCl and sodium hydroxide (NaOH) were used for the pH calibration. (all reagents from Sigma-Aldrich)

3.3.2.2.2 Polyaniline and polypyrrole synthesis.

The materials used in the synthesis of water-dispersible CP suspensions consisted of aniline ($\geq 99,5\%$, Aldrich, San Louis, MO, US), pyrrole ($\geq 99\%$, Aldrich, San Louis, MO, US), ammonium persulfate ($\geq 98\%$, Fluka Bucharest, Romania), poly (sodium 4-styrenesulfonate) (PSS) solution (Mw 70,000, 30% wt), and (Mw 200,000, 30% wt) purchased from Sigma Aldrich (San Louis, MO, US).

3.3.2.2.3 PANI and PPy ink formulation.

PANI:PSS and PPy:PSS were formulated adding the proper amount of MilliQ water (MQ); Triton X100 as surfactant and Glycerol and DMSO as conductor promoter. Details of all the prepared formulations are contained in Table S1.

3.3.2.2.4 Inks characterization. DLS.

The particle size distribution of the suspensions was determined by dynamic light scattering in diluted samples (1:10) using a Zetasizer ZEN3600 (Malvern Panalytical, Malvern, United Kingdom).

3.3.2.2.5 FTIR Spectra.

PANI:PSS and PPy:PSS IR spectra were obtained using IR spectrometer (Nicolet iS10, Thermo Fisher Scientific). For sample preparation, suspension were lyophilized and then combined with potassium bromide (KBr) to be compressed between two platens and to form the pellet to be analyzed.

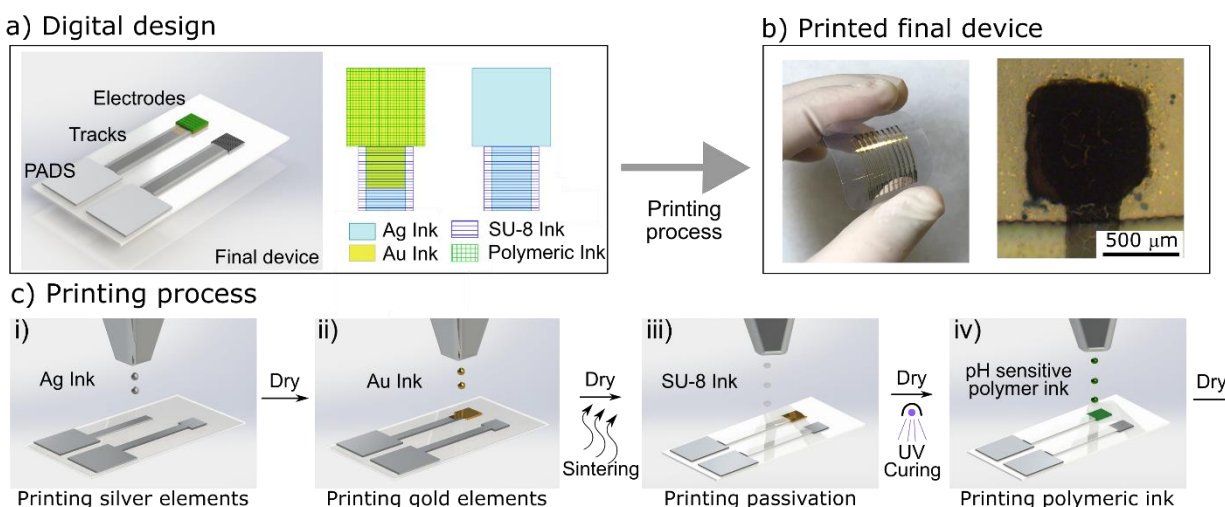


Figure 3.12. Fully inkjet printed pH sensor.

a) Digital design of the pH sensor. b) Final printed platform with 9 IE and 1 pRE and microscope image of the printed polymeric electrodes. c) Inkjet printing steps: i) printing of Ag RE, tracks, and pads, followed by a dry step; ii) printing of the Au IE, followed by a dry and thermal sintering of both metallic Au and Ag layers; iii) printing of the dielectric SU-8, drying and UV cross-linking; iv) printing of CP inks, followed by a drying step.

3.3.2.2.6 Microscope images.

Field Emission Scanning Electron Microscopy (FESEM) images were taken to observe the nanostructure with a field-emission Zeiss Merlin FESEM (Oberkochen, Germany). The film of the samples was prepared depositing a droplet of the suspension on a silicon substrate and let dry on a vacuum drier at room temperature.

3.3.2.2.7 Fabrication of solid-state pH sensor.

The pH sensor structure was fabricated with IJP technology, using the same approach that we reported in our previous work.^{289,296} Basically, a drop-on-demand Dimatix Material Printer (DMP 2831 for Fujifilm Dimatix, Inc., USA) was used with the 10 pL printhead. The sensor structure was digitally designed using CleWin 5 software (Figure 3.12a) and then exported to BMP to load in the Dimatix Bitmap editor. The printing process was carried out in standard laboratory conditions without particles-filter, temperature, and humidity control. Microelectrodes and CP inks (PANI:PSS, PPy:PSS and PANI:PSS/PPy:PSS) were printed on PEN substrate, as detailed in Figure 3.12c. The complete fabrication of the pH sensor can be easily understood as two steps: The printing process of the metallic microelectrodes, and the electrodes modification. In the first step (c.i), the silver (Ag) elements were first printed: the reference electrode (RE) of 800 x 800 μm , tracks, and pads with a drop spacing (DS) of 20 μm followed by a dry step at 80 $^{\circ}\text{C}$ for 15 min. Then, the Au-Np ink was printed (c.ii) to obtain a 1 mm^2 indicator electrode (IE), with a DS of 15 μm , the platen temperature was set to 40 $^{\circ}\text{C}$ and the printhead temperature was set to 30 $^{\circ}\text{C}$. Au elements were dried as before, and both inks were finally sintered in the oven at 140 $^{\circ}\text{C}$ for 30 min. Then the dielectric ink SU-8 was printed (c.iii) on Ag tracks to isolate and define the active electrode area and pads with a DS of 15 μm . First, a soft bake on hot plate at 100 $^{\circ}\text{C}$ for 5 min followed by an UV treatment for 30 sec to polymerize this layer by polymer cross-linking. For the fabrication of microelectrodes with the other Au ink Au-Pc, the DS used was 25 μm , and the platen and printhead temperature was set to 35 $^{\circ}\text{C}$.

The second step consisted of the printing process of the pH sensitive polymer ink over the Au microelectrode (c.iv), and the chlorination of the Ag RE. Initially, the CP inks were sonified for 5 minutes in order to uniformly disperse the solid content. Then, the inks were filtered through a polar ultrafilter of a 0.45 μm pore size and introduced into the ink cartridge. To achieve a good pattern definition substrate, the cartridge nozzles were heated at 40 $^{\circ}\text{C}$ and 35 $^{\circ}\text{C}$ respectively. Three layers of CP inks were printed wet-on-wet on top the Au IE with a DS of 10 μm , and dried for 15 min at 120 $^{\circ}\text{C}$. The Ag RE was chlorinated by cyclic voltammetry (detailed in the Supplementary Information (SI) Figure S1) in 0.1 M HCl, scanning the potential from 0 V to 0.2 V versus Ag/AgCl commercial reference electrode at 20 mV s^{-1} to obtain a stable Ag/AgCl pseudo-reference electrode (pRE). A final printed platform on PEN substrate with nine IE and one pRE and a microscope image of the printed CP electrodes can be observed in Figure 3.12b.

3.3.2.2.8 Morphological characterization of printed CP.

The printed polymeric films were analyzed using an optical microscope (DM4000M LEICA, Germany), a profilometer (KLA Tencor P-15), and a scanning electron microscope (SEM, Auriga40 from Carl Zeiss, Germany).

3.3.2.2.9 pH measurements.

The open-circuit potential (OCP) of the inkjet-printed electrodes was measured by a PalmSens3 electrochemical station (De Indruk, Netherland). Measurements were carried out in various commercial pH buffer solutions ranging from pH 3 to 10. Sequential immersion in buffer solutions was followed by a cleaning step with deionized water to avoid cross-contamination. For each test, the electrodes were immersed in the buffer for 30 s, and the potential between IE and pRE was recorded. The base-acid titration was done from basic (NaOH) to acid (HCl) standardized solutions with concentrations of 0.01 mM, 0.1 mM, 0.001 M, 0.01 M, 0.1 M, and 1 M, which was magnetically stirred. Additionally, the pH value was recorded with a commercial pH-meter (GLP22, Crison) in both experiments.

3.3.2.3 Results and discussion

3.3.2.3.1 Synthesis and characterization of printable polymeric pH-sensitive inks.

To obtain the CP inks for IJP, water-dispersible particles of PANI and PPy were synthesized through electrostatic interaction suspension method as described in the materials and methods section. This method is especially suitable to obtain CPs suspensions with the ability to form a continuous conductive film as it has been previously reported for PANI^{183,297} and PPy^{298–300}. The distinctive feature of this procedure consists of involving electrostatic forces produced between monomer and polyelectrolyte to allow obtaining stable suspensions during the oxidative polymerization. This allows obtaining a controlled size distribution to fulfill one of the most restrictive IJP requirements. The supporting polyelectrolyte used was PSS solution as charge- balancing dopant during the polymerization. Considering that the application of the suspensions is an IJP ink, we studied the influence of the molecular weight of PSS which takes a critical role both in the properties of the ink (size distribution, stability) and in the properties of the printed film. In the current literature, it has been reported that high PSS molecular weight presents some advantages in term of superior electrical and electrochemical performance^{301,302}. However, there are very few references about the effect of PSS molecular weight on

the size distribution, suspension stability and film formation properties of PANI:PSS and PPy:PSS suspensions. With this in mind, four different suspensions were prepared, (PANI:PSS(I), PANI:PSS(II), PPy:PPS(I), and PPy:PPS(II)) using PSS with two different molecular weights 70.000 Da for (I) suspensions and 200.000 Da for (II). After the synthesis, stable suspensions of both PANI (green color, Figure 3.13a.i) and PPy (black color, Figure 3.13b.i) were obtained for the two PSS used. Obtaining PANI:PSS and PPy:PSS suspensions through electrostatic interaction synthesis was confirmed through IR analysis as detailed in SI Figure S2a and b. None of the suspensions obtained presented signs of precipitation after 6 months at room temperature. Size distribution of the PANI:PSS and PPy:PSS formulations was studied through DLS. We observed that, PANI:PSS and PPy:PSS suspensions presented a monodisperse size distribution in all cases, regardless of the monomer used or the PSS molecular weights.

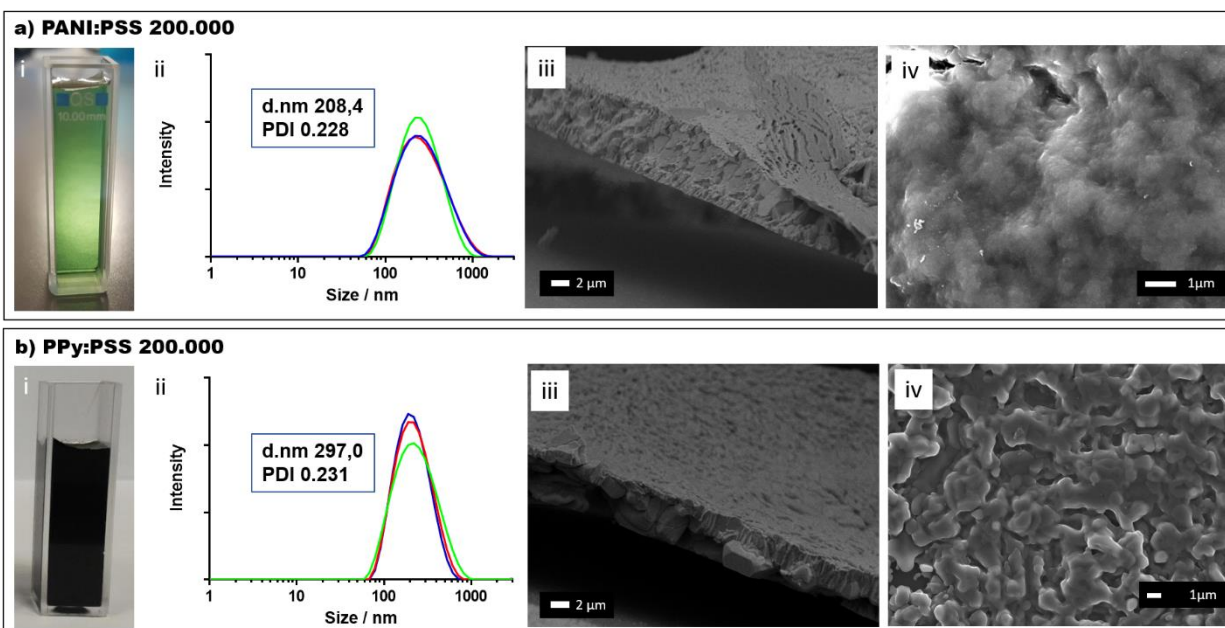


Figure 3.13. PANI and PPy ink characterization.

Characterization of CPs suspensions. PANI:PSS(II) suspension (a) and PPy:PSS(II) suspension (b): i) solutions; ii) particle size distribution and iii) FESEM profile image; iv) FESEM film image.

Considering the dependence of PANI polymer on the pH media, the synthesis of PANI:PSS suspensions was optimized at pH 2 to maximize the number of PANI:PSS particles (data shown in Figure S3). The particle size average values were around 200 nm, as shown in Figure 3.13a.ii) for PANI:PSS(II) and b.ii) for PPy:PSS(II) (values for PANI:PSS(I) and PPy:PSS(I) are shown in the SI

Figure S4). The zeta potential of the suspensions was also measured, obtaining a value around -20 mV for PSS of Mw 70.000 and around -40 mV for the PSS of 200.000 (data shown in Figure S5). The mean value combined with particle size distribution (PDI) values around 0.2 obtained for each suspension fulfilled the requirements of IJP to avoid the clogging of the printer nozzle. All the suspensions were correctly filtered using a 0.2 μm PTFE filter before each printing for the elimination of any possible higher particles to prevent the nozzle clogging.

After filtering, the suspensions were able to form a continuous film on a silicon substrate after air drying. FESEM images revealed a continuous structure with a well-defined layer thickness of approximately 5 μm for PANI:PSS (Figure 3.13a.iii) and 7 μm for PPy:PSS (Figure 3.13b.iii) for all the film suspensions studied (SI Figure S6). No significant differences were observed in the morphology for PANI:PSS or PPy:PSS samples where a different molecular weight PSS was used during their synthesis (Figure 3.13a.iv and b.iv for Mw 200.000 PSS). As can be seen, both images present a globular morphology due to the interaction between the oxidant and the structuring agent during polymerization³⁰³. It is of interest to note that PANI:PSS globular shape revealed a smoother morphology when compared with PPy:PSS, possibly originated by a coalescence phenomenon produced during the drying process.

These four aqueous suspensions were used as the basis for IJP ink formulations. The studied suspensions were formulated using a surfactant (1,5 % (w/v) of Triton X100), to adjust the surface tension of the ink prior to the printing. Surface tension data of the evaluated formulation inks are detailed in Table S2 of the SI. Furthermore, to increase electric conductivity, dimethyl sulfoxide (DMSO) and glycerol (Gly) were used as a secondary dopant. Gly addition also contributes to adjust the viscosity of the CPs formulation and the presence of DMSO and Gly shows a stabilization of polymer benzoic structure once the film is formed^{304–309}. Hence, this intrinsic conjugation of benzoic structure allows a better electron mobility through polymeric chains, which in turn enhances the electroactivity of CPs. This effect, which is broadly studied for polymers such as the gold standard PEDOT:PSS, is not so widely studied for PANI and PPy formulations and even less when they are applied as a pH sensor.

3.3.2.3.2 Polymeric inks printing process.

Once formulated, the inks were printed using an inkjet printer to obtain a sensor array. Printing parameters were adjusted to obtain a continuous drop ejection for PANI:PSS(I) and (II) and, PPy:PSS(I) and (II) inks printing. Waveform and printing parameters were obtained considering polymeric ink

properties to have a reliable printing process of developed polymeric inks (SI Figure S7). As described in the literature, the ink-substrate interaction alters the ink deposition, hence the drop spacing (DS) selection between two consecutive drops and the printer platen temperature determines the quality of the printed pattern on a specific substrate.³¹⁰ The DS determines the resolution and density in X- and Y-axes of the printed samples, for example, a DS of 15 μm represents a print resolution of 1693 dpi (dots per inch). The platen temperature plays a critical role on drops evaporation that it is directly related to line formation, pattern definition and coffee-ring effect. To evaluate an optimum DS, a line pattern test was performed with DS from 5 to 140 μm .⁵⁵

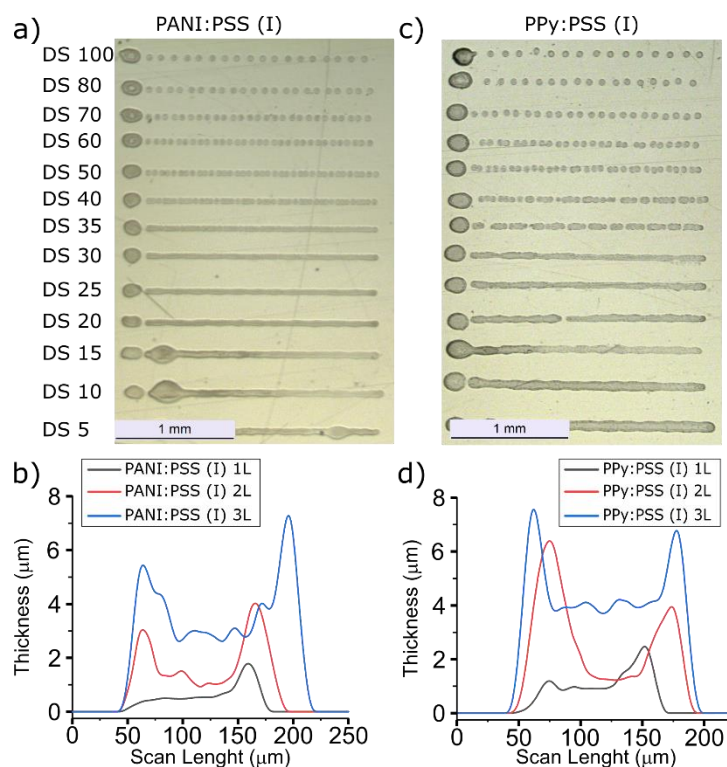


Figure 3.14. Printing characterization of polymeric inks.

Line patterns printed on PEN substrate for a) PANI:PSS(I) and b) PPy:PSS(I) formulated inks. Cross-section profile for c) PANI:PSS(I) and d) PPy:PSS(I) for 1L, 2L or 3L.

Figure 3.14 shows the printed line patterns for PANI:PSS(I) (a), PPy:PSS(I) (b). Both inks present more or less the same behavior and no main differences can be observed with the other formulations using Mw 200.000 PSS (data not shown). However, depending on the selected DS, different performance can be observed. When the chosen DS is too small (5 μm), bulging effects appear due to an excess of deposited material. For DS values of 40 μm or higher, the formation of isolated drops that are not able to form a continuous line can be observed. The proposed inks have optimized DS values between DS

10 and 35 μm that allow the printing of a homogeneous and continuous line. Apart from the line pattern evaluation, experimentally it has been observed that DS values higher than 10 μm do not allow the overlap of contiguous printed lines, as can be observed in SI Figure S8. This can be explained by a fast evaporation of ink solvents or interaction between ink and substrate helped by drop kinetics. Also optimized was the substrate temperature, which was set to 40 $^{\circ}\text{C}$ to obtain a balance between solvent evaporation, ink spreading, and linewidth. Temperatures lower than 40 $^{\circ}\text{C}$ produced an excessive spreading and the formation of inconsistent lines due to the slower evaporation of the ink, and temperatures higher than 40 $^{\circ}\text{C}$ showed thinner lines and exaggerated coffee-ring effects as a result of rapid solvent evaporation. Finally, a DS of 10 μm at 40 $^{\circ}\text{C}$ was determined as the optimal point to obtain the most homogeneous lines with a controlled coffee-ring effect to print the polymeric suspensions onto the Au microelectrodes.

Furthermore, different number of CPs layers were printed wet-on-wet and evaluated latter in the profilometer (one (1L), two (2L) and three layers (3L)). A desired thickness of around 1-3 μm should be achieved to decrease the CP film electrical resistance, decrease the pH behavior hysteresis, increase pH sensor life-time, and ensure a good repeatability as previously reported.³¹¹⁻³¹³ Four layers (4L) were also tested, however these conditions were not under consideration because the films were completely detached when being immersed in an aqueous solution, as shown in Figure S9, due to an excess of material over the metallic electrode. Profilometer measurements are shown in Figure 3c for PANI:PSS(I) and 3d for PPy:PSS(II); the well-known coffee-ring effect was observed for all the printed layers, being necessary 3L for achieving a non-uniform thickness of around 3 μm in the central part of the pattern. After printing, PANI and PPy films with PSS of Mw 70.000, revealed a good stability in aqueous media indicating its suitability as sensor. However, when a PSS of Mw 200.000 was used, the polymeric film was completely detached after a few minutes of being in contact with the aqueous media. Thus, we selected the PANI:PSS(I) and PPy:PSS(I) inks for its evaluation and validation as a pH sensor.

3.3.2.3.3 Evaluation of the printed CPs inks as pH sensor.

For the evaluation of the polymeric printed films, potentiometric pH measurements were carried out by measuring the open circuit potential at room temperature. Sensors were placed three times in the same buffer solution to evaluate the pH response and repeatability of the polymeric film. Considering the applicability of this sensor in biological applications, in addition to evaluating its sensitivity and linearity, special attention was paid to the physiological pH range (around pH 7.5).

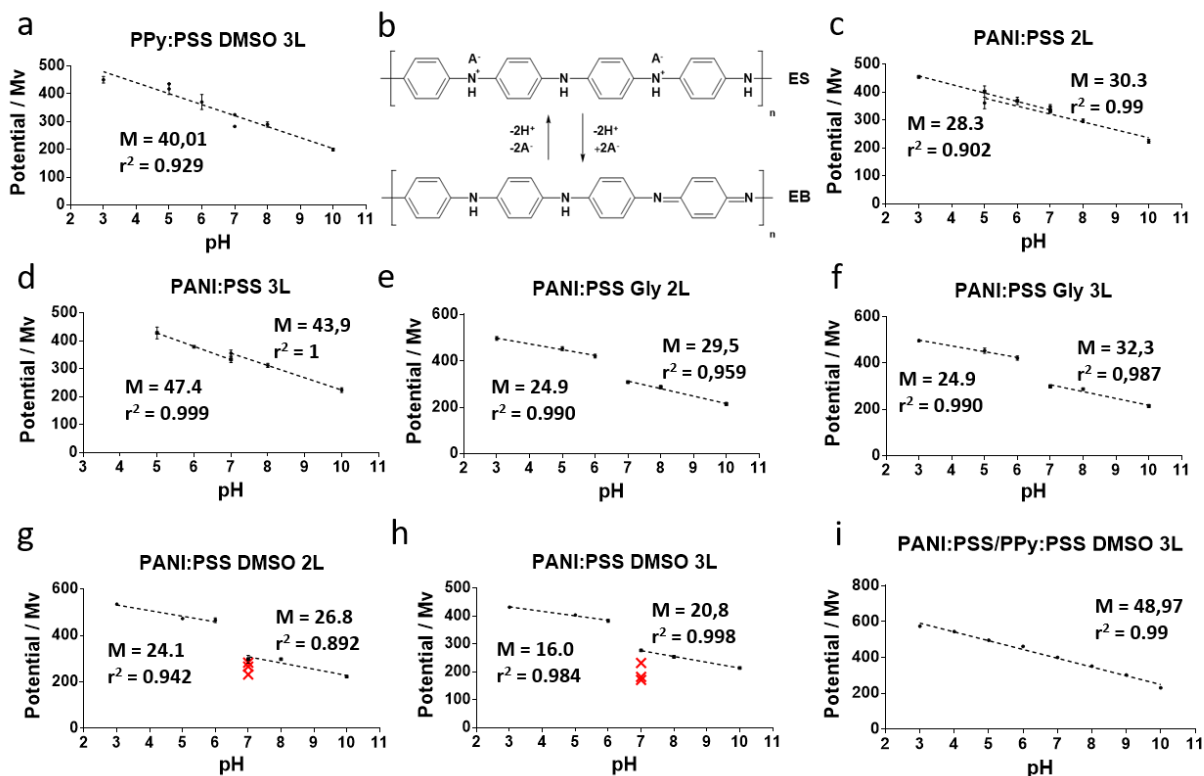


Figure 3.15. pH calibration of PANI and PPy printed films.

Plots of potentials against pH value reading from pH meter for (a) PPy:PSS + DMSO 3L, (b) Structure of PANI macromolecule changes due to protonation/deprotonation, (c) PANI:PSS 2L, (d) PANI:PSS 3L, (e) PANI:PSS + Gly 2L, (f) PANI:PSS + Gly 3L, (g) PANI:PSS + DMSO 2L, (h) PANI:PSS + DMSO 3L, (i) PANI:PSS/PPy:PSS + DMSO 3L ($n = 3$, variation coefficient below 5%).

Figure 3.15 shows the potentiometric pH measurements of the evaluated formulations of PANI:PSS(I) and PPy:PSS(I). PPy:PSS(I) formulation revealed a poor linearity in the selected pH range even when a secondary dopant (DMSO) was used to enhance the polymer electroactivity (Figure 3.15a). This behavior of PPy as a pH sensor is described in the literature for similar devices³¹⁴

For PANI:PSS(I), the potential decreases with the increase of the pH, revealing two good linear regions similarly to the behavior of electrodeposited PANI pH sensors but with less pronounced changes in the slopes³¹⁵. The presence of these regions is ascribed to the pH dependent emeraldine salt (ES) – emeraldine base (EB) transition of PANI macromolecules, where, depending on the pH, there is a different level of protonation of the EB imine groups (Figure 3.15b). This protonation – deprotonation of PANI structure provides its electroactive properties allowing changes in the potential output signal, which reveals two different slopes corresponding to the protonation levels, where the acid pH region

allows higher slope values indicating better electron mobility and high electroactive behavior of the polymer. A result of this behavior can be seen in the printed sensors of PANI:PSS(I) without conductivity promoters, where two linear regions can be observed in Figure 3.15c and d corresponding to a film of 2L or 3L, respectively. The linear regions present in PANI:PSS(I) 2L and 3L films presented similar slopes (28.3 mV/pH for pH 3 – 7 region and 30.3 mV/pH for the pH 7 – 10 region). These changes may be attributed to the presence of sulfonate groups present in PSS which generates local acidic regions that allows the regulation of PANI protonation. Although PANI:PSS films reduce the effect of the structure change by improving the linearity of the sensor response, the neutral pH zone still presents a poorly defined signal. PANI:PSS(I) films formulated with a conductivity promoter such as Glycerol (Figure 3.15e and f) or DMSO (Figure 3.15g and h) only magnified the effect of structure protonation, presenting higher differences between the potential output signal of the two regions. This effect is clearly visible for PANI:PSS samples with DMSO, where the measurement performed at pH 7 presented a high deviation. Increasing the number of layers of printed PANI:PSS film from 2 to 3 did not produce any significant improvement in this sense.

To improve the measurements in the physiological region as well as the linearity in the studied range of pH, we used a formulation that combines PANI:PSS(I) and PPy:PSS(I) (PANI:PSS/PPy:PSS). We hypothesized that when electron mobility cannot be carried out through the PANI chain due to the EB / ES structure change, the PPy chain supports electron mobility. First, we optimized the IJP conditions of the two polymers together. It was observed that mixing PANI:PSS(I) with PPy:PSS(I) (1:1 v/v) allowed the printability of a stable polymeric sensor. Figure S10 of the SI shows the line pattern of this new ink and the corresponding cross-section profile for 1L to 3L, as previously done for PANI and PPy base inks. In this case, the DS optimized is also 10 μm . However, the cross-section profiles show how the ink accumulates in the central part, noted by the distribution of the material. We observed that the most homogeneous film was achieved with 3 L, with a thickness of about 5 μm .

Secondly, we studied the sensor response at different pHs. Figure 3.15i shows potential against pH plot for PANI:PSS/PPy:PSS sensor. The potentiometric pH measurements revealed a good linearity in the range of pH 3 to pH 10. These results confirm our hypothesis, because not only did we solve the drawbacks of PANI:PSS at the physiological range of pH but we also increased the stability of the PPy:PSS films. Furthermore, the sub-Nernstian response was in good agreement with other reported sensitivities for polymeric pH based sensors^{291,315–318}. All measurements subsequently performed were

done with the PANI:PSS/PPy:PSS ink printed over the Au microelectrodes with a platen temperature of 40 °C, DS of 10 μm, and 3 L.

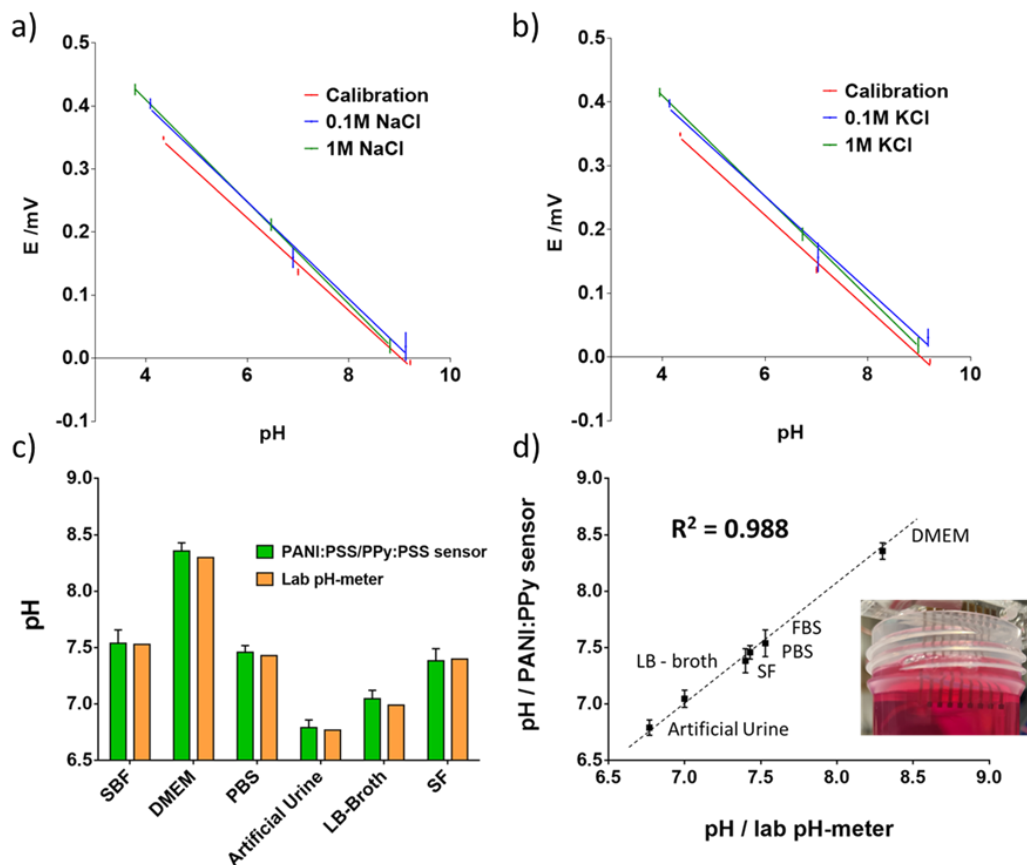


Figure 3.16. Interferences study for PANI:PSS/PPy:PSS sensor.

Potential interfering ions test for PANI:PSS/PPy:PSS sensors: Na⁺ (a) and K⁺ (b). Determination of pH value for a set of mediums used in the bioengineering field: Comparison between PANI:PSS/PPy:PSS sensors ($n = 3$) with a laboratory pH-meter (c) and compared using a linear correlation (d).

Selectivity is one of the most important factors in potentiometric sensors and defines the ability to specifically measure hydronium ions in the presence of other ions. For this reason, we evaluated the potentiometric selectivity performance of the developed pH sensor against major potential interfering sodium (Na⁺) and potassium (K⁺) ions observing the voltage drifts at different pH for constant ion concentrations (Figure 3.16a and b). Potential against pH plots of buffered solution in the presence of Na⁺ and K⁺ revealed small voltage drifts similar to other similar devices described in the literature^{319,320}. Based on these results, the presence of Na⁺ and K⁺ does not interfere with the pH measurements of real unknown solution. In this context, the performance of the PANI:PSS/PPy:PSS sensor was evaluated

using 6 standard solutions of unknown pH used in the field of bioengineering: simulated body fluid (SBF), Dulbecco's Modified Eagle Medium (DMEM), Phosphate Buffer Saline (PBS), Artificial Urine, Luria-Bertani Broth (LB-Broth) and commercial Corning SF medium. Figure 3.16c shows the pH value of the solutions measured using the PANI:PSS/PPy:PSS sensor compared with a conventional pH-meter with a glass electrode. The pH of these real solutions were determined revealing no significant differences between the measurements carried out with the PANI:PSS/PPy:PSS sensor and with the laboratory pH-meter. From a qualitative point of view, Figure 3.16d shows the correlation of the pH values of the two electrodes for the 6 evaluated solutions. As shown, the linear regression presents a coefficient of determination of 0.988, indicating the good agreement between values and demonstrating that the developed sensors present the same behavior that a laboratory device.

3.3.2.3.4 Effect of the gold substrate on the Nernstian-behavior of the pH sensor response.

In this section, we explore the utilization of an Au-based printed electrode modified with a phthalocyanine (Pc) as a method to increase the sensitivity of the polymeric-based pH sensor. The commercial Au-Pc metallic ink used to print the Au electrodes was modified with a derivative metal-free phthalocyanine, which presented a delocalized planar structure, promoting the formation of large π -conjugated regions. These regions, directly in contact with the surface of the Au nanoparticle, improved the electrical pathway among them³²¹ allowing good conduction characteristics equivalent to those of the conventional nanoinks (Au-Np) with a minimum heat treatment (usually sinterings at 100-120 °C for several minutes gives well-conducted patterns). As previously described, the incorporation of phthalocyanine into PPy or PANI chains results in the increase of the delocalized regions, enhancing the doping level of the CP, the electron mobility and the electroactivity^{322,323}.

Figure 3.17 shows the interactions of the Au-Pc ink together with the CPs. Once the PANI:PSS/PPy:PSS ink was printed onto the Au-Pc microelectrode, the π – conjugated regions of the PANI, PPy and PSS interacted with the π – conjugated regions of Au-Pc, enhancing the electron mobility between the printed Au-Pc substrate and the polymeric film in comparison with the bare Au-Np ink

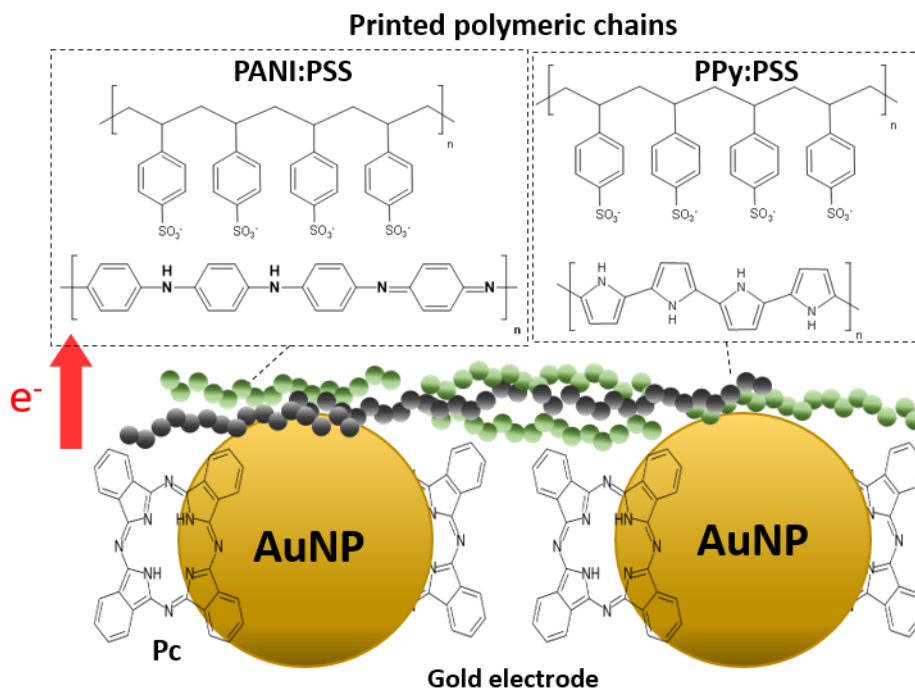


Figure 3.17. Chemical schematic illustration of AuNP ink and polymers.

Schematic illustration of π – junction of Au-Pc ink modified with phthalocyanine and PANI:PSS/PPy:PSS polymeric chain.

Figure 3.18a shows the effect of Pc in direct contact with the PANI:PSS/PPy:PSS based sensor. pH calibration was performed for PANI:PSS/PPy:PSS printed on non-modified Au substrate (Au-Np) revealing a Nernstian sensitivity of 48.5 ± 0.5 mV/pH with a high correlation coefficient r^2 of 0.990 in the all pH ranges (3 to 10), in good agreement with other previously reported CPs based pH sensors.³¹² When the PANI:PSS/PPy:PSS polymeric film was printed onto the Au-Pc, a super-Nernstian response of 81.2 ± 0.5 mV/pH with high linearity was achieved. Table 3-3 summarizes the most recent papers on conducting polymers used for pH sensing. As can be observed, our work has the highest sensitivities achieved for a polymeric based sensor²⁹⁰. As stated before, this increase in sensitivity can be explained due to enhanced electron mobility between the Au-Pc substrate and PANI:PSS/PPy:PSS. The utilization of Au-Pc ink to generate a high delocalized π -region between the electrode and the PANI:PSS/PPy:PSS printed polymeric film is not only interesting in terms of obtaining a high sensitive pH sensor, it also describes a strategy that could be implemented in other CPs to increase electroactivity, thus unlocking new applications.

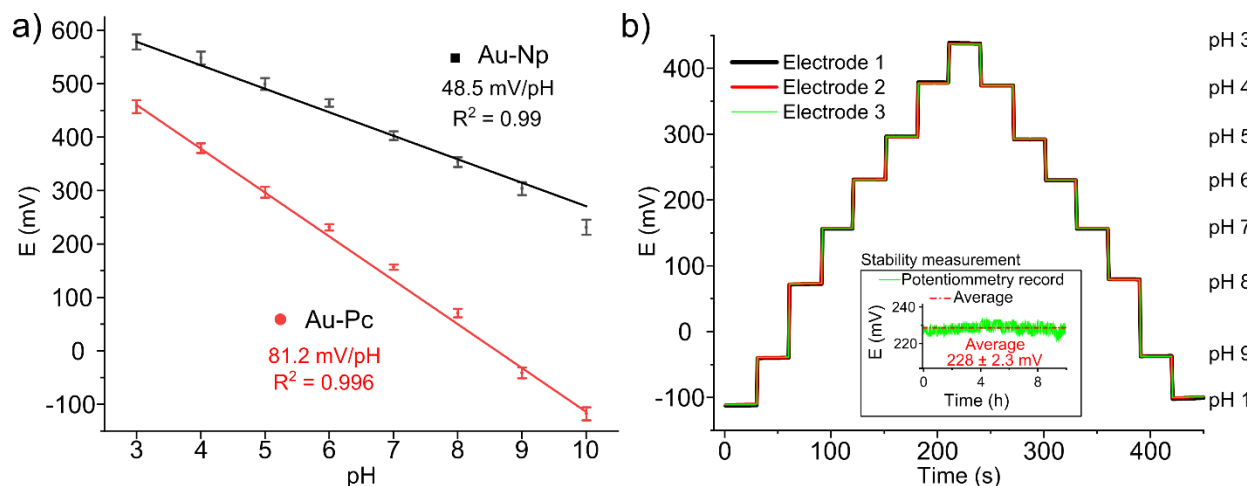


Figure 3.18. PANI:PSS/PPy:PSS pH calibration curves.

Calibration curves of PANI:PSS/PPy:PSS. a) Sensor sensitivity of PANI:PSS/PPy:PSS on Au-Np and Au-Pc microelectrodes in the pH range of 3-10 ($n = 3$, variation coefficient below 3% for Au-Pc and below 4% for Au-Np). b) Repeatability of the electrode of PANI:PSS/PPy:PSS on Au-Pc at different pH values from 3 to 10 (Inset: mid-term pH sensor stability at pH 6 for 10 hours).

The complete evaluation of the pH sensing characteristics required a reproducibility study of the PANI:PSS/PPy:PSS printed on top of the Au-Pc microelectrode. Three independent microelectrodes, made from the same fabrication batch, were measured by OCP and the base-to-acid and acid-to-base changes were studied. Figure 3.18b shows the response of each individual microelectrode, and as can be observed, the potential responses for each one almost overlap, indicating an excellent reproducibility. The average sensitivity of the three electrodes is 81.2 mV/pH with an average variation coefficient for each pH level under 0.5% (Table S3), confirming a good repeatability of PANI:PSS/PPy:PSS sensor with a the correlation coefficient larger than 0.996 for all measurements. The mid-term stability of the pH sensor near protonation and deprotonation regions was further investigated by measuring its potential drift over 10 hours at room temperature. For this purpose, the platform was immersed in pH 6 buffered solution (Figure 3.18b inset) and continuously measured. Although some slight potential fluctuations can be explained by temperature changes, the sensor shows an excellent stability of continuous reading over a 10 h test resulting in a potential drift of 0.2 mV/h, an average reading of 228 mV and a standard deviation of 2.3 mV, thus providing reliable pH read-outs for long measurements.

Table 3-3. CPs-based pH sensors on the literature.

Comparison of selected works from the literature, highlighting the conducting polymers used for pH sensing, the fabrication technique used for the deposition of the conducting polymer, pH range and sensitivity. Abbreviations: CNT (Carbon Nanotubes), MWCNT (Multiwalled Carbon Nanotubes), DBSA (Dodecyl Benzene Sulfonic Acid), PU (Polyurethane), and PSS (Sodium 4-styrenesulfonate).

Conducting Polymer	Technique	pH range	Sensitivity (mV/pH)	Reference
PPy	Electropolymerization	2 to 12	54.67 ± 0.7	324
PANI nanofibers	Polymerization	3.9 to 10.1	62.4	325
PANI nanopillar	Soft lithography	2.38 to 11.61	60.3	326
PANI	Electropolymerization	5 to 7	-	294
PANI	Electropolymerization	5.5 to 8	59.2	295
PPy + CNT, PANI + CNT	Electrodeposition	1 to 13	59	327
PANI	Laser carbonized	4 to 10	51	328
PANI	Coating	4 to 10	50	312
PANI	Coating	4 to 8	54 ± 0.51	329
PANI + CNT	Electrodeposition	1 to 13	58	330
PPy	Electropolymerization	3 to 10	46	331
PANI + DBSA	Spin coating	5.4 to 8.6	58.57	92
PANI + MWCNT	Screen printing	2 to 11	20.63	332
PANI + PU	Electrospinning	2 to 7	60	93
PANI	Electrodeposition	4 to 8	60.6	333
PANI + PPy + PSS	Inkjet printing	3 to 10	81.2 ± 0.5	This work

3.3.2.3.5 Validation of the PANI:PSS/PPy:PSS film as pH sensor.

To evaluate if the PANI:PSS/PPy:PSS sensor is good candidate for local pH determination, pH titration was studied. Titration was performed over a range of molarities (from 0.01 mM to 1 M), from NaOH to HCl by addition of a specific volume of acid. Figure 3.19a shows the titration plot of aqueous NaOH with HCl. Results obtained for monoprotic titration of strong alkalis with strong acids are comparable with results obtained with commercial glass electrode. The PANI:PSS/PPy:PSS sensor presented had a

reasonable detection limit (0.01 mM), a concentration range (from 1 M to 0.01 mM) and a pH range (from 3 to 10) compared with previous studies^{290,334}. The theoretical equivalence point for this titration is 10 mL at pH 7, due to pKa of NaOH and HCl. Figure 3.19b shows the experimental calculated equivalence points for all concentrations and their standard deviation. The sensors present good performance and accuracy, allowing detection of pH changes even ± 0.01 pH units with a high sensitivity of 81.05 ± 0.08 mV/pH. The same behavior was observed when the titration was performed from the acidic to basic range as shown in Figure S11. An equivalence point determined at pH 7 of 10 mL and a detection limit of 0.01 mM was obtained.

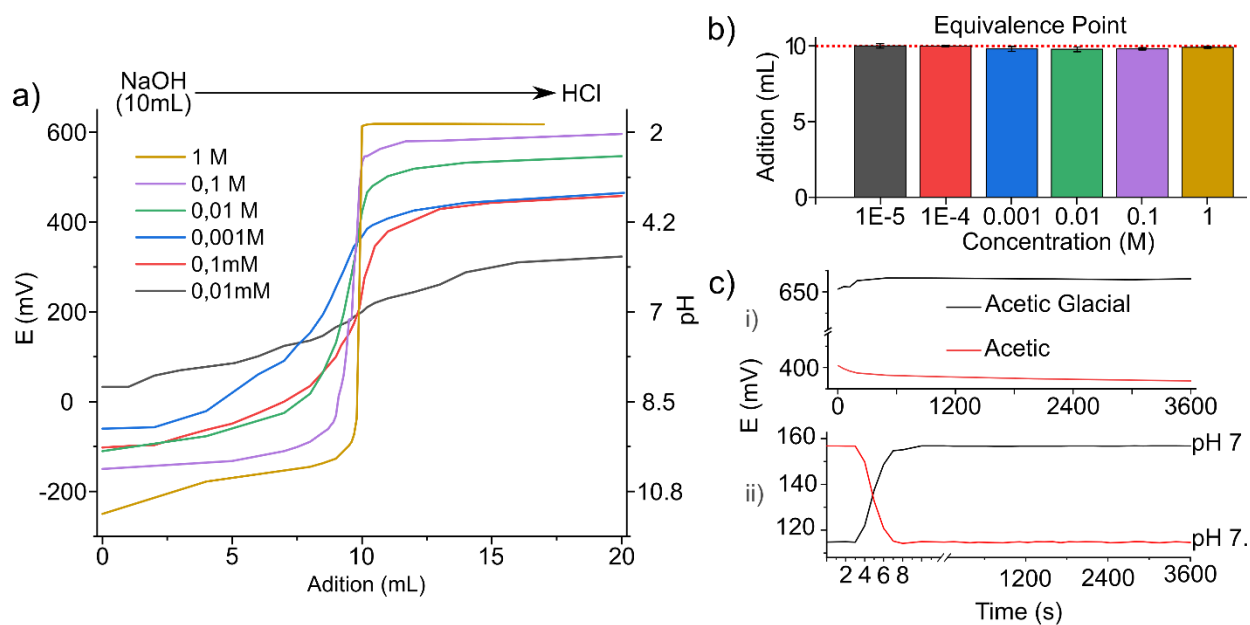


Figure 3.19. Titrations and stability study of PANI:PSS/PPy:PSS pH sensor.

Titration of strong base with strong acid. a) Potentiometric pH titration curves for NaOH and HCl at the indicated molarity, b) Representation of equivalence point for each molarity, on red dots the theoretical value, and c) Stability of the pH sensor in acid conditions, acetic and acetic glacial acid (i) and buffer solutions at pH 7 and 7.5 (ii).

Figure 3.19c.i shows the stability of PANI:PSS/PPy:PSS sensor for 1 hour in acetic acid and acetic glacial acid showing a stabilization time of 300 s for these low pH values, a small drift of 1 mV/h for acetic glacial and 6 mV/h for acetic acid. This proves the good behavior of the sensor in extreme pH conditions allowing its utilization on non-aqueous media. The stability was also measured in aqueous buffer solutions at pH 7 and 7.5 (Figure 3.19c.ii) to demonstrate how the sensors met the proposed benchmarks, showing that the response time was achieved within 7 seconds, and a small drift of 1.5 mV/h for pH 7 and 1.8 mV/h for pH 7.5. The sensitivity did not alter after 2 hours in extreme

conditions obtaining values of 80.7 mV/pH of the PANI:PSS/PPy:PSS sensor (data not shown). This result demonstrates that PANI:PSS/PPy:PSS polymeric film is not affected after performing measurements in non-aqueous acid media. Additionally, since the substrate proposed is flexible, the pH sensor evaluation was completed verifying that the sensor response remained unaltered after repeated bending tests. For this, a proof of concept was carried out to verify how sensor sensitivity evolves after being subjected to different bending cycles (Figure S12 of the SI). It was found that after 50 bending cycles of 90 °, the sensitivity of the sensors remained stable around 77 and 78 mV/pH, demonstrating that the sensors flexibility did not affect the pH sensor response.

3.3.2.4 Conclusions

We have presented a novel approach for fabricating a stable pH sensor using a highly rough printed Au ink as a substrate metal electrode. The pH sensors were completely fabricated with IJP based on PANI:PSS / PPy:PSS inks deposited on a gold microelectrode printed on a flexible substrate. The different approaches allowed the optimization of pH sensor properties and in particular IJP inks formulation allowed the improvement of the pH sensor sensitivity. Furthermore, the combination of PANI:PSS and PPy:PSS particles improved the linearity of pH against potential as well as expanding the pH range (from pH 3 to 10) and resolving problems of PANI sensors regarding physiological pH, thereby promoting utilization in biological applications. The use of a gold ink modified with Pc for the gold microelectrode substrate, revealed an enhancement of electron mobility between the conducting polymer chains and the gold nanoparticles, generating a delocalized π -region that improved the electroactivity. In this regard, the sensor reached a linear super-Nernstian response (81.2 ± 0.5 mV/pH unit), one of the highest sensitivity values for a polymeric pH sensor reported to date.

The characterization of the sensor also revealed a wide range of versatile properties that extends the range of possible applications. Furthermore, the sensor presented high stability in aqueous and non-aqueous media (acetic acid) confirming its ability to perform highly accurate titration measurements by detecting small changes in the concentration of strong monoprotic alkalis with strong acid (0.01M).

Supplementary Information (Section 6.2)

Pseudo-reference electrode chlorination and stability characterization; Ink formulations; Surface tension ink formulations; IR spectra characterization; CP suspensions – pH dependence; DLS characterization;

Zeta Potential Characterization; FESEM images; Parameters of printing process; images of printing test and non-adherence of polymeric film; PANI:PSS/PPy:PSS line pattern study; Variation coefficient; Titration of strong acid with strong base; pH sensor sensitivity after bending.

Acknowledgment

M. Zea would like to acknowledge his financial support covered by Fundación Centro de Estudios Interdisciplinarios Básicos y Aplicados (CEIBA)-Gobernación de Bolívar (Colombia). This work was supported by the Spanish government-funded project RTI2018-096786-B-I00, and RTI2018-102070-B-C21 by Ministerio de Ciencia, Innovación y Universidades (MINECO/FEDER, EU). The authors also want to thank the support of the Generalitat de Catalunya to 2017-SGR-988 and to 2017- SGR 1559, and the SU-8 Unit of the CIBER in Bioengineering, Biomaterials, and Nanomedicine (CIBER-BBN) at the IMB-CNM (CSIC) of ICTS "NANBIOSIS." This work has also made use of the Spanish ICTS Network MICRONANOFABS partially supported by MEINCOM.

Corresponding Author

* E-mail: gemma.gabriel@imb-cnm.csic.es.

Author Contributions

‡ M.Zea and R.Texido contributed equally to this work. The manuscript was written through contributions of all authors. / All authors have given approval to the final version of the manuscript.

Notes

The authors declare no competing financial interest.

Chapter 4 | Inkjet printed PoC devices

This chapter includes a brief explanation and description of PoC devices. Followed by the need of develop low-cost, disposable, and reliable electrochemical sensors for the incorporation in PoC. Next, the effect of printing on paper and its property of tuning electrochemical active area is presented. Finally, a novel cortisol paper-based printed sensor is presented.

4.1. Overview of PoC

Compared with standard laboratory testing, PoC diagnostics are rapid, simple, and inexpensive, and thus have great accessibility to resource-limited settings^{335,336}. Therefore, POC diagnostics are essential to initiate and scale up on-site medical care for the prevention and control of infectious diseases³³⁷⁻³⁴⁰. Point-of-care testing (PoCT) involves a paradigm shift from classical deferred diagnostics to near-patient analysis, providing real-time results for an early diagnosis, facilitating treatment implementation and selection, and reducing disease complications³⁴¹. The use of PoCT devices offers a promising solution to this situation, allowing to provide diagnostic information near the site of the patient and in real time³⁴². Figure 4.1 show an overview of the latest advances in developing PoC devices. Most PoCT devices can work with small volumes of biological samples and reagents, offering unique advantages such as a low assay cost, fast turnaround time, simple-to-use operation, and fully integrated devices implementable in resource-limited settings^{16,343}.

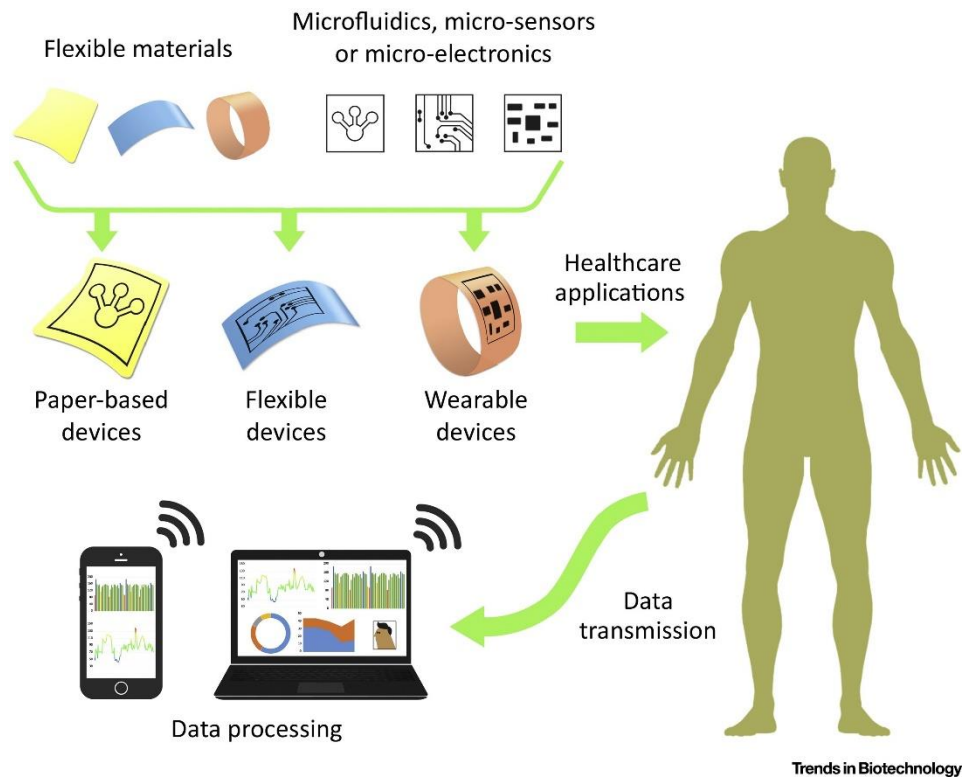


Figure 4.1. Overview of PoC devices for healthcare applications.
Source ³⁴⁴.

The PoC devices offer an enhanced diagnostic tool and will play an increasingly important role in controlling disease outbreaks, rising the survival rate of patients, and improving overall the quality of life of the citizens. Similar advantages that apply to diagnostics at mobile health units in isolated settlements, where the strategies currently available are unfeasible, because personalized medicine will be possible only if diagnostic devices can be used by or close to patients³⁴⁵. PoCT break the actual chain of diagnostic of conventional laboratory-based testing where the samples must be collected, stored, and transported to the centralized facilities, having to wait for long periods of time before the samples are analyzed by trained personnel and the results are sent back to the clinicians and reach the patients³⁴⁶. Furthermore, the use of PoC diagnostic devices could reduce as well the medical costs, and the risk of sample mislabeling and mishandling³⁴⁷. The PoC capability to diagnose or monitor diseases is increasingly important to population health, chronic disease, and to prevent severe admissions and readmissions.

Additionally, PoC devices allow to healthcare patient and health enthusiastic to monitor their own health, in consequence the devices need to be analytically valid, user-friendly and clinically valid in presential and tele medicine³⁴⁶. These requirements enable remote diagnosis and monitoring at center stage. To meet these requirements a PoC device must have a robust and reliable system for sample treatment (if it is needed), sensing, signal processing, signal output, and electrical or chemical source.

The menu of analytes is being expanded beyond vital signs, many hormones, proteins, and even virus are gaining a huge attention. At the same time, integration of data from PoCT into electronic health records and utilization of artificial intelligence (AI) and data analytics for data mining to achieve rapid and accurate diagnosis are assuming greater importance. Still almost all alternative (no glucose) PoC devices market available today, depend on colorimetric detection or cellphone image analysis³⁴⁸. Cellphone cameras can recognize small differences in color tone, as can be confirmed even in simple home experiments. And the cellphone app can assign quantifiable values to these tonality differences could be used to maximize the potential of the quantification of an analyte. However colorimetric detection combined with cellphone has certain drawbacks such as, qualitative results (color reaction), adapters or other devices need to be connected to the cellphone, shadows, each cellphone has a different design and size, different cameras, among others³⁴⁸.

Electrochemical detection offers quantitative results with high reliability, resolution, and low limit of detection. Electrochemical sensors are a mainstay of analytical chemistry as demands for increasingly selective and sensitive detection methods grow. Additionally, they are inexpensive, simple, and adaptable

to demanding environments where robust, miniaturized analytical methods are required³⁴⁹. Flexible substrate-based PoC devices, particularly with integrated electrochemical sensors not only significantly enhance sensitivity but also allow for continuous on-body health monitoring in a noninvasive mode³⁴⁴. These advantages put electrochemical sensors on flexible substrates in the focus to develop new reliable, robust, and accurate PoC device.

4.2. Overview of inkjet printed PoC devices

Inkjet printing technology provides as it is stated above a rapid and inexpensive way to generate prototyping iterations because no clean room is required, thus enabling low-cost, open-source research prototypes for proof-of-concept studies, and mass production of final device³⁴⁶. Examples of PoC device components that can be printed include sample pre-treatment devices, microfluidic reagents, blood mixer, fluid actuation unit, detector adapter, housing unit, or sensor. Inkjet printing technology provides accurate control of dispensing ink, precise positioning, and flexibility in printing patterns. However, in PoC manufacturing clogging of the nozzle can be a problem, since the dispensing solution can contain complex protein stabilizers and/or big particles, additionally the use of new substrates add more complexity to the printing process. Proper process optimization is required for the manufacturing process of PoC devices.

However, most PoC sensors for commercial use are still fabricated by using screen-printing and less frequently by more expensive and clean-room based photolithographic techniques. Even though these processes are quite automated and established, they require masks for each deposited layer and employed material, which can lead to alignment issues³⁵⁰. Furthermore, additional costs and time for the design and preparation of new masks need to be considered in case the design of sensors must be changed. This is even more critical for prototyping than for batch production. On the other hand, inkjet printing allows in a fast and reiterative manner multi-layer/material deposition and the production of combinatorial material libraries. Nowadays printer represents an ideal platform for sensor prototype development, but also industrial production^{114,351}.

To print PoC devices with high performance, there are several key considerations required, including the pattern quality, device flexibility/stretchability and device durability³⁵². A well define and integrated pattern is a prerequisite to develop inkjet printed device, since a uniform and high-resolution pattern enhances the device stability and can help minimize the device size. Large flexibility/stretchability and

long durability ensure the device adaptability for substrate bending. For instance, uniform homogeneous patterns diminish situation such as short circuits and heterogeneous conductivity. In printed electronics for PoC, high resolution patterns enable reduce used area of printed components, which provide an excellent handicap in the develop of a PoC portable device. In addition to area usage, the performance of the printed device is enhanced, by mean of higher conductivity and density for circuits, larger bandwidth and higher switching speed for transistor, and better connection for sensors³⁵³.

PoC devices, including electronic accessories, display, sensors, battery, tend to be bent, stretched, or squash during the usage, and even more when they are handled by the final consumer (self-use patient/user PoC device). Consequently, flexibility and stretchability are primary mechanical consideration when it comes to inkjet printed PoC. To meet the requirements, a huge effort have been done on exploring more suitable substrates and inks. Plastic and paper substrates despite their lack of stretchability, are the most used in electronic accessories due their flexibility. Other substrates that have been used in inkjet printed PoC devices are textiles, elastomers, among others.

Plastic-based printed PoC devices offer hydrophobic and condensing surface and high mechanical strength, additionally plastic substrate ensures excellent printed patterns. Nevertheless, the glass transition temperature must be considered when it comes to the ink need of sintering, as it is commented in section 2.4. It is essential for the progress of printed PoC devices develop strategies for low or no temperature process in addition of exploring novel inks. Moreover, achieving this requirement, it can be applied to other substrates with low glass transition temperature.

Textile-based printed PoC devices represent a flexible, long-lasting, conformable, and lightweight PoC platform that can be mechanically/manually stretched, bent, sheared, or twisted. Printed PoC textiles are candidate for flexible wearables PoC (on clothes). Several printed electronics parts for PoC devices on textile have been reported such as antennas, electroluminescent sensors and capacitors³⁵⁴⁻³⁵⁶. However, until the date, there is a limited number of publications on inkjet printing of textile-based PoC devices due to the intrinsic methodical challenges of printing onto fabric/textile substrates. Explicitly it is difficult to achieve a highly conductive continuous track on the rough material with a thin inkjet printed layer and also as the majority of fabrics cannot withstand temperatures above 150 °C. PoC on textile has a long path to wander but several method for printing on textile are under study^{357,358}.

Paper-based printed PoC devices present many advantages for printed PoCs. Not only because it is widely available and inexpensive, paper also lightweight, biodegradable and can be rolled or folded into 3D or 2D configurations (discussed in section 4.3.2)^{62,359}. Even though the attractive attributes, paper substrate comes with some shortcomings when it serves as substrate for inkjet printing process, such as overspreading due to capillarity, porosity, fiber interaction with inks and high-temperature post processing³⁵². Low viscosity inks tend to be absorbed by paper, which could lead to pattern overspreading with no define boundaries and poor electrical properties. To avoid this drawback and to prevent pattern irregularities, many strategies could be follow such as hydrophobic barriers, paper coating, roughness treatments, and even modifying paper fabrication process³⁶⁰⁻³⁶⁴. The printing process on paper is a on development and promising process that need the effort of the researching community to overcome actual challenges and obtain low-cost, reliable, disposable, biodegradable, and high performance printed PoC devices.

4.3. Paper-based PoC devices

A wide variety of paper substrate have been use for the fabrication of PoC devices but two main kinds have been most utilized to fabricate PoCT devices^{365,366}. One is nitrocellulose membrane which is the key material for lateral flow assays³⁶⁷. The other one is cellulose fiber-based substrate, such as filter paper and chromatography paper, which are the major substrates of dipsticks and PADS³⁶⁸. By virtue of the abundance and physical properties of cellulose, paper cellulose-based devices are often considered to be novel platforms for inexpensive, portable, and simple devices. The work done in this thesis is based in the last one (cellulose filter).

4.3.1. Cellulose substrate composition and applications

Many papers are composed majorly by cellulose fiber, these fibers come mainly from wood. The composition of the wood-fiber depends on the type of wood and pulping process. Three methods of pulping are the most used³⁶⁸. Chemical pulping, low or high pH is used to decompose the lignin in wood selectively, releasing fibers from wood ships. Mechanical pulping consists in ground the wood to get a pulp, so the result is cellulose, lignin, and pitch (fatty acids and resin). And the third method is fully bleached pulp that is white and is used to make filter paper and copy machine paper. Only small quantities of lignin remain in a fully bleached pulp. To obtain the final product, either to influence the

final properties or to facilitate the paper making, several polymeric additives are use. From the perspective of PoC device fabrication is important to know these additives that determine the chemistry of the substrate.

As it is known cellulose fiber-based substrate are porous, its hydrophilic properties allow the material to take more than their own mass of water. Writing, printing, and some packaging papers are usually treated with an hydrophobic treatment to increased contact angle and lower water rate penetration³⁶⁹. Additionally, coated paper is also used where the substrate properties emulate almost a plastic films protecting the paper from water absorption.

Cellulose fibers that conform a piece of paper, are hollow tubes ~ 1.5 mm long, $20 \mu\text{m}$ wide, and $\sim 2 \mu\text{m}$ thickness. Since paper fabrication process is a filtration, the fibers are mainly layered in the x,y plane^{370,371}. Generally, paper is described by three properties: capillarity, thickness, and basis weight. An estimation of pore volume can be obtained from thickness and basis weight, also other properties can be estimate from these three properties such as, density, pore size, among others³⁶⁸.

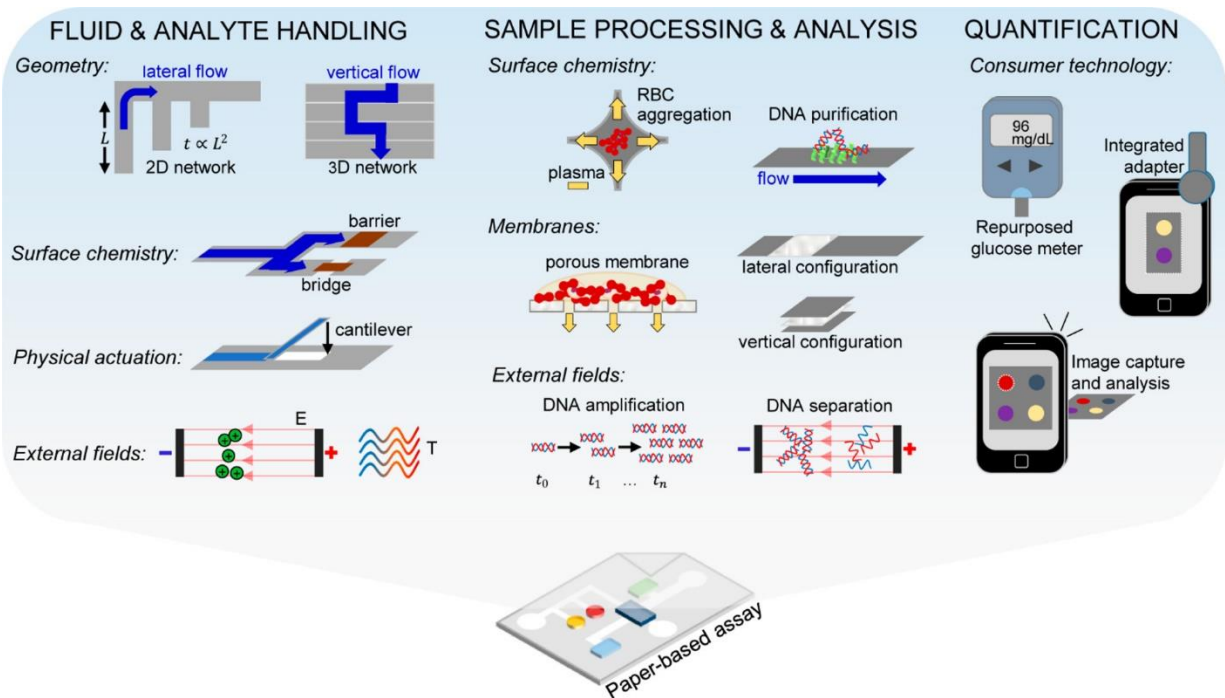


Figure 4.2. Analytical Capabilities of paper-based PoC

Paper-based assays with strategies for fluid and analyte handling, sample processing and analysis, and quantification. Source from ³⁷².

It is important to remark that paper is a very anisotropic material³⁷³. The mass distribution along the thickness is usually not constant. The common distribution is low density near the surface and maximum density in the center. Fiber orientation is another concern of the paper fabrication process, the orientation defines fluid transportation along the substrate. The orientation of the fiber is highly related to direction that paper was made on the paper machine. Consequently, liquid transportation along the strips of the substrate in a lateral-flow device usually depend on the angle at which the substrate was cut.

The property of moving fluid along the strips by capillary force, it is one of the most attractive to use paper substrate in PoC devices. This property allows lateral flow without the need of pumping or/and external energy. Additionally, the paper substrate offers filtration properties that can be adjust (pore size and fiber density) in the fabrication process, it can be treated with hydrophobic materials to create channels and split the sample (fluid) to transported to different locations³⁷⁴, it is a low-cost substrate, biodegradable, eco-friendly, among others.

Another property of paper substrate that start to be on develop is its intrinsic roughness or 3D structure, some studies have showed that an enhanced in the electrochemical performance of paper-based

electrodes or electric elements could be attributed to their highly porous structure with a large surface area, which decreased the transport length scale of the ions and electrons^{375,376}. Additionally, the paper porous structured coated by a conductive material (electrode) provide an effective pathway for ion transport and could act as favor electrolyte reservoirs due to the water-swelling effect of cellulose fiber in aqueous mediums³⁷⁷. As result, fabricated paper-based electrodes have a lower internal resistance caused by dense packing of the metal structure due to the porous 3D networks of the cellulose paper. Moreover, this 3D structure lead to a higher electrode surface area that it could trigger higher electrochemical active area.

A wide range of applications can be done with paper-based PoC as is shown in Figure 4.2, from detection of pathogens in food, water and air that has a huge society-health implications to biomedical diagnostic tools that apply to each individual particularly. The challenge is to achieve sensitivity, selectivity, and fast response while being inexpensive and in according with circular economy. And here is where electrochemical detection and paper substrate can be combined to develop PoC devices in the pathway of reliable, accurate, and circular-economy devices.

4.3.2. Electrochemical detection on paper

As it mentioned above a large majority of reported paper-based sensors relies in colorimetric detection method, which basically measure a color intensity generated by a reaction between the analyte and reagents in the paper, this intensity usually depends on analyte concentration. Specifically designed tools have been designed to provide optical quantitative interpretation such as cellphones, and others offer optical qualitative interpretation^{378,379}. These dependence to color intensity or reaction present limited accuracy and sensitivity, as result this colorimetric devices show a high rate of false-positive and false negative test results^{380,381}.

In the past years, the most effective transduction methods have been deployed on paper substrate in order to reduce cost and adapt to market demands, also gathering accurate and quantitative results, these methods include fluorescence, chemiluminescence, electrochemiluminescence, and electrochemical sensing. Evidently, these mechanisms have their own advantages and disadvantages. However electrochemical detection remains among the most promising detection tool, it is an effective and versatile method with high accuracy, fast results, and reliability. The electrochemical method provides improved sensitivity and selectivity compared with actual colorimetric methods³⁸². Nevertheless, there

are still some crucial challenges to overcome the wide range of application of paper based PoC devices, such as, miniaturization, integration, and cost.

Nowadays electrochemical detection on paper substrate obtain highly comparable results in terms of sensitivity and specificity to detection produced by the more conventional benchtop techniques (Liquid chromatography, UV-Vis spectroscopy, and inductively coupled plasma-mass spectroscopy)³⁸². However, in order to improve electrochemical paper-based devices (EPAD) a development of multiplexed tests on EPADs are highly desirable³⁸³. This is because sample treatments such as, collection, filtration, extraction, storage, and analysis can be carried out on the paper substrate in a single multiplexed EPAD, which facilitate the electrochemical reading³⁸⁴. Figure 4.3 shows a multiplex EPAD develop for the detection of glucose and protein.

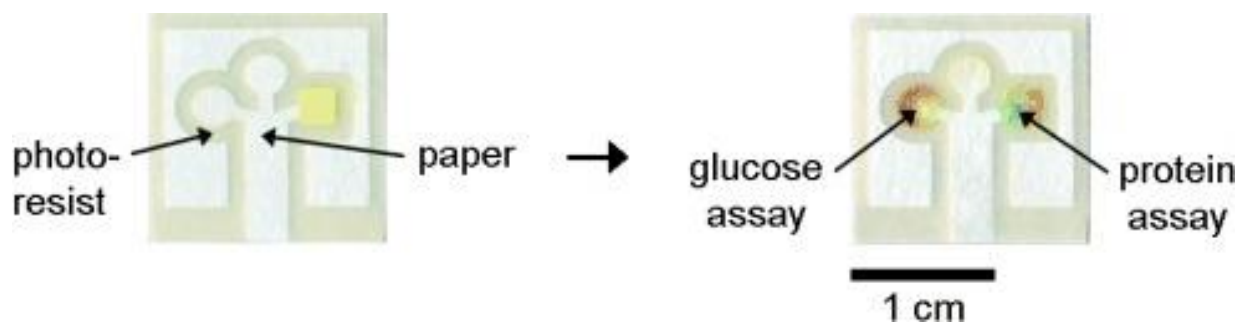


Figure 4.3. Multiplexed EPAD for detection of glucose and protein in urine.
EPAD device. Source: ⁶⁰

Depending on the desire test (analyte to read), the device fabrication can vary from the construction of a stack (vertical flow, Figure 4.2), barrier wall, and electrode to electrode surface modification using antibodies. Barriers are the most often used technique in EPAD fabrication process, it allows the discrimination of hydrophobic and hydrophilic areas to prevent the backflow of a solution and to allow reactions to be carried out in a specific zone or/and the flow of the sample in a determine channel. Fabrication of this modification can be performed by free-hand cutting, wet etching, or another equipment-based technique. Independently of the application, materials, deposition thickness and uniformity, device dimension, and space limitation parameters must be considered and optimized for optimal fabrication.

In terms of electrode assembly, a wide variety of materials can be used, and they contribute conductive, semi-conductive, or dielectric properties to the EPAD. The assembly of the electrodes can be done by several methods such as screen printing, inkjet printing, or pencil drawing onto desire area (hydrophobic or hydrophilic)³⁸⁵. The arrangement of the electrodes and paper device can be in 2D or 3D structures. In 2D structures, all the device (channels and sensors) is along a single flat strip. And in 3D, generally the electrodes and channels are assembled in different pieces of the substrate, which are stacked or folded during the measurement^{386,387}.

EPADs can be easily produced in various configurations thanks to the inherent properties of the paper material, including adjustable thickness, flexibility, and hydrophilicity. Moreover, the high roughness and porosity of paper substrates result useful to collect, store, separate, extract and concentrate the sample, facilitate the integrated operation of different assay steps, and improve the response of the electrochemical sensor³⁴¹. The substrate matrix fiber distribution reduces the effect of heat from convection of a fluid caused by random motion, vibration, turbulence, and heating³⁸⁸. Additionally, a stationary test can be easily transformed to a flow measurement by making the reagents flow across the sensor device. At the same time, EPADs provide a very convenient combination of sample pre-treatment and capillary passive self-pumping for fluid transport for self-powered hand-held electrochemistry commercial readers¹⁰⁸.

The current areas of interest for EPADs development include the improvement of the technologies available for paper and electrode fabrication and modification; the development of simple and low-cost mass fabrication methods that could lead to successful commercialization of these devices; and the design and fabrication of inexpensive miniaturized platforms of enhanced detection sensitivity³⁸⁹.

4.3.3. Paper-based PoC devices

Paper, as a substrate for the fabrication of flexible devices, offers a set of properties that are completely different from the properties of the plastics used in conventional flexible technology. It can be folded, unfolded, and creased for storage in small spaces or to form three-dimensional self-standing structures, it can be combined with micro-portable analytical devices or paper-based microfluidics, it can be easy handled to cut or fold, it can be porous or breathable useful for adhesive wearable applications, among others¹³⁶. For all of these properties, paper substrate has attracted more and more attention. For example, Abe et al.⁷⁶ in 2008, demonstrated an inkjet printing method for the fabrication of complete microfluidic

multianalyte chemical sensing paper, featuring microfluidic channels connecting a central sample inlet area with three different sensing areas and a reference area (Figure 4.4). However, until today, any paper-based PoC device has been reported. The main advancements on paper substrate have been done in the development of the electrochemical platforms.

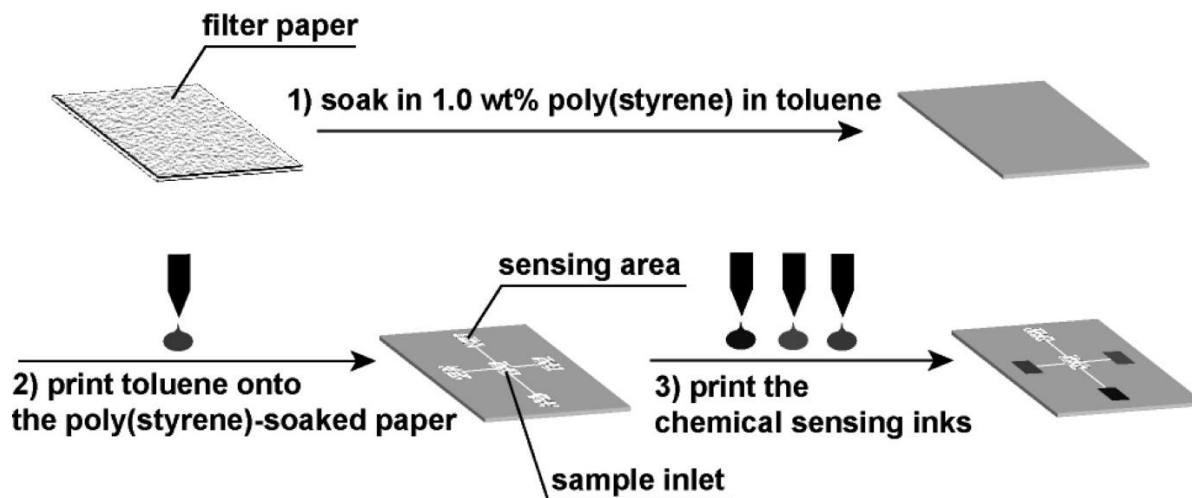


Figure 4.4. Schematic representation of the inkjet printed multianalyte device.

Schematic representation of the fabrication process of the inkjet-printed microfluidic multianalyte chemical sensing paper featuring microfluidic channels connecting a central sample inlet area with three different sensing areas and a reference area. Source ⁷⁶

Herein Inkjet printing is a promising approach to fabricate PoC devices on paper substrate, with the necessary electronic, conductive tracks, and sensors. Given the advantages of the inkjet printing technology, it has been used by many groups to develop printed electrochemical platforms on paper. For instance, in 2013 Määttä et al.²⁴² develop one of the first inkjet printed paper-based electrochemical sensors (Figure 4.5). They presented an inkjet printed three-electrode electrochemical platform on a multilayer-coated recyclable paper, with the WE, CE and RE. They printed the electrodes and conductive tracks, an AgCl layer was electrochemically deposited on the RE to achieve an Ag/AgCl RE, and a reaction well was formed on the paper platform using PDMS. They used the platform as a pH sensor, modifying the WE electrode with electropolymerized polyaniline. Furthermore, they also modified the WE with glucose oxidase to obtain a glucose biosensor. A fully inkjet printed paper-based electrochemical sensing platform was presented by Da Costa et al.¹⁰⁰, which consists of carbon nanotube-printed WE, RE, and CE on paper (unspecified). Also, an inkjet printed electrochemical non-enzymatic hydrogen peroxide sensor was presented by Shamkhalichenar and Choi ³⁹⁰, using carbon nanotubes.

Other researchers have contributed to achieve fully inkjet-printed paper-based sensors through present paper substrate modifications and suggesting another approach. Glavan et al.³⁹¹ describe a rapid, simple method for altering the surface chemistry of paper by treatment with organosilanes in the gas phase. Silane turns the paper hydrophobic, so resistant to wetting by the high surface tension liquids such as water, while it preserves all the other properties flexibility, rugosity, and porosity allowing the passage of gas as the untreated paper. Also, Zhang et al.³⁹² presented the same approach but using inkjet printing to print the silane on the desired area, making the paper hydrophobic just in the printed patterns. This approach allows to print inks almost with the same behavior of printing on plastic, because the substrate after the silane treatment behaves as a plastic substrate, in terms of printing resolution as no ink spreading is presented.

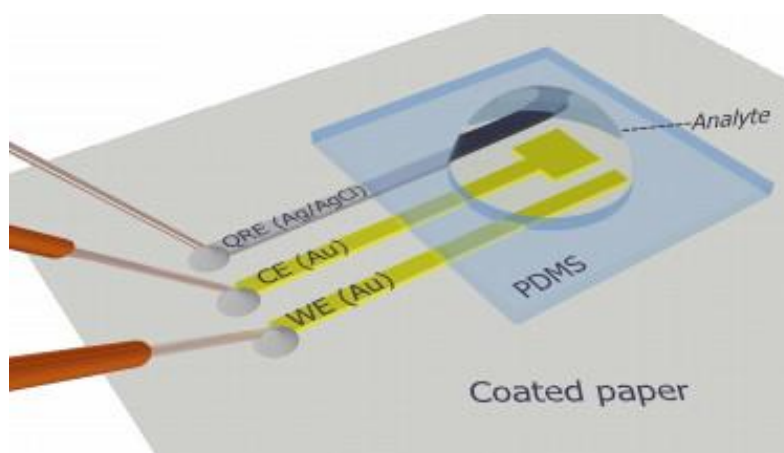


Figure 4.5. Schematic illustration of inkjet printed three-electrode platform.

A schematic illustration of the inkjet printed three-electrode platform with connected probes on the left and analyte solution droplet in the reaction well. Source: ²⁴²

With the developments above commented until this moment in the field of inkjet printed electrochemical sensors, it is easy to believe that in a near future hybrid PoC devices will be on research. These can be formed by a printed electrochemical sensor; the sample treatment can be done in the substrate itself and the reading can be done by a hybrid microfabricated potentiostat. However, all reported inkjet printed electrochemical platforms until today have downsides. They are made on coated paper, the electrode modification is made by other techniques, or the platforms are not fully inkjet printed (the dielectric or the RE, etc). A long path remaining to range but this is a young technology with a lot to exploit.

4.3.4. Publication III: Inkjet-printed Paper-based Electrochemical Sensors: Tuning Active Area through Surface Modification

The first paper presented in this Chapter, **Publication III**, is a submitted article about the development of a three-electrode electrochemical cell fabricated fully by inkjet printing on a porous paper substrate. The article is focused in four methodologies for treat the substrate in order to obtain conductive printed material on top. Different results are obtained from the four treatments, on all cases the three-electrode cell can be developed, however each electrode has a different active electrochemical area.

This article has been edited from the version submitted to Advanced Materials Technologies (edition consist in formatting and numbering figures, references, tables, and equations in accordance with the thesis manuscript, however acronym corresponds to the article):

Miguel Zea, Ana Moya, Rosa Villa, and Gemma Gabriela. **Inkjet-printed Paper-based Electrochemical Sensors: Tuning Active Area through Surface Modification**. Submitted

This work has been also presented in different conferences with their corresponding Proceedings:

- ❖ Conference **Transducer – Eurosenors XXXIII2019**: Miguel Zea, Ana Moya, Imad Abrao-Nemeir, Juan Gallardo-Gonzalez, Nadia Zine, Abdelhamid Errachid, Rosa Villa, and Gemma Gabriel. All Inkjet Printing Sensor Device on Paper: for Immunosensors Applications.
- ❖ Conference **Nano Today2019**: Miguel Zea, Ana Moya, Imad Abrao-Nemeir, Hamdi Ben Halima, Nadia Zine, Abdelhamid Errachid, Rosa Villa, Gemma Gabriel. Flexible inkjet printed device for detection of cortisol in Saliva.
- ❖ Conference **FLEX MEMS & SENSORS2020**: Miguel Zea, Ana Moya, Eloi Ramon, Gemma Gabriel. Development of inkjet printed biosensors on flexible and porous substrates. Oral Presentation.

Inkjet-printed Paper-based Electrochemical Sensors: Tuning Active Area through Surface Modification.

Miguel Zea^{a,b}, Ana Moya^a, Rosa Villa^{a,c}, Gemma Gabriel^{a,c,*}

^a Instituto de Microelectrónica de Barcelona, IMB-CNM (CSIC), Esfera UAB, Campus Universitat Autònoma de Barcelona, 08193, Bellaterra, Barcelona, Spain.

^b PhD in Electrical and Telecommunication engineering, Universitat Autònoma de Barcelona, (UAB)

^c CIBER in Bioengineering, Biomaterials and Nanomedicine (CIBER-BBN)

Keywords: Inkjet-Printed Electrodes, Real/Active Surface Area, paper substrate.

*Note: The supplementary information of this article can be found in section 6.2 (Figures and tables number with S of prefix are inserted there).

Abstract.

The need for portable, low-cost, disposable and faster analyses methods has pushed the fast growing of Point-Of-Care (POC) devices. Among the different types of POC, electrochemical paper-based analytical devices (ePADs) provide more reliable measurements, higher sensitivity and selectivity than single electrode detection or colorimetric paper-based sensors. Traditional fabrication methods are highly reported and show lacks in reliability and endurance. The need of disposable, simpler and accurate devices has opened a new research field that focusing on simpler fabrication steps and quantitative results. To achieve this, we propose the direct printing of three electrochemical electrodes using gold and silver inks, which are compatible with inkjet printing technology and paper substrate. Additionally, four strategies of the paper substrate are evaluated; printing the active elements directly on the hydrophilic bare paper, a hydrophobic gas-phase or a selective printed silanized paper, and a hydrophobic coating that blocks the surface porosity. Thanks to the ability of the inks to conform the cellulose fibers, the resulting working electrodes tune their electrochemical active area related to their substrate modification, showing higher active electrochemical area when the roughness is increased. The obtained peak currents (I_p) in the best case is 2.7-times higher than theoretical Randle-Sěvčik I_p for corresponding planar electrode. The fabrication approach presented here is highly suitable for the development of low-cost, eco-friendly, disposable, and flexible electroanalytical tools

4.3.4.1 introduction

Inkjet-printed based electrochemical sensors is a growing area of interest^{55,102,289} particularly for applications that require cost-efficiency, single use, and disposable sensors, even portable or wearable³⁹³. Inkjet printing (IJP) technology allows the digital deposition of functional materials in microscale dimensions on a wide range of substrates, simplifying iterative design changes during the initial development stages. It is a non-contact approach that allows the mask-less deposition of materials owing the precise control of picoliter volumes and saving the overall fabrication time and costs. Moreover, IJP also permits to have customized geometries and it is compatible with low temperature processes¹⁸⁶. Although screen-printed sensors are nowadays the most reported ones¹⁰², recent advances have demonstrated that inkjet-printed and paper-based electrochemical sensors provide a reliable solution for many applications^{100,393}.

Paper has emerged as a strong competitive substrate for diagnostic devices due to its attractive properties, including flexibility and conformability, hydrophilicity and high mechanical strength^{394–397}. These excellent characteristics allow paper to possess excellent performance for the fabrication of paper-based devices. Meanwhile, it is environmentally friendly, reusable/recyclable at any extent, biodegradable and biocompatible^{396,398–400}. This makes that paper-based sensors are increasingly gaining attention due to the global trend and compromise around the “green electronics”. Thereby, paper offers a flexible, disposable, and low-cost solution to develop sensors by IJP technology.

Paper-based analytical devices (PADs) are in the spotlight to develop flexible, disposable, and simpler devices taking advantage of their microfluidic properties^{379,401}. PADs typically include an arrangement of hydrophilic/hydrophobic microstructures patterned in the paper using techniques such as wax printing, photolithography or chemical vapour-phase deposition among others.⁴⁰² PADs in combination with all the advantages of an electrochemical sensor (ePAD) was demonstrated in 2009 by Dungchai *et al.*⁴⁰³ showing more reliable measurements than single microelectrode detection or colorimetric PAD sensors⁴⁰⁴. Electrochemical detection is an attractive alternative detection scheme for paper-based microfluidics due to its small size, portability, low cost, high sensitivity, and high selectivity by proper choice of detection potential and/or electrode material⁴⁰³. Therefore, their use in many applications such as; biomedical, environmental, clinical analysis, food processing, and chemical industry fields has highly increased^{404–407}.

Different strategies have been used up to date trying to integrate electrodes on paper substrate^{403,408–410}. First works obtained ePADs with materials such as carbon, silver (Ag) and gold (Au) printed on paper^{403,410} usually by screen printing. Later microelectrodes were first fabricated on a separate paper substrate and then integrated on the final paper substrate^{408,411} trying to improve the sensitivity of the system. Ko *et al.* fabricated an electrochemical sensor by printing a carbon nanotube conductive ink on printed electrodes using a commercial office inkjet printer³⁶⁴. Li *et al.* in 2016 designed an origami paper-based analytical device to electrochemically detect glucose, they directly wrote the electrodes on paper by pencils⁴¹².

An important parameter for use electrochemical sensors is the effective electrochemical active area. This parameter can be determined by methods based on charge transfer either diffusion controlled or not controlled by diffusion. These methods are based on cyclic voltammetry (CV) and electrochemical impedance spectrometry (EIS)⁴¹³. The determination of the electrochemical active area has been object

of many researches using different oxide species to study its mass transport and adsorption on electrode surface area^{413–416}.

The motivation of this work is to study different strategies to develop a full inkjet-printed sensor on flexible and porous paper substrate. All of them represent valuable alternatives and efficient fabrication methods using available commercial inks that can be easily printed and sintered at low temperature. The electrochemical sensors incorporate the three active elements (counter, working, and reference electrode) to perform electrochemical-based measurements. The printing of conductive inks directly onto the porous substrate is not straightforward and must be studied in order to avoid short circuits and a non-defined electrode area. In this work we want to explore and compare different approaches of modifying the surface of the paper for obtaining conductive patterns, and to study how these modifications directly affect the active area of the working electrode (WE) of the electrochemical sensor. Specifically, the main objective is to study the wettability modification of the paper and the porosity sealing before the fabrication of the electrochemical sensor. In order to print the inks on the substrate, four different hydrophilic-hydrophobic approaches were evaluated which at the end allow obtaining four different electrochemical active areas, which fundamentally affects to the final sensor performance, sensitivity and response time. The ability to tune the electrochemical active area allows to move the IJP technology several steps forward in the fabrication of electrochemical devices, increasing sensitivity and adjusting response times. Two of the four fabrication routes proposed here are fully printed steps by IJP, which is very attractive due to the low-cost characteristics as pave the way for the development of disposable devices in a broad range of applications. The development of this technology will allow the direct access of reliable easy-to-use diagnostic tests.

4.3.4.2 Experimental Section

4.3.4.2.1 Chemical and Materials.

For the development of the microelectrodes, three commercially available inks were used. A low-curing Au colloidal ink (DryCure Au-J 1010B from Colloidal Ink Co., Ltd, Japan), a Ag nanoparticle ink (Dupont-PE410 from USA), and a dielectric photoresist SU-8 ink (SU-8 2002 from MicroChem, USA). For the formulation of the silane ink, it was used 1H,1H,2H,2H-perfluorooctyltriethoxysilane (POTS from abcr, Germany) as hydrophobic precursor, tetraethyl orthosilicate 98+% (TEOS from Merck), ethanol absolute, HCl and water. The above mentioned inks are all specifically formulated for the use of the drop-on-demand inkjet technology, concretely a piezoelectric Dimatix Material Printer (DMP2831

from FUJIFILM-Dimatix, Inc., USA). Whatman® cellulose paper grade 1 (WHA3001861 from Merck) with a thickness of 0.18 mm, porosity of 0.686, and pore diameter of 11 μm was used as substrate.

Ethanol, Phosphate buffered saline (PBS), potassium nitrate (KNO_3), potassium hexacyanoferrate (III) ($\text{K}_3[\text{Fe}(\text{CN})_6]$), potassium hexacyanoferrate(II) trihydrate ($\text{K}_4[\text{Fe}(\text{CN})_6]$), hydrochloric acid (HCl, 1M) and potassium chloride (KCl), all from Merck (Spain) were used as received.

4.3.4.2.2 Silane ink formulation.

The silane ink used as hydrophobic precursor was prepared following previous report^{392,417} optimizing it for its use in the piezoelectric printer. It contains 24 mL of ethanol, 2 mL of water, 3 μL of HCl 1M, 1 mL of TEOS and 1.5 mL of POTS. First the ethanol, water and HCl are stirred for 1 minute. With a continuous stirring TEOS and POTS are added and kept stirring for 24 hours at ambient temperature.

4.3.4.2.3 Fabrication of PADs by inkjet printing.

The fabrication process is visually described in Figure 4.6. It can be separated in two major steps; the first one is the paper treatment (Figure 4.6a), which prepares the substrate to receive the conductive inks, and the second one (Figure 4.6b) is the printing of the electrodes structures. Printing patterns were designed using CleWin 5 software, which .dxf file was imported with the Dimatix Bitmap editor. The three-microelectrodes array consists of a Au WE, a Au counter electrode (CE) and a Ag pseudo-reference electrode (pRE). The dielectric SU-8 ink was used for the tracks passivation and to define the electrode area, obtaining the final device.

The *paper treatments* (Figure 4.6a) here proposed have been thought to achieve a hydrophobic o blocked surface of the paper. Three methods were selected (vapour-phase silanization, printing silane and printing of a blocking primer layer) and then compared with the untreated paper. The bare paper was used as received (a.i) and was only cleaned with a nitrogen gun. The vapour-phase silanization reaction (a.ii) was performed in a vacuum chamber at 95 °C using 500 μL of POTS in a beaker to supply the silanization reagent in the vapour phase. Sample was leaved in the vacuum chamber for 15 minutes to allow proper reaction of POTS with the sample. This time and temperature depend on chamber and sample size, so the process here described it is useful for the silanization of an area $\pm 200 \text{ cm}^2$ of paper in a chamber of 2.6 L. The reaction occurs readily with the silanizing agent in the vapour phase and requires no sophisticated equipment apart from a low-pressure chamber and a source of heat. The entire

process is described by Glavan *et al.*³⁹¹ Another method to get the substrate hydrophobic is printing a specially formulated silane ink directly to the paper obtaining a homogeneous printed film (a.iii). The silane ink was filtered by 0.22 μm syringe filter and 2 mL were loaded into printer cartridge that has 10 pL nominal drop volume printheads having 16 nozzles each with a diameter of 21.5 μL . The silane ink was inkjet-printed onto the desired areas of the paper where the sensors will be placed through 1 to 3 printing passes (layers), with a separation between drops (drop spacing, DS) in X and Y axis of 10 μm . Finally, inkjet-printed silane layer was heated in an oven at 100 $^{\circ}\text{C}$ for 1h to evaporate the solvents. The fourth strategy was the printing of SU-8 primer layer (a.iv) on the paper substrate in order to selectively seal the porosity where the sensors will be placed obtaining a smooth and non-porous surface⁴¹⁸. The primer layer was locally inkjet-printed on desired area through 1 to 6 printing passes (layers) with a DS of 15 μm , blocking the minimal paper area in order to not affect the properties of the paper substrate. The curing of the SU-8 was done by UV treatment for 30 s. With this strategy a conductive flat material can be obtained after the printing of the primer layer³¹ (Figure 4.6a.iv).

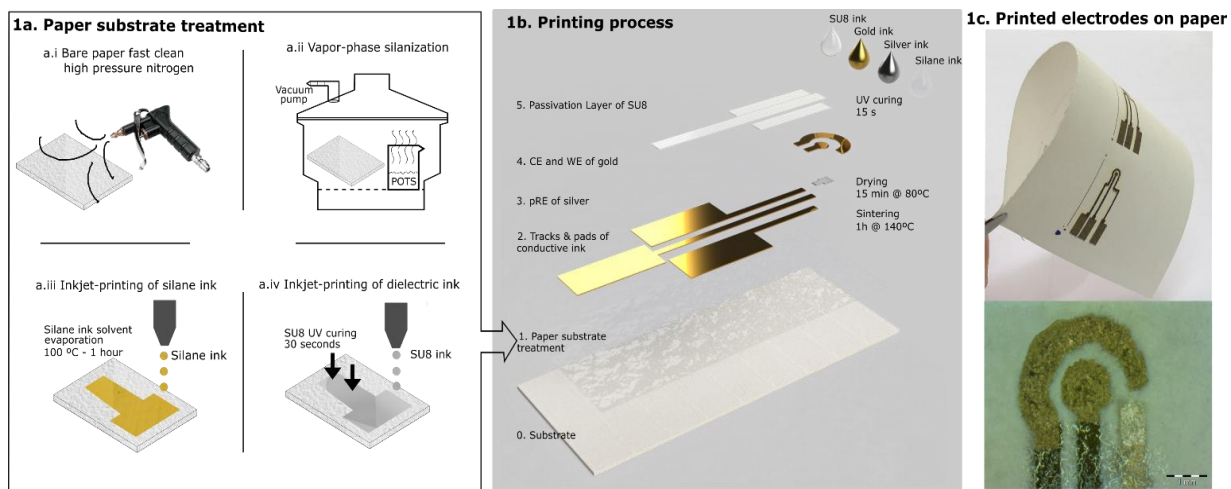


Figure 4.6. Fabrication process of a paper-based inkjet printed sensor.

Fabrication process of the electrochemical sensor on paper. 1a) Schematic treatments proposed over the bare paper: cleaning the bare paper (i), vapour-phase silanization performed in a vacuum chamber (ii), inkjet-printing of a formulated silane ink (iii), and inkjet-printing of the dielectric SU-8 ink (iv). 1b) Simplified manufacturing steps illustrating the printing of Au WE and CE electrodes, and Ag RE, 1c) Photographs of the printed Au and Ag electrodes on the porous flexible Whatman paper.

The second step is the *IJP process* of the microelectrodes (Figure 4.6b). Two individual ink cartridges were filled with one of each metal-based ink (Au and Ag). Optimization of the IJP process was done as we previously reported^{31,55}. The first step was the IJP of the Ag pRE of 600 x 600 μm^2 (a geometric

surface area (GSA) of 0.36 mm²) with a DS 20 μm and dried at 80 °C for 15 min. Au WE of 1 mm diameter (GSA of 0.785 mm²), CE (with a geometric area > 3.14 mm²), tracks and pads were inkjet-printed using a DS of 15 μm. Then, both inks were thermally dried at 80 °C for 15 min and then sintered in an oven at 140 °C for 1h. Afterwards, another cartridge with SU-8 ink was used to inkjet-printed in order to define the microelectrodes area and to insulate the tracks for connections with DS of 15 μm, then cured using a UV lamp for 30 s. Finally, two post-process steps were required. First, the RE was chlorinated by CV in 0.1 M HCl, scanning potential from 0 to 0.2 V against Ag/AgCl commercial reference electrode (RE) (Metrohm, Germany) and Pt CE (Metrohm, Germany) at 20 mV/s to obtain a stable pRE. Second, the Au WE was electrochemically activated by differential amperometric pulses voltammetry (5 pulses of 5 s from 0 to -0.2 V) in PBS. Both processes were performed using an 8-channel potentiostat 1030A Electrochemical Analyzer (CH Instruments, USA).

4.3.4.2.4 Substrate characterization.

The characterization of the surface energy of each treated substrate was performed by measuring the water contact angle (WCA) system (DataPhysics Instruments, Germany) at room temperature (20 °C) using a 4 μL deionized water droplet as the liquid probe. A morphological characterization of the papers was made by scanning electron microscopy (SEM, Auriga-40 from Carl Zeiss, Germany) and optical microscopy (DM4000M LEICA, Germany).

4.3.4.2.5 Electrical characterization.

The conductivity of the different Au and Ag inks was determined on the different proposed paper treatments, evaluating the effect of each treatment and the number of printed layers. For each substrate, we inkjet-printed Van der Pauw structures from 1 to 3 layers of the metallic inks in order to know the sheet resistance by a 4-points technique using a Hewlett Packard HP4155 Semiconductor Parameter Analyzer connected to a manual probe station PM5 (Süss Microtec GmbH, Germany).

4.3.4.2.6 Electrochemical characterization.

After chlorinated the pRE, potential stability was evaluated by potentiometry technique in KCl 3M against a commercial Ag/AgCl reference exhibiting good stability with low drift⁴¹⁹. After WE activation, CV at 25 mV/s in ferro/ferricyanide (5 mM) were carried out on the electrodes to compare the electrochemical properties against external RE and CE, and internal pRE and CE.

4.3.4.2.7 Active area determination.

The electrochemical active areas of the electrodes were calculated running CV at different scan rates from 5 mV/s to 1 V/s (5, 10, 25, 50, 75, 100, 200, 500, and 1000 mV/s) in ferro/ferricyanide to obtain peak current values (I_p). The electrochemical active area was calculated using Randles-Sěvčik equations for reversible electrochemical process^{414,420}. In addition, the electron transfer kinetics was studied using Matsuda and Ayabe approach. It was measured the electron transfer rate constant from the $\Delta E_p - \text{Log}(v)$ ^{421,422}.

4.3.4.3 Results and Discussion

In this work, Whatman Grade 1 has been chosen as the most extensively paper substrate⁴²³ for microfluidic sensing platforms in a wide range of applications such as clinical analysis, healthcare, agriculture, food industry, and even air pollution monitoring⁴²⁴⁻⁴²⁷. In addition of using the bare paper as a substrate, three different methods are compared to allow us to develop conductive layers on top of it. Each one of these methods changes the hydrophilicity and roughness properties of the paper allowing tuning active electrochemical area depending on the treatment.

4.3.4.3.1 Characterization of the wettability of treated papers.

The development of an electrochemical inkjet-printed sensor on paper is not straightforward due to its intrinsic high roughness and high porosity. Although cellulose is an insulator material, it has a modulable hydrophilic property as it allows the penetration of aqueous liquids within its fiber matrix. The surface wettability, indicated by the hydrophilic or hydrophobic nature of the substrate, is very important to be controlled because it determines the final resolution and quality of the printed patterns⁴²⁸. On a hydrophilic substrate, the generated droplets spread after deposition resulting in larger sizes than the original designed size⁴²⁹.

Whitesides group introduced to the scientific world the electrochemical paper-based devices⁴³⁰ in 2007 using wax. Wax in this work has been excluded due to the need of the sintering process after the wax pattern. Alternatively, silane is a strategy that enables to grow a monolayer of hydrophobic material onto the paper substrate. This layer gets the paper hydrophobic and help to obtain uniform lines of ink on the surface^{431,432}. Furthermore, this method is simple, low-cost, and fast. The bare paper is compared in this section with two hydrophobized papers treated with POTS (one printed and the other vapour-phase

silanization reaction) and a blocked paper treated with SU-8. POTS is a fluorinated alkyl silane (see Figure S1 in the Supplementary Information) that is mostly used for improving the wettability of the substrate by lowering the surface energy. It facilitates a superhydrophobic coating by enriching the surface with CF_3 groups and a WCA above 150° ⁴³³.

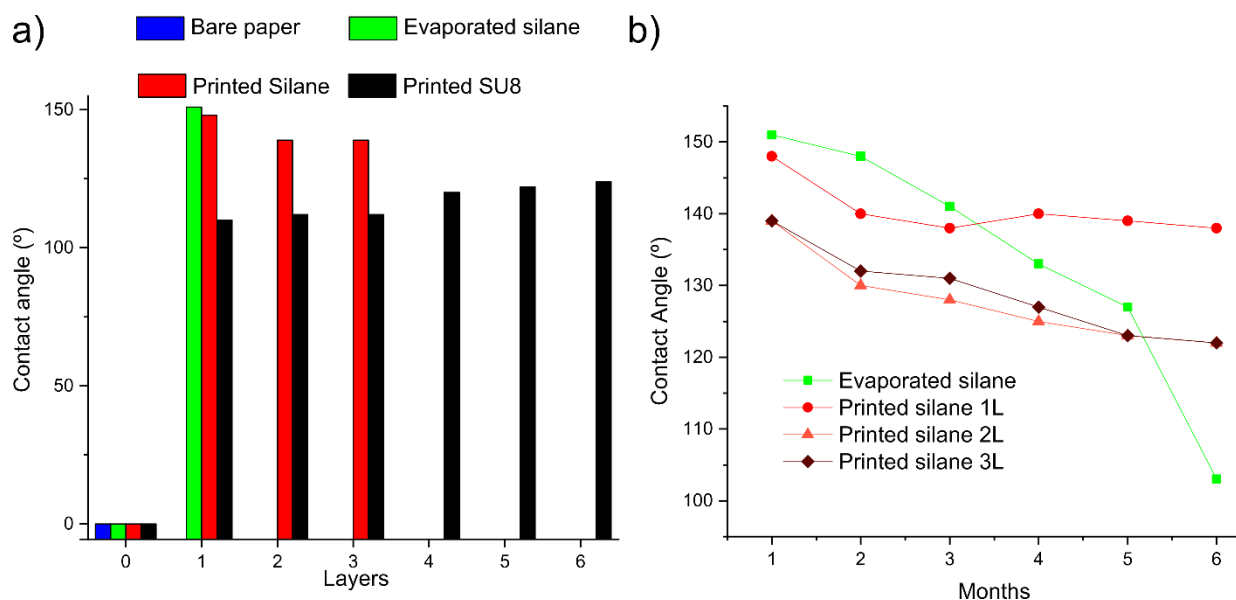


Figure 4.7. Water contact angle study on treated paper.

a) Static WCA measurements of water droplets on bare paper, gas-phase silanized paper, 1 to 3 layers of printed silane and 1 to 6 layers of printed SU-8. b) WCA stability of hydrophobic surface upon 5 months of silanized surface.

The surface wettability of the paper is one of the critical parameters to characterize after a hydrophobic treatment and it is typically characterized by the contact angle technique. While contact angle decreases (hydrophobicity decreases) hydrophilicity and so the wettability increase. Figure 4.7 depicts the static distilled WCAs (corresponding optical images are shown in Figure S2 in the Supplementary Information) measurements that were performed after each paper treatment method. As expected, the bare paper WCA is 0° due to the hydrophilic properties of this filter paper substrate. SEM images (Figure 4.8) of treated and untreated papers were also taken to study the morphological changes after each treatment. As shown in Figure 4.8a, the bare substrate, Whatman paper Grade 1, has a pore size around $10 - 20 \mu\text{m}$. It can be easily appreciated an intrinsic porous and fiber mesh structure that explains its medium retention and flow rate behavior.

Gas-phase silanization is the first chosen treatment because, as it does not modify the roughness of the paper, leads to a maximum active surface area, and consequently it can be used as a control method. WCA measurement for the evaporated silane is $151 \pm 0.5^\circ$ ($n = 3$), which means that the organosilane successfully reacts with the hydroxyl groups of cellulose paper surface to turn it superhydrophobic. WCA results agree with the ones found by Glavan *et al.*³⁹¹ SEM images of gas-phase silanized paper (Figure 4.8b) show no structural changes due this non-contact process, however it can be appreciated a nanostructured roughness on the fibers that may be responsible of the hydrophobic property as suggested by Zhang *et al.*³⁹². The procedure is simple because it does not require pre- or post-treatment steps and it is completed within minutes. However, this silanization methodology transforms the entire substrate into hydrophobic removing the hydrophilic properties of paper that can be used for example as filter or microfluidics. The only way to avoid an entire hydrophobization is the use of a mask, nevertheless, as the silanization is a colorless process, it becomes difficult to align on top of it.

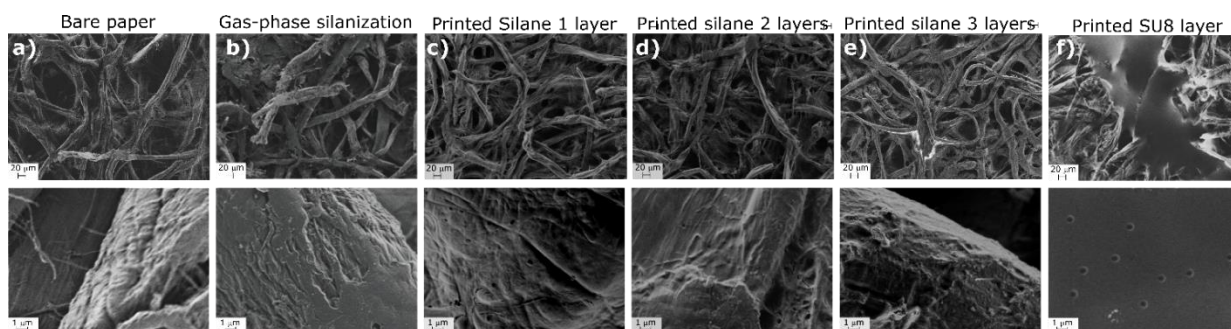


Figure 4.8. SEM images of paper treatments.

SEM images at two magnifications of (a) bare paper, (b) paper modified with vapour-phase silanization, and (c) 1, (d) 2 and (e) 3 layers of printed silane ink and (f) blocked paper with 6 layers of primer SU-8 line.

Alternatively, we propose to form a hydrophobic coating using IJP technique by a specifically formulated POTS silane ink, which avoids the difficult process of using a mask, allows the precise deposition of the ink in the desired pattern, and requires less material consumption. The first approach of printing a silane solution was reported by Zhang *et al.*³⁹² They used a hydrophobic precursor to develop Janus superwetting papers for the patterning of microfluidic channels in a paper-based analytical device. Using the same principle, we printed from 1 to 3 layers of the proposed silane ink. WCA measurements ($n = 3$) were $148 \pm 2^\circ$ for 1 layer, $140 \pm 0.5^\circ$ for 2 layers and $140 \pm 0.5^\circ$ for 3 layers. Measurements indicate that the printed silane layers successfully lead to a hydrophobic functionalization of the paper. The WCA decrease in the case of 2 and 3 layers could be explained by studying both sides of the paper. One silane

layer leads to the printed side of the paper hydrophobic, remaining the other one hydrophilic. However, 2 and 3 silane layers leads to both sides of the paper hydrophobic (picture shown in Figure S3 in the Supplementary Information). This can be explained by the small drop volume dispensed (10 μL) and the time printing process. Less silane ink leads to a more rapid evaporation of solvents remaining the silane mostly on the top half of the paper. While for 2 and 3 layers, the printing process is longer in time and the accumulated quantity of silane ink entail to the penetration of ink through the substrate leading to both sides hydrophobic, and so, the WCA is slightly decreased. Notably for printed silane (Figure 4.8c, d, e) the nanostructured roughness can be also appreciated, differences between layers of printed silane are hardly noticed in SEM images due the spread of the ink inside the substrate.

Another method to get a surface hydrophobic is using the concept of a printed primer layer to partially seal the substrate porosity allowing the deposition of smooth layers on top of it as demonstrated in our previous work of Moya *et al.*³¹ In this case, the dielectric SU-8 ink is chosen. Using the same principle, we evaluated the printing of several layers of SU-8 on the paper. The WCA of printed SU-8 from 1 to 6 layers were measured obtaining results from $110 \pm 10^\circ$ to $124 \pm 0.6^\circ$ respectively. These values demonstrate that from the first printed SU-8 layer a hydrophobic surface is formed, however a great WCA deviation is observed. A water droplet deposited on the top of paper covered with one SU-8 layer is quickly absorbed due to an incomplete covering of paper fibers. To allow a complete blocking of the porosity and to obtain a higher WCA with lower deviation, several layers of SU-8 were printed on top the previous one, finally getting a minimum deviation for the case of 6 layers. This can be easily understood by observing the SEM topographic pictures. As can be seen in Figure 4.8f, a line of 200 μm width printed with 6 layers already blocks the porosity of the paper and the surface of the printed area is almost smooth, which allows the drop water to remain stable on the sealed paper. It has been found that the WCA of 6 layers of SU-8 is comparable with the one on polyethylene terephthalate (PET) substrate⁴³⁴. The number of printed SU-8 layers could be decreased by increasing the DS. The selected DS for SU-8 was 15 μm , which means a 1693 dot per inch (dpi), and it was chosen as the minimum one that allows enough resolution to obtain well-defined structures. Lower DS, slows down the printing process, which entails longer printing time between the printing and the curing steps, which causes scattered patterns as the ink has more time to penetrate into the paper⁴¹⁸. As it has been previously observed increasing printing layers of SU-8 leads to a more homogeneous film of metallic inks that are going to be on top and decreases sheet resistance of printed patterns⁴³². The electrical characterization will be further discussed in the electrical characterization section

Evaluation of the Surface Coatings Durability. Additionally, a stability test of the different treated papers was done to evaluate the durability of their hydrophobicity. Samples were stored in the dark, with no controlled temperature and humidity conditions. Regular static WCAs were measured for 6 months (Figure 4.7b) to observe the evolution of the surface coatings. The printed SU-8 and printed silane treated surface remains hydrophobic for six months with inevitable losses. In the case of the gas-phase silanized paper, WCA values stay above 93% of the original value for the first three months, then it continues degrading until it reaches 66% of the initial value after 6 months. This phenomenon responds to the oxidation of the silane that induces the degradation of hydrophobic surface. The printed silane inks suffer a lower degradation in comparison with the evaporated ones. One layer remains over the 93% of initial WCA value and above 87% for 2 and 3 layers. Degradation of printed silane is proportional in all three cases, however for one layer is lower. This could be explained due to a fastest drying process for one layer as more silane ink remains on the cellulose fiber surface. On the other hand, 2 and 3 layers drying process allows the ink to spread along the substrate.

Experimentally is demonstrated that the oxidation of the printed silanes does not impact as much as the evaporated ones, and this must be related with the amount of silane deposited in the surface. From the stability point of view, and even taking into account the overall decrease in the WCA over time, the substrates remain hydrophobic for almost half a year, thus demonstrating that the manufacturing method for the substrate treatment is highly stable.

Roughness is a direct metric of surface topography, and the wettability is a direct measure of surface chemistry. According to above presented modifications we face the electrical characterization on 4 types of substrates: 1) the bare paper that is rough and hydrophilic; 2 and 3) the gas-phase silanized paper and the 3 layers of printed silane that are rough and hydrophobic, 4) the blocked paper with 6 layers of SU-8 that is planar and hydrophobic.

4.3.4.3.2 Printing of the conductive inks onto treated and untreated paper.

The printing behavior of metal-based inks on top of the bare paper and the several treated papers was studied. One, two and three layers of the Ag and Au conductive inks were printed in Van der Pauw structures of $4 \times 4 \text{ mm}^2$ over the several proposed substrates⁴³⁵. These structures were printed on the four paper substrates at same condition of resolution (DS $15 \mu\text{m}$ for Au ink, and $20 \mu\text{m}$ for Ag ink), the patterns were dried 15 min at $80 \text{ }^\circ\text{C}$ and sintered 1 h at $140 \text{ }^\circ\text{C}$. The ink penetration in the proposed

paper substrates did not allow measuring the thickness of each layer, so this section is based on sheet resistance values comparison as we are unable to calculate the final conductivity of the inks on paper and compare them to bulk materials. Cross-section optical images of Au ink printed on bare paper and SU-8 coated paper are shown in Figure S4 in the Supplementary Information, demonstrating the difficulty of measuring the layer thickness of the inks on these type of substrates.

Firstly, sheet resistance of Au and Ag inks on SU-8 was evaluated as wettability studies were not conclusive to determine the optimum SU-8 number of layers. Figure S5 in the Supplementary Information shows the measured sheet resistance versus the number of layers for the Au (S5a) and Ag (S5b). Au has a particular behaviour; 1, 2 and 3 layers exhibit a very similar electrical behaviour, and the same occur with 4, 5 and 6 layers. Printing 3 Au layers over SU-8 obtained reasonable sheet resistances values independently of the number of SU-8 layers, ranging from $4.3 \pm 0.75 \Omega/\square$ over 1 SU-8 layer to $1.2 \pm 0.3 \Omega/\square$ over 6 SU-8 layers. On the other hand, Ag ink on SU-8 presented sheet resistance values of $0.03 \Omega/\square$ starting from a single layer of Ag, but at least 4 layers of SU-8. Being ideal sheet resistance values less than $1 \Omega/\square$ compared with a common PET substrate⁵⁵, we decided to work with 6 layers of SU-8.

Figure 4.9 shows the measured sheet resistance values versus the number of Au (Figure 4.9a) and Ag (Figure 4.9b) layers on bare paper, vapour-phase and printed silanized paper, and on 6L SU-8 printed paper. One Au layer shows higher resistance than subsequent layers, ranging from $40 \pm 5 \Omega/\square$ on printed silane to $2510 \pm 200 \Omega/\square$ on bare paper. The sheet resistance decreases considerably printing a second layer, from $4 \pm 1.2 \Omega/\square$ on bare paper to $15 \pm 2 \Omega/\square$ on SU-8. A third layer of Au ink led to a further decrease in sheet resistance meeting in the 4 treatment-cases around $1.2 \pm 0.3 \Omega/\square$. The Au ink follows the same behaviour as observed in our previous works³¹ over SU-8, the increasing thickness of metallic ink decreases the sheet resistance, and also an improvement on the reproducibility of the resulting conductivity. So, 3 layers of Au ink achieve reasonable conductivities, reaching values from $1.20 \pm 0.34 \Omega/\square$ to $1.34 \pm 0.27 \Omega/\square$.

In the case of Ag, sheet resistance values follow the same behavior as for Au ink on bare paper and the gas-phase and printed silanized paper. Two layers of Ag are enough to achieve values lower than $1 \Omega/\square$ over all the paper treated substrates, reaching values from $0.17 \pm 0.0051 \Omega/\square$ to $0.5 \pm 0.015 \Omega/\square$. On the other hand, Ag printed on 6L of SU-8 has sheet resistance values around $0.015 \pm 0.005 \Omega/\square$ since

the first printed layer. These good conductivity values allow us to work with 2 layers of Ag ink over all the paper substrates.

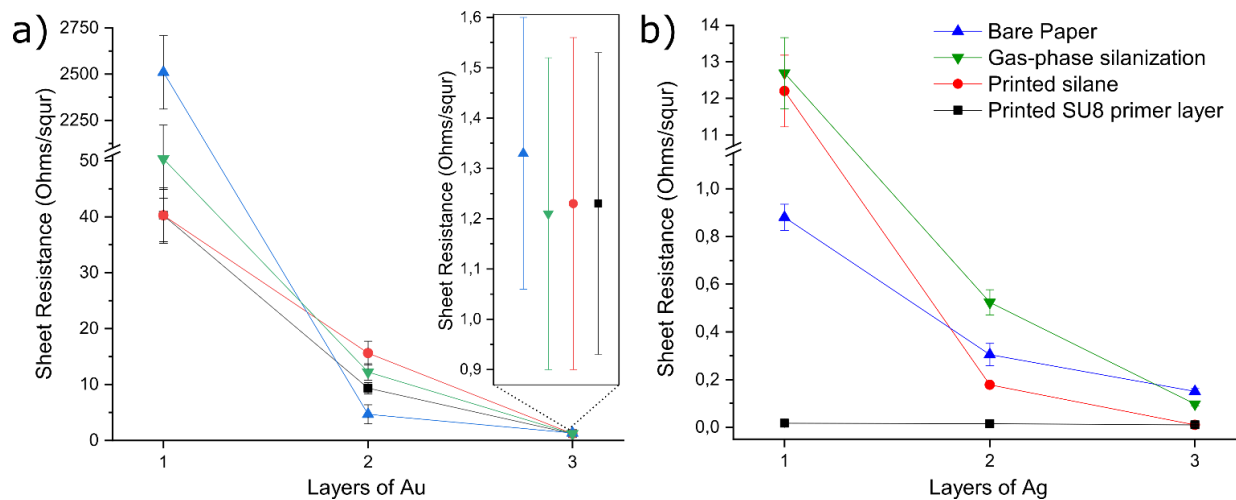


Figure 4.9. Electrical characterization of metallic inks on paper.

Evolution of the sheet resistance measurements calculated from Van der Pauw structures against the different number of layers of Ag (a) and Au (b) ink on bare paper, vapour-phase silanized paper, silanized printed paper and blocked SU-8 paper.

4.3.4.3.3 Printing process on treated paper and morphological characterization.

An electrochemical three electrode system was used for the development of the sensors following the fabrication procedure described in the experimental section. In particular, the sensors evaluated here have a WE diameter of 1 mm. Our efforts have focused on determining the optimal printing conditions to form a highly conductive layer on the proposed substrates. However, and given the sheet resistance values found in the previous section, it was decided to print on the different substrates, using the same conditions. To summarize, 3 layers of Au and 2 layers of Ag were selected as the resulting sheet resistances of about 1.2 and 0.1 Ω/\square respectively allow to print any electrical patterns with good conductivity. The electrodes (WE and CE) were printed with Au, and only the RE area was printed with Ag. The SU-8 primer ink and the silane ink were printed on the paper to selectively modify the hydrophobic properties only in the sensors area.

As the fabrication procedure for all selected substrates follow the same printing steps and curing procedures, the WE are comparable among them. So, the possible variations observed of the electrochemical behaviour can be directly attributed to differences of the effective active area of the WE that depend on the roughness and porosity of the respective substrates observed.

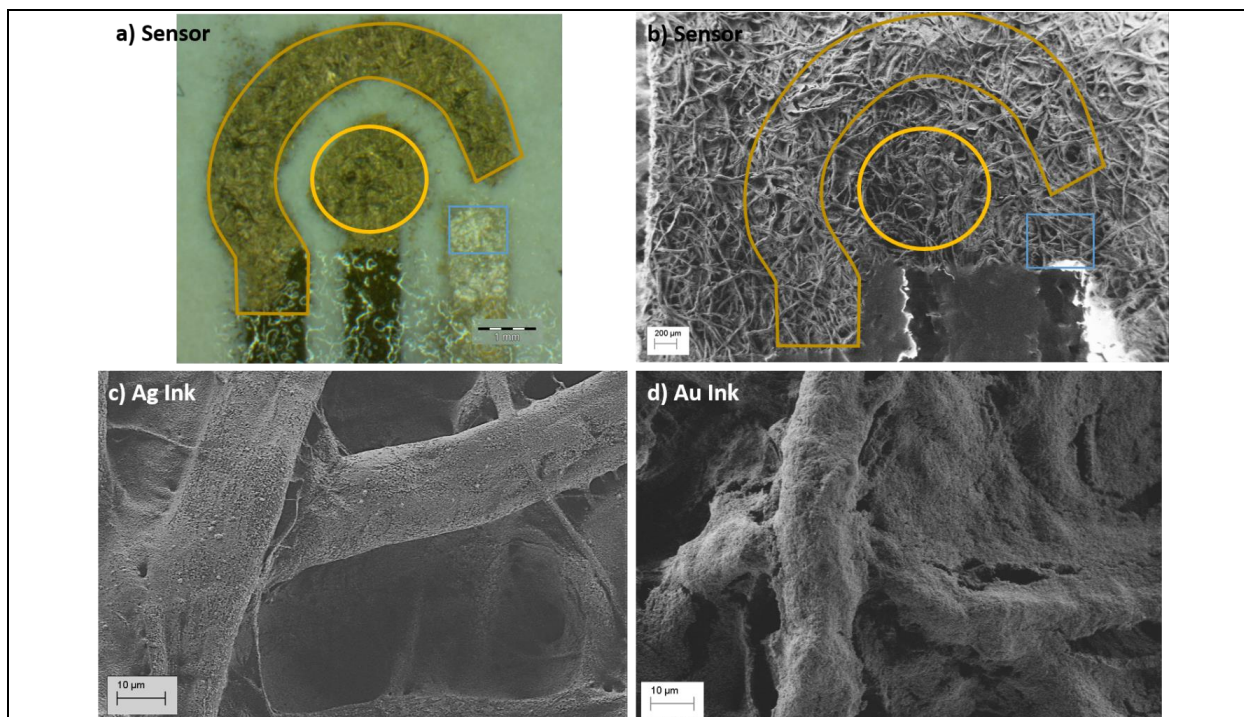


Figure 4.10. Optical characterization of inkjet printed patterns on paper.

(a) Optical, (b) SEM image of the printed sensor on bare paper highlighted in yellow the limits of the WE and CE printed with gold and in blue the RE printed with Ag. SEM images of Ag (c) and Au (d) coating on bare paper, with the formation of a three-dimensional (3D) network of metallic conductive material.

Figure 4.10 shows optical and SEM images of Au and Ag printed patterns onto bare paper substrate after printing the sensor. The limits of the WE, CE and RE patterns have been highlighted in the optical image (a) and the corresponding ones have also been highlighted on the correspondingly SEM image (b). The metallic conductive features can not be observed at low magnification under SEM microscopy, however, it is possible to see the presence of the dielectric SU-8 that delimits the electrode area as a brilliant feature on the bottom part of the picture (transparent in the optical image), and this allows to properly locate the different electrodes. The presence of Ag (c) and Au ink (d) are observed at higher magnifications, and they show how the ink coatings conform the cellulose fibers, a typical phenomenon that is observed for electrically conductive polymeric coatings on textile fibers⁵⁴. The inks are able to form a three-dimensional (3D) network on the cellulose fibers, which allows to explain the enhanced mechanical stability and flexibility that the final device have. However more solid content is appreciated for the Au ink (d) as it is necessary three layers to achieve good conductivities, and this produces accumulation of the ink and the apparition of small cracks. The same behaviour is also observed in the silanized paper substrates.

4.3.4.3.4 Electrochemical characterization of printed three array electrode.

The electrochemical reversibility of the WEs was assessed by CV using the equimolar 10 mM electrochemically reversible hexacyanoferrate (III/II) redox couple $[\text{Fe}(\text{CN})_6]^{3-} + e^- \leftrightarrow [\text{Fe}(\text{CN})_6]^{4-}$. Figure 4.11a shows the voltammograms obtained for the Au microelectrode printed directly on the bare paper. This response was greatly improved after an electrochemical activation step, since no significant cathodic or anodic peaks was observed before it. After WE activation peaks were well defined according to a reversible redox process, and ΔE was decreased to 85 mV, closer to the theoretical 59 mV for a single electron transfer on a perfect Au surface^{436,437}. The larger ΔE values can be caused by layer holes and cracks that are observed in the SEM pictures of the Au ink over the cellulose fibers of the paper, and also by surfactants or solvents that are still remaining after the drying and sintering process⁴³⁸. As can be seen, the electrochemical activation is essential to have a good electrochemical performance of WE. An external configuration with commercially available RE and CE electrodes was used to compare the integrated printed pRE and CE (Figure 4.11b). The integration of the CE (black line), as expected, does not produce any change in the measured potential. On the other hand, the integration of the pRE (blue line) produces a potential shift of 95 mV attributed to the absence of the chloride solution present in a double layer Ag/AgCl RE. This behavior was also observed for all the 4 treated paper substrates (data not shown).

The electrochemical characterization in ferro/ferricyanide of printed WEs on 4 treated papers cases with the CE and pRE integrated microelectrodes are compared in Figure 4.11c. All cases show a well-defined voltammogram denoting good reversibility, however peak current decreases in the cases of the coated paper with the silane and SU-8 ink as can be seen in Table 4-1. Electrochemical results of printed electrodes on paper.. Figure S6 in the Supplementary Information shows the main electrochemical response of a 1 mm diameter Au WE printed on a planar PET substrate used in this work for comparison purposes. These data have been added to Table 4-1. Electrochemical results of printed electrodes on paper.. There is a clear relationship between the intrinsic roughness of the paper substrate and the anodic (I_p , indicating that an increase of the roughness allows a higher real electrochemical surface area. As the roughness of the substrate increases the active electrochemical area also increases, for this reason the inkjet-printed WE on bare paper substrate shows, as expected, the highest I_p , being it approximately 23 μA . On the other hand, the blocked paper with SU-8 shows almost the half current response compared to the bare paper, 16 μA . This can be explained as this polymer achieve almost a flat

coating on paper as previously observed in the SEM images, so it is the most similar case to the common planar plastic films prepared for printed electronics. However, the primer layer can not overcome all fiber irregularities and the roughness is determined as $3.1 \mu\text{m}$ of RMS, as a result, I_p value on SU-8 is slightly higher ($16 \mu\text{A}$) than on the planar PET substrate ($12 \mu\text{A}$).

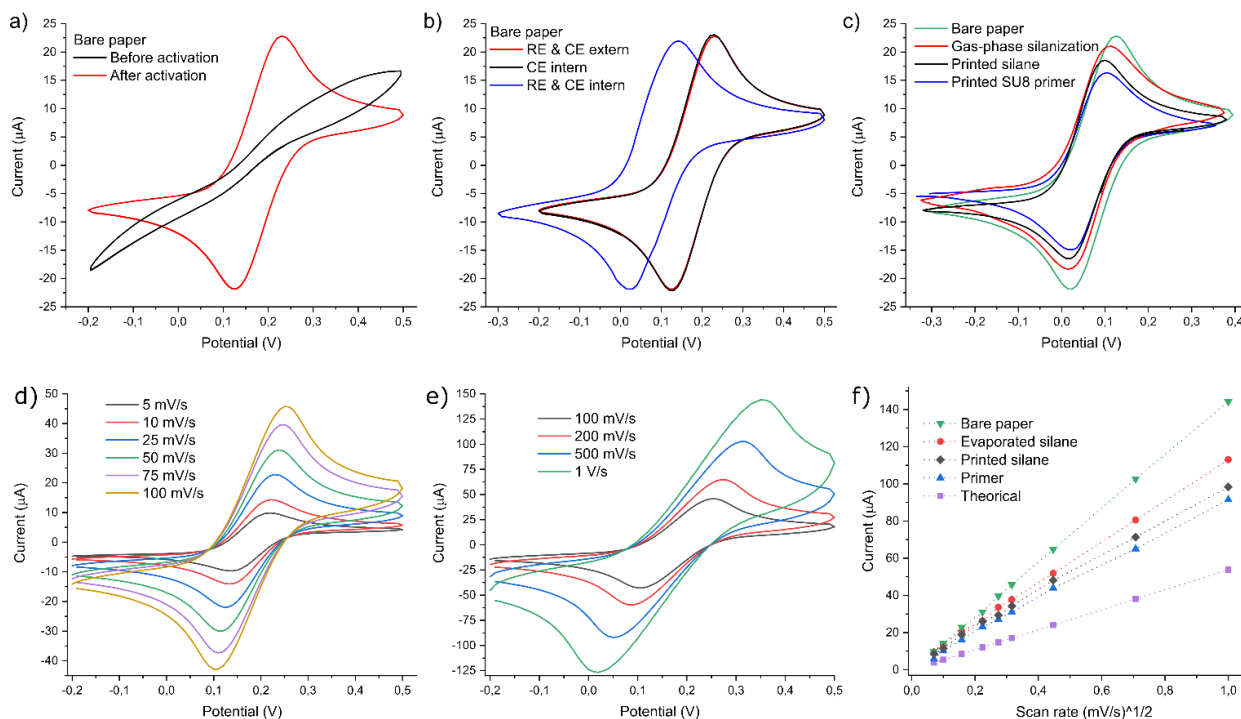


Figure 4.11. Electrochemical characterization of three-electrode cell on paper.

Cyclic voltammograms corresponding to the measurements of equimolar mixtures 10 mM ferro/ferricyanide redox couple in 0.1 M KNO_3 a) Au microelectrode on bare paper before and after activation at 25 mV/s vs Ag/AgCl RE; b) Au microelectrode on bare paper using external commercial RE and CE configuration versus integrated printed electrodes at 25 mV/s; c) Au WE printed on the four paper cases at 25 mV/s vs Ag/AgCl RE; d, e) Au microelectrode on bare paper varying scan rate from 5 to until 1000 mV/s; f) comparison between the theoretical Randle-Sěvčík equation prediction for a 1 mm Au WE vs experimental current peaks on 4 treated papers in function of square root of the scan rate.

In between the bare and the blocked paper, there are the WE printed on vapour-phase silanized paper that has a current response of $21 \mu\text{A}$, very similar to the bare paper, and the silane printed paper has an I_p of $20 \mu\text{A}$. The gas-phase silanization treatment grows a monolayer of silane onto the paper substrate that creates a nano hydrophobic layer coating which slightly reduces the bare paper porosity and roughness, allowing an easiest ink spreading onto the substrate that results in a lower I_p compared to the paper. Whereas, the silane drops deposited on paper, even with their infimum 10 pL dispensed volume, produce a high level of humidification that causes fiber compression. In consequence, their

roughness is less than for the vapour treated paper, leading to a decrease in the current response. As most of the kinetic parameters of the electrode reaction need to be discussed related to the unit area, there are various electrochemical methods that determine the real surface area of the electrodes⁴³⁹. In our case, we are working with a reversible reaction, so Randles-Sěvčik's equation governs the magnitude of the voltammetric current, and it is the most common method used for determining the effective surface area⁴²⁰. From the voltammograms varying the scan rate from 5 mV/s to 1000 mV/s (Figure 4.11d, e for bare paper substrate) it can be calculated Randles-Sěvčik's plots shown in Figure 4.11f, following the equation 1 detailed in the Supplementary Information. Clearly for all substrates current increases linearly as a function of the square root of the scan rate as is typical for a diffusion-controlled process. From the slope of these plots, the real electrode area has been calculated and detailed in Table 4-1. Electrochemical results of printed electrodes on paper.. As can be seen, the real electrochemical surface area of a WE printed on bare paper (2,12 mm²) is much larger, almost doubles the area of one WE printed on a planar substrate which is 1,09 mm² and triplicates the theoretical GSA (0,785 mm²). This is a direct consequence of the substrate roughness, as the effect of the intrinsic roughness of the gold ink is observed when the WE on PET is compared to the theoretical planar value, being the electrode is 1.4-fold higher than the theoretical one. So, the relation of A_{real} divided by the A_{geo} can be used as an estimation of a roughness factor (R_f). Again, R_f of the blocked paper with SU-8 is close to the printed on planar PET, 1,8-fold, and slightly higher can be found de paper silanized by the printing method, 2,2-fold, and the gas-phase silanized one, 2.4-fold.

The value of the electron transfer rate constant (k_s) has been calculated using the well know method of Matsuda-Ayabe⁴⁴⁰ using the equation 2 detailed in the Supplementary Information. Fig. S7 in the Supplementary Information shows the determination of k_s . At $\Lambda=1$, which occurs at the scan rate at which ΔE_p begins to depart from ideality that in our sensors is at 100 mV/s, k_s was calculated as $1.44 \cdot 10^{-4}$ cm/s for all the four substrate cases. That means that our system can be considered quasi-reversible allowing to perform analytical electrochemical techniques. In summary, our WEs show I_p increase in a wide range of scan rates and they have a quasi-reversible behavior.

Table 4-1. Electrochemical results of printed electrodes on paper.

Substrate	Substrate Roughness (μm)	ΔE_p (mV)	I_p anodic (μA) 25 mV/s	Real Electrode Area Randles-Ševčík (mm^2)	$R_f = A_{\text{real}}/A_{\text{geo}}^*$
Bare-paper	5.5	85	22.8 ± 0.6	2,12	2.7
Gas-phase silanized paper	5.3	75	20.7 ± 0.6	1,91	2.4
Silane printed paper	4.4	73	18.8 ± 0.3	1,73	2.2
SU-8 printed paper	3.1	70	16.0 ± 0.2	1,47	1,8
PET	3,65 nm	73	11.8 ± 0.3	1,09	1,4
Theoretical	---	59	8.50	0,785	1

4.3.4.4 conclusions

We present a novel approach for fabricating a three-array electrode on paper using 4 treatment-cases to tune the electrochemical active area. The electrodes were fabricated by additive non-contact digital IJP technology and consists of three different materials that were patterned on the 4 treatment-cases: Au, Ag and SU-8. Paper was treated in 4 different ways in order to tune the surface where patterns were printed; bare-paper, vapour-phase silanization, printing silane and printing primer. For the first time, the fabrication and characterization of a full inkjet WE, CE and pRE with Au and Ag inks on paper is presented. In addition, by surface modification we were able to tune the electrochemical active area, which for prospective application in electrochemical sensors. The characterization of WEs on 4 treatment cases shows that on bare paper we obtained an I_p value of $22.8 \mu\text{A}$ (at 75 mV/s) that is 2.12 folds higher than theoretical I_p for same electrode dimensions, and even the WE printed on SU-8 with the lower I_p shows 1.47 folds higher than theoretical. Moreover, I_p values show linear behavior in a wide range of scan rates from 5 mV/s to 1 V/s, and the system can be considered quasi-reversible kinetics allowing the use of electrodes in most electrochemical applications. In addition, we have also demonstrated the successful combination of this rapid prototyping technique on low-cost, eco-friendly, and biodegradable paper substrate. Due its versatility and adaptability, the three-array electrode can lead toward the generation of green, wearable, flexible, microfluidic and high-resolution devices.

Supplementary Information (Section [Error! No se encuentra el origen de la referencia.]

Chemical structure POTS, WCA, hydrophobic image, cross-section, sheet resistance, electrochemical study, Randles-Sěvčik's equation.

Acknowledgements

M. Zea would like to acknowledge his financial support covered by Fundaci3n Centro de Estudios Interdisciplinarios B3sicos y Aplicados (CEIBA)-Gobernaci3n de Bolivar (Colombia). This work was supported by the Spanish government-funded project RTI2018-096786-B-I00, and RTI2018-102070-B-C21 by Ministerio de Ciencia, Innovaci3n y Universidades (MICIU/FEDER, EU). The authors also want to thank the support of the SU-8 Unit of the CIBER in Bioengineering, Biomaterials, and Nanomedicine (CIBER-BBN) at the IMB-CNM (CSIC) of ICTS "NANBIOSIS." This work has also made use of the Spanish ICTS Network MICRONANOFABS partially supported by MEINCOM. This work was also partially supported by the EU H2020 research and innovation program KardiaTool with agreement N^o 768686, POC4Allergies through the ERA PerMed program (Reference Number: ERAPERMED2019-127 and from CAMPUS FRANCE program agreement PHC PROCOPE 40544QH.

Corresponding Author

* E-mail: gemma.gabriel@imb-cnm.csic.es. Tel:+34 935 947700

Author Contributions

The manuscript was written through contributions of all authors. / All authors have given approval to the final version of the manuscript.

Notes

The authors declare no competing financial interest.

4.4. Cortisol sensing

Cortisol, a steroid hormone, is a biomarker for numerous diseases and plays an important role in the regulation of various physiological processes such as blood pressure, glucose levels, and carbohydrate metabolism. It also plays an important role in homeostasis of the cardiovascular, immune, renal, skeletal and endocrine system⁴⁴¹⁻⁴⁴³. Chromatographic techniques have been traditionally used to detect cortisol. However, this technique has many downsides such as assay formation, system complexity, and multistep extraction/purification that limits its application in the field. In order to overcome these downsides and with the recent advances in sensing technologies, the objective is to develop miniaturized and reliable platform for cortisol detection, various immunoassays sensing strategies are being explored. However, electrochemical immunosensing of cortisol is considered as a recent advancement towards PoC applications.⁴⁴⁴

4.4.1. Publication IV: Electrochemical sensors for cortisol detections: almost there

The second paper presented in this Chapter, **Publication IV**, is a published review about the electrochemical sensing techniques to detect cortisol, entitle: Electrochemical sensors for cortisol detections: almost there. This review takes a detailed look at the current state-of-the-art in electrochemical cortisol detection in the last five years. During which time, the necessity for real-time and continuous monitoring of cortisol levels for fast diagnosis has come to the fore.

This article has been edited from the version published in TrAC Trends in Analytical Chemistry, with permission from Elsevier (edition consist in formatting and numbering figures, references, tables, and equations in accordance with the thesis manuscript, however acronym corresponds to the article):

Miguel Zea, Francesca G. Bellagambi, Hamdi Ben Halima, Nadia Zine, Rosa Villa, Gemma Gabriel, and Abdelhamid Errachid. **Electrochemical sensors for cortisol detections: almost there**. TrAC Trends in Analytical Chemistry 2020, 132, 116058; <https://doi.org/10.1016/j.trac.2020.116058>.

Electrochemical sensors for cortisol detections: almost there.

Miguel Zea^{1,2}, Francesca G. Bellagambi³, Hamdi Ben Halima³, Nadia Zine³, Rosa Villa^{1,4}, Gemma Gabriel^{1,4}, and Abdelhamid Errachid^{3,**}*

¹ Instituto de Microelectrónica de Barcelona, IMB-CNM (CSIC), Bellaterra, Spain.

² Ph.D. in Electrical and Telecommunication Engineering, Universitat Autònoma de Barcelona (UAB).

³ Université de Lyon, Institut des Sciences Analytiques, UMR5280, CNRS, Villeurbanne, France.

⁴ CIBER de Bioingeniería, Biomateriales y Nanomedicina (CIBER-BBN), Spain.

Keywords: Cortisol; Immunosensor; Healthcare; Electrochemical sensor; Hormone

Abstract.

Mostly known as “the stress hormone,” cortisol has many essential functions in humans due to its involvement in regulation of blood pressure, immune system, metabolism of protein, carbohydrate, adipose, and anti-inflammatory action. Since a right cortisol balance is essential for human health, many efforts are currently being made to monitor the cortisol level in the human body. Cortisol levels are usually monitored in blood, plasma, serum, oral fluid, sweat, and hair samples through immunochemical and analytical methods, but in the last decade, electrochemical measurements are proving to be reliable techniques for cortisol quantification in biological matrices with the advantages of a fast response by portable and wearable devices. This review gathers the most recent developments and works on electrochemical sensors for cortisol detection, highlighting their high technology maturity and potential for clinical applications

4.4.1.1 Introduction

Human cortisol (11 β ,17 α ,21-Trihydroxypregn-4-ene-3,20-dione) is a steroid hormone, one of the major glucocorticoids synthesized in the zona fasciculata of the adrenal cortex. Cortisol release is regulated by the hypothalamic-pituitary-adrenal (HPA) axis response. The HPA axis is the central stress response system in humans, which is characterized by hypothalamic release of corticotropin-releasing factor (CRF). When CRF binds to CRF receptors on the anterior pituitary gland, the adrenocorticotrophic hormone (ACTH) is released. This later binds to receptors on the adrenal cortex and stimulates adrenal release of cortisol. This path^{445,446}, schematically shown in Fig. 1, ends when cortisol is released into bloodstream and diffused to different tissues.

Cortisol, as with other steroid hormones, can cross the cytoplasmic membrane because of its fat-soluble properties and acts as primary messenger. Cortisol plays many essential functions in humans because it is involved in several metabolic pathways. For example, during bleeding, cortisol acts in the formation of glucose and activates the anti-inflammatory and anti-stress pathways. It also plays a role in the liver and muscle glycogenolysis, the separation of glycogen in glucose-1-phosphate and glucose. Cortisol helps in the activation of glycogen phosphorylase, which is essential for adrenaline to influence glycogenolysis. For the nutritionist community, cortisol also plays an essential role in human nutrition⁴⁴⁷, as well as dieting alters cortisol level⁴⁴⁸. It regulates energy by selecting the right type and amount of substrate (carbohydrate, fat, or protein) the body needs to meet the physiological demands placed on it.

However, if there is an elevated level of cortisol over a long period, it can lead to a breakdown of a muscle ^{449–451}. Also, when it is chronically elevated, cortisol can have deleterious effects on weight, immune function, and chronic disease risk. Due to the presence of glucocorticoid receptors in almost every cell of the body, cortisol affects many organ systems, such as musculoskeletal, cardiovascular, respiratory, endocrine, and nervous ⁴⁵².

Cortisol can reduce the activity of the immune system by stopping the multiplication of T-cells by rendering the interleukin-2 producer T-cells unresponsive to interleukin-1 and unable to produce the T-cell growth factor of IL-2 ⁴⁵³. It can also reduce bone formation, developing in the long term osteoporosis ⁴⁵⁴. Cortisol permits an increase of the glomerular filtration rate and the renal plasma flow from the kidneys, leading to an increase of phosphate excretion as well as sodium and water retention. However, it also increases the sodium and water absorption and potassium excretion in the intestines ⁴⁵⁵.

In the absence of pathological conditions, the amount of plasmatic cortisol changes during the day following a well-established circadian rhythm. Cortisol levels are minimal around midnight, start rising in the early morning (around 4 a.m.), and reach a peak 30–40 min after awakening, then slowly decrease during the day ^{456–458}. Examples of reference concentration ranges found in different biological fluids from nominally healthy subjects are listed in Table 4-2.

The amount of cortisol produced and released into the bloodstream is highly regulated by the human body to ensure the correct balance. The body responds to stress or danger, increasing the metabolism of glucose, controlling blood pressure, and reducing inflammation. Cortisol is also needed for the “fight or flight” response by the autonomic nervous system, which is a healthy, natural response to perceived threats. Abnormal levels may represent health effects. Symptoms of too much cortisol include weight gain, particularly around the abdomen and face, thin and fragile skin that is slow to heal, acne, for women facial hair, irregular menstrual periods, fertility problems, susceptibility to stress, pain, fatigue, muscle wastage and hyperglycemia ^{459–462}. Symptoms of low cortisol include tiredness, nausea, vomiting, weight loss, muscle weakness, and pain in the abdomen ^{463,464}.

Table 4-2. Cortisol usual levels in human fluids.

Cortisol levels in different biological matrices in nominally healthy subjects (*Cortisol level in urine is measured over a 24 h period, and it is referred as the 24 h urinary free cortisol test.)

Sample	Cortisol normal ranges*	Ref.
Blood	25 µg/mL (morning), 2 µg/mL (midnight)	444
Serum	45 – 227 ng/mL (morning), 17– 141 ng/mL (evening)	465
Urine	21458 – 149696 ng/24h	465
	44000 – 140000 ng/24h	466
Saliva	1 – 12 ng/mL (morning), 0.1 – 3 ng/mL (evening)	467
	1 – 10 ng/mL (morning), 0.5 – 2 (evening)	465
Sweat	8 – 142 ng/mL	468
Hair	18 – 153 pg/mg	469
	40 – 128 pg/mg	470
Interstitial fluid	12 – 34 ng/mL (morning), 9 – 13 ng/mL (evening)	471

Modifications of cortisol levels caused by stress are now a public health concern; long stress exposition can lead to high levels of cortisol, which can create an allostatic load (a stress accumulation with the time) and causes various physical modifications in the human body ⁴⁷². Cortisol is also known to unfavorably affect classic cardiovascular risk factors such as hypertension and insulin resistance ^{459,473}. During pregnancy, stress hormones and the production of cortisol are necessary for healthy fetal organ development and for preparing the fetus for uterine life, but excessive stress can have negative influences on fetal development, in particular on brain development ⁴⁷⁴. There are several factors that can reduce cortisol levels, such as magnesium after aerobic exercise ⁴⁷⁵; omega-3 fatty acids, and fish oil ⁴⁷⁶; massage ⁴⁷⁷; and laughing and humor ⁴⁷⁸.

Metabolism of cortisol takes place mainly in the liver, where by means of reductases it is converted to tetrahydrometabolites (THMs), which are then excreted in urine. More than 90% of circulating cortisol is bound cortisol to cortisol-binding globulin and to albumin. There is a small amount of biologically active free cortisol which can bind to glucocorticoid receptors and initiate physiological events, so it is

considered responsible for biological functions of the hormone. This free cortisol passively diffuses, as detailed in Figure 4.12. Cortisol secretion pathway in humans., into oral fluids via ultra-filtration⁴⁶⁷. As a consequence, salivary cortisol levels correlate very well ($r = 0.7, p < 0.05$) with the free cortisol in the blood^{479,480}. This high agreement is due to the fact that cortisol is lipid-soluble and enters saliva by passive diffusion through the cells of the salivary gland, so that its concentration in saliva does not depend on flow rate, thereby giving a clinically useful index of unbound plasma levels^{481–484}. Cortisol diffusion to sweat is similar to salivary cortisol concentrations via ultra-filtration, which represent the free unbound fraction of cortisol in the blood and correlate with salivary cortisol concentrations ($r^2 = 0.30, P < 0.05$)⁴⁶⁸. Indeed, the significant correlation between cortisol in sweat and saliva suggests that both may reflect acute hypothalamo-pituitary-adrenal activity⁴⁸⁵. Cortisol can also be detected in hair and urine. This review will describe the relevance of sensing cortisol, the techniques that have been used for measuring it, the importance of the development of electrochemical detection, and the most relevant characteristics of electrochemical detection of cortisol published works from 2013.

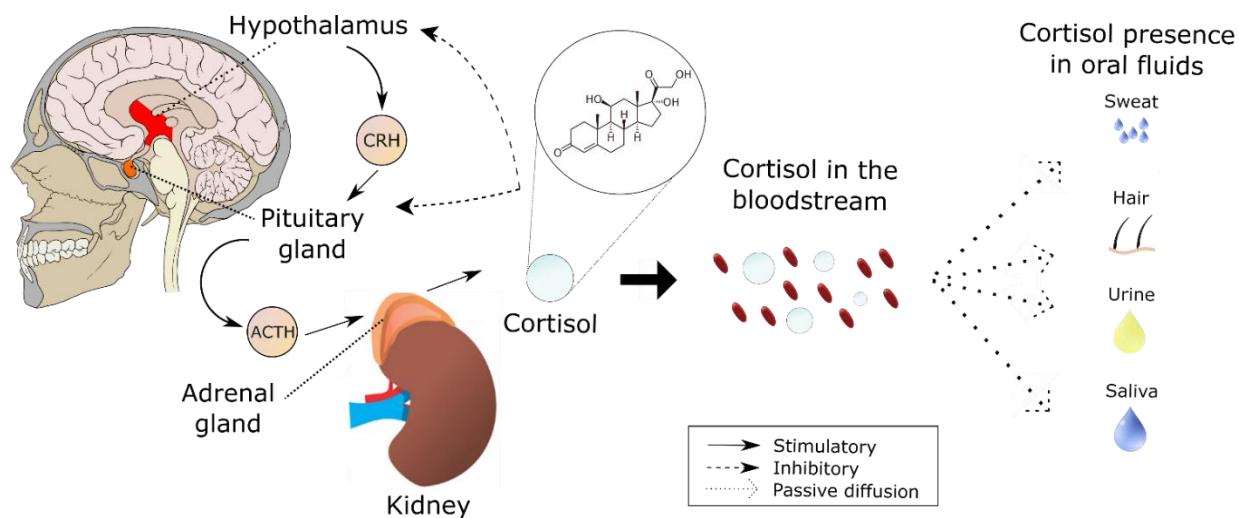


Figure 4.12. Cortisol secretion pathway in humans.

Cortisol generation path in human body. The free cortisol is released into bloodstream and diffused to different oral fluids by passive diffusion.

4.4.1.2 Quantitative sensing of cortisol

Immunosensing techniques or immunoassays (IA) with different sensing receptors and transducers are considered as significant developments and promising tools in screening methods^{486,487}. The use of immunosensors for cortisol detection is advantageous in terms of increased sensitivity, decreased limit of detection (LOD), cost-effectiveness, ease of use, and reduced need for expensive reagents.

Specifically, the most frequently used immunoassay is enzyme-linked immunosorbent assay (ELISA). IA assessment measures the presence of cortisol molecules in the solution using antibodies, while in ELISA, the antibody is linked with an enzyme to react with the antigen, and this reaction produces a detectable change of color ⁴⁸⁸.

Tandem mass spectrometry (MS/MS) is different from immunoassay assessments as it consists of measuring the mass-to-charge ratio of ions with the obtained spectra providing the isotopic signature. This technique is considered the gold standard for cortisol assessment because of its high specificity and sensitivity ⁴⁸⁹. However, it has critical specific disadvantages in that it requires trained personnel and specialized equipment, which, compared to conventional IA's, make MS/MS methodology in its present form unsuitable for the development of portable analytic applications.

The lateral flow immunoassay was the first technique to detect cortisol out of laboratories ⁴⁹⁰. Nowadays, it is a well-known technique based on a liquid analyte (e.g. blood, sweat) that is absorbed and moved through the device. The most studied lateral flow devices are colorimetric, so the reaction is a change of color. However, recent developments employ quantitative biomarkers with the use of image analysis and electrochemical sensors ^{491–493}.

Additionally, multiple biosensing platforms have been proposed by Shetty and Yamaguchi ⁴⁹⁴ for bio-sample analytical purposes using antibodies. This methodology can be based on either antigen/antibody binding (immunoassays), which has been reported from the 1980s for labeled cortisol for fluoroimmunoassay ⁴⁹⁵; nucleic acid interactions (DNA, RNA) ⁴⁹⁶; and chemical or enzymatic interactions ⁴⁹⁷, which combined with the biomarker of interest can prescribe the specimens of preference and the way to collect them. However, most samples need to be treated before being processed, mostly for the separation of macromolecules that interfere during measurement. Many techniques have been developed to avoid sample treatments in order to obtain reliable results ^{498–500}. However, the pre-treatment of samples has not been the focus of recent research as more effort has been put into detecting cortisol in a non-invasive way.

4.4.1.2.1 Cortisol in biological matrices

Nowadays, there are multiple analytical methods for the determination of cortisol in biological matrices, such as urine, hair, sweat, blood, and saliva. Only unbound cortisol is bioactive; thus, the quantification of free cortisol is of superior biological relevance compared with total cortisol quantification.

Urine. Cortisol level in urine is measured over a 24 h period, and it is referred to as the 24 h urinary-free cortisol test. The concentration of cortisol in urine is correlated to unbound, and biologically active cortisol in blood, and its determination was first reported in 1968 by Murphy et al.⁵⁰¹ via a protein-binding radioassay. Since then, many improvements have been made in the determination of cortisol in urine in relation to the problem of its unknown cross-reacting interferences. The determination of the urinary concentration of cortisol can be carried out by protein binding assays, RIA, MS/MS, thin-layer chromatography (TLC), and fluorimetry^{502,503}.

Serum and plasma. Overcome the interferences due to cross-reaction of steroids or other substances is the main limitation in determining cortisol levels in serum and plasma. Cortisol levels are generally measured by immunochemical methods^{504,505}, as well as RIAs and rapid automated chemiluminescence immunoassays^{503,506}.

Hair. The use of hair as a biological sample has gained considerable attention over the last two decades and is mainly exploited in forensic sciences, toxicology, doping control, and clinical diagnostics. Cortisol is known to deposit in the shaft of the hair, so the first-centimeter segment of hair closest to the scalp approximates to the last month's cortisol production, and it continues proportionally^{507,508}. The cortisol is extracted from the hair using methanol to obtain a treatable sample^{469,509}. Different approaches have been used to measure cortisol in hair, such as ELISA^{469,510}, or more simply, enzyme immunoassays (EIA) or RIA⁵¹¹.

Sweat. Cortisol in sweat represents the free unbound fraction of cortisol in the blood and likely free cortisol⁵¹². Sweat cortisol may also reflect hypothalamic-pituitary-adrenal activity⁴⁸⁵. Sweat cortisol concentrations have been significantly correlated with the time of day ($r^2 = 20.44$, $P < 0.01$) and with salivary cortisol concentrations ($r^2 = 0.30$, $P < 0.05$). The first reported method for analyzing sweat cortisol was ELISA⁴⁶⁸, since when several methods have been reported, such as high-performance liquid

chromatography (HPLC) coupled to MS (HPLC-MS)⁵¹³; thin-layer chromatography (TLC)⁵¹⁴; and immunosensor⁵¹⁵.

Blood. Cortisol in bloodstream circulates in both bound and free forms with a half-life of around 80 min⁴⁴¹. Typically, assays for measuring cortisol in blood involve measuring the total cortisol (bound and free) and then the active fraction. Blood, however, is afflicted by many drawbacks⁵¹⁶, so measuring free cortisol in blood is complex, time-consuming, and expensive and includes ultrafiltration, equilibrium dialysis, and steady-state gel filtration. For this reason, cortisol in blood is usually measured from serum by immunoassays^{517,518}.

Saliva. The advantages of determining steroid hormones by saliva analysis have already been abundantly reported⁵¹⁹, and salivary cortisol determination has been reported from 1969⁵²⁰ but the lack of sensitivity and accuracy hampered the research until the late 70s⁵²¹ with RIAs development. Even if salivary cortisol is highly correlated with the amount of blood cortisol⁵²², cortisol levels in saliva are about 100-fold lower than blood⁵²³. For this reason, high sensitivity assays with low LODs are required for efficient detection of cortisol concentration in saliva⁴⁴⁴. Analytical techniques such as HPLC-MS/MS⁴⁶⁷, and immunosensors^{444,524–527} have been demonstrated effective for measuring cortisol in saliva.

4.4.1.3 Electrochemical cortisol detection

As shown above, there are several types of transducers for cortisol detection as they depend on signal generation (viz. electrochemical or optical) or property changes (such as a change in mass). The most common transducer for cortisol is the optical detection with a high sensitive measurement of the target molecules. However, they require sophisticated clinical lab-scale instruments and have limitations regarding their point-of-care regimes' expensive reagents and bulky optical detectors. The main alternative is the use of electrochemical immunosensors, which are well-known analytical methods because of their extremely low detection limits. This technique is based on the principle of measuring the changes in the electrical properties of a conductive material due to the absorption of the target analyte on the surface, commonly functionalized with antibodies. The working principle of an electrochemical sensor consists of a transducer element, Figure 4.13a, covered by a recognition element, Figure 4.13b and c, and this one interacts with the target analyte, Figure 4.13d. As a consequence of this interaction, the electrochemical transducer transforms the chemical change into an electrical signal that can be related to the concentration of the analyte, Figure 4.13e. The immunosensors, where the recognition element is

an antibody, are the most common analytical tools in which the electrical signal can be processed, recorded, and displayed due to the formation of antigen-antibody (Ag-Ab) complex. In this review, all the sensor commented parts will be discussed in detail.

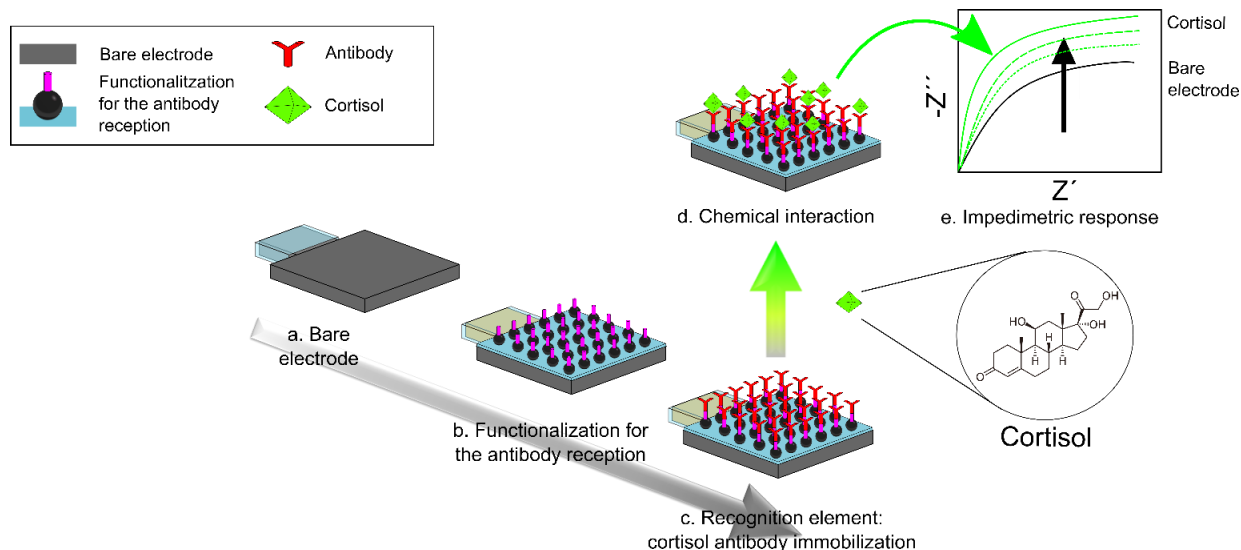


Figure 4.13. Schematic example of functionalization process of an electrode.

An example of an antibody functionalized electrode and its electrochemical response toward cortisol by electrochemical impedance spectroscopy. Stepwise fabrication of immunosensor a) bare electrode, b) preparation for the reception of antibody (generally with carboxylic groups), c) Immobilization of the antibody, e) detection of cortisol molecule, and f) usual impedimetric measurement for cortisol detection.

The fact that cortisol levels vary according to daily activities has led to research on wearable and portable point of care (PoC) devices able to rapidly detect cortisol in-situ and able to monitor in a non-invasive way the personal stress level with a minimal disturbance of daily routines. PoCs obviate the need for expensive equipment, tedious sample preparations, lengthy procedures, and technical expertise⁵²⁸. An electrochemical-driven sensing platform can be used to develop simple and miniaturized biosensors that are required for PoC devices using relatively simple and low-cost instrumentation⁵²⁹ compared with other transduction methods, allowing on-site analysis. Furthermore, it is more accurate and more sensitive; it enables low LOD even in the femtomolar range. It allows a measure in small intervals of time, offering accurate information in small changes of the analyte concentration. These above-commented characteristics make the electrochemical detection, compared with conventional techniques, a reliable, quantitative, and easier-to-use technique for PoC cortisol sensing, which gives them enormous potential for improving patient health at a clinical level⁴⁰⁴.

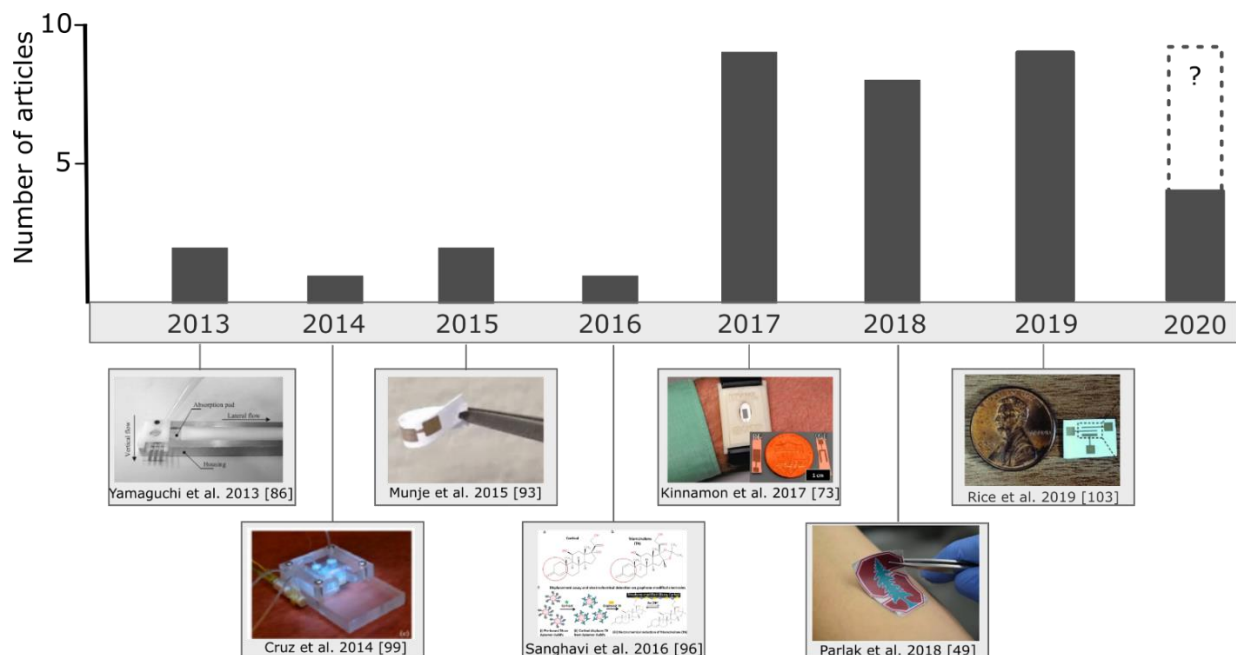


Figure 4.14. Number of published articles about electrochemical cortisol detection.

Recent growth in the number of publications on cortisol electrochemical detection with the most recent papers on electrochemical biosensors for detecting cortisol in biological matrices.

In recent years, mainly from 2014, publications of electrochemical cortisol measurement by sensing techniques have increased exponentially. Before this date, accurate and reliable results were not selective enough to detect just cortisol molecules due to their similarity with other molecules. Figure 4.14 shows the growth in the number of publications on electrochemical detection of cortisol in the past seven years. As proposed by Dungchai et al.⁴⁰³, electrochemical detection is an attractive alternative detection scheme for paper-based microfluidics due to its small size, portability, low cost, high sensitivity, and high selectivity by proper choice of detection potential and/or electrode material. Moreover, an additional advantage of electrochemical detection is the simplicity of the instrumentation resulting in low electrical power requirements for in-field use⁵³⁰, as demonstrated by the numerous current hand-held analyzers (i.e., glucometer, pH meter, uric acid meter, etc.) and the potential of miniaturization of both the device itself and the required instrumentation. In 2014, Singh et al.⁵²⁶ and Kaushik et al.⁴⁴⁴ reviewed the most relevant reports on electrochemical sensing of cortisol up to 2014. However, there have been many advances, and in the remainder of this article, we review the most relevant research on the detection of cortisol by electrochemical techniques, and the use of anti-cortisol antibody electro addressed or electrochemically bound on electrode surfaces.

4.4.1.3.1 Electrochemical techniques for cortisol detection

One of the most popular electrochemical techniques is cyclic voltammetry (CV). CV records changes in current while varying the potential applied to the working electrode at a constant scan rate in forward and reverse directions. CV is used to study the electrochemical properties of the working electrode to adsorb a molecule or an analyte. In order to increase speed and sensitivity, many forms of potential modulation (other than just a simple staircase ramp) have been tried over the years. Differential pulse voltammetry (DPV), normal pulse voltammetry (NPV), and square-wave voltammetry (SWV) have also been reported. Electrochemical impedance spectroscopy (EIS) measures the electrical properties of the material on the working electrode via application of a sinusoidal AC excitation signal. EIS is a quite sensitive electrochemical technique, and it quantifies molecules with higher LOD compared with ELISA. It presents some significant advantages: it is non-destructive, provides time-dependent quantitative information, and it is possible to extract an equivalent electrical model that is an electrical fingerprint of its properties and interactions. Table 4-3 summarizes the most recent papers on electrochemical biosensors for detecting cortisol in biological matrices, and the following sections give an overview of the main achievements, limitations, and opportunities in this topic area.

4.4.1.3.2 Transduction element

The solid support that acts as the transduction element that constitutes the electrode, sometimes called a matrix, can be considered the heart of the biosensor. The performance of the biosensor is highly dependent on the transduction matrix and on the immobilization of the final recognition biomolecule. Much research has focused on one or both topics, and we will first review the most important improvements regarding the composition of the transduction element. The chemical properties of the electrode mark the bioreceptor immobilization and the final biosensor stability. In this sense, the most common materials used as electrodes are carbon and gold (see Table 4-3). Materials that show enhanced electro-catalytic activity and good electron-transfer kinetics are the ones most considered for forming the electrode as this improves the biosensor response.

In general, the metal oxides are materials that meet the requirements mentioned above and are good candidates to be used as transduction materials. The most studied metal oxides in this respect are nickel oxide (NiO) and zinc oxide (ZnO). Dhull et al.⁵³¹ fabricated a non-invasive electrochemical immunosensor for the detection of salivary cortisol using sputtered NiO thin film as a sensing platform.

This study used an increase in surface roughness of the NiO (about 5.09 nm) to improve charge transfer properties. The final sensor achieved LOD of 0.32 pg/mL in a broad range of linearity from 1 pg/mL to 10 µg/mL and a stability of 9 weeks. Munje et al.⁵³² developed an immunosensor based on ZnO deposited by pulsed laser on a nanoporous flexible polyamide for wearable diagnostics of cortisol in synthetic and human sweat. They measured impedance and observed double-layer capacitance changes due to the antibody-hormone interactions at diagnostic concentrations. The immunosensor showed a high sensitivity of detection of 1 pg/mL cortisol in synthetic sweat and 1 ng/mL in human sweat.

Electrode modification with graphene has attracted much attention because of its high surface area, high biocompatibility, and the possibility to increase sensitivity by facilitating the electron transfer between the electroactive species and the surface of the electrode. In this way, Tuteja et al.⁵³³ proposed the use of graphene embedded on screen-printed electrodes. They took advantage of graphene to bioconjugate antibodies and demonstrate how a higher surface activity of graphene improved electrocatalytic activity. When reduced to graphene oxide, graphene has special properties that make the material ideal for use in biosensors. It can be functionalized by π - π electrostatic interactions, and the presence of the oxidized groups allows a great variety of chemical functionalizations. Furthermore, they proposed a dual working electrode configuration for the cortisol and lactate monitoring using the chronoamperometric technique. They achieved good selectivity and practical applicability for the cortisol sensing, with a LOD of 0.1 ng/mL over a wide detection range from 0.1 to 200 ng/mL, with a fast response time less than ≤ 1 min compared with the 3–5 hours that is usually needed with ELISA.

Kinnamon et al.⁵¹⁵ reported, for the first time, the use of molybdenum disulfide (MoS₂) nanosheets integrated into nanoporous flexible electrode system for detecting cortisol. Nanoscaled 2D MoS₂ has a high surface area ratio and a high presence of sulfur terminated edges and corners that enable their chemical functionalization. They obtained a flexible wearable device to detect cortisol in human sweat in the range from 1 ng/mL to 500 ng/mL with a LOD of 1 ng/mL by EIS.

4.4.1.3.3 Recognition element

One of the critical points for a successful cortisol biosensor is the presence of a relevant recognition element that is mainly responsible for the cortisol capture. The most widely used strategy is the use of antibodies. S. Khan et al.⁵³⁴ report an electrochemical immunosensor with enhanced sensitivity for detecting human salivary cortisol in pg/mL range thanks to the use of bovine serum albumin (BSA) in

comparison with the most common used ethanolamine. They found that 1 % BSA was enough to be used as an effective sensitivity enhancer, in addition to optimizing the other two parameters: anti-cortisol antibody covalently attached to Au electrodes and saliva sample incubation time on the sensor chip. They used EIS to evaluate the cortisol levels of the saliva samples with a LOD of 0.87 ± 0.12 pg/mL in a wide concentration range from 1 pg/mL to 10 ng/mL ($R^2 = 0.9831$).

However, the use of antibodies has several shortcomings: they cannot be synthesized *in vitro*, they exhibit drawbacks in their variability and cross-reactivity, and steric limitations arise as antibodies are big molecules in comparison with the small analytes to be measured. They also show denaturalization when stored for a period, and taken together; these characteristics imply inherent limitations on these types of sensors. The field of aptamers has been growing in recent years and is already considered a conventional bioreceptor. One of the most relevant studies was done by Sanghavi et al.⁵³⁵. They demonstrated a recognition system based on an aptamer functionalized with gold nanoparticles pre-bound with electroactive triamcinolone in a microfluidic device. EIS measurement gave signal linearity in a five-log cortisol concentration range from 10 μ g/mL to 30 pg/mL of cortisol and exhibited rapid binding kinetics of 2.5 min for each assay and small sample volumes (< 1 μ L). In this study, aptamer showed low interferences with progesterone, testosterone, and estradiol.

Due to the challenges associated with affinity and the continuous monitoring of cortisol, new approximations have been proposed. Manickam et al.⁵³⁶ reported an approach for the rapid detection of salivary cortisol without the use of any specialized antibody or enzyme. They demonstrated, for the first time, the use of a molecularly imprinted polymer (MIP) using cortisol as a model analyte. MIP is designed to replace natural antibodies, offering higher stability and cost-effectiveness. The electropolymerization of pyrrole over the electrode surface in the presence of cortisol produced a cortisol MIP film. In order to remove the entrapped template to form the complementary imprinted sites, the best strategy found was the electrochemical over-oxidation of polypyrrole. This MIP biosensor uses CV for the detection of cortisol concentrations, showed a LOD of 1 pM in a linear range from 1 pM to 10 μ M ($R^2 = 0.9925$). Furthermore, they showed that the sensitivity of the sensor remained over 90% after seven cycles of elution/rebinding, while the sensitivity decreased by 10% after 4 weeks of storage at room temperature, indicating that the sensor can be used multiple times.

One year later, Parlak et al.⁴⁹¹ also used a tailor-made polymeric membrane following the MIP methodology and demonstrated again that a stable and selective molecular recognition of cortisol can

be achieved. Manickam et al.⁵³⁷ also proposed the use of a composite formed by metalloporphyrin (MTTPs) and multiwalled carbon nanotubes (MWCNTs) on screen printed carbon electrodes. The catalytic activity of MTTPs was investigated in this work, and the electrochemical reduction of cortisol was found to be ultra-sensitive for the combination of MTTPs and MWCNTs. Detection of cortisol was in a range from 1 nM to 50 nM with a LOD as low as 50 fM and a sensitivity of 0.38 nM in saliva samples.

4.4.1.3.4 Devices

The first attempts to improve the usability of these types of electrochemical biosensors were their integration in microfluidic systems, as this strategy decreases both the probability of human error and the required sample volume. However, this type of system has limited use as a PoC. In this sense, Cruz et al.⁵³⁸ report a miniaturized potentiostat to perform a full range of CV measurements for the immune detection of cortisol integrated with a microfluidic system formed by a sample and buffers reservoirs, a fluid control system and an assay chamber. They demonstrated that this customized device was able to detect cortisol in a detection range of 10 pM to 500 nM showing a sensitivity of 1.24 μ M. Vasudev et al.⁵³⁹ developed a fully automated 3D microfluidic system with an integrated electrochemical biosensing platform for the detection of cortisol of microfabricated interdigitated Au electrodes. Cortisol was detected in a linear range of 10 pM to 100 nM at a sensitivity of 0.207 μ A/M.

The measurement of cortisol in the bio-fluids mentioned above will become increasingly relevant in on-site clinical diagnosis and in the stress level monitoring of cortisol. In the roadmap of diagnostic medical devices, the next step after the identification of a reliable technology, is the development of PoC devices for prevention and health monitoring. It is for this reason that novel designs of PoC are being proposed for several groups. One example can be found in the work of Yamaguchi et al.⁵²⁷, who proposes a biosensing cartridge based on a cortisol immunosensor for non-invasive and quantitative analysis of salivary cortisol. The portable cartridge incorporates a fluid control mechanism based on a vertical flow where the immune reaction occurs combined with a lateral flow over an absorption pad responsible for the absorption of the unreacted GOD-labeled cortisol by capillary action. Using the relative detected current through the working electrode from a competitive reaction between the analyte and glucose oxidase of an amperometric system, a cortisol detection in the range of 0.1 to 10 ng/mL was achieved in 35 min.

One of the most advanced wearable devices for cortisol sensing is presented by Parlak et al.⁴⁹¹. They designed a wearable patch to measure cortisol in human sweat collected during exercise that integrates an organic electrochemical transistor (OECT) and a flexible microfluidic device for sweat skin sensing. The whole device is fabricated on a flexible and stretchable elastomeric substrate. The skin-like microfluidic device was able to collect newly generated sweat and deliver it to the sensor interface. Electrodes were brush-printed on a tailor-made synthetic and biomimetic polymeric membrane. They measured currents in the transistor for stable and selective molecular recognition of human cortisol, and the detection range was between 0,01 to 10 μ M and the measured time was less than 1 min and LOD down to 1 pg/mL. Madhu et al.⁵⁴⁰ present a technology to obtain a binder-free and superwetable ZnO nanorods electrochemical immunosensor for the detection of cortisol in sweat integrated into a coating of flexible carbon yarns. The biocompatibility and cytotoxicity effects of this immunosensor are also presented, as it is a sensor thought to be fabricated on fabrics providing an ease of use of a wearable sensor.

Table 4-3. Published works of electrochemical cortisol detection.

Comparison of selected works from the literature, highlighting their detecting properties as detection technique, electrode material, immobilizing biomolecule, sample, detection range, detection limit, and test time. Abbreviations: Monoclonal cortisol antibodies (C-mAb), Anticortisol antibodies (C-Ab), Reduced Graphene oxide (RGo).

Detection technique	Electrode	Immobilizing biomolecule	Sample	Detection range*	LOD**	Ref
Amperometry	Pt	C-MAb	Human saliva	0.1 to 10 ng/mL ($R^2 = 0.98$)	-	527
	Au	C-Ab	Fish plasma	1.25 to 200 ng/mL ($R^2 = 0.964$)	-	541
	RGo	C-Ab	Human saliva and sweat	0.1 to 200 ng/mL ($R^2 = 0.98$)	0.1 ng/mL	533
	Au	C-Ab	Human sweat	1 pg/mL to 100 ng/mL	-	542
CV	Au	C-Ab	PBS with Fe(II)/Fe(III)	0.003 to 36 ng/mL ($R^2 = 0.997$)	10 pg/mL	539

	Au	C-mAb	Fe(II)/Fe(III)	0.003 to 181 ng/ml ($R^2 = 0.989$)	0.36 pg/mL	538
						536
	Carbon	Imprinted polymer	PBS with Fe(II)/Fe(III)	0.36 pg/mL to 3624 ng/mL ($R^2 = 0.9925$)	3624 ng/mL	543
	ITO	C-Ab IgG-DI	Human serum	10.8 pg/mL to 0.36 μ g/mL	10.8 pg/mL	544
	NiO	C-Ab	PBS	0.01 to 10 μ g/mL	14 μ AmL/ μ g	537
	Carbon	MWNTs + metalloporphyrins	Human saliva	1.81 to 36.2 ng/mL ($R^2 = 0.998$)	18 fg/mL	545
	---	Imprinted polymer	Human Urine	1 to 1000 ag/mL	2 ag/mL	491
OECT	ITO	Imprinted polymer	Human sweat	3.6 to 3624 ng/mL	2.86 μ A/dec**	546
SWV	Au nanowires	C-mAb	Blood serum	3.6 to 28.9 μ g/mL ($R^2 = 0.998$)	7.4 μ g/mL	547
	Graphite	mAb IgG + C-mAb	Human saliva	0.5 to 55.1 ng/mL ($R^2 = 0.97$)	1.7 ng/mL	548
	ITO	Ferrocene tagged C-Ab	Zebrafish whole-body artificial saliva	0.001-50 ng/mL	1.03 pg/mL	549
DPV	Au NPs + RGo carbon	C-Ab	Human serum	0.1 to 1000 ng/mL ($R^2 = 0.992$)	0.05 ng/mL	550
	AuNPs/MoS ₂ /AuNPs	C-mAb	Saliva	0.18 to 72 ng/mL	40 pg/mL	531
DPV, CV	NiO	C-Ab	Human saliva	1 pg/mL to 10 μ g/mL	0.32 pg/mL	551
	2D disulfide nanoflakes	C-mAb + BSA	Human saliva	3.6 to 36.24 μ g/mL ($R^2 = 0.997$)	0.036 ng/mL	

	Carbon yarn	C-mAb + BSA	Human sweat	1 fg/mL to 1 μg/mL (R ² = 0.998)	0.005 fg/mL	552
	ZnO nanorods - yarn based	C-mAb	Human sweat	1 fg/mL to 1 μg/mL	0.45 fg/mL CV 0.098 fg/mL DPV	540
EIS, CV	Au NPs + PANI	C-mAb + BSA	PBS	0.36 pg/mL to 36.245 ng/mL (R ² = 0.989)	1.63 μA/M**	553
	1D & 2D ZnO nanoflakes	C-mAb	Human saliva	3.6 pg/mL to 36.2 ng/mL	0.36 pg/mL	554
EIS	Au	C-mAb	Interstitial fluid in vitro	0.36 pg/mL to 36.245 ng/mL (R ² = 0.997)	0.36 pg/mL	555
	ZnO	C-Ab	Synthetic and human sweat	10 to 200 ng/mL (R ² = 0.996)	1 pg/mL (synthetic sweat) 1 ng/mL (human sweat)	532
	Graphene + Au NPs	Aptamer	Human serum	10 to 30 pg/mL (R ² = 0.995)	10 pg/mL	535
	Au	C-Ab + BSA	Fish plasma	1.44 to 21.7 μg/mL	2.75 μg/mL	556
	RGo	C-Ab + BSA	Human saliva	0.0036 to 36.2 ng/mL (R ² = 0.93)	0.036 ng/mL	557
	Graphene and amphiphilic polymer	C-Ab	Human saliva	1 pg/mL to 10 ng/mL (R ² = 0.977)	1 pg/mL	558
	Palladium + MoS ₂	C-Ab	Human sweat	1 to 500 ng/mL	1 ng/mL	515

			(R ² = 0.998)		
Au	C-mAb	Human sweat	0.001 to 200 ng/mL	-	559
Au	C-mAb		[ng/mL]	[ng/mL]	560
		Human serum,	50 to 200	10	
		whole blood,	50 to 200	10	
		saliva,	1 to 40	1	
		sweat	10 to 150	10	
Au	C-Ab + BSA	Human saliva	0.001 to 10 ng/mL	0.87 pg/mL	534
			(R ² = 0.9831)		
-	C-mAb	Human tears	0.05 to 200 ng/mL	21.66 ng/mL	561
			(R ² = 0.986)		
Carbon	Imprinted polymer	Human saliva	0.18 to 23.19 ng/mL	0.05 ng/mL	562
			(R ² = 0.993)		

*The units have been converted to adequate values in g/mL just to facilitate the reader the data comparison (cortisol Mw = 362,46 g/mol)

**Works that only detail the sensitivity

4.4.1.4 Conclusions and Future perspectives

Reliable and accurate devices for quantitative analyses may represent a crucial inflection point to diagnose several diseases. This review highlights the relevance of electrochemical detection of cortisol, paying particular attention to the past five years, during which time, the necessity for real-time and continuous monitoring of cortisol levels for fast diagnosis has come to the fore. Electrochemical immunosensors meet requirements for detection of cortisol in both physiological and pathological ranges, for low LOD and with the key advantages of fast response times, rapid and continuous measurement, and a much lower use of reagents. Furthermore, biosensing devices can be easily integrated into PoC devices. Therefore, in the next couple of years, reliable, accurate, quantitative electrochemical sensors for the detection of cortisol can be expected to drive the large-scale distribution of PoC devices for a non-invasive, rapid, accurate, and real-time cortisol detection in biological fluids.

While most papers currently report single-use sensors due to their immunosensor properties, the optimum goal is the development of wearable and reusable devices able to provide real-time monitoring with the typical sensitivity of an immunosensor, as well as all its advantages. However, developing an ideal PoC sensor to comply with the sample rigor and LoD still present a challenge, and current issues such as antibody stability in ambient environments, their high cost of production, and possible cross-reactivity with interferences (i.e., aldosterone, progesterone, and prednisolone) must be overcome. More improvements will need to be made to increase the sensitivity and specificity of these devices.

Corresponding Authors

* E-mail: gemma.gabriel@imb-cnm.csic.es

** E-mail: abdelhamid.errachid@isa-lyon.fr

Author Contributions

All authors contributed to the drafting of the manuscript. The corresponding authors provided to the manuscript review. All authors have approved the final version of the manuscript.

Notes

Authors declare no competing financial interest.

Acknowledgments

M. Zea would like to acknowledge his financial support covered by Fundación Centro de Estudios Interdisciplinarios Básicos y Aplicados (CEIBA)-Gobernación de Bolívar (Colombia). This work was supported by the Spanish government-funded project RTI2018-096786-B-I00, and RTI2018-102070-B-C21 by Ministerio de Ciencia, Innovación y Universidades (MINECO/FEDER, EU). The authors also want to thank the support of the Generalitat de Catalunya to 2017-SGR-988, and the SU-8 Unit of the CIBER in Bioengineering, Biomaterials, and Nanomedicine (CIBER-BBN) at the IMB-CNM (CSIC) of ICTS "NANBIOSIS." This work has also made use of the Spanish ICTS Network MICRONANOFABS partially supported by MEINCOM. This work was also partially supported by the EU H2020 research and innovation program KardiaTool with agreement N° 768686 and from CAMPUS FRANCE program agreement PHC PROCOPE 40544QH.

4.4.2. Publication V: A Fully Paper-Based Electrochemical Sensor Made by Inkjet Printing for Saliva Cortisol Detection

The third paper presented in this Chapter, **Publication V**, is a submitted article about the development of a fully inkjet printed cortisol immunosensor on a porous paper substrate. The article is focused in the development, characterization, and biofunctionalization of inkjet printed pattern on a porous paper substrate for the detection of cortisol in human saliva. A novel proposal of cortisol sensor is proposed in this article, showing high sensitivity and do not show interferences with interesting cytoquines and proteins.

This article has been edited from the version submitted to ACS Applied Materials & Interfaces, with permission from ACS (edition consist in formatting and numbering figures, references, tables, and equations in accordance with the thesis manuscript, however acronym corresponds to the article):

Miguel Zea, Hamdi Ben-Halima, Ana Moya, Rosa Villa, Nadia Zine, Abdelhamid Errachid; and Gemma Gabriel. **A Fully Paper-Based Electrochemical Sensor Made by Inkjet Printing for Saliva Cortisol Detection**. Submitted

This work has been also presented in different conferences with their corresponding Proceedings:

- ❖ Conference **Transducer – Eurosensors XXXIII2019**: Miguel Zea, Ana Moya, Imad Abrao-Nemeir, Juan Gallardo-Gonzalez, Nadia Zine, Abdelhamid Errachid, Rosa Villa, and Gemma Gabriel. All Inkjet Printing Sensor Device on Paper: for Immunosensors Applications. Poster presentation
- ❖ Conference **Nano Today2019**: Miguel Zea, Ana Moya, Imad Abrao-Nemeir, Hamdi Ben Halima, Nadia Zine, Abdelhamid Errachid, Rosa Villa, Gemma Gabriel. Flexible inkjet printed device for detection of cortisol in Saliva. Poster presentation
- ❖ Conference **FLEX MEMS & SENSORS2020**: Miguel Zea, Ana Moya, Eloi Ramon, Gemma Gabriel. Development of inkjet printed biosensors on flexible and porous substrates. Oral presentation.

A Fully Paper-Based Electrochemical Sensor Made by Inkjet Printing for Saliva Cortisol Detection

Miguel Zea^{‡‡}, Hamdi Ben-Halima[§], Ana Moya[‡], Rosa Villa^{‡¶}, Nadia Zine[§],

Abdelhamid Errachid[§] and Gemma Gabriel^{‡¶}*

[†]Instituto de Microelectrónica de Barcelona IMB-CNM (CSIC), Campus Universitat Autònoma de Barcelona, 08193 Cerdanyola del Vallès, Barcelona, Spain

[‡]PhD in Electrical and Telecommunication Engineering, Universitat Autònoma de Barcelona (UAB), Bellaterra, Barcelona, Spain

[§] Université Claude Bernard Lyon 1, Institut des Sciences Analytiques (ISA), 5 rue de la Doua, 69100, Villeurbanne, Lyon, France

[¶]CIBER de Bioingeniería, Biomateriales y Nanomedicina (CIBER-BBN)

Keywords: Inkjet Printing, paper substrate, cortisol, stress hormone, electrochemical impedance spectroscopy, electrochemical sensor.

*Note: The supplementary information of this article can be found in section 6.4 (Figures and tables number with S of prefix are inserted there).

Abstract

Electrochemical paper-based analytical devices (ePADs) have emerged as innovative approaches, transforming the field of Point-of-Care (PoC) devices and wearable devices by offering a low-cost, disposable or reusable, easily scalable, versatile and with a low environmental-footprint method for real-time diagnostics or readings on-site. The achievement of sensing in real sample with complex matrix of interferences by ensuring good readings and accurate results remains a fundamental challenge for ePADs. The need to build a solid, factual, and cost-effective ePAD is the primary justification. The development of a sensor for cortisol detection in everyday life has many applications, including healthcare, sports, high-risk jobs, among others. In this paper, a functional all-inkjet paper-based electrochemical immunosensor using gold (Au) printed ink as transducer was used for the detection of salivary cortisol with Electrochemical Impedance Spectroscopy (EIS). Covalent binding of Cortisol monoclonal-antibody onto the printed Au surface was achieved through the electrodeposition of 4-carboxymethylaniline (CMA), and non-specific binding was avoided with ethanolamine passivation. The ePAD shows a linear response between the physiological cortisol range in standard solution, artificial saliva, and human saliva (5 - 20 ng/mL), with sensitivity of 25, 23, and 19 $\Omega \cdot \text{ng/mL}$ with a $R^2 = 0.995$, $R^2 = 0.979$, and $R^2 = 0.99$ and a limit of detection (LOD) of 1.18, 1.09, and 0.81 ng/mL, respectively. An interferences study was also carried out against Tumor Necrosis Factor- α (TNF- α) and N-Terminal pro B-type natriuretic peptide (NT-proBNP), which yielded excellent results. Our proposed fabrication method is the first, as far as we know, cortisol biosensor made by inkjet printing technology, moreover it has been developed on a paper substrate that allows to reach higher electrochemical active surface area with same 2D dimensions. This novel ePAD will significantly simplify the fabrication process, reduce environmental-footprint, and lower fabrication costs.

4.4.2.1 Introduction

Paper-based devices have been used in the development of sensors for bioanalytical methods usually know as PADs or μ PADs, due to its biocompatibility, lightweight, chemical stability, biodegradability, 3D fibrous structure, availability, easy production, inertness to generally utilized reagents, and easy modification.⁵⁶³ PADs or μ PADs usually comprise an arrangement of hydrophilic channels and hydrophobic structures that can be easy patterned on paper substrate using printing or cutting technologies.⁴⁰² Enabling devices to have a pump-free microfluidic system.^{341,399,564} Recent works show

paper as one of the most widely used substrates for the development of disposable, low-cost, and eco-friendly sensing devices.^{565,566}

The development of effective point-of-care devices employing electrochemical paper-based analytical device has potentially set the stage for creating devices that are more portable, simpler, disposable, reliable, and highly sensitive. They provide more reliable measurements than colorimetric or single electrode sensors.⁴⁰⁴

ePADs can now be used in a wide range of areas, including biomedical, food processing, environmental, clinical analysis, and the chemical industry, among others.⁴⁰⁶ Electrochemical sensors are inexpensive, have high sensitivity and selectivity, a wide variety of detection techniques, can be miniaturized, and can perform a variety of assays.⁵⁶⁷ Therefore, ePADs allow the miniaturization of electrodes and their deposition using a variety of technologies.⁵⁶⁶ However, screen-printing still remains the most technique for the production of electrodes on ePADs.⁵⁶³ However, innovation is critical to the advancement, and research efforts have been made towards innovations in this field in search of a game changer ePADs fabrication technique. Therefore, the inkjet printing technology appear to be promising.

The inkjet printing technology has many advantages over traditional ePADs fabrication techniques, including easy layout modifications without the use of screen or stencils, waste reduction and non-contact deposition.² Because of its non-contact deposition process, inkjet printing prevents substrate contamination; additionally, it allows the technology to be compatible with delicate or super-thin paper substrates that would be compromised by force application using another technique. Paper-based devices combined with inkjet printing technology are paving the way for inkjet printed ePADs for biological and chemical sensing.¹⁰² However, most inkjet printed-based ePADs to date are simple cases in which basic chemicals are used without any further electrode modification or complex analyte to measure/detect.^{100,102,125,242,390}

The aim of this research is to fabricate an inkjet printed-based ePADs for cortisol detection on a real physiological sample (saliva), demonstrating the capability of an inkjet printed electrode on paper to be bio-functionalized with antibodies and detect cortisol hormone. Cortisol hormone is commonly used as an important biomarker of human and animal stress, which is why it is mostly known as “the stress hormone”. Cortisol, on the other hand, plays many important roles in humans, including blood pressure control, immune system regulation, protein, carbohydrate, and adipose metabolism, and anti-

inflammatory action. Many attempts are being made to improve cortisol sensors because of their ties to diseases such as Cushing syndrome, Addison's disease, stress, and even heart failure.⁵⁶⁸ Over the last decade, electrochemical measurements have demonstrated reliable cortisol detection even in biological matrices such as plasma, blood, serum, sweat, saliva, and hair, with the benefits of a fast and precise response by portable and wearable devices.⁵⁶⁹ Immunoassays or immunosensing techniques with different transducers and sensing receptors are leading the way in screening methods innovation.^{486,487} Recent developments use quantitative biomarkers with the adoption of electrochemical sensors and image analysis.⁴⁹¹⁻⁴⁹³ However, the most reliable and widely used method in portable and disposable devices for cortisol detection is based in antigen/antibody binding.⁵⁷⁰ Image analysis methods, on the other hand, require sophisticated equipment and bulky optical detectors, while electrochemical sensors allow the development of portable and wearable point of care devices. In order to have a cortisol electrochemical sensor, transducer surface must be modified to interact with cortisol molecules and register changes in the transducer's electrical properties. To the best of our knowledge, a cortisol electrochemical sensor made by inkjet printing technology that detects cortisol in a physiological sample is yet to be reported in the literature. Therefore, we present a novel biosensing fully printed platform on paper that detects cortisol in physiological range in untreated human saliva. This is, as far as we know, the first printed paper-based platform to detect cortisol, paving the way for the development of printed paper-based biosensing systems based on inkjet printing technology.

This platform contains four Au working microelectrodes (WEs), two Au counter microelectrodes (CEs), and two pseudo-references (REs) allowing a simultaneous detection for $n = 4$ of samples. Cortisol antibodies were successfully immobilized on WEs and cortisol detection was performed by Electrochemical Impedance Spectroscopy (EIS). Our proposed printed paper-based biosensing platform is very attractive due to its innovation and novelty; additionally, it establishes the first steps in the detection of cortisol using inkjet printing technology, which we believe can be scaled in the detection of other hormones and cytokines.

4.4.2.2 Materials and methods

4.4.2.2.1 Materials and chemicals

For the development of the printed platform, we used three commercially available inks. A low-curing Au colloidal ink (DryCure Au-J 1010B from Colloidal Ink Co., Ltd, Japan), silver (Ag) nanoparticle ink (Dupont-PE410, USA), and SU-8 ink (2002 from MicroChem, USA). Additionally, a silane-based ink

was formulated¹³⁹² for substrate treatment using Tetraethyl orthosilicate 98+% (TEOS), 1H,1H,2H,2H-perfluorooctyltriethoxysilane (POTS, from abcr GmbH, Deutschland), absolute ethanol, hydrochloric acid 36% (HCl), and distilled water. All the ink formulations were printed with a drop-on-demand Dimatix Materials Printer (DMP 2831 from Fujifilm Dimatix, USA). HCl (0.1 M) was used for the chlorination of the printed Ag electrode, and potassium chloride (KCl, 0.1 M) for testing the pseudo-reference electrode (pRE). Whatman cellulose paper grade 1 (WHA3001861) with a thickness of 180 μm with a porosity of 0.686 and pore diameter of 11 μm was used as substrate.

Phosphate buffered saline (PBS), potassium hexacyanoferrate (III) ($\text{K}_3[\text{Fe}(\text{CN})_6]$) and potassium hexacyanoferrate (II) trihydrate ($\text{K}_4[\text{Fe}(\text{CN})_6]$) were used for activation and characterization of the printed microelectrodes. 4-carboxymethylaniline (CMA), N-hydroxysuccinimide (NHS), N-(3-dimethylaminopropyl)-N'-ethylcarbodiimide hydrochloride (EDC-HCl), sodium chloride (NaCl), sodium nitrate (NaNO_2), and ethanolamine (from Fluka, France) were used for sensor biofunctionalization. For the preparation of the artificial saliva, we used sodium chloride (NaCl, purity $\geq 99.5\%$), potassium chloride (KCl, purity 99-100.5%), sodium phosphate dibasic (NaHPO_4 , PharmaGrade), calcium chloride (CaCl_2 , purity $\geq 93\%$), mucin (from pork stomach extract, type II), and urea. All reagents mentioned above were purchased from Merck KGaA (except the ones that mention another) and were used without further purification.

To detect cortisol; anti-Cortisol monoclonal antibody (Cat. No. XM210) was purchased from Novus Biological (France), hydrocortisone (cortisol, Cat. No. ab141250) was purchased from Abcam (France), human TNF- α antigens (TNF- α) (Car. No. 210-TA) was purchased from R&D Systems (France), and NT-proBNP (Cat. No. 8NT2) was from HyTest (Finland).

4.4.2.2.2 Preparation of aliquots

Following supplier protocol, Cortisol monoclonal-antibody (anti-Cortisol), and antigens TNF- α , NT-proBNP and cortisol were reconstituted in PBS buffer solution to obtain a concentration of 1 $\mu\text{g}/\text{mL}$ to then prepare the aliquots with a concentration of 100 $\mu\text{g}/\text{mL}$ for stock them in the freezer at $-20\text{ }^\circ\text{C}$.

Aliquots of anti-Cortisol, TNF- α , and NT-proBNP with a concentration of 10 $\mu\text{g}/\text{mL}$ were prepared by dissolving the indicate amount of PBS in the stock solutions. The standard solutions for the detection of cortisol containing different concentrations 5, 10, 15 and 20 ng/mL were prepared taking the

appropriate amount of stock solution (100 µg/mL) and adding it to the correct amount of buffer solution.

The same procedure was performed to obtain standard solutions of antibody and antigens in artificial saliva in the same concentration range that were prepared before. Artificial saliva has been prepared as is described,⁵⁷¹ by dissolving 0.6 g/L of sodium phosphate dibasic (Na₂HPO₄), 0.6 g/L of anhydrous calcium chloride (CaCl₂), 0.4 g/L of potassium chloride (KCl), 0.4 g/L of sodium chloride (NaCl), 4 g/L mucin, and 4 g/L urea in deionized water, adjusted to pH 7.2 by adding NaOH or HCl (both 0.1 M), sterilized by autoclaving and stored at -4 °C until use.

4.4.2.2.3 Biosensor inkjet platform fabrication

The construction of the inkjet printed microelectrodes on paper was done as we previously demonstrated⁵⁷². Basically, a drop-on-demand Dimatix Material Printer (DMP 2831 for Fujifilm Dimatix, Inc., USA) was used with the 10 pL printhead. The microelectrodes structure was digitally designed using CleWin 5 software then exported to BMP to load in the Dimatix Bitmap editor. The printing process was carried out in standard laboratory conditions without particles-filter, temperature, and humidity control. However, in this study, we faced a challenge of attach antibodies on the electrodes with all processes for bio-functionalization that it needs.

Furthermore, an electrochemical platform with four working electrodes (WE), two references (RE) and two counter electrodes (CE) was designed for this study, enabling us to achieve four samples n = 4) in each trial and facilitate future applications.

Figure 4.15a shows the fabrication steps for obtaining a full inkjet printed sensor on paper substrate. The complete fabrication of the printed platform can be easily understood as two steps: The printing process of the metallic microelectrodes and then the electrodes modification. In the first step, the silane ink was first printed (a.ii) to obtain a hydrophobic surface where platform will take place, followed by printing Ag ink (a.iii) to obtain the Ag elements: the RE (500 x 500 µm), tracks, and pads, with a Drop Spacing (DS) of 20 µm. Ag elements were dried at 80 °C for 15 min. Then, the four Au WEs were printed (a.iv) 800 x 800 µm and two 800 x 3000 µm CEs, with a DS of 15 µm, and it was dried as before. Both inks were finally sintered in the oven at 140 °C for 60 min. Then the dielectric ink SU-8 was printed (a.v) on Ag tracks to isolate and define the active electrode area and pads with a DS of 15 µm. It was

cured, first with a soft bake on hot plate at 100 °C for 5 min followed by an UV treatment for 30 sec to polymerize this layer by polymer cross-linking. A picture of the final fabricated platform is shown in Figure 4.15b.

a) Printing process

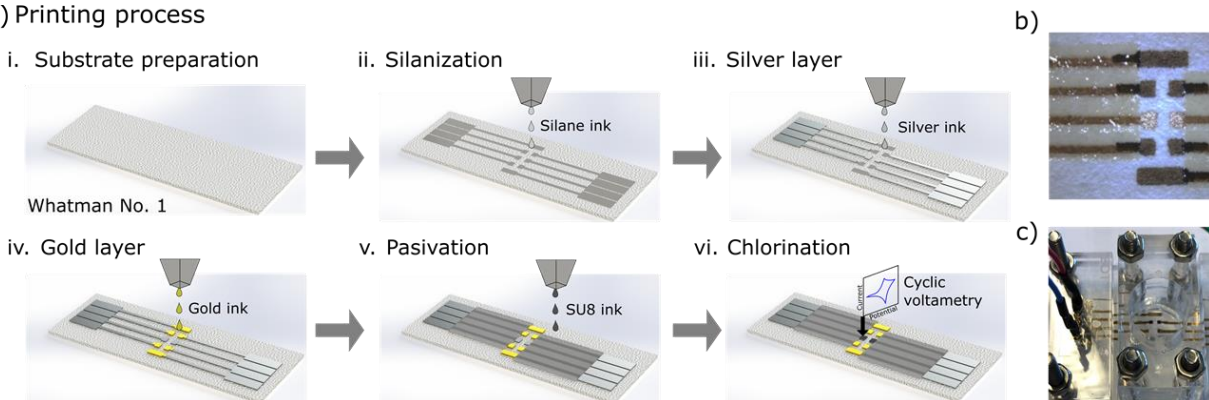


Figure 4.15. Fabrication process of cortisol immunosensor.

a) Illustration of the biosensor platform fabrication process: (i) Substrate preparation; (ii) Printing silane ink for turning the substrate hydrophobic; (iii) Printing of the Ag pRE, connections and pads followed by a drying step; (iv) Printing Au ink WEs, followed by a sintering step; (v) Printing of the passivation SU-8 layer, followed by soft bake and UV curing; (vi) Chlorination by CV of silver elements to form the pRE-electrode. b) Picture of the biosensor platform. c) Customized electrochemical interface fabricated in Poly(methyl methacrylate) with movable add-ons for the use of up to four microelectrodes in static conditions

The second step, two electrochemical procedures were required to obtain a functional electrochemical platform. Firstly, the Ag RE was chlorinated (a.vi) by cyclic voltammetry (CV) (Figure S1) in 0.1 M HCl, scanning the potential from 0 V to 0.2 V versus Ag/AgCl commercial reference electrode (RE) at 20 mV/s to obtain a stable Ag/AgCl pRE. Secondly, the Au WEs were electrochemically activated by amperometric pulses (5 pulses of 5 s from 0 to -0.2 V) in PBS.⁴³⁷

4.4.2.2.4 Optimization of CMA electrodeposition

CMA 5 mM solution was selected to determine optimum electrodeposition parameters for coating printed Au WEs with a range in CV speeds (25, 50, and 80 mV/s) and CV cycles (5, 6, and 7), and CV in ferro/ferricyanide was carried out to analysis results.

4.4.2.2.5 Bio-functionalization of gold surface

There are several steps involved in the bio-functionalization of WEs. The WEs were first electrochemically activated as described above (Figure 4.16a), and then their characterization was studied using CV in ferro/ferricyanide (10 mM) solution. CV was also used in the above CMA electrodeposition.^{525,571} Basically, 5 mM CMA was prepared in deionized water with 15 mM HCl and 15 mM NaNO₂. The solution was used directly from the fridge at 4 °C to perform the CMA electrodeposition. The printed platform was placed in an electrochemical cell (as shown in Figure 1c) with the CMA solution, where seven cycles at 25 mV/s from -1.2 to 0.2 V were applied by CV to ensure an appropriate CMA blocking layer (Figure 2b), after which the printed platform was rinsed with water and dried with nitrogen. Activation of the carboxylic acid groups of CMA molecules was done by incubation of EDC/NHS (0.4 M/0.1 M) in ethanol for 1 h at room temperature (Figure 4.16c), consequently, rinse with HCl 0.1 M to remove EDC/NHS excess, and immediately incubated anti-Cortisol at 5 µg/mL for 90 min in the fridge at 4 °C (Figure 4.16d). Printed platform was then rinsed with PBS and ethanolamine solution (1% in PBS) was incubated for 30 min to deactivate remained active carboxylic acid groups (Figure 4.16e).

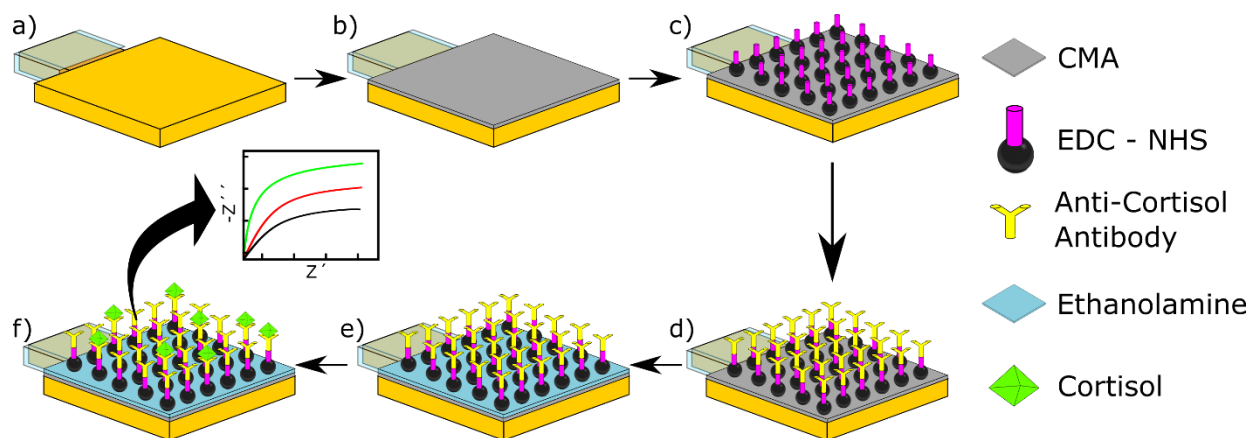


Figure 4.16. Biofunctionalization of an inkjet printed electrode.

Schematic recreation of the bio-functionalization of a WE. a) Representation of a activated gold electrode. b) Electrodeposition of CMA on gold WEs by applying CV. c) CMA activation by incubation of mixture EDC-NHS. d) Bio-functionalization through incubation with Anti-Cortisol antibodies. e) Deactivation of the remained active groups by incubation in ethanolamine solution. f) Incubation of the platform into cortisol solution followed by detection of cortisol by EIS.

For cortisol detection (Figure 4.16e), standard solutions containing different concentrations of cortisol (5, 10, 15, and 20 ng/mL) were incubated. Each incubation was performed for 30 min at 4 °C to ensure

antigen conservation. After each incubation, the sensor platform was rinsed with abundantly PBS. Finally, the sensor platform was immersed in ferro/ferricyanide to carry the EIS for at least 5 min to avoid absorptions and miss readings.

4.4.2.2.6 Determination of cortisol antigen

EIS were performed to detect cortisol in standard solution (PBS), artificial saliva, and human saliva with different concentration (5, 10, 15, and 20 ng/mL) using ferro/ferricyanide parameter were set at; equilibration time 0 s, fixed potential scan with $E_{dc} = 0.154$ V and $E_{ac} = 0.01$ V within the frequencies 0.7 and 1000 Hz over a 5 minutes period. The error of the immunosensor was also calculated by performing measurements in quadruplicate taking advantage of the printed platform.

4.4.2.2.7 Human saliva sampling procedure

Saliva samples were collected from five nominally healthy volunteers using the Salivette® (Art. No. 51.1534.500, Sarstedt, Germany) sampling device, it is specially intended for cortisol determination in saliva. The volunteers were asked to move the swab in the oral cavity for 2 min at a self-selected pace. Saliva was recovered by centrifugation of devices at 7000 rpm for 5 min at 4 °C. A pooled saliva sample was prepared by mixing all collected samples. It was then used to prepare samples for the calibration curve with spikes of cortisol antigen similarly to what have done in section 4.4.2.2.2.

4.4.2.3 Results and discussion

4.4.2.3.1 Characterization of the functionalized gold surface

The fully printed platform on paper and the customized electrochemical interface fabricated in Poly(methyl methacrylate) with movable add-ons for the use of up to four microelectrodes in static conditions (Figure 4.15c) detection was previously reported by our group⁵⁷². CV curves for reduction and oxidation reaction of ferro/ferricyanide of bare Au electrodes before and after activation are shown in Figure 4.17a. As can be observed electrodes activation is a crucial step to ensure performance of the electrodes. The two characteristics redox peaks are clearly on plot, which were assigned to the electron reduction and oxidation reactions of ferro/ferricyanide. Anti-Cortisol was immobilized onto Au microelectrodes through CMA molecules. CMA molecules have been electrochemically deposited onto Au WEs by using CV technique as is shown in Figure 4.17b, the scan rate was at 25 mV/s and the switching potential was scanned between -1.2 to 0.2 V for 7 cycles. Figure 4.17c shows CV performed

ferro/ferricyanide for Au WE before and after CMA deposition. The oxidoreduction peaks of activated WE have totally disappeared after CMA deposition due to the weak electron transfer kinetics of ferro/ferricyanide caused by the CMA blocking layer. To immobilize the antibodies on the electrode surface, carboxylic acid groups of CMA molecules has been activated by incubation in EDC/NHS in ethanol solution for 1 h at room temperature. Afterward, the device has been washed with HCl 0.1 M to remove the excess of EDC/NHS and immediately incubated in PBS solution containing anti-Cortisol for 90 min at 4 °C. Afterward, the remained active carboxylic acid groups have been deactivated by incubation in ethanolamine solution (1% in PBS) for 30 min at room temperature. This step is very important to prevent nonspecific bonding at the detection stage.

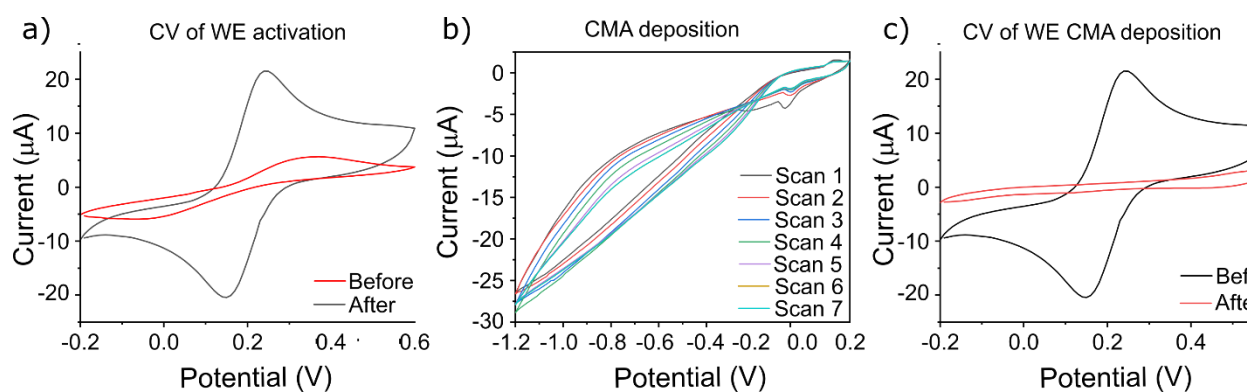


Figure 4.17. Electrochemical characterization of biofunctionalization.

a) CV of ferro/ferricyanide redox couple before and after the activation of WEs, b) Seven CV cycles applied to WEs for deposition, c) CV of gold WE before and after CMA deposition

4.4.2.3.2 Optimization of CMA deposition

Owing printed Au intrinsic properties (roughness, nanoparticles structures, non-planar structure, among others, show in Figure S2) CMA electrodeposition must be optimized to immobilize an optimal amount of anti-Cortisol antibodies on WEs. CMA must be electrodeposited onto Au creating a blocking CMA coating layer, therefore the oxidoreduction peaks of ferro/ferricyanide of CMA blocked Au microelectrode have to disappear due to weak electron transfer kinetics between ferro/ferricyanide and CMA. A set of experiments were performed in order to obtain a planar response in ferro/ferricyanide after CMA deposition. 5 mM CMA solution was used to run electrodeposition CVs with a range in CV speeds of 25, 50, and 80 mV/s and CV cycles 5, 6, and 7, Figure S3 in the supporting information shows electrodeposition curves. Electrodeposition CVs showed a broad irreversible cathodic wave with a peak at different potentials, indicating the attachments of CMA molecules onto Au surface by diazonium salt

reduction. On the first cycle cathodic current was higher than consequent cycles similarly to reported for microfabricated⁴⁸⁶, and even screen Au electrodes⁵⁷³ pointing out the path to follow. Finally, CVs in ferro/ferricyanide were carried out to analysis results of CMA electrodeposition (Figure S2). Seven cycles at 25 mV/s from -1.2 to 0.2 V CMA electrodeposition show a CV in ferro/ferricyanide planar without oxido/reduction peaks and capacitive charge, these mentioned parameters were selected for the CMA electrodeposition.

4.4.2.3.3 Detection and interference of cortisol in standard solution

The EIS plots of the platform ($n = 4$) biosensor at different concentrations of cortisol are shown in Figure 4.18a in Nyquist plot presentation. The first semi-circle corresponds to the immobilized anti-Cortisol. After the incubation of the biofunctionalized WE in 5 ng/mL of cortisol, the second Nyquist plot semi-circle has increased from the first showing thus an increase in impedance which confirm the biorecognition between antibodies and their corresponding antigens cortisol (Figure 4.18a). Nyquist plot semi-circles have continued to increase by increasing the concentration of cortisol antigens which highlight the good sensitivity of the biosensor. The increase in the diameter of the Nyquist plots is attributed to the binding of cortisol to immobilized anti-Cortisol antibody on the WE, producing an insulating layer that decreases the electron transfer for the redox probe. Nyquist plot semi circles were then fitted using Randles equivalent circuit model (Figure 4.18b inset) where R_s (solution resistance), R_p (charge-transfer resistance), and CPE (constant phase element), an equivalent model of double-layer capacitance.⁵⁷⁴ The real part of impedance ($\text{Re}(Z)$) increased as function of cortisol concentration. This was due to the increase of the R_p between WE and electrolyte as the bonding of cortisol increase onto the WE. Therefore, the increase of R_p is directly related to the sensitivity of the biosensor. The normalized data, shown in Figure 4.18b were presented as $\Delta R/R$ (where $\Delta R = R_p(\text{cortisol}) - R_p(\text{antibodies}) / R_p(\text{antibodies})$) as a function of cortisol concentration. Normalized data reveals a linear detection range for cortisol concentrations in the range of measurements. The biosensor exhibits a sensitivity of $25 \Omega \cdot \text{ng/mL}$ with a correlation coefficient of 0.995 and a limit of detection (LOD) of 1.18 ng/mL. Therefore, in order to investigate the selectivity, additional tests were performed using solutions containing interesting cytokines TNF- α , symptom of an infection and NT-proBNP that was identified as the Au standard biomarker for HF diagnosis and therapy monitoring.

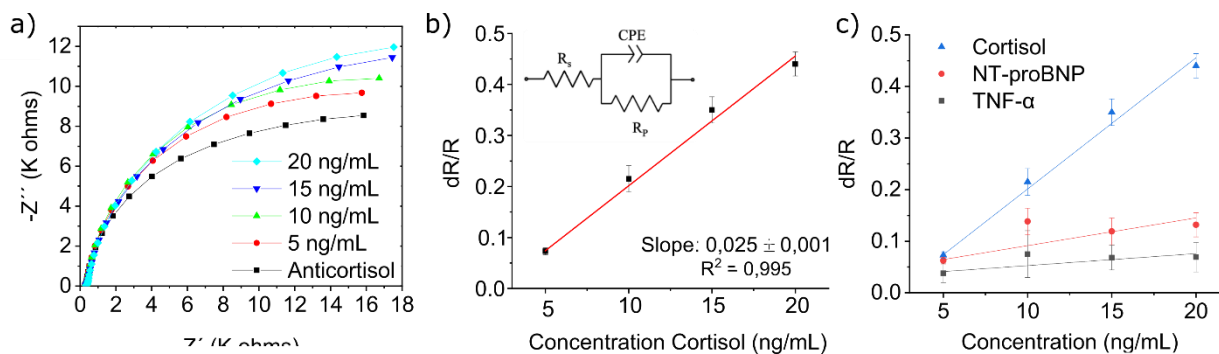


Figure 4.18. Detection of cortisol in standard solution.

a) Nyquist impedance plots (at PBS) of cortisol solution analyzed by EIS. b) Calibration curve for normalized data obtained from EIS studies for different cortisol concentration (caption: Randles equivalent circuit model). c) Linearity curve for normalized data obtained from EIS studies for interference NT-proBNP and TNF- α .

These cytokines are also present in saliva; however, they have not inherent interference with cortisol due to structure differences, but interference test is necessary to prove biosensor selectivity. Additionally, knowing that biosensor does not show interference with these cytokines open the scenario to have a multiparametric platform. To this end, new biosensors have been biofunctionalized with anti-Cortisol using the procedure previously described, and then tested by EIS with cytokines (NT-proBNP and TNF- α) instead of cortisol. Here the biosensor was highly selective and sensitive to cortisol if compared to cytokines response (Figure 4.18c) which confirm the high selectivity of the developed biosensors. As seen in Figure 4.18c, the biosensor showed a higher selectivity to cortisol compared to NT-proBNP and TNF- α . The detection of cortisol demonstrates linearity upon increasing the concentration, with a sensitivity of $25 \Omega \cdot \text{ng/mL}$, but significant reduced current values were found by analyzing NT-proBNP (with a sensitivity of $3 \Omega \cdot \text{ng/mL}$) and TNF- α (with a sensitivity of $1 \Omega \cdot \text{ng/mL}$) standard solutions.

4.4.2.3.4 Detection of cortisol in artificial saliva

Artificial saliva was prepared as described in section 4.4.2.2.2 and used to simulate real saliva matrix. Here the same principle of EIS analyses performed before was made for cortisol detection using artificial saliva as buffer. First, in order to test the no specific adsorption, the biosensor previously biofunctionalized with anti-Cortisol was incubated for 30 min many times in unspiked artificial saliva (without any cortisol concentration) (Figure 4.19a). Here the first Nyquist plot semi-circle corresponds to the antibodies immobilized onto microelectrodes. The biosensor was rinsed abundantly with PBS and incubated another time (without cortisol) in artificial saliva for 30 min in order to see if there is an

increased phenomenon of adsorption. Nyquist plot were superimposed even after a third incubation without cortisol (data not shown). In order to observe deeply the effect of artificial saliva on the EIS analyses, different concentration (5, 10, 15, and 20 ng/ml) of cortisol were prepared using artificial saliva as buffer. A shift between the first and the second Nyquist plot semi-circles (Figure 4.19a) was observed after the first incubation of the biosensor in artificial saliva containing 5 ng/ml of cortisol. Consequently, the Nyquist plot semi-circles have increased with increasing concentration of cortisol, highlighting the cortisol detection in artificial saliva if compared to the previous test. Normalized data has also been plotted (Figure 4.19b) showing a sensitivity of $23 \Omega \cdot \text{ng/mL}$ with a correlation coefficient of 0.979 and LOD of 1.09 ng/mL.

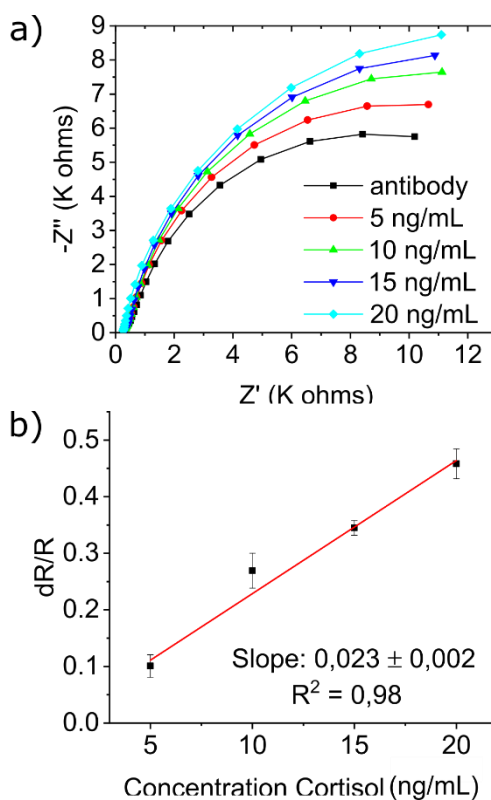


Figure 4.19. Cortisol detection in artificial saliva.

a) Nyquist impedance plots (at artificial saliva) of cortisol solution analyzed by EIS. b) Linearity curve for normalized data obtained from EIS studies for different cortisol concentration in artificial saliva.

Therefore, the biosensor was able to detect specifically cortisol within a complex matrix showing similar results than standard solution. Matrix effects are often caused by the alteration of ionization efficiency of target analytes in the presence of coeluting compounds in the same matrix. Matrix effects can be observed either as a loss in response (ion suppression) or as an increase in response (ion enhancement).⁵⁷⁵

Both the ion suppression and enhancement dramatically affect analytical performance of a method.⁵⁷⁶ However, our biosensing platform shows a small deviation in sensitivity showing a good performance of detecting cortisol even in a complex matrix.

4.4.2.3.5 Detection of cortisol in human saliva

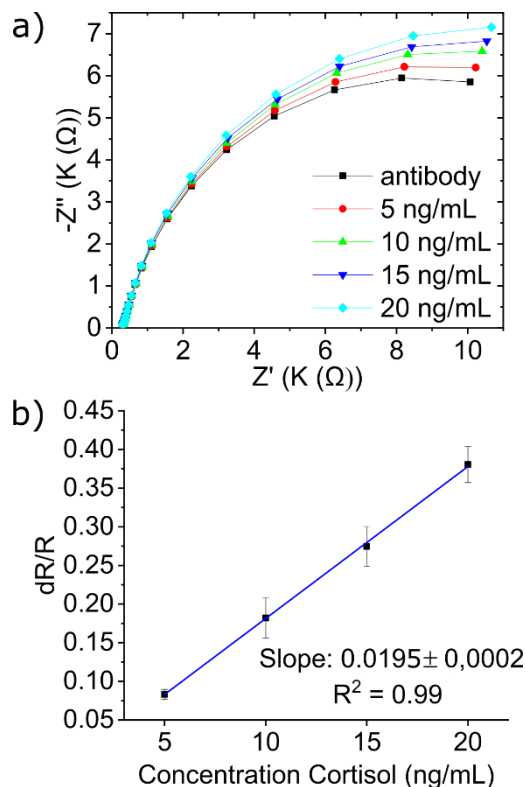


Figure 4.20. Cortisol detection in human saliva.

a) Nyquist impedance plots (at real saliva) of cortisol solution analyzed by EIS. b) Linearity curve for normalized data obtained from EIS studies for different cortisol concentration in real saliva.

The biosensor was biofunctionalized with anti-Cortisol and tested for real human saliva. As made for artificial saliva, the biosensor was incubated in human saliva for varying lengths of time to study nonspecific bonding in physiological medium. Same procedure was done, for each concentration, the biosensor was incubated in cortisol solution for 30 min, followed by PBS washing and EIS measurement showed in Figure 4.20a. The first Nyquist plot semi-circle corresponds to the anti-Cortisol. After the first incubation (5 ng/mL) in human saliva, the second Nyquist plot semi-circle has shifted from the first showing an increase in impedance which means bonding and detection. The biosensor was rinsed

abundantly with PBS and incubated (10 ng/mL) to observe if there is an increased phenomenon of bonding or detection, here the third Nyquist plot semi-circle (10 ng/mL) has increased from the second showing biorecognition phenomenon. The same phenomenon was observed for cortisol concentration of 15 and 20 ng/mL. It is clear that the diameter of the Nyquist plots increases with increasing cortisol concentration as we have seen before. Normalized data are shown in Figure 4.20b, for human saliva the biosensor sensitivity is $19 \Omega \cdot \text{ng/mL}$ with a correlation coefficient of 0.99 and LOD of 0.81 ng/mL, demonstrating the feasibility of cortisol detection even in human saliva samples, also avoiding matrix effect in the saliva. The small reduction in sensitivity can be explain due to interaction of cortisol hormone with ions in the artificial saliva and human saliva, which modify the electrical charge of the cortisol.⁵⁷⁷

A comparison with selected cortisol antibody-based electrochemical sensors in the literature is summarized in Table 1. Here, our proposed biosensing platform shows similar response or even better LOD than other reported works. This demonstrates the potential of the present work in contrast with recent published works. Also, the proposed methodology offers a novel fabrication method by inkjet printing technology, and the intrinsic properties that a paper-based device offer (low-cost, pump-free microfluidic, eco-friendly, among others). Moreover, proposed biosensing platform allow to measure cortisol with four microelectrodes using the same sample or even in the future measure four different analytes, thus demonstrating the biosensing platform applicability.

Table 4-4. Comparisson of published similar cortisol immunosensors.
Comparison of different cortisol electrochemical detection.

Electrode	Technique	Matrix	Linear Range (ng/mL)	Limit of Detection (ng/mL)	Ref.
Inkjet Printed Au	EIS	Standard solution	5 to 20	1.18	This work
Inkjet Printed Au	EIS	Artificial saliva	5 to 20	1.09	This work
Inkjet Printed Au	EIS	Human saliva	5 to 20	0.81	This work
E-beam evaporated Au	EIS	Human saliva	1 to 40	1	560
Screen printed Au	EIS	Human tears	0.05 to 200	21.66	561
Screen printed graphite	SWV*	Human saliva	0.5 to 55.1	1.7	547
Screen printed carbon	CA**	Standard solution	0.1 to 200	0.1	533
Screen printed Ni-SPE	CV	Human saliva	90 to 9000	26.82	578

*Square wave voltammetry

**Chronoamperometry

4.4.2.4 Conclusions

The development of a new biosensor platform for the detection of cortisol in human saliva samples by EIS is presented in this study. The biosensor platform is based on inkjet printed Au electrodes on paper substrate, and bio-functionalization was optimized for this additive rough technology. The biosensing platform was bio-functionalized by CMA electrodeposition and anti-Cortisol antibodies immobilization, resulting in a sensitive device with a good performance and sensitivity for the detection of cortisol, even in presence of other potential interferences such as NT-proBNP and TNF- α . Tests performed in both artificial saliva and human saliva demonstrated the biosensing platform's capability to detect cortisol in physiological ranges, with a linear relationship between increasing cortisol concentration and charge transfer resistance. The biosensing platform also showed very promising results also in analyzed artificial saliva and human saliva. Furthermore, the biosensing printed platform allows further implementation of a multiparametric biosensing tool for diagnosis or/and monitorization of related diseases using saliva samples.

Corresponding Author

* E-mail: gemma.gabriel@imb-cnm.csic.es

Author Contributions

All authors contributed to the drafting of the manuscript. The corresponding authors provided to the manuscript review. All authors have approved the final version of the manuscript.

Notes

Authors declare no competing financial interest.

Acknowledgments

M. Zea would like to acknowledge his financial support covered by Fundación Centro de Estudios Interdisciplinarios Básicos y Aplicados (CEIBA)-Gobernación de Bolívar (Colombia). This work was supported by the Spanish government-funded project RTI2018-096786-B-I00, and RTI2018-102070-B-C21 by Ministerio de Ciencia, Innovación y Universidades (MINECO/FEDER, EU). The authors also want to thank the support of the Generalitat de Catalunya to 2017-SGR-988, and the SU-8 Unit of the CIBER in Bioengineering, Biomaterials, and Nanomedicine (CIBER-BBN) at the IMB-CNM (CSIC) of ICTS "NANBIOSIS." This work has also made use of the Spanish ICTS Network MICRONANOFABS partially supported by MEINCOM. This work was also partially supported by the EU H2020 research and innovation program KardiaTool with agreement N° 768686 and from CAMPUS FRANCE program agreement PHC PROCOPE 40544QH.

Chapter 5 | Conclusion and further work

This Chapter describes the most relevant goals achieved during the development of the present thesis work to cover the necessities to develop the inkjet printing technology and its integration with PoC device systems.

5.1. Concluding remarks

As the development of low-cost sensor for PoC devices is mainly based in to develop functional, reliable, and low-cost sensors and easy to incorporate to the system, the aim of this thesis work has been the development of these biosensors using inkjet printing technology that fulfill all the requirements to fabricate them.

The main goal has been to develop novel printed sensors with unique features such as, novel ink, fully printed, and implementation of a new substrate. Specifically, the developed sensors were designed allowing their integration with portable potentiostat. Inkjet printing technique has been employed during this work, using three different substrates and two novel inks. Also, it shows the possibility of use metal inks on substrates with low glass-transition temperature.

In the development of the inkjet printing technology, in this thesis work, four sensing platforms have been proposed. The final fabricated devices are shown in Figure 5.1.

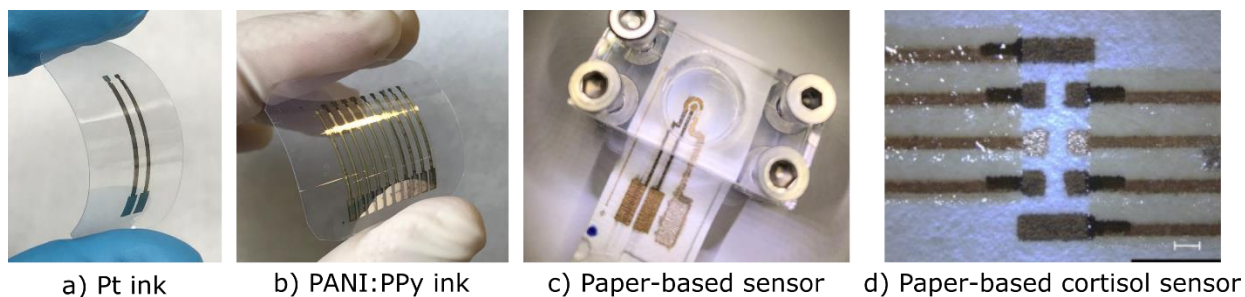


Figure 5.1 Developed sensors in this thesis.

Images of the sensing devices presented in this thesis, a) novel Pt ink-based pH sensor, b) fully printed pH sensor, c) Inkjet printed strategies on porous paper, and d) paper-based printed cortisol sensor

The first two developed sensing platforms (Figure 5.1a)) were develop on a plastic substrate. The first is a pH sensor based in a novel Pt ink, which enhanced the adhesion of IrOx sensing layer thin film allowing sensor operation over a year. Following by a fully-printed pH sensor is develop (Figure 5.1b)), where a specially designed PANI/PPy ink is synthesize and set-up for inkjet printing. This ink was printed on a singular chemical functionalization of gold ink with phthalocyanine (Pc), increased the

sensor sensitivity. The other two developed platforms were fabricated on a porous paper substrate, the initial work was to develop a printed strategy on the substrate, and at the end four treatment strategies were described in order to obtain a three-electrode system (Figure 5.1c)). And finally, using one of the printing paper strategies to develop a cortisol sensor on this substrate (Figure 5.1d)).

The main results of the thesis are presented schematically in Figure 5.2. As can be seen, the progression of the work has been always looking for a simpler, reliable, cost-efficiently and friendly devices while adapting these approaches to the requirements of each system.

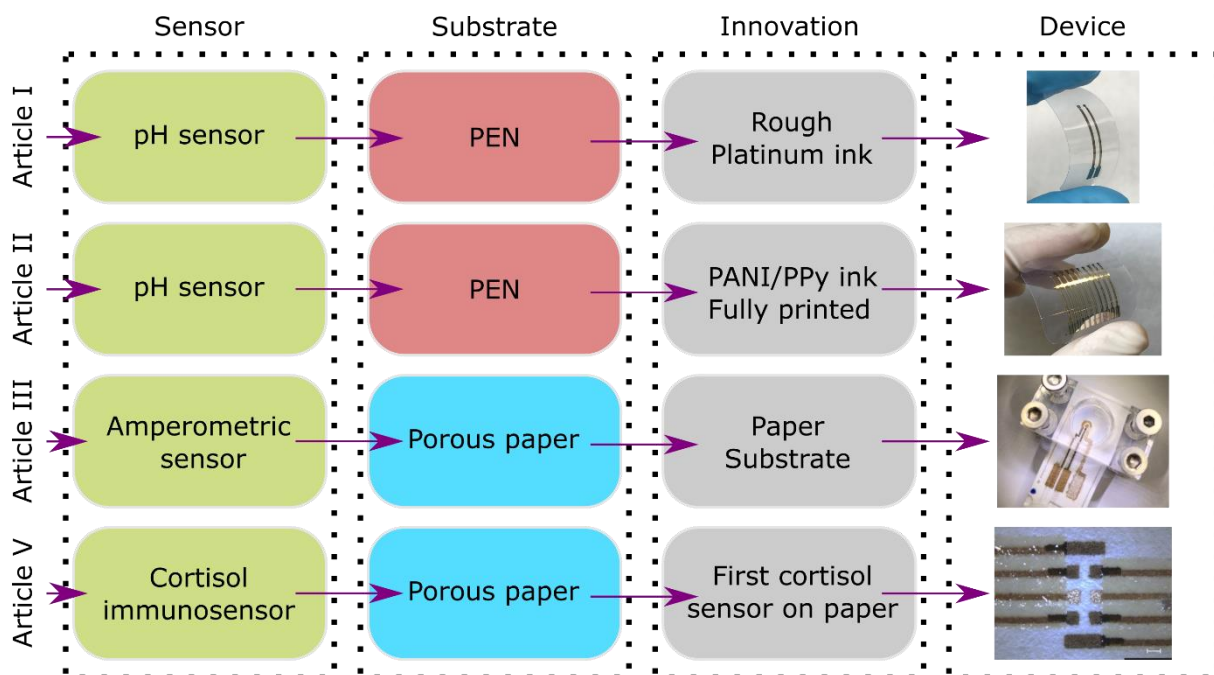


Figure 5.2. Summarized conclusion of the thesis.

Summarized of the evolution of the thesis showing the key advances to solve different sensing applications.

Following, specific conclusions of sensors on plastic and paper substrate are presented.

PEN substrate

Sensor development on plastic substrates is highly reported and studied. However, the development of new materials still a challenge. Here the development of two novel inks is presents and their application, both are applied to pH sensing layer.

The first pH sensor has been addressed with the development and characterization of a novel Pt ink to enhance the performance of EIROF sensitive: The results of these work can be summarized as:

- ❖ The developed pH sensor is based on a nanostructured EIROF sensing layer on such a printed rough Pt electrode, which has been demonstrated to have an excellent adhesion to the Pt.
- ❖ The pH sensors exhibit a linear super-Nernstian (71.43 mV/pH) response in a wide pH range, with an excellent reproducibility and a rapid response time.
- ❖ This improved adhesion of the EIROF layer is also demonstrated by the evaluation of the sensor over 1 year.
- ❖ Sensor was test under fluidic flow, where fluxes ranging from 0.1 to 1 mL/min do not alter the pH sensor response.

The second work presents for the first time a fully printed pH sensor. For achieve this goal a novel PANI/PPy ink was developed. The results of these work can be summarized as:

- ❖ The pH sensors were completely fabricated with inkjet based on PANI/PPy inks deposited on a gold microelectrode printed on a flexible substrate.
- ❖ The combination of PANI/PPy particles improved the linearity of pH against potential as well as expanding the pH range (from pH 3 to 10) and resolving problems of PANI sensors.
- ❖ The use of a gold ink modified with Pc for the gold microelectrode substrate, revealed an enhancement of electron mobility between the conducting polymer chains and the gold nanoparticles, generating a super-Nernstian response (81.2 ± 0.5 mV/pH unit).
- ❖ The sensor presented high stability in aqueous and non-aqueous media (acetic acid) confirming its ability to perform highly accurate titration measurements by detecting small changes in the concentration of strong monoprotic alkalis with strong acid.

Porous paper substrate

The need of develop electrochemical sensors on paper substrate due to its microfluidic properties, low-cost, environmentally friendly, and flexibility is increasing every day. It is in this context that the second part of this thesis work has been focused on the development of electrochemical sensor on porous paper. Inkjet printing technology allow the fabrication of metallic ink electrodes, which permit to be applied in a wide range of substrates, including delicate substrates.

The third sensor is an electrochemical platform made on porous paper substrate, during its fabrication 4 printing strategies were considered, which allow the tuning of the electrochemical active area of electrodes. The results of the work can be summarized as:

- ❖ A novel approach for fabricating a three-array electrode on paper using 4 treatment-cases to tune the electrochemical active area is presented.
- ❖ For the first time, the fabrication and characterization of a full inkjet WE, CE and pRE with Au, SU8, and Ag inks on paper is presented.
- ❖ The characterization of WEs on 4 treatment cases shows that on bare paper we obtained an I_p value of 48 μ A (at 75 mV/s) that is 2.5 folds higher than theoretical I_p for same electrode dimensions, and even the WE printed on SU-8 with the lower I_p shows 1.3 folds higher than theoretical.
- ❖ A successful combination of this rapid prototyping technique on low-cost, eco-friendly, and biodegradable paper substrate is done.

The fourth sensor is a novel printed immunosensor, based on a four-electrode platform fabricated on paper substrate. The electrodes were bio-functionalized to obtain a cortisol immunosensor. This developed sensor is also easy to use with a portable potentiostat. The immunosensor detect cortisol in human saliva turning this sensor in easy compatible PoC device. The results of the work can be summarized as:

- ❖ The biosensor platform is based on inkjet printed Au electrodes on paper substrate, and bio-functionalization was optimized for this additive rough technology.
- ❖ The biosensing platform was bio-functionalized by CMA electrodeposition and anti-Cortisol antibodies immobilization, resulting in a sensitive device with a good performance and sensitivity for the detection of cortisol, even in presence of other potential interferences such as NT-proBNP and TNF- α .
- ❖ Tests performed in both artificial saliva and human saliva demonstrated the biosensing platform's capability to detect cortisol in physiological ranges, with a linear relationship.
- ❖ the biosensing printed platform allows further implementation of a multiparametric biosensing tool for diagnosis or/and monitorization of related diseases using saliva samples.

Listed PhD outcomes

Here is listed a short summary of the achievement during this PhD program.

4 published articles in first quartile journals.

- Miguel Zea, Ana Moya, Marco Fritsch, Eloi Ramon, Rosa Villa, and Gemma Gabriel, Enhanced performance stability of iridium oxide based pH sensors fabricated on rough inkjet-printed platinum. 2019, 11, 16, 15160–15169, <https://doi-org.ure.uab.cat/10.1021/acsami.9b03085>.
- Miguel Zea, Francesca G. Bellagambi, Hamdi Ben Halima, Nadia Zine, Rosa Villa, Gemma Gabriel, and Abdelhamid Errachid. Electrochemical sensors for cortisol detections: almost there. TrAC Trends in Analytical Chemistry 2020, 132, 116058; <https://doi.org/10.1016/j.trac.2020.116058>.
- Miguel Zea, Robert Texido, Rosa Villa, Salvador Borrós and Gemma Gabriel. Specially designed polyaniline/polypyrrole ink for a fully printed high sensitive pH microsensor. Accepted on 22/06/2021. <https://doi.org/10.1021/acsami.1c08043>.
- Moya, A.; Ortega-Ribera, M.; Guimerà, X.; Sowade, E.; Zea, M.; Illa, X.; Ramon, E.; Villa, R.; Gracia-Sancho, J.; Gabriel, G. Online Oxygen Monitoring Using Integrated Inkjet-Printed Sensors in a Liver-on-a-Chip System. Lab on a Chip 2018, 18 (14), 2023–2035. <https://doi.org/10.1039/C8LC00456K>.

2 published conference paper

- Zea, M.; Moya, A.; Abrao-Nemeir, I.; Gallardo-Gonzalez, J.; Zine, N.; Errachid, A.; Villa, R.; Gabriel, G. All Inkjet Printing Sensor Device on Paper: For Immunosensors Applications. In 2019 20th International Conference on Solid-State Sensors, Actuators and Microsystems Eurosensors XXXIII (TRANSDUCERS EUROSENSORS XXXIII); 2019; pp 2472–2475. <https://doi.org/10.1109/TRANSDUCERS.2019.8808473>.
- A.Moya, M. Zea, E. Sowade, R. Villa, E. Ramon, R.R. Baumann, G. Gabriel. Inkjet-Printed Dissolved Oxygen and pH Sensors on Flexible Plastic Substrates. Volume 10246, Smart Sensors, Actuators, and MEMS VIII; 102460F (2017); doi: 10.1117/12.2264912.

2 submitted articles in first quartile journals.

- Miguel Zea, Ana Moya, Rosa Villa, and Gemma Gabriela. **Inkjet-printed Paper-based Electrochemical Sensors: Tuning Active Area through Surface Modification.** Submitted
- Miguel Zea, Hamdi Ben-Halima, Ana Moya, Rosa Villa, Nadia Zine, Abdelhamid Errachid; and Gemma Gabriel. **A Fully Paper-Based Electrochemical Sensor Made by Inkjet Printing for Saliva Cortisol Detection.** Submitted

2 oral presentations in international congress.

- Conference **Ibersensor – TMSB2018**: M. Zea, A. Moya, M. Fritsch, E. Ramon, R. Villa, and G. Gabriel. ENHANCED PH SENSOR PERFORMANCE ON ROUGH INKJET-PRINTED PLATINUM. Oral presentation.
- Conference **FLEX MEMS & SENSORS2020**: Miguel Zea, Ana Moya, Eloi Ramon, Gemma Gabriel. Development of inkjet printed biosensors on flexible and porous substrates. Oral Presentation.
- Conference **SPIE2017**: A.Moya, M. Zea, E. Sowade, R. Villa, E. Ramon, R.R. Baumann, G. Gabriel. Inkjet-Printed Dissolved Oxygen and pH Sensors on Flexible Plastic Substrates. Oral presentation. Proceedings Volume 10246, Smart Sensors, Actuators, and MEMS VIII; 102460F (2017); doi: 10.1117/12.2264912.

3 poster presentations in international congress.

- Conference **jPHD2017**: M. Zea, A. Moya, I. Gimenez, R. Villa, and G. Gabriel. Miniaturized multi-sensing platform for pH and Dissolved Oxygen monitoring in Organ-On-a-Chip systems. Poster presentation.
- Conference Transducer – **Eurosenors XXXIII2019**: Miguel Zea, Ana Moya, Imad Abrao-Nemeir, Juan Gallardo-Gonzalez, Nadia Zine, Abdelhamid Errachid, Rosa Villa, and Gemma Gabriel. All Inkjet Printing Sensor Device on Paper: for Immunosensors Applications. Poster presentation
- Conference **Nano Today2019**: Miguel Zea, Ana Moya, Imad Abrao-Nemeir, Hamdi Ben Halima, Nadia Zine, Abdelhamid Errachid, Rosa Villa, Gemma Gabriel. Flexible inkjet printed device for detection of cortisol in Saliva. Poster presentation

International internship of 6 months.

- Research internship at Institute of Science Analytical for 6 months, supervised by professor Abdelhamid Errachid. During this internship: I developed inkjet printed cortisol immunosensors on plastic and paper substrate.

3 collaborations with external research groups.

- Collaboration with the group of Dr. Salvador Borrós from the Grup d'Enginyeria de Materials (GEMAT) of the Insitut Químic de Sarrià (IQS). Implementation of PANI i Ppy inks for pH sensing on flexinle substrate
- Collaboration with the group of Dr. Jasmina Casals from the MicroTech Lab of the Polytechnic University of Catalonia (UPC). Micro-pillars implementation for blood plasma separation printed on plastic and paper substrates.
- Collaboration with the group of Dr. Ignacio Giménez of the Centro Investigación Biomédica de Aragón (CIBA) and with Dr. Luis Fernández of the Applied Mechanics and Bioengineering (AMB) group of the University of Zaragoza within the INKCELL project: Multi-sensing platform OD and pH in Inkjet printing and manufacture of microfluidic camera.

Among other achievements

Chapter 6 | Supplementary of published Articles

This chapter includes the supplementary files of the published or submitted articles.

6.1. Supplementary of Publication I

Enhanced performance stability of iridium oxide based pH sensors fabricated on rough inkjet-printed platinum

*Miguel Zea^{†,‡,k} Ana Moya^{†,¶,k} Marco Fritsch,[§] Eloi Ramon,[†] Rosa Villa,^{†,¶} and Gemma
Gabriel^{†,¶,*}*

[†]Instituto de Microelectrónica de Barcelona IMB-CNM (CSIC), Campus Universitat Autònoma
de Barcelona, 08193 Cerdanyola del Vallès, Barcelona, Spain

[‡]PhD in Electrical and Telecommunication Engineering, Universitat Autònoma de Barcelona
(UAB)

[¶]CIBER de Bioingeniería, Biomateriales y Nanomedicina (CIBER-BBN)

[§]Fraunhofer IKTS Institute, Winterbergstrasse 28, 01277 Dresden, Germany

^kThese authors contributed equally to this work

AUTHOR INFORMATION

Corresponding Author

*E-mail: gemma.gabriel@imb-cnm.csic.es

Cost analysis of the IJP pH sensor

Table S1. Calculation of the material costs per sensor.

pH electrode	Value	Ink quantity [ml]	Cost ink [€/ml]	Cost per sensor [€]
PET substrate	---	---	---	0,07000
Pt	151	0,00000151	50,70	0,00008
Ag	6711	0,00006711	20,01	0,00134
SU-8	22538	0,00022538	1,38	0,00031
Approximate cost per sensor (Substrate, pRE and IE)				0,07173

Pseudo-reference electrode

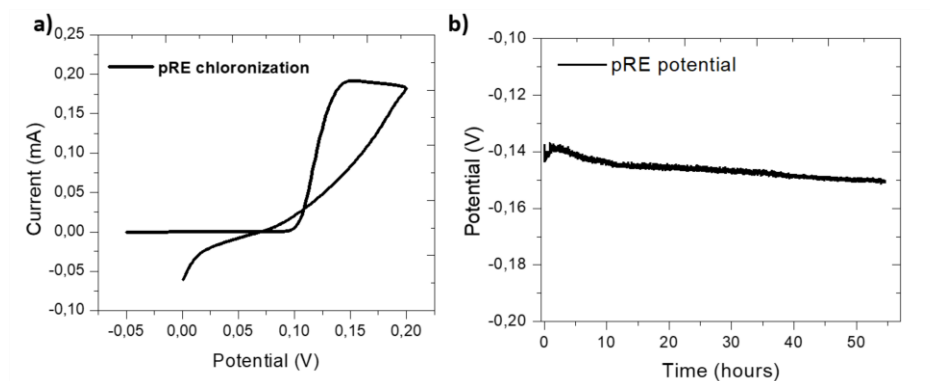


Figure S1. a) CV in HCl 0.1 M at a scan rate of 20 mV/s applied for the chlorinated process of the printed Ag electrode, b) Potential stability in KCl (0.1 M) evaluated against a commercial Ag/AgCl reference electrode (RE) of the developed Ag/AgCl pRE over time.

Iridium oxide electrodeposition

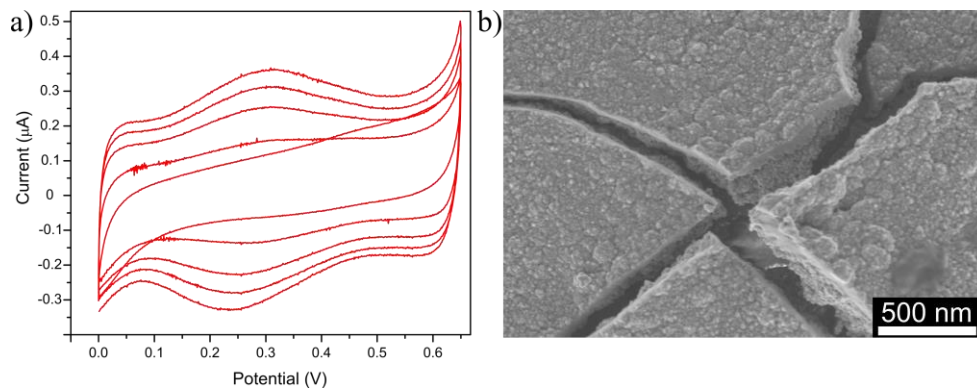


Figure S2. a) Growth of EIROF on printed Pt microelectrode ($GSA = 0.009 \text{ cm}^2$) by cyclic voltammetry method at a scan rate of 10 mV/s (50 cycles). b) SEM image of EIROF, where it can be distinguished inside the crack a thin layer of EIROF (approximately 150 nm) deposited on the Pt nanoparticles.

Pt ink characterization

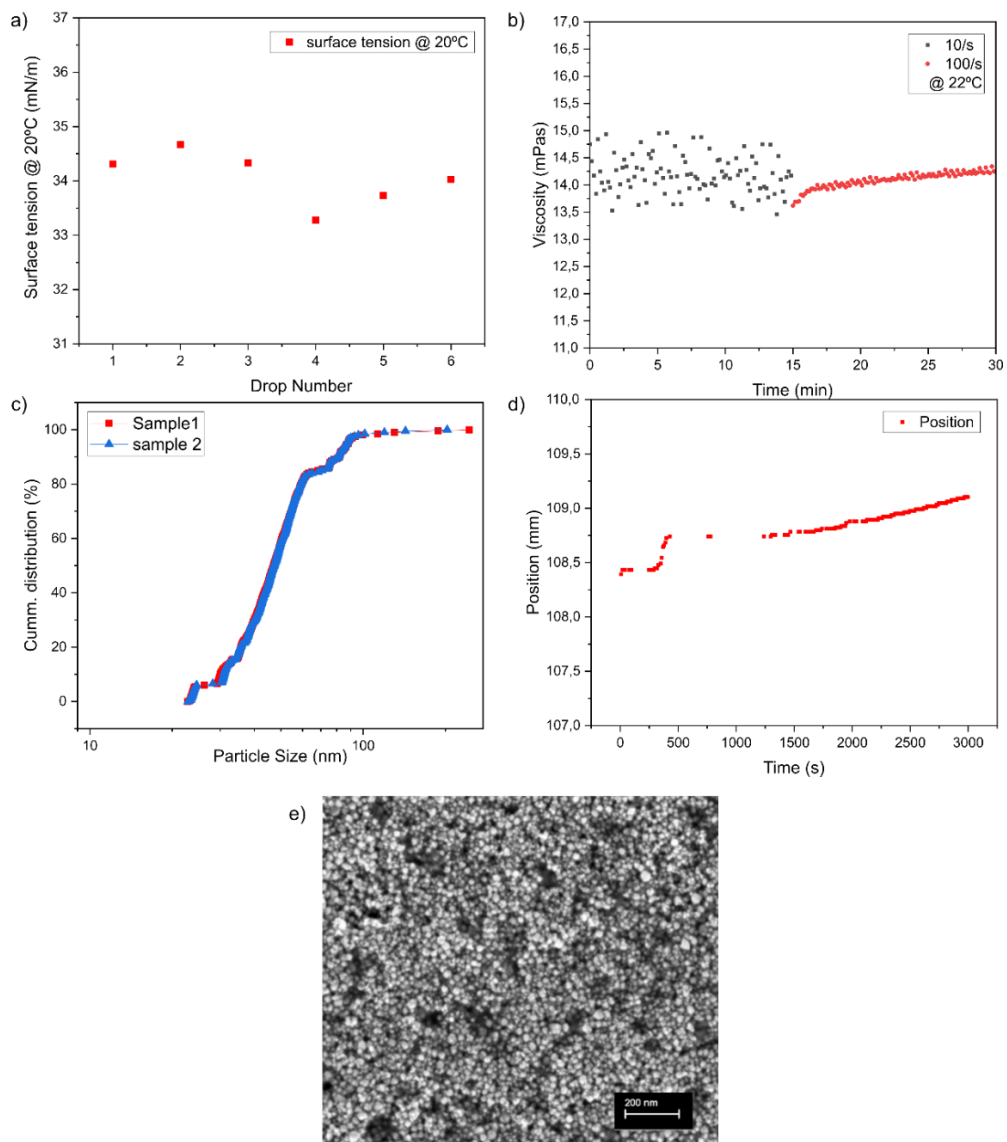


Figure S3. Pt ink rheological properties a) Surface tension, b) Viscosity, c) Particle size distribution, d) Sedimentation rate, e) SEM image of the Pt ink after drying on a sample holder at 80 °C for 10 min.

Inkjet Printing fabrication

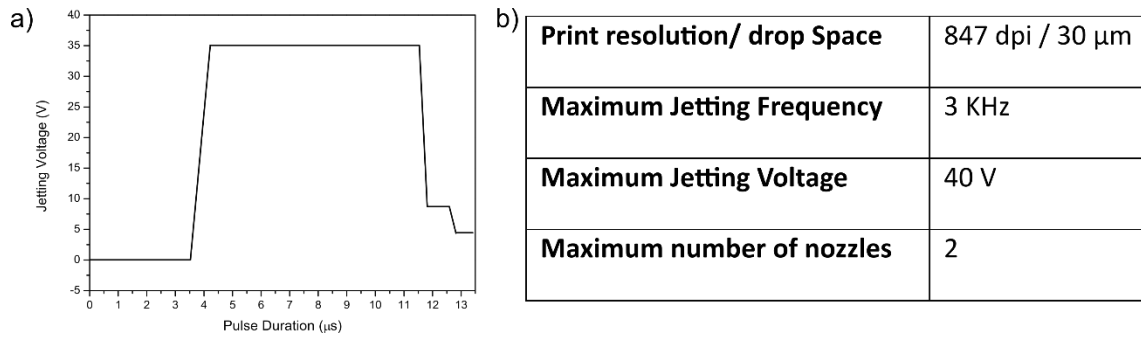


Figure S4. Optimized waveform and parameters applied to the piezoelectric transducer of the printhead for the Pt ink printing develop to fine-tune the drop ejection of the inkjet printhead.

Pt line pattern test

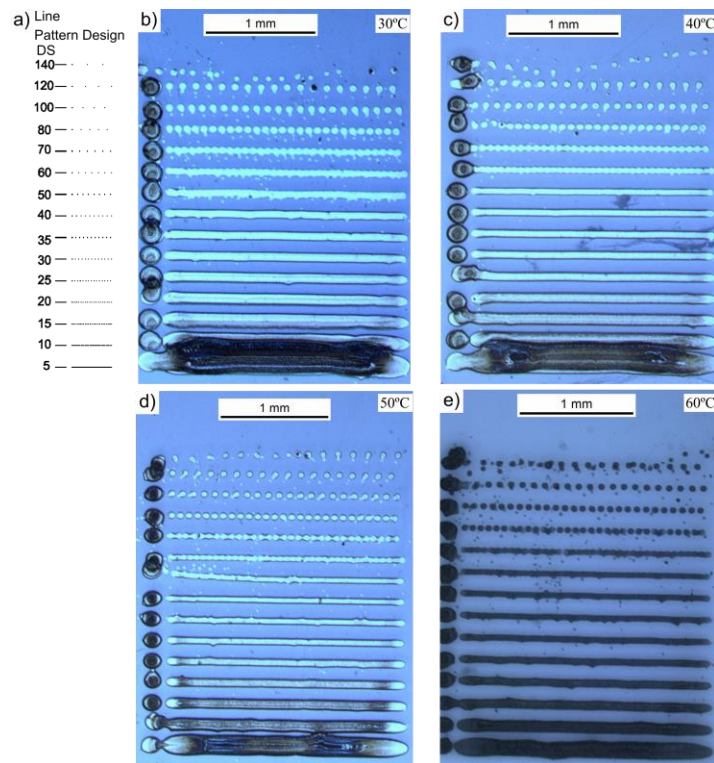


Figure S5. a) Line pattern design, distance in μm . b) Line pattern of Pt ink on platen at 30 °C, c) 40 °C, d) 50 °C and e) 60 °C.

EIROF pH sensor response time and stability

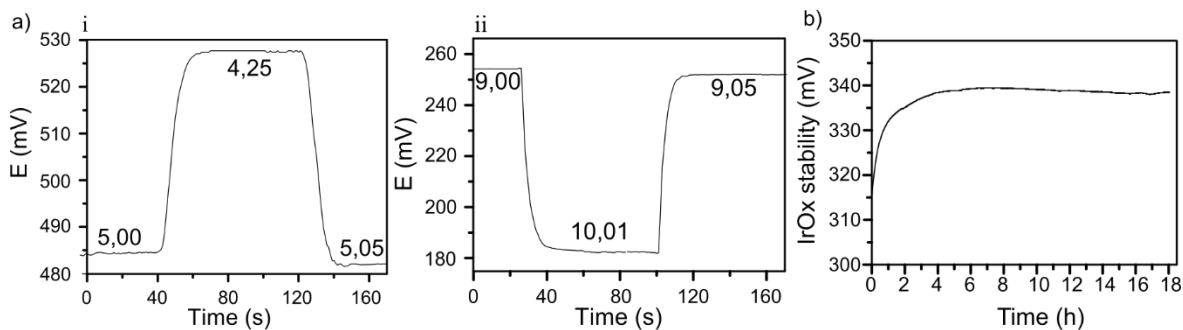


Figure S6. a) Response time to a pH step in acid medium (i) and alkaline medium (ii). b) Drift recording in buffer solution at pH 7 of an EIROF microelectrode stored in dry conditions for 9 months. The first 4h is the conditioning step. The potential drift is calculated to be 0.2 mV/h.

Microfluidic chamber fabrication

To validate the adhesion of IrOx and stability of pH sensor on liquid flow, a home-made microfluidic chamber was fabricated in PMMA. The fabrication process started by designing the chamber on CorelDraw. Upper and bottom PMMA plates were cut in CO₂ laser systems (Epilog mini 24, Epilog Laser). Screws holes, microfluidic channels and fluid inlets/outlets were defined using a CNC milling machine (MDX-40A, Roland DG). The microfluidic channel was defined with a 1 mm thick silicone that was cut using a vinyl cutter (CAMP-1 Servo GX-24, Roland DG Corporation). The cut silicone and printed flexible pH sensor was sandwiched between the upper and lower plates and tightened using screws. Fluid connections were made using silicone tubing (inner diameter of 0.8 mm) and mini luer connectors for easy and quick release.

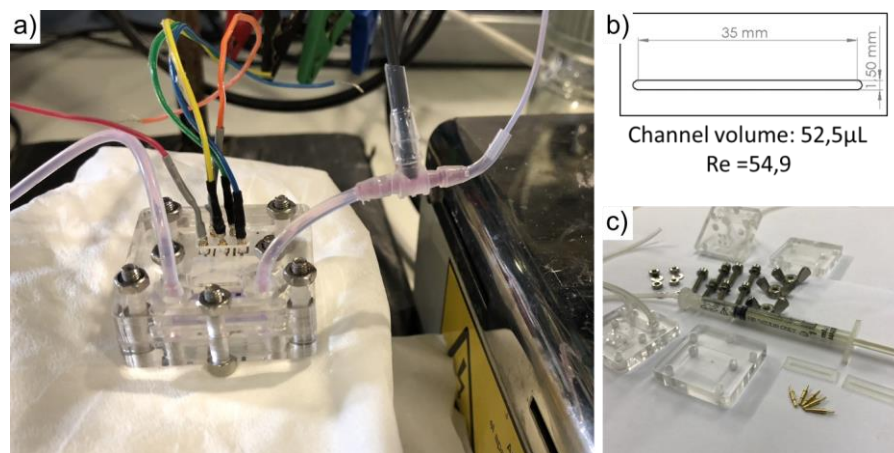


Figure S7. a) Image of the PMMA fabricated microfluidic chamber with a connection for an external RE. b) Channel dimensions, volume and calculated Reynolds number. c) Fabricated pieces to assembly the microfluidic chamber.

6.2. Supplementary of Publication II

Specially designed polyaniline/polypyrrole ink for a fully printed high sensitive pH microsensor.

Miguel Zea,^{†,‡} Robert Texido[§], Rosa Villa^{†,¶}, Salvador Borrós[§] and Gemma Gabriel^{†,¶,}*

[†]Instituto de Microelectrónica de Barcelona IMB-CNM (CSIC), Campus Universitat Autònoma de Barcelona, 08193 Cerdanyola del Vallès, Barcelona, Spain

[‡]PhD in Electrical and Telecommunication Engineering, Universitat Autònoma de Barcelona (UAB)

[§] Grup d'Enginyeria de Materials, Institut Químic de Sarrià-Universitat Ramon Llull, via Augusta 390, 08017 Barcelona, Spain

[¶]CIBER de Bioingeniería, Biomateriales y Nanomedicina (CIBER-BBN)

AUTHOR INFORMATION

Corresponding Author

*E-mail: gemma.gabriel@imb-cnm.csic.es

Pseudo-reference electrode

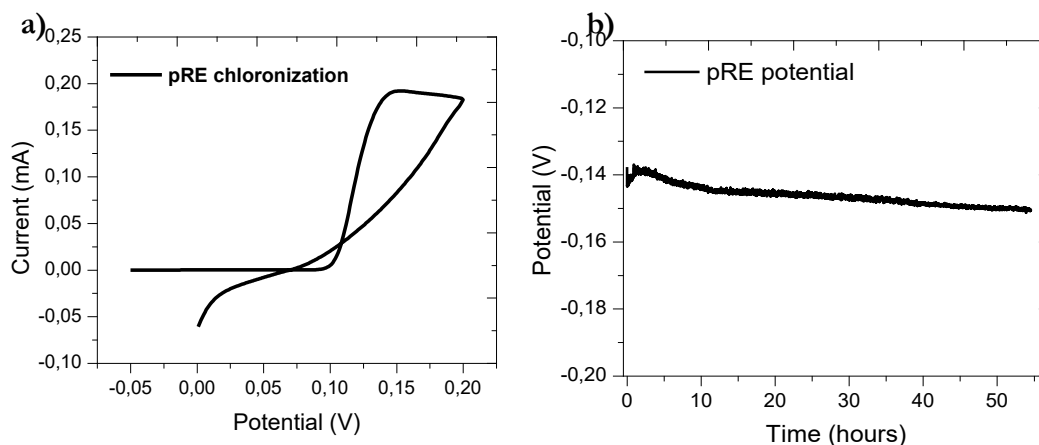


Figure S1. a) CV in HCl 0.1 M at a scan rate of 20 mV/s applied for the chlorinated process of the printed Ag electrode, b) Potential stability in KCl (0.1 M) evaluated against a commercial Ag/AgCl reference electrode (RE) of the developed Ag/AgCl pRE over time.

PANI:PSS and PPy:PSS formulations

Formulations			
PANI:PSS (Mz 70.000) solution diluted 1:1 MQ water	Triton X100 1.5% v/v		
	Triton X100 1.5% v/v	DMSO 5% v/v	
	Triton X100 1.5% v/v	Gly 5% v/v	
PANI:PSS (Mz 200.000) solution diluted 1:1 MQ water	Triton X100 1.5% v/v		
	Triton X100 1.5% v/v	DMSO 5% v/v	
	Triton X100 1.5% v/v	Gly 5% v/v	
PPy:PSS (Mz 70.000) solution diluted 1:1 MQ water	Triton X100 1.5% v/v		
	Triton X100 1.5% v/v	DMSO 5% v/v	
	Triton X100 1.5% v/v	Gly 5% v/v	
PPy:PSS (Mz 200.000) solution diluted 1:1 MQ water	Triton X100 1.5% v/v		
	Triton X100 1.5% v/v	DMSO 5% v/v	
	Triton X100 1.5% v/v	Gly 5% v/v	

Table S1. Formulations of inkjet printing inks obtained from PANI:PSS / PPy:PSS suspensions

Surface tension of PANI:PSS / PPy:PSS formulations

Formulations							Standard mN/m	deviation	
PANI:PSS (Mz 70.000) solution diluted 1:1 water	MQ	Triton X100	1.5%	v/v	DMSO 5%	v/v	59,7	1,3	
		Triton X100	1.5%				Gly 5%	59,2	1,5
		Triton X100	1.5%				Gly 5%	59,3	1,8
PANI:PSS (Mz 200.000) solution diluted 1:1 water	MQ	Triton X100	1.5%	v/v	DMSO 5%	v/v	59,7	1,2	
		Triton X100	1.5%				Gly 5%	59,2	1,5
		Triton X100	1.5%				Gly 5%	59,4	2,1
PPy:PSS (Mz 70.000) solution diluted 1:1 water	MQ	Triton X100	1.5%	v/v	DMSO 5%	v/v	59,7	1,2	
		Triton X100	1.5%				Gly 5%	59,9	2,6
		Triton X100	1.5%				Gly 5%	59,8	1,5
PPy:PSS (Mz 200.000) solution diluted 1:1 water	MQ	Triton X100	1.5%	v/v	DMSO 5%	v/v	61,4	2,8	
		Triton X100	1.5%				Gly 5%	60,1	1,8
		Triton X100	1.5%				Gly 5%	59,7	1,9
Table	PANI:PSS + PPy:PSS (Mz 70.000)+MQ water (1:1:1)		Triton X100	1.5%	DMSO 5%	v/v	60,5	1,6	

Surface tension of the formulations of inkjet printing inks obtained from PANI:PSS / PPy:PSS suspensions

IR spectra characterization

PANI:PSS and PPy:PSS suspension were characterized using FTIR spectra to validate the obtention of the CPs suspension. For PANI, main PANI bands are present in FTIR (Figure S2 a): 1578 cm⁻¹ band correspond to C = C stretching of PANI quinoid groups and 1486 cm⁻¹ C = C stretching of benzenoid groups highlighted in the green bar. Also, it is possible to identify the 1294 cm⁻¹ band of stretching vibration of secondary amine C – N band and 830 cm⁻¹ band corresponding at C – H out-of -plane deformation vibration of the benzenoid groups⁵⁷⁹. The FTIR also presented the sulfonic acid vibration bands at 1138 and 1110 cm⁻¹, 803 cm⁻¹ band corresponding to out-of-plane bending vibration of the C-H band of p-disubstituted benzene ring and 505 cm⁻¹ band corresponding to – SO₃H group stretch^{579,580}. These bands confirm the presence of a p – substituted benzene group with sulfonic acid in the PANI microparticles.

IR spectre for PPy:PSS 70.000, revealed the principal bands of both compounds as was expected (Figure S2 b). Typical pyrrole ring vibration bands at 1550cm^{-1} , 930cm^{-1} and 770cm^{-1} along with C – N stretch band (1189cm^{-1}) and 666cm^{-1} from primary amine wagging confirms the presence of PPy in the structure^{581,582}. The FTIR also presented the sulfonic acid vibration bands at 1033 and 1004cm^{-1} observed previously in the PANI FTIR (Figure S2 a) confirming the presence of the polyelectrolyte^{579,580}.

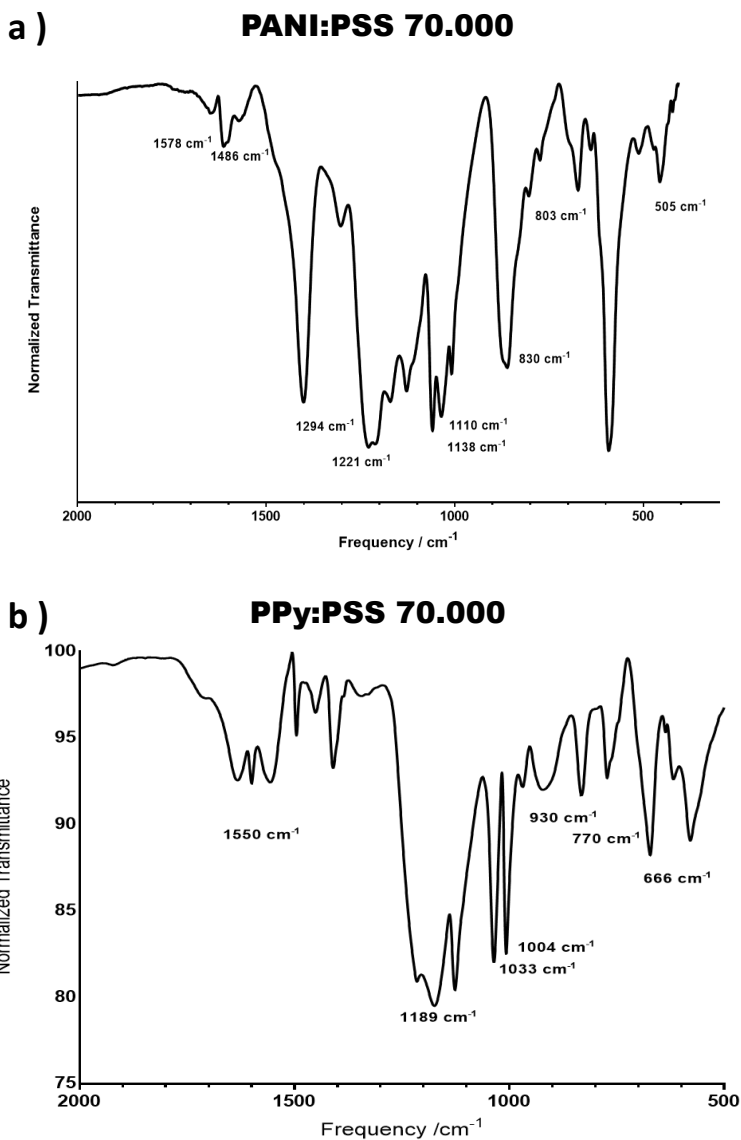


Figure S2. FTIR spectra of PANI:PSS Mw 70.000 (a) and PPy:PSS Mw 70.000 (b).

CP suspensions – pH dependence

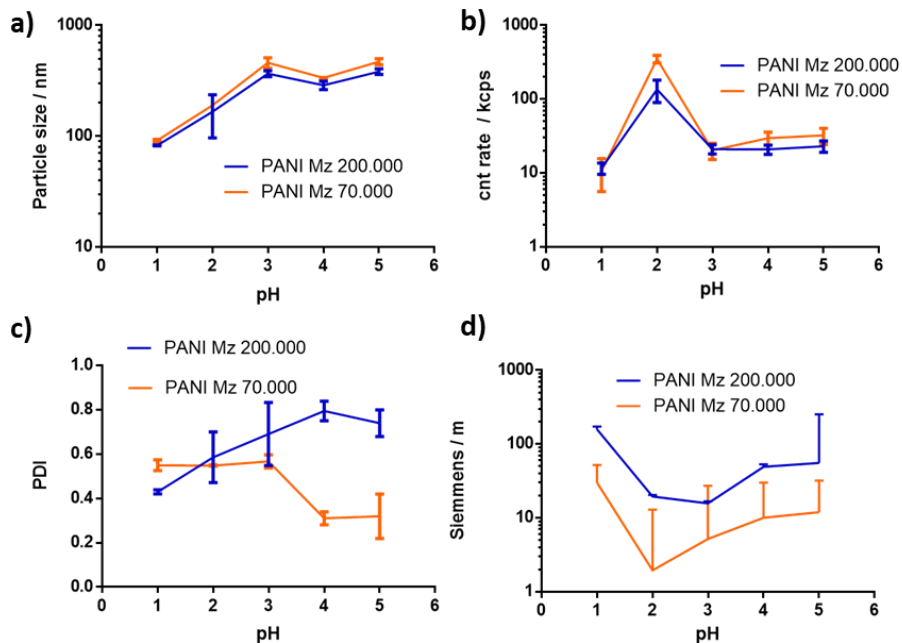


Figure S3. Effect of the pH of the synthesis media on PANI:PSS suspension parameters: Particle size mean (a), count rate of the DLS measurement, indicating number of particles in media (b), Polydispersity of the suspensions (c) and conductivity of the obtained film (d).

DLS characterization

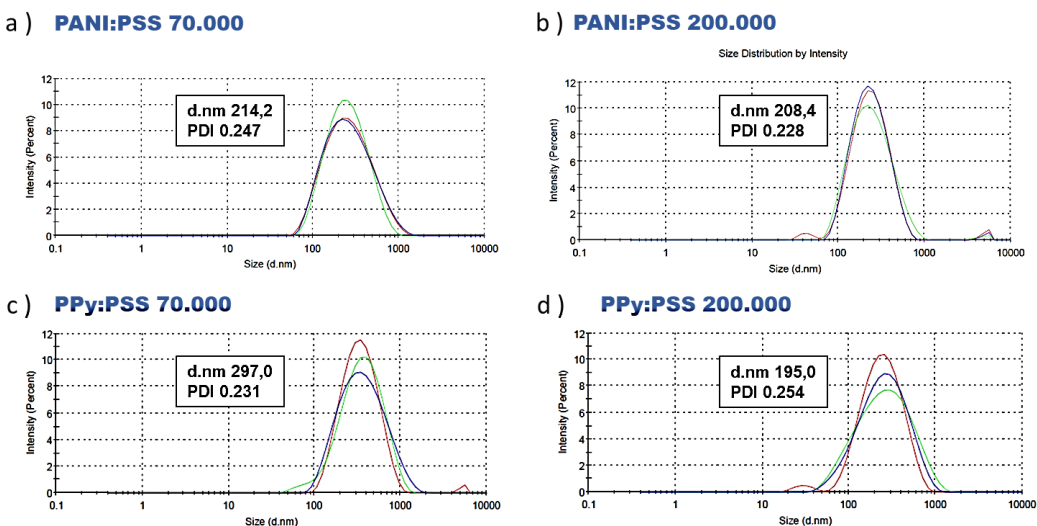


Figure S4. Particle size distribution profile obtained through DLS for CP suspensions after its synthesis: PANI:PSS with PSS molecular weight of Mw 70.000 and 200.000 (a and b) and PPy:PSS with a Mw of 70.000 and 200.000 (c and d).

Zeta potential characterization

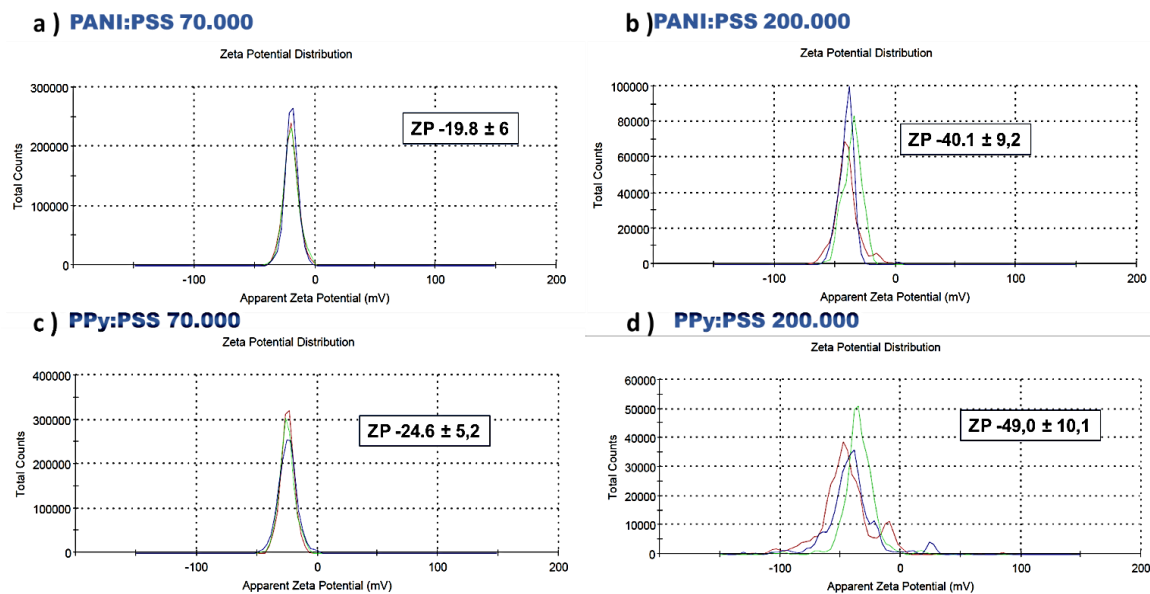


Figure S5. Zeta potential profile obtained through DLS for CP suspensions after its synthesis: PANI:PSS with PSS molecular weight of Mw 70.000 and 200.000 (a and b) and PPy:PSS with a Mw of 70.000 and 200.000 (c and d).

FESEM images

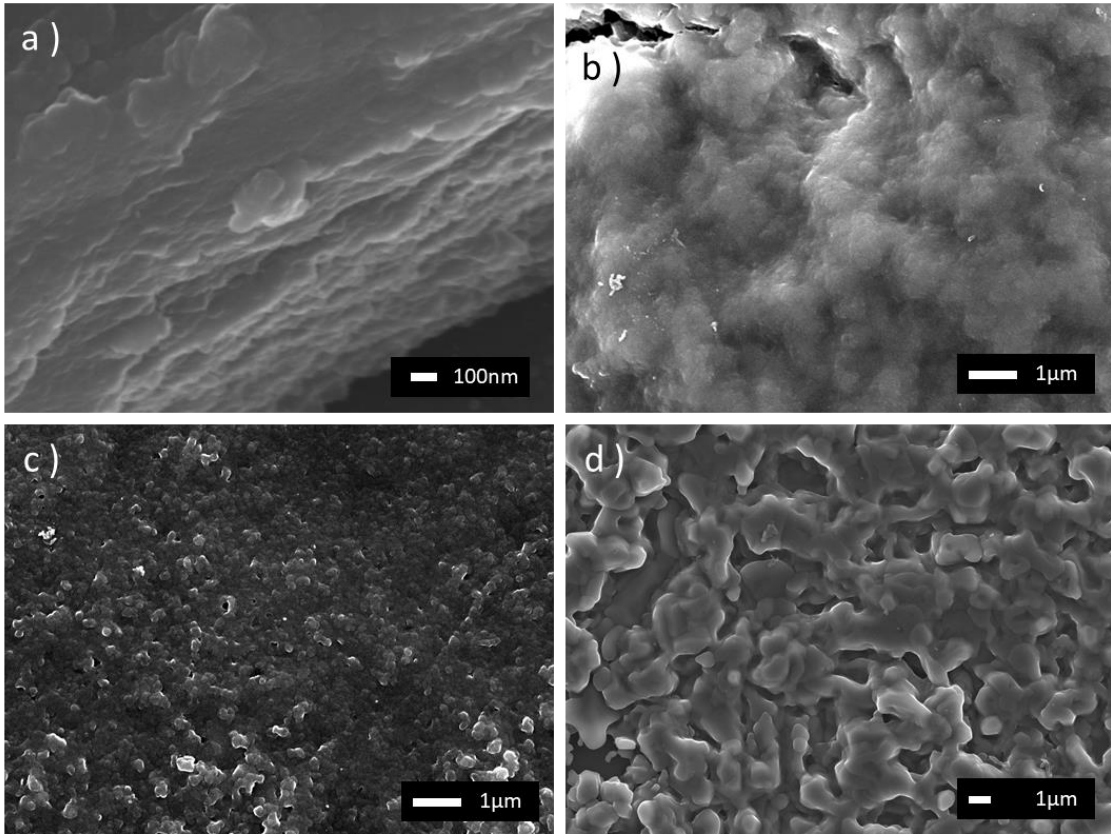
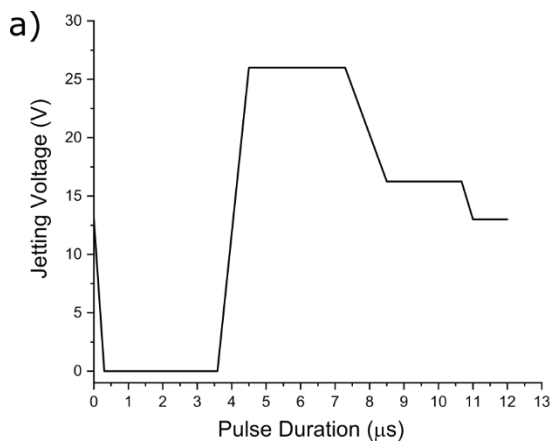


Figure S6. FESEM images of CP suspension films: a) PANI:PSS Mz 70.000, b) PANI:PSS Mz 200.000, c) PPy:PSS Mz 70.000 and d) PPy:PSS Mz 200.000.

Inkjet Printing fabrication

Waveform was develop to fine-tune the drop ejection of the inkjet printheads.



b)

Print resolution / Drop space	2540 dpi / 10 µm
Maximum jetting frequency	5 KHz
Maximum Jetting Voltage	26 V
Maximum number of Nozzles	15

Figure S7. Optimized waveform and parameters applied to the piezoelectric transducer of the printhead for the CP inks printing developed to fine-tune the drop ejection of the inkjet printhead.

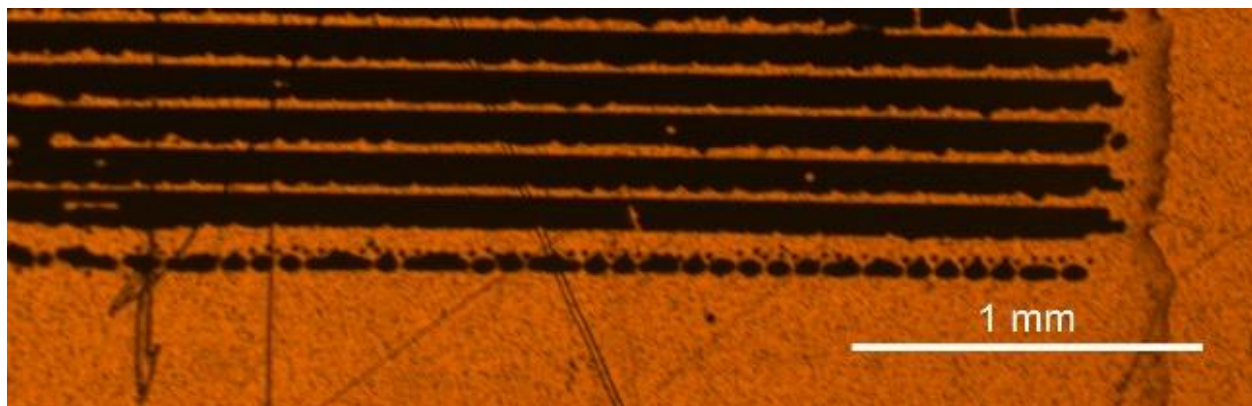


Figure S8. Image of a square printed at DS 10 μm . This DS or higher do not allow the overlap of contiguous printed lines.

Non-adherence of polymeric film

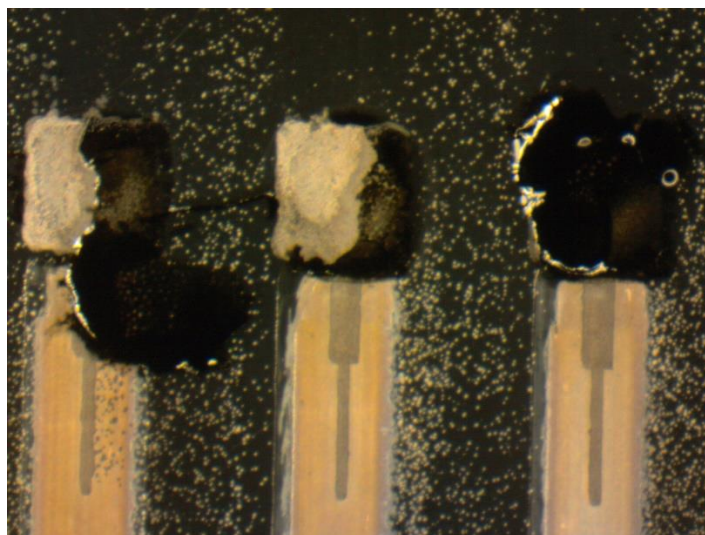


Figure S9. Four layers (4L) of the printed CP produce films that are completely detached when being immersed in an aqueous solution due to an excess of material over the metallic electrode.

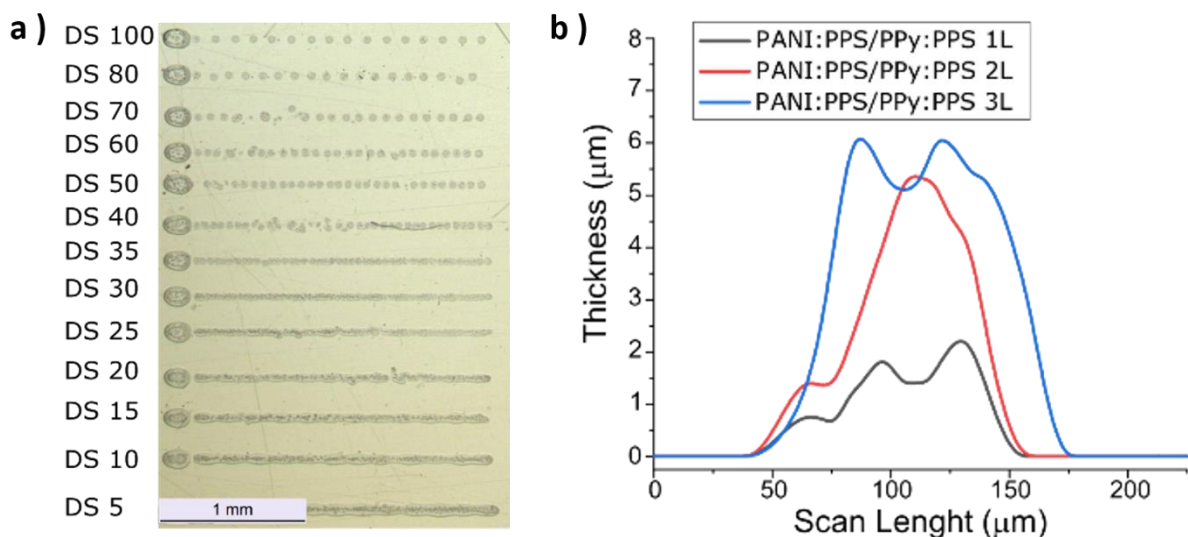


Figure S10. a) Line pattern printed on PEN substrate for PANI:PSS/PPy:PSS specially formulated ink and b) the cross-section profiles for 1L, 2L and 3L.

Volts				
pH	Electrode 1	Electrode 2	Electrode 3	CV (%)
10	-0,11235	-0,11098	-0,11123	0,65642434
9	-0,03994	-0,03894	-0,03888	1,52130896
8	0,07205	0,07296	0,07307	0,77200719
7	0,15627	0,15694	0,15701	0,26191204
6	0,23104	0,23081	0,23082	0,05691322
5	0,29630	0,29583	0,29582	0,09317697
4	0,37870	0,37715	0,37714	0,23830115
3	0,45789	0,45899	0,45800	0,13207177

Table S3. Variation coefficient of calibration in figure 6 with the PANI:PSS/PPy:PSS ink.

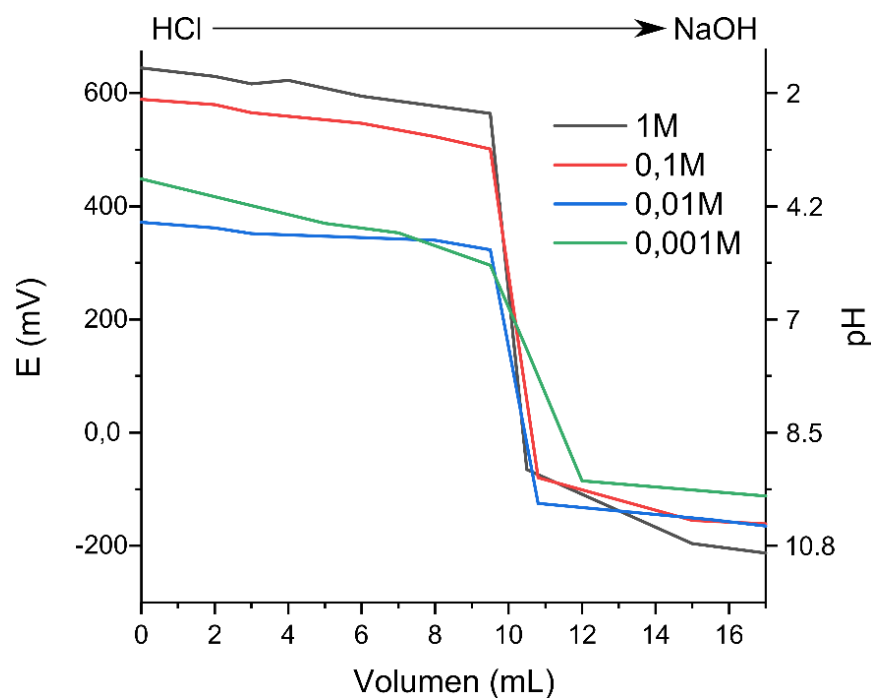


Figure S11. Titration of strong acid with strong base: Potentiometric pH titration curves for HCl and NaOH at the indicated molarity

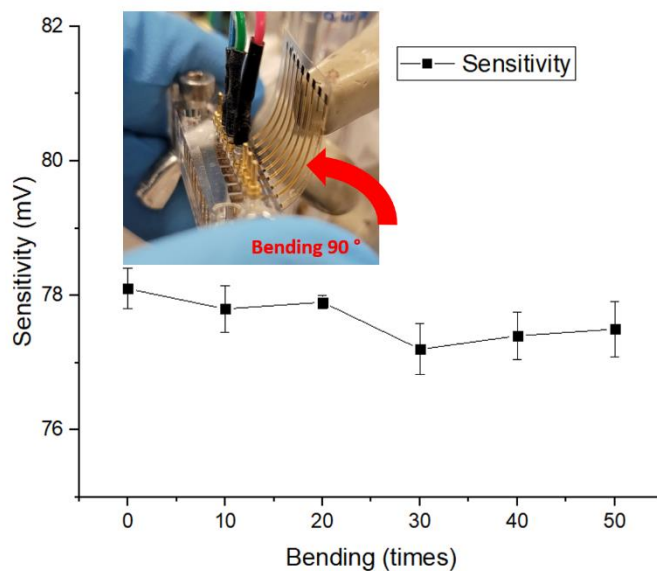


Figure S12. Evolution of the pH sensor sensitivity after a simple bending test where the electrode platform is cyclically bended 90 °.

6.3. Supplementary of Publication III

Inkjet-printed Paper-based Electrochemical Sensors: Tuning Active Area through Surface Modification.

Miguel Zea^{a,b}, Ana Moya^a, Rosa Villa^{a,c}, Gemma Gabriel^{a,c,*}

^a Instituto de Microelectrónica de Barcelona, IMB-CNM (CSIC), Esfera UAB, Campus Universitat Autònoma de Barcelona, 08193, Bellaterra, Barcelona, Spain.

^b PhD in Electrical and Telecommunication engineering, Universitat Autònoma de Barcelona, (UAB)

^c CIBER in Bioengineering, Biomaterials and Nanomedicine (CIBER-BBN)

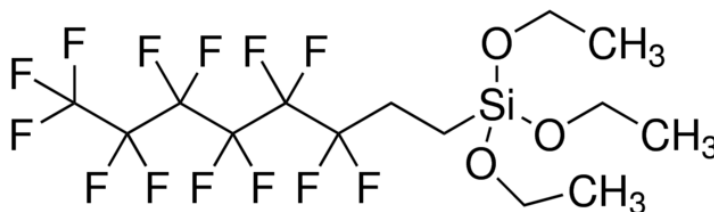


Figure S1. Chemical structure of 1H,1H,2H,2H-perfluorooctyltriethoxysilane (POTS), with a empirical Formula (Hill Notation): C₁₄H₁₉F₁₃O₃Si

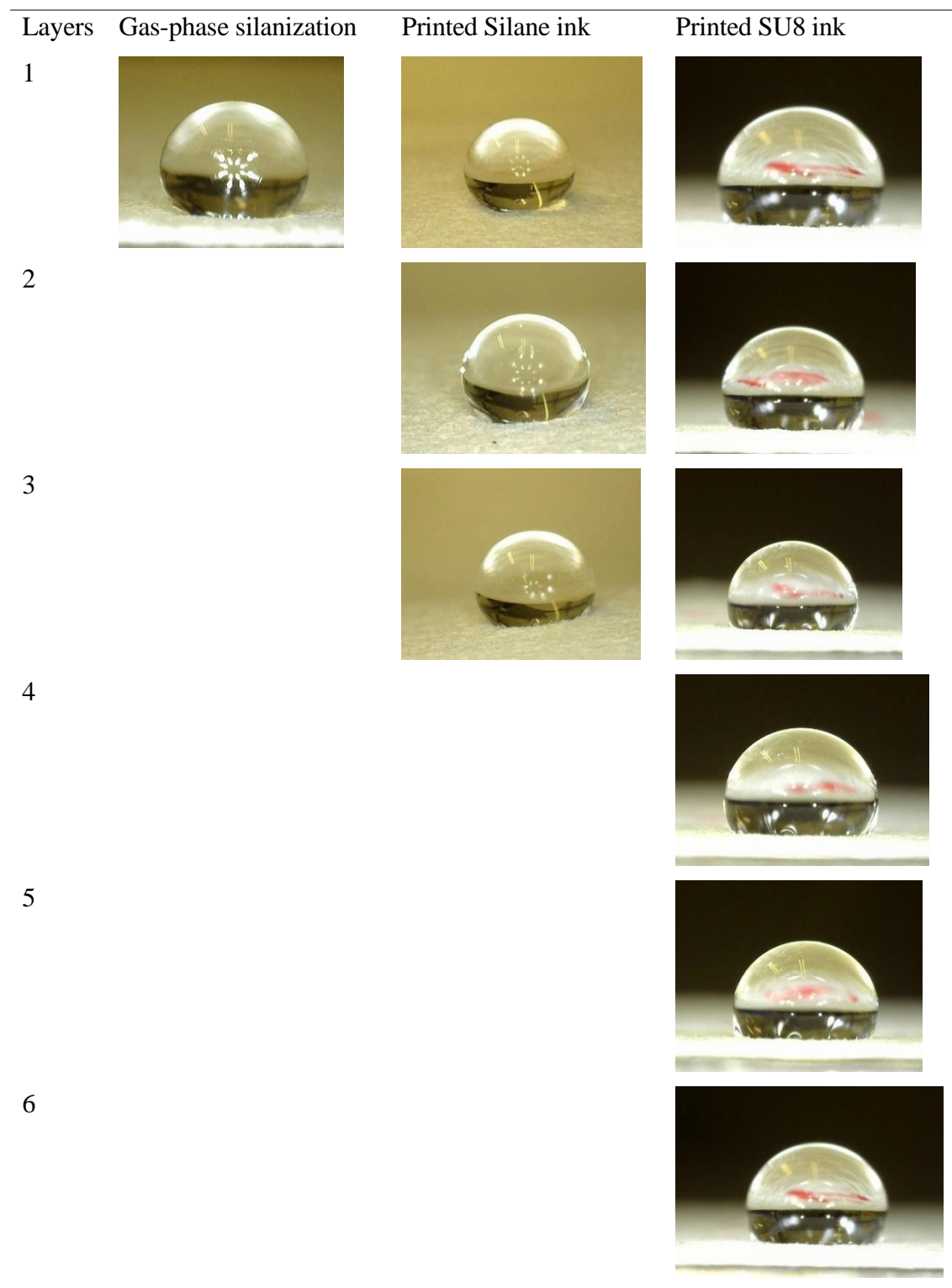


Figure S2. Optical images of a droplet of distilled water deposited on a gas-phase silanized paper, on a printed paper with a silane ink, and on a blocked paper printed with SU8.

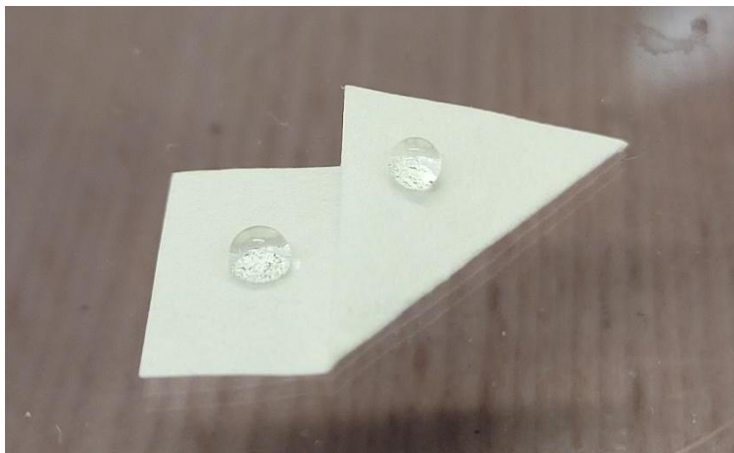


Figure S3. Deposited water droplet on both faces of a Whatman paper Grade 1 paper printed with 2 layers of silane ink denoting that both sides of the paper are hydrophobic. The same happens with the paper printed with 3 layers of silane ink.

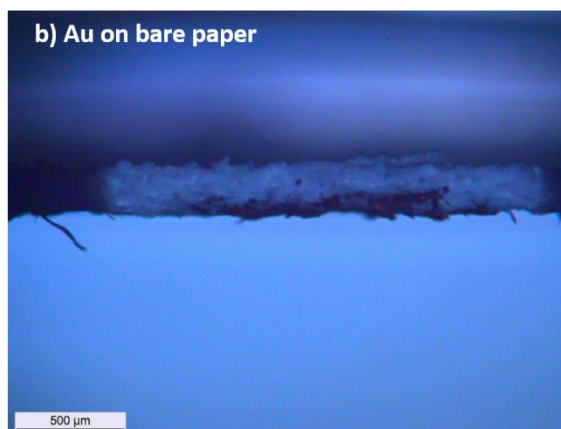
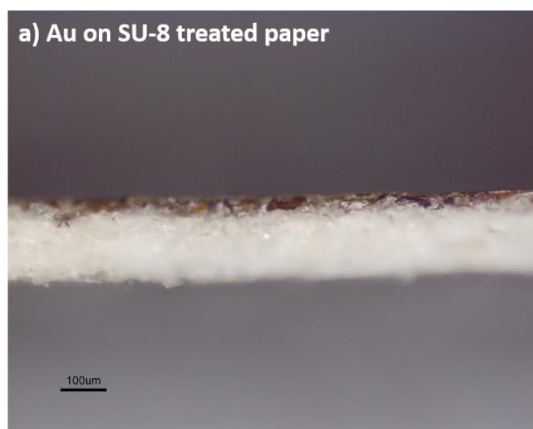


Figure S4. A)

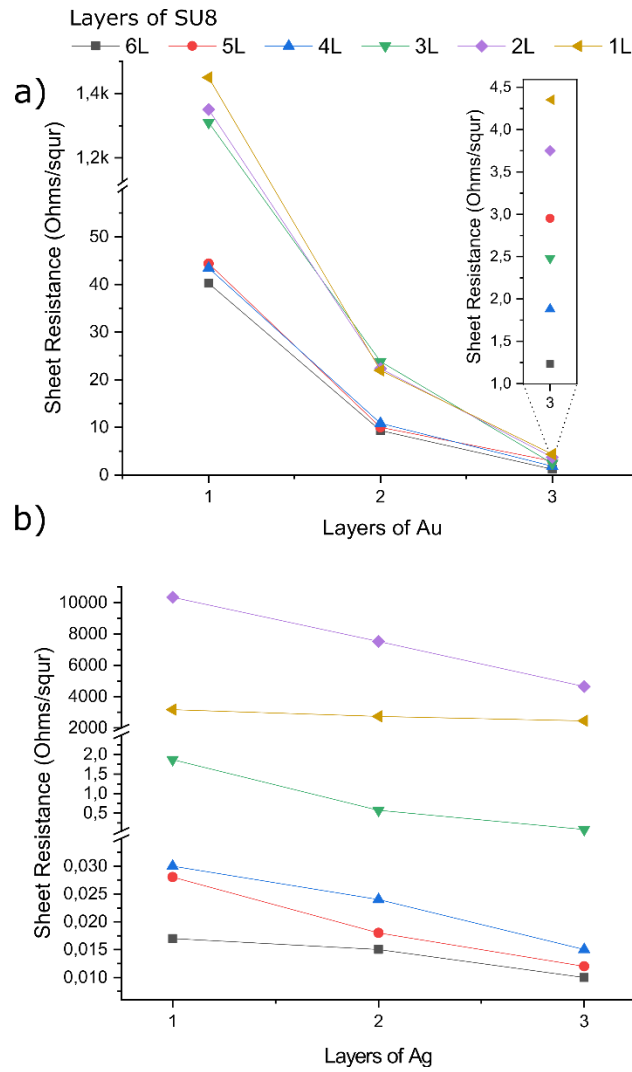


Figure S5. Sheet resistance values determined from van der Pauw structures for 1, 2 and 3 layers of Au (a) and Ag (b) over 1 to 6 layers of SU8.

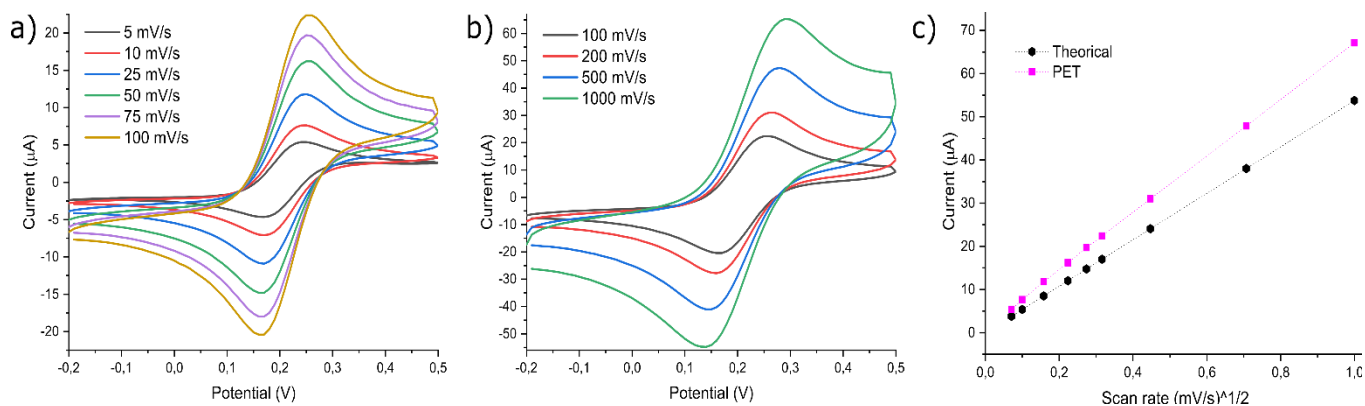


Figure S6. Cyclic voltammograms corresponding to the measurements of equimolar mixtures ferro/ferricyanide redox couple in 0.1 M KNO₃. A) and b) Au microelectrode on PET substrate varying scan rate from 5 to until 1000 mV/s; c) comparison between the theoretical Randle-Sěvčík equation prediction for a 1 mm Au WE vs experimental current peaks of Au microelectrode on PET in function of square root of the scan rate.

To determine if the electrodes are working properly we compared the obtained I_p with the theory, using Randles-Sěvčík's equation:

$$I_p = 0.4463 \cdot \left(\frac{F^3}{RT}\right)^{\frac{1}{2}} \cdot n^{\frac{3}{2}} \cdot A \cdot D^{\frac{1}{2}} \cdot R_0 \cdot v^{\frac{1}{2}} \quad (1)$$

where n is the number of electrons participating in the redox process, F is the Faraday Constant [$C \cdot mol^{-1}$], A is the electrochemically active electrode area [m^2], R_0 is the initial concentration of analyte [$mol \cdot m^{-3}$], D is the diffusion coefficient [$m^2 \cdot s^{-1}$], v is the scan rate [$V \cdot s^{-1}$], R is the gas constant [$J \cdot K^{-1} \cdot mol^{-1}$] and T is the temperature [K]. The diffusion coefficient value here used is $6.5 \times 10^{-10} m^2/s$ for ferrocyanide.

The value of the electron transfer rate constant (k_s), was calculated using the approach described by Matsuda and Ayabe⁴⁴⁰ using the relation of the heterogeneous charge transfer:

$$\Lambda = k_s \cdot (n \cdot F \cdot v \cdot D / R \cdot T)^{-1/2} \quad (2)$$

k_s is determined at $\Lambda=1$, which occurs at the scan rate at which ΔE_p begins to depart from ideality, The rest of parameters are the same involved in equation 1.

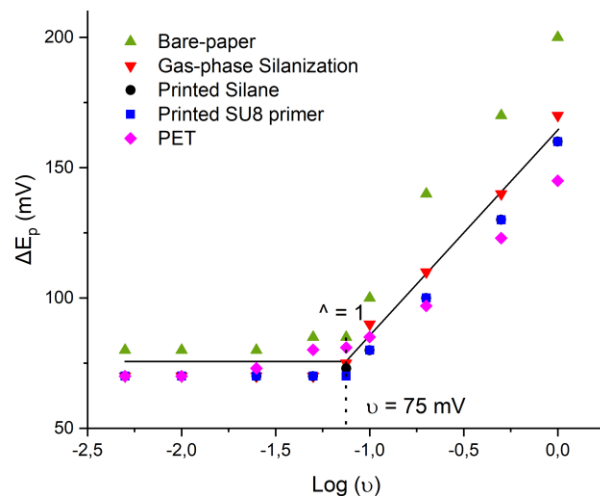


Figure S7. Peak to peak separation of the Cyclic voltammetry Ferro/Ferricyanide redox couple, versus the logarithmic of the scan rate, that shows when the heterogeneous charge transfer $\Lambda=1$ for the 4 treatment-cases.

6.4. Supplementary of Publication V

A Fully Paper-Based Electrochemical Sensor Made by Inkjet Printing for Saliva Cortisol Detection.

*Miguel Zea^{†,‡}, Hamdi Ben-Halima[§], Ana Moya[†], Rosa Villa^{†,¶}, Nadia Zine[§], Abdelhamid
Errachid[§] and Gemma Gabriel^{†,¶,*}*

[†]Instituto de Microelectrónica de Barcelona IMB-CNM (CSIC), Campus Universitat Autònoma de Barcelona, 08193 Cerdanyola
del Vallès, Barcelona, Spain

[‡]PhD in Electrical and Telecommunication Engineering, Universitat Autònoma de Barcelona (UAB), Bellaterra, Barcelona,
Spain

[§] Université Claude Bernard Lyon 1, Institut des Sciences Analytiques (ISA), 5 rue de la Doua, 69100, Villeurbanne, Lyon,
France

[¶]CIBER de Bioingeniería, Biomateriales y Nanomedicina (CIBER-BBN)

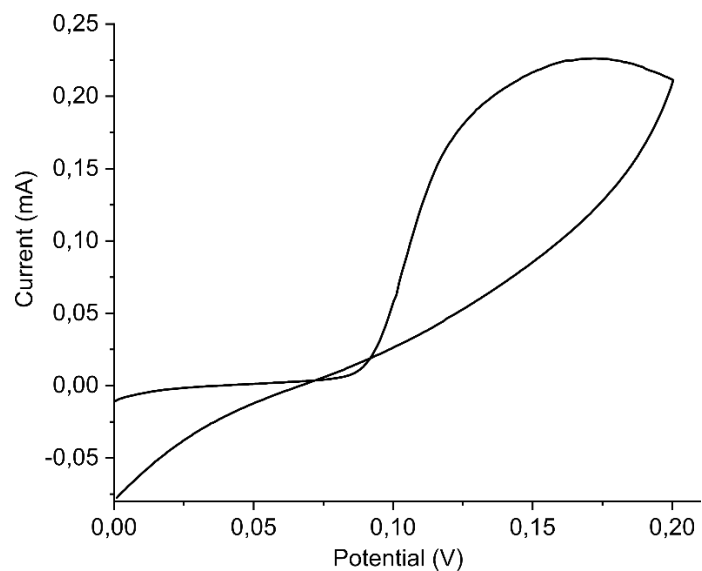


Figure S1. CV in HCl 0.1 M at a scan rate of 20 mV/s applied for the chlorinated process of the printed Ag electrode on paper.

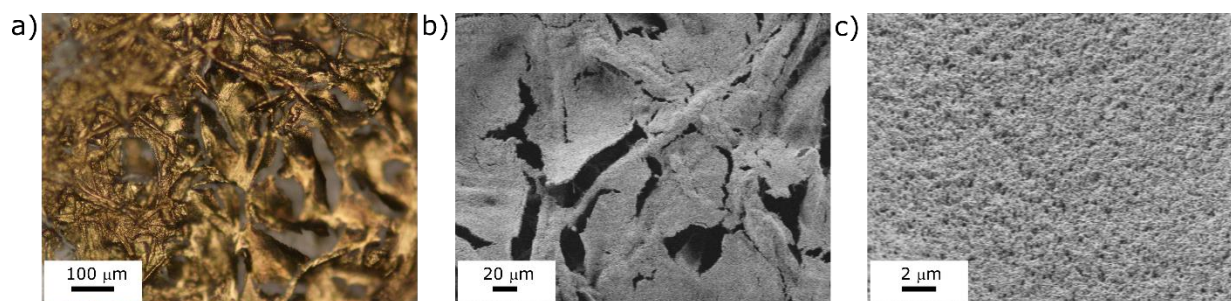


Figure S2. Au printed microelectrode on paper substrate a) digital microscope image; b) and c) SEM images.

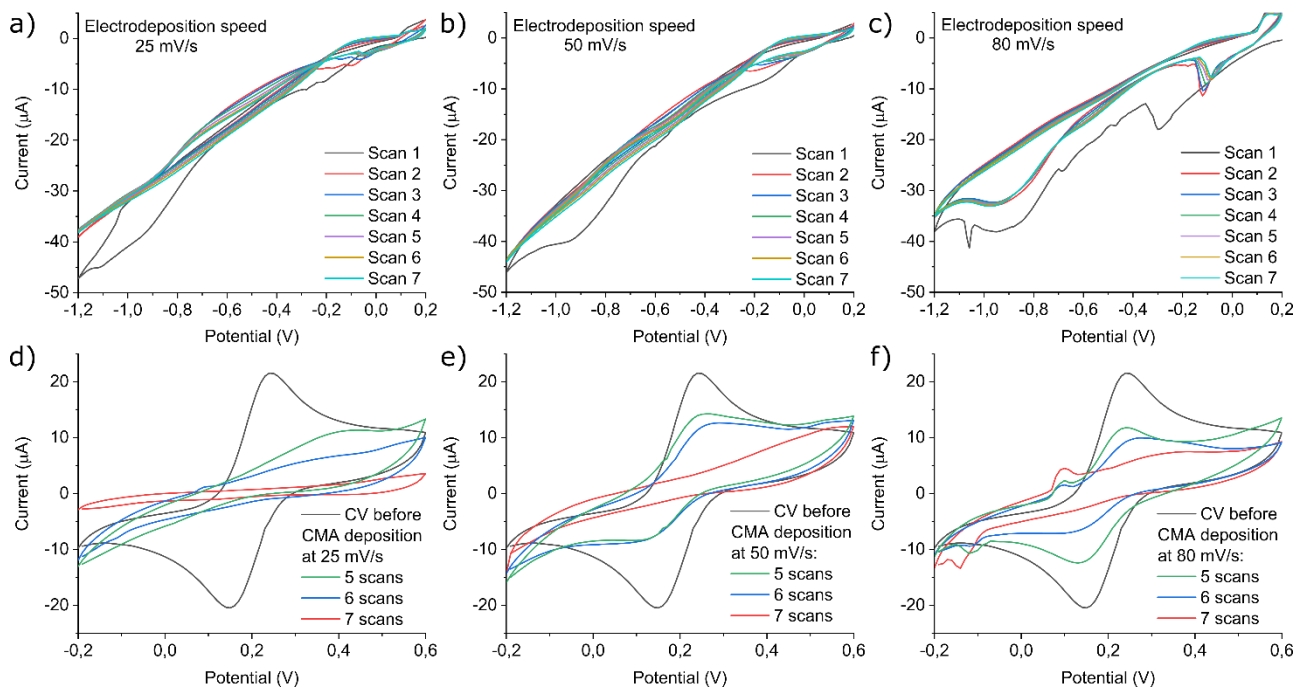


Figure S3. Cyclic voltammograms of CMA electrodeposition onto gold WEs. Potential was scanned from 0.2 V to -1.2 V. 5, 6, and 7 cycles were performed at different scan rates a) 25 mV/s, b) 50 mV/s, and c) 80 mV/s. Cyclic voltammograms of activated WEs before CMA deposition and after 5, 6, and 7 scans of CMA deposition varying scan rate speed d) 25 mV/s, e) 50 mV/s, and f) 80 mV/s.

References |

- (1) Foster, R. N. *Innovation: The Attacker's Advantage*; Summit books, 1988.
- (2) Moya, A.; Gabriel, G.; Villa, R.; Javier del Campo, F. Inkjet-Printed Electrochemical Sensors. *Current Opinion in Electrochemistry* **2017**, *3* (1), 29–39. <https://doi.org/10.1016/j.coelec.2017.05.003>.
- (3) Al-Halhouli, A.; Qitouqa, H.; Alashqar, A.; Abu-Khalaf, J. Inkjet Printing for the Fabrication of Flexible/Stretchable Wearable Electronic Devices and Sensors. *Sensor Review* **2018**, *38* (4), 438–452. <https://doi.org/10.1108/SR-07-2017-0126>.
- (4) Singh, M.; Haverinen, H. M.; Dhagat, P.; Jabbour, G. E. Inkjet Printing—Process and Its Applications. *Advanced Materials* **2010**, *22* (6), 673–685. <https://doi.org/10.1002/adma.200901141>.
- (5) Haghdoost, F.; Mottaghitlab, V.; Haghi, A. K. Comfortable Textile-Based Electrode for Wearable Electrocardiogram. *Sensor Review* **2015**, *35* (1), 20–29. <https://doi.org/10.1108/SR-08-2013-719>.
- (6) Adly, N.; Rinklin, P.; Wolfrum, B. Inkjet Printing for Biosensors and Bioelectronics. *Organic Bioelectronics for Life Science and Healthcare* **2019**, *56*, 243.
- (7) Alemdar, H.; Ersoy, C. Wireless Sensor Networks for Healthcare: A Survey. *Computer Networks* **2010**, *54* (15), 2688–2710. <https://doi.org/10.1016/j.comnet.2010.05.003>.
- (8) Population structure and ageing - Statistics Explained https://ec.europa.eu/eurostat/statistics-explained/index.php/Population_structure_and_ageing (accessed 2021 -04 -26).
- (9) Sherratt, R. S.; Dey, N. Low-Power Wearable Healthcare Sensors. *Electronics* **2020**, *9* (6), 892. <https://doi.org/10.3390/electronics9060892>.
- (10) Drew Barbara J.; Califf Robert M.; Funk Marjorie; Kaufman Elizabeth S.; Krucoff Mitchell W.; Laks Michael M.; Macfarlane Peter W.; Sommargren Claire; Swiryn Steven; Van Hare George F. Practice Standards for Electrocardiographic Monitoring in Hospital Settings. *Circulation* **2004**, *110* (17), 2721–2746. <https://doi.org/10.1161/01.CIR.0000145144.56673.59>.
- (11) Domingo, M. C. An Overview of the Internet of Things for People with Disabilities. *Journal of Network and Computer Applications* **2012**, *35* (2), 584–596. <https://doi.org/10.1016/j.jnca.2011.10.015>.
- (12) Frattasi, S.; Biomedical, I. S. on A. S. in; Technologies, C. *Proceedings of the 4th International Symposium on Applied Sciences in Biomedical and Communication Technologies: 2011, Barcelona, Spain: ISABEL '11*; ACM, 2011.

- (13) Bandodkar, A. J.; Jeerapan, I.; Wang, J. Wearable Chemical Sensors: Present Challenges and Future Prospects. *ACS Sens.* **2016**, *1* (5), 464–482. <https://doi.org/10.1021/acssensors.6b00250>.
- (14) Wen, F.; He, T.; Liu, H.; Chen, H.-Y.; Zhang, T.; Lee, C. Advances in Chemical Sensing Technology for Enabling the Next-Generation Self-Sustainable Integrated Wearable System in the IoT Era. *Nano Energy* **2020**, *78*, 105155. <https://doi.org/10.1016/j.nanoen.2020.105155>.
- (15) Stetter, J. R.; Penrose, W. R.; Yao, S. Sensors, Chemical Sensors, Electrochemical Sensors, and ECS. *J. Electrochem. Soc.* **2003**, *150* (2), S11. <https://doi.org/10.1149/1.1539051>.
- (16) Gubala, V.; Harris, L. F.; Ricco, A. J.; Tan, M. X.; Williams, D. E. Point of Care Diagnostics: Status and Future. *Anal. Chem.* **2012**, *84* (2), 487–515. <https://doi.org/10.1021/ac2030199>.
- (17) J. Meagher, R.; V. Hatch, A.; F. Renzi, R.; K. Singh, A. An Integrated Microfluidic Platform for Sensitive and Rapid Detection of Biological Toxins. *Lab on a Chip* **2008**, *8* (12), 2046–2053. <https://doi.org/10.1039/B815152K>.
- (18) Abel, G. Current Status and Future Prospects of Point-of-Care Testing around the Globe. *Expert Review of Molecular Diagnostics* **2015**, *15* (7), 853–855. <https://doi.org/10.1586/14737159.2015.1060126>.
- (19) Westgard, S. A.; Goldschmidt, H. M. J.; Ehrmeyer, S. S. POCT Analysts' Perspective: Practices and Wants for Improvement. *The Journal of Applied Laboratory Medicine* **2020**, *5* (3), 480–493. <https://doi.org/10.1093/jalm/jfaa037>.
- (20) Ferreira, C. E.; Guerra, J. C.; Shessarenko, N.; Scartezini, M.; Franca, C. N.; Colombini, M. P.; Berlitz, F.; Machado, A. M.; Campana, G. A.; Faulhaber, A. C.; others. Point-of-Care Testing: General Aspects. *Clinical laboratory* **2018**, *64* (1), 1–9.
- (21) Briggs, C.; Carter, J.; Lee, S.-H.; Sandhaus, L.; Simon-Lopez, R.; Corrons, J.-L. V. ICSH Guideline for Worldwide Point-of-Care Testing in Haematology with Special Reference to the Complete Blood Count. *International Journal of Laboratory Hematology* **2008**, *30* (2), 105–116. <https://doi.org/10.1111/j.1751-553X.2008.01050.x>.
- (22) Luppá, P. B.; Müller, C.; Schlichtiger, A.; Schlebusch, H. Point-of-Care Testing (POCT): Current Techniques and Future Perspectives. *TrAC Trends in Analytical Chemistry* **2011**, *30* (6), 887–898. <https://doi.org/10.1016/j.trac.2011.01.019>.
- (23) Giasuddin, A. Point-of-Care Testing (POCT): Importance in Emergency Medical/Health Care. *Bangladesh Journal of Medical Biochemistry* **2017**, *10* (2), 43–44.
- (24) Korhonen, J.; Honkasalo, A.; Seppälä, J. Circular Economy: The Concept and Its Limitations. *Ecological Economics* **2018**, *143*, 37–46. <https://doi.org/10.1016/j.ecolecon.2017.06.041>.

- (25) Lakshmi, U.; Hofmann, M.; Valencia, S.; Wilcox, L.; Mankoff, J.; Arriaga, R. I. “Point-of-Care Manufacturing”: Maker Perspectives on Digital Fabrication in Medical Practice. *Proc. ACM Hum.-Comput. Interact.* **2019**, *3* (CSCW), 91:1-91:23. <https://doi.org/10.1145/3359193>.
- (26) Hue, P. L. Le Technologies, Inc., Beaverton, Oregon. *J. of Imaging Science and Technology* **1998**, *42*, 49–62.
- (27) Rayleigh, Lord. On the Instability of Jets. *Proceedings of the London mathematical society* **1878**, *1* (1), 4–13.
- (28) Fundamentals of Inkjet Printing: The Science of Inkjet and Droplets | Wiley <https://www.wiley.com/en-us/Fundamentals+of+Inkjet+Printing%3A+The+Science+of+Inkjet+and+Droplets-p-9783527337859> (accessed 2021 -05 -04).
- (29) Wong, W. S.; Salleo, A. *Flexible Electronics: Materials and Applications*; Springer Science & Business Media, 2009; Vol. 11.
- (30) Crowley, K.; Morrin, A.; Hernandez, A.; O’Malley, E.; Whitten, P. G.; Wallace, G. G.; Smyth, M. R.; Killard, A. J. Fabrication of an Ammonia Gas Sensor Using Inkjet-Printed Polyaniline Nanoparticles. *Talanta* **2008**, *77* (2), 710–717. <https://doi.org/10.1016/j.talanta.2008.07.022>.
- (31) Moya, A.; Ortega-Ribera, M.; Guimerà, X.; Sowade, E.; Zea, M.; Illa, X.; Ramon, E.; Villa, R.; Gracia-Sancho, J.; Gabriel, G. Online Oxygen Monitoring Using Integrated Inkjet-Printed Sensors in a Liver-on-a-Chip System. *Lab on a Chip* **2018**, *18* (14), 2023–2035. <https://doi.org/10.1039/C8LC00456K>.
- (32) Andò, B.; Baglio, S.; Bulsara, A. R.; Emery, T.; Marletta, V.; Pistorio, A. Low-Cost Inkjet Printing Technology for the Rapid Prototyping of Transducers. *Sensors* **2017**, *17* (4), 748. <https://doi.org/10.3390/s17040748>.
- (33) Hutchings, I. M.; Martin, G. D. *Inkjet Technology for Digital Fabrication*; Wiley Online Library, 2013.
- (34) Khan, A.; Rahman, K.; Ali, S.; Khan, S.; Wang, B.; Bermak, A. Fabrication of Circuits by Multi-Nozzle Electrohydrodynamic Inkjet Printing for Soft Wearable Electronics. *Journal of Materials Research* **2021**. <https://doi.org/10.1557/s43578-021-00188-4>.
- (35) Yang, P.; Zhang, L.; Kang, D. J.; Strahl, R.; Kraus, T. High-Resolution Inkjet Printing of Quantum Dot Light-Emitting Microdiode Arrays. *Advanced Optical Materials* **2020**, *8* (1), 1901429. <https://doi.org/10.1002/adom.201901429>.

- (36) Graphic Monthly Canada, Printing Industry Magazine for the Canadian Graphics Arts Industry including Top 100 Printers <http://www.graphicmonthly.ca/?id=68> (accessed 2021 -05 -10).
- (37) Inkjet Printers Market Size, Share & Trends Report, 2020-2027 <https://www.grandviewresearch.com/industry-analysis/emerging-inkjet-printing-market> (accessed 2021 -05 -10).
- (38) Martin, G. D.; Hutchings, I. M. Fundamentals of Inkjet Technology. *Inkjet Technology for Digital Fabrication. John Wiley & Sons Ltd* **2013**, 21–44.
- (39) Le, H. P. Progress and Trends in Ink-Jet Printing Technology. *Journal of Imaging Science and Technology* **1998**, *42* (1), 49–62.
- (40) Alamán, J.; Alicante, R.; Peña, J. I.; Sánchez-Somolinos, C. Inkjet Printing of Functional Materials for Optical and Photonic Applications. *Materials* **2016**, *9* (11), 910. <https://doi.org/10.3390/ma9110910>.
- (41) Hoath, S. D. *Fundamentals of Inkjet Printing: The Science of Inkjet and Droplets*; John Wiley & Sons, 2016.
- (42) Setti, L.; Piana, C.; Bonazzi, S.; Ballarin, B.; Frascaro, D.; Fraleoni-Morgera, A.; Giuliani, S. Thermal Inkjet Technology for the Microdeposition of Biological Molecules as a Viable Route for the Realization of Biosensors. *Analytical Letters* **2004**, *37* (8), 1559–1570. <https://doi.org/10.1081/AL-120037587>.
- (43) Bogy, D. B.; Talke, F. E. Experimental and Theoretical Study of Wave Propagation Phenomena in Drop-on-Demand Ink Jet Devices. *IBM Journal of Research and Development* **1984**, *28* (3), 314–321. <https://doi.org/10.1147/rd.283.0314>.
- (44) Gan, H. Y.; Shan, X.; Eriksson, T.; Lok, B. K.; Lam, Y. C. Reduction of Droplet Volume by Controlling Actuating Waveforms in Inkjet Printing for Micro-Pattern Formation. *J. Micromech. Microeng.* **2009**, *19* (5), 055010. <https://doi.org/10.1088/0960-1317/19/5/055010>.
- (45) Kwon, K.-S. Experimental Analysis of Waveform Effects on Satellite and Ligament Behavior Via in Situ Measurement of the Drop-on-Demand Drop Formation Curve and the Instantaneous Jetting Speed Curve. *J. Micromech. Microeng.* **2010**, *20* (11), 115005. <https://doi.org/10.1088/0960-1317/20/11/115005>.
- (46) DIMATIX DMP-2800 SERIES USER MANUAL Pdf Download | ManualsLib <https://www.manualslib.com/manual/1238531/Dimatix-Dmp-2800-Series.html> (accessed 2021 -05 -26).

- (47) de Gans, B.-J.; Duineveld, P. C.; Schubert, U. S. Inkjet Printing of Polymers: State of the Art and Future Developments. *Advanced Materials* **2004**, *16* (3), 203–213. <https://doi.org/10.1002/adma.200300385>.
- (48) Moya Lara, A. Integrated Sensors for Overcoming Organ-on-a-Chip Monitoring Challenges. Ph.D. Thesis, Universitat Autònoma de Barcelona, 2017.
- (49) Kumar, A.; Mandal, S.; Barui, S.; Vasireddi, R.; Gbureck, U.; Gelinsky, M.; Basu, B. Low Temperature Additive Manufacturing of Three Dimensional Scaffolds for Bone-Tissue Engineering Applications: Processing Related Challenges and Property Assessment. *Materials Science and Engineering: R: Reports* **2016**, *103*, 1–39. <https://doi.org/10.1016/j.mser.2016.01.001>.
- (50) Magdassi, S.; Grouchko, M.; Berezin, O.; Kamyshny, A. Triggering the Sintering of Silver Nanoparticles at Room Temperature. *ACS Nano* **2010**, *4* (4), 1943–1948. <https://doi.org/10.1021/nn901868t>.
- (51) Szczech, J.; Megaridis, C.; Zhang, J.; Gamota, D. Ink Jet Processing of Metallic Nanoparticle Suspensions for Electronic Circuitry Fabrication. *Microscale Thermophysical Engineering* **2004**, *8* (4), 327–339. <https://doi.org/10.1080/10893950490516884>.
- (52) Kamyshny, A.; Magdassi, S. Conductive Nanomaterials for Printed Electronics. *Small* **2014**, *10* (17), 3515–3535. <https://doi.org/10.1002/sml.201303000>.
- (53) Kipphan, H. *Handbook of Print Media: Technologies and Production Methods*; Springer Science & Business Media, 2001.
- (54) Ian Gibson, I. G. *Additive Manufacturing Technologies 3D Printing, Rapid Prototyping, and Direct Digital Manufacturing*; Springer, 2015.
- (55) Moya, A.; Sowade, E.; del Campo, F. J.; Mitra, K. Y.; Ramon, E.; Villa, R.; Baumann, R. R.; Gabriel, G. All-Inkjet-Printed Dissolved Oxygen Sensors on Flexible Plastic Substrates. *Organic Electronics* **2016**, *39*, 168–176. <https://doi.org/10.1016/j.orgel.2016.10.002>.
- (56) Tehrani, B. K.; Mariotti, C.; Cook, B. S.; Roselli, L.; Tentzeris, M. M. Development, Characterization, and Processing of Thin and Thick Inkjet-Printed Dielectric Films. *Organic Electronics* **2016**, *29*, 135–141. <https://doi.org/10.1016/j.orgel.2015.11.022>.
- (57) Bitto, J.; Tehrani, B.; Cook, B.; Tentzeris, M. Fully Inkjet-Printed Multilayer Microstrip Patch Antenna for Ku-Band Applications. In *2014 IEEE Antennas and Propagation Society International Symposium (APSURSI)*; 2014; pp 854–855. <https://doi.org/10.1109/APS.2014.6904755>.
- (58) Cui, Z. *Printed Electronics: Materials, Technologies and Applications*; John Wiley & Sons, 2016.

- (59) Morseletto, P. Targets for a Circular Economy. *Resources, Conservation and Recycling* **2020**, *153*, 104553. <https://doi.org/10.1016/j.resconrec.2019.104553>.
- (60) Martinez, A. W.; Phillips, S. T.; Butte, M. J.; Whitesides, G. M. Patterned Paper as a Platform for Inexpensive, Low-Volume, Portable Bioassays. *Angewandte Chemie International Edition* **2007**, *46* (8), 1318–1320. <https://doi.org/10.1002/anie.200603817>.
- (61) Cruz, S. M. F.; Rocha, L. A.; Viana, J. C. *Printing Technologies on Flexible Substrates for Printed Electronics*; IntechOpen, 2018. <https://doi.org/10.5772/intechopen.76161>.
- (62) Yamada, K.; Henares, T. G.; Suzuki, K.; Citterio, D. Paper-Based Inkjet-Printed Microfluidic Analytical Devices. *Angewandte Chemie International Edition* **2015**, *54* (18), 5294–5310. <https://doi.org/10.1002/anie.201411508>.
- (63) Pabst, O.; Perelaer, J.; Beckert, E.; Schubert, U. S.; Eberhardt, R.; Tünnermann, A. All Inkjet-Printed Piezoelectric Polymer Actuators: Characterization and Applications for Micropumps in Lab-on-a-Chip Systems. *Organic Electronics* **2013**, *14* (12), 3423–3429. <https://doi.org/10.1016/j.orgel.2013.09.009>.
- (64) Pang, C.; Lee, G.-Y.; Kim, T.; Kim, S. M.; Kim, H. N.; Ahn, S.-H.; Suh, K.-Y. A Flexible and Highly Sensitive Strain-Gauge Sensor Using Reversible Interlocking of Nanofibres. *Nature Mater* **2012**, *11* (9), 795–801. <https://doi.org/10.1038/nmat3380>.
- (65) Fuller, S. B.; Wilhelm, E. J.; Jacobson, J. M. Ink-Jet Printed Nanoparticle Microelectromechanical Systems. *Journal of Microelectromechanical Systems* **2002**, *11* (1), 54–60. <https://doi.org/10.1109/84.982863>.
- (66) Srichan, C.; Saikrajang, T.; Lomas, T.; Jomphoak, A.; Maturros, T.; Phokaratkul, D.; Kerdcharoen, T.; Tuantranont, A. Inkjet Printing PEDOT:PSS Using Desktop Inkjet Printer. In *2009 6th International Conference on Electrical Engineering/Electronics, Computer, Telecommunications and Information Technology*; 2009; Vol. 01, pp 465–468. <https://doi.org/10.1109/ECTICON.2009.5137049>.
- (67) Rieu, M.; Camara, M.; Tournier, G.; Viricelle, J.-P.; Pijolat, C.; de Rooij, N. F.; Briand, D. Fully Inkjet Printed SnO₂ Gas Sensor on Plastic Substrate. *Sensors and Actuators B: Chemical* **2016**, *236*, 1091–1097. <https://doi.org/10.1016/j.snb.2016.06.042>.
- (68) Pereira da Silva Neves, M. M.; González-García, M. B.; Hernández-Santos, D.; Fanjul-Bolado, P. Future Trends in the Market for Electrochemical Biosensing. *Current Opinion in Electrochemistry* **2018**, *10*, 107–111. <https://doi.org/10.1016/j.coelec.2018.05.002>.
- (69) Patranabi, D. *Sensors and Transducers*; PHI Learning Pvt. Ltd., 2003.
- (70) Christiansen, D.; Alexander, C. K.; Jurgen, R. K. *Standard Handbook of Electronic Engineering*; McGraw-Hill Education, 2005.

- (71) Leopold, N.; Busche, S.; Gauglitz, G.; Lendl, B. IR Absorption and Reflectometric Interference Spectroscopy (RIfS) Combined to a New Sensing Approach for Gas Analytes Absorbed into Thin Polymer Films. *Spectrochimica Acta Part A: Molecular and Biomolecular Spectroscopy* **2009**, *72* (5), 994–999. <https://doi.org/10.1016/j.saa.2008.12.032>.
- (72) Spadavecchia, J.; Ciccarella, G.; Siciliano, P.; Capone, S.; Rella, R. Spin-Coated Thin Films of Metal Porphyrin–Phthalocyanine Blend for an Optochemical Sensor of Alcohol Vapours. *Sensors and Actuators B: Chemical* **2004**, *100* (1), 88–93. <https://doi.org/10.1016/j.snb.2003.12.027>.
- (73) Pacquit, A.; Frisby, J.; Diamond, D.; Lau, K. T.; Farrell, A.; Quilty, B.; Diamond, D. Development of a Smart Packaging for the Monitoring of Fish Spoilage. *Food Chemistry* **2007**, *102* (2), 466–470. <https://doi.org/10.1016/j.foodchem.2006.05.052>.
- (74) Correia, V.; Caparros, C.; Casellas, C.; Francesch, L.; Rocha, J. G.; Lanceros-Mendez, S. Development of Inkjet Printed Strain Sensors. *Smart Mater. Struct.* **2013**, *22* (10), 105028. <https://doi.org/10.1088/0964-1726/22/10/105028>.
- (75) Andò, B.; Baglio, S.; La Malfa, S.; L'Episcopo, G. All Inkjet Printed System for Strain Measurement. In *2011 IEEE SENSORS*; 2011; pp 215–217. <https://doi.org/10.1109/ICSENS.2011.6127295>.
- (76) Abe, K.; Suzuki, K.; Citterio, D. Inkjet-Printed Microfluidic Multianalyte Chemical Sensing Paper. *Anal. Chem.* **2008**, *80* (18), 6928–6934. <https://doi.org/10.1021/ac800604v>.
- (77) Hasenbank, M. S.; Edwards, T.; Fu, E.; Garzon, R.; Kosar, T. F.; Look, M.; Mashadi-Hosseini, A.; Yager, P. Demonstration of Multi-Analyte Patterning Using Piezoelectric Inkjet Printing of Multiple Layers. *Analytica Chimica Acta* **2008**, *611* (1), 80–88. <https://doi.org/10.1016/j.aca.2008.01.048>.
- (78) Chung, S.; Kim, S. O.; Kwon, S.-K.; Lee, C.; Hong, Y. All-Inkjet-Printed Organic Thin-Film Transistor Inverter on Flexible Plastic Substrate. *IEEE Electron Device Letters* **2011**, *32* (8), 1134–1136. <https://doi.org/10.1109/LED.2011.2156757>.
- (79) Thévenot, D. R.; Toth, K.; Durst, R. A.; Wilson, G. S. Electrochemical Biosensors: Recommended Definitions and Classification. International Union of Pure and Applied Chemistry: Physical Chemistry Division, Commission I.7 (Biophysical Chemistry); Analytical Chemistry Division, Commission V.5 (Electroanalytical Chemistry).1. *Biosensors and Bioelectronics* **2001**, *16* (1), 121–131. [https://doi.org/10.1016/S0956-5663\(01\)00115-4](https://doi.org/10.1016/S0956-5663(01)00115-4).
- (80) Gpel, W.; Hesse, J.; Zemel, J. N. Sensors a Comprehensive Survey. Vol. 1, Fundamentals and General Aspects. **1989**.

- (81) Nyholm, L. Electrochemical Techniques for Lab-on-a-Chip Applications. *Analyst* **2005**, *130* (5), 599–605. <https://doi.org/10.1039/B415004J>.
- (82) Bergveld, P.; Thevenot, D. In *Advances in Biosensors, Supplement 1 (APF Turner, Ed.)*; JAI Press, London, UK, 1993.
- (83) Bagotsky, V. S. *Fundamentals of Electrochemistry*; John Wiley & Sons, 2005; Vol. 44.
- (84) Vondrák, J. *Electrochemical Methods: Fundamentals and Applications: By AJ Bard and LR Faulkner; Published by Wiley, New York, 1980; Xviii+ 718 Pp.; Price, pounds 33.65 (Hard Cover), pounds 13.00 (Soft Cover); ISBN 0-471-05542-5; Elsevier, 1983.*
- (85) Alegret, S.; Valle, M. del; Merkoçi, A. *Sensores electroquímicos: introducción a los quimiosensores y biosensores : curso teórico-práctico*; Univ. Autònoma de Barcelona, 2004.
- (86) Cremer, M. *Über Die Ursache Der Elektromotorischen Eigenschaften Der Gewebe, Zugleich Ein Beitrag Zur Lehre von Den Polyphasischen Elektrolytketten*; R. Oldenbourg, 1906.
- (87) Ross, J. W. Calcium-Selective Electrode with Liquid Ion Exchanger. *Science* **1967**, *156* (3780), 1378–1379. <https://doi.org/10.1126/science.156.3780.1378>.
- (88) Bloch, R.; Shatkay, A.; Saroff, H. Fabrication and Evaluation of Membranes as Specific Electrodes for Calcium Ions. *Biophysical journal* **1967**, *7* (6), 865–877.
- (89) Forster, R. J.; Keyes, T. E. Ion-Selective Electrodes in Environmental Analysis. *Encyclopedia of Analytical Chemistry: Applications, Theory and Instrumentation* **2006**.
- (90) Bühlmann, P.; Pretsch, E.; Bakker, E. Carrier-Based Ion-Selective Electrodes and Bulk Optodes. 2. Ionophores for Potentiometric and Optical Sensors. *Chemical Reviews* **1998**, *98* (4), 1593–1688.
- (91) James, H. J.; Carmack, G.; Freiser, H. Coated Wire Ion-Selective Electrodes. *Analytical chemistry* **1972**, *44* (4), 856–857.
- (92) Li, Y.; Mao, Y.; Xiao, C.; Xu, X.; Li, X. Flexible PH Sensor Based on a Conductive PANI Membrane for PH Monitoring. *RSC Advances* **2020**, *10* (1), 21–28. <https://doi.org/10.1039/C9RA09188B>.
- (93) Hou, X.; Zhou, Y.; Liu, Y.; Wang, L.; Wang, J. Coaxial Electrospun Flexible PANI/PU Fibers as Highly Sensitive PH Wearable Sensor. *J Mater Sci* **2020**, *55* (33), 16033–16047. <https://doi.org/10.1007/s10853-020-05110-7>.
- (94) Hu, J.; Stein, A.; Bühlmann, P. Rational Design of All-Solid-State Ion-Selective Electrodes and Reference Electrodes. *TrAC Trends in Analytical Chemistry* **2016**, *76*, 102–114. <https://doi.org/10.1016/j.trac.2015.11.004>.

- (95) Moya, A.; Pol, R.; Martínez-Cuadrado, A.; Villa, R.; Gabriel, G.; Baeza, M. Stable Full-Inkjet-Printed Solid-State Ag/AgCl Reference Electrode. *Anal. Chem.* **2019**, *91* (24), 15539–15546. <https://doi.org/10.1021/acs.analchem.9b03441>.
- (96) Grossi, M.; Riccò, B. Electrical Impedance Spectroscopy (EIS) for Biological Analysis and Food Characterization: A Review. *Journal of Sensors and Sensor Systems* **2017**, *6* (2), 303–325. <https://doi.org/10.5194/jsss-6-303-2017>.
- (97) Nernst, W. Methode Zur Bestimmung von Dielektrizitätskonstanten. *Zeitschrift für Physikalische Chemie* **1894**, *14* (1), 622–663.
- (98) GABRIELLI, C. Méthodes Electrochimiques: Mesures d'impédances. *Techniques de l'ingénieur. Corrosion vieillissement* **1998**, No. P2210.
- (99) Hou, L.; Cui, Y.; Xu, M.; Gao, Z.; Huang, J.; Tang, D. Graphene Oxide-Labeled Sandwich-Type Impedimetric Immunoassay with Sensitive Enhancement Based on Enzymatic 4-Chloro-1-Naphthol Oxidation. *Biosensors and Bioelectronics* **2013**, *47*, 149–156. <https://doi.org/10.1016/j.bios.2013.02.035>.
- (100) Costa, T. H. da; Song, E.; Tortorich, R. P.; Choi, J.-W. A Paper-Based Electrochemical Sensor Using Inkjet-Printed Carbon Nanotube Electrodes. *ECS J. Solid State Sci. Technol.* **2015**, *4* (10), S3044–S3047. <https://doi.org/10.1149/2.0121510jss>.
- (101) Tortorich, R. P.; Song, E.; Choi, J.-W. Inkjet-Printed Carbon Nanotube Electrodes with Low Sheet Resistance for Electrochemical Sensor Applications. *J. Electrochem. Soc.* **2014**, *161* (2), B3044–B3048. <https://doi.org/10.1149/2.008402jes>.
- (102) Tortorich, R. P.; Shamkhalichenar, H.; Choi, J.-W. Inkjet-Printed and Paper-Based Electrochemical Sensors. *Applied Sciences* **2018**, *8* (2), 288. <https://doi.org/10.3390/app8020288>.
- (103) Ceradrop - Inkjet Technology, Aerosol Jet, Digital Printing, Printed Electronics, Smart 3D, 3D, Piezoelectric inkjet printer <http://www.ceradrop.com/en/products/f-serie/> (accessed 2021 -06 -18).
- (104) Nilsson, D.; Kugler, T.; Svensson, P.-O.; Berggren, M. An All-Organic Sensor–Transistor Based on a Novel Electrochemical Transducer Concept Printed Electrochemical Sensors on Paper. *Sensors and Actuators B: Chemical* **2002**, *86* (2), 193–197. [https://doi.org/10.1016/S0925-4005\(02\)00170-3](https://doi.org/10.1016/S0925-4005(02)00170-3).
- (105) Lee, C.-W.; Nam, D.-H.; Han, Y.-S.; Chung, K.-C.; Gong, M.-S. Humidity Sensors Fabricated with Polyelectrolyte Membrane Using an Ink-Jet Printing Technique and Their Electrical Properties. *Sensors and Actuators B: Chemical* **2005**, *109* (2), 334–340. <https://doi.org/10.1016/j.snb.2004.12.070>.

- (106) Sjöberg, P.; Määttänen, A.; Vanamo, U.; Novell, M.; Ihalainen, P.; Andrade, F. J.; Bobacka, J.; Peltonen, J. Paper-Based Potentiometric Ion Sensors Constructed on Ink-Jet Printed Gold Electrodes. *Sensors and Actuators B: Chemical* **2016**, *224*, 325–332. <https://doi.org/10.1016/j.snb.2015.10.051>.
- (107) Pavinatto, F. J.; Paschoal, C. W. A.; Arias, A. C. Printed and Flexible Biosensor for Antioxidants Using Interdigitated Ink-Jetted Electrodes and Gravure-Deposited Active Layer. *Biosensors and Bioelectronics* **2015**, *67*, 553–559. <https://doi.org/10.1016/j.bios.2014.09.039>.
- (108) Nie, Z.; Deiss, F.; Liu, X.; Akbulut, O.; Whitesides, G. M. Integration of Paper-Based Microfluidic Devices with Commercial Electrochemical Readers. *Lab Chip* **2010**, *10* (22), 3163–3169. <https://doi.org/10.1039/C0LC00237B>.
- (109) Pandhi, T.; Cornwell, C.; Fujimoto, K.; Barnes, P.; Cox, J.; Xiong, H.; Davis, P. H.; Subbaraman, H.; Koehne, J. E.; Estrada, D. Fully Inkjet-Printed Multilayered Graphene-Based Flexible Electrodes for Repeatable Electrochemical Response. *RSC Adv.* **2020**, *10* (63), 38205–38219. <https://doi.org/10.1039/D0RA04786D>.
- (110) Le, D. D.; Nguyen, T. N. N.; Doan, D. C. T.; Dang, T. M. D.; Dang, M. C. Fabrication of Interdigitated Electrodes by Inkjet Printing Technology for Application in Ammonia Sensing. *Adv. Nat. Sci.: Nanosci. Nanotechnol.* **2016**, *7* (2), 025002. <https://doi.org/10.1088/2043-6262/7/2/025002>.
- (111) Y. Adly, N.; Bachmann, B.; J. Krause, K.; Offenhäusser, A.; Wolfrum, B.; Yakushenko, A. Three-Dimensional Inkjet-Printed Redox Cycling Sensor. *RSC Advances* **2017**, *7* (9), 5473–5479. <https://doi.org/10.1039/C6RA27170G>.
- (112) Khan, Y.; Pavinatto, F. J.; Lin, M. C.; Liao, A.; Swisher, S. L.; Mann, K.; Subramanian, V.; Maharbiz, M. M.; Arias, A. C. Inkjet-Printed Flexible Gold Electrode Arrays for Bioelectronic Interfaces. *Advanced Functional Materials* **2016**, *26* (7), 1004–1013. <https://doi.org/10.1002/adfm.201503316>.
- (113) Xu, Z.; Dong, Q.; Otieno, B.; Liu, Y.; Williams, I.; Cai, D.; Li, Y.; Lei, Y.; Li, B. Real-Time in Situ Sensing of Multiple Water Quality Related Parameters Using Micro-Electrode Array (MEA) Fabricated by Inkjet-Printing Technology (IPT). *Sensors and Actuators B: Chemical* **2016**, *237*, 1108–1119. <https://doi.org/10.1016/j.snb.2016.09.040>.
- (114) Jović, M.; Zhu, Y.; Lesch, A.; Bondarenko, A.; Cortés-Salazar, F.; Gumy, F.; Girault, H. H. Inkjet-Printed Microtiter Plates for Portable Electrochemical Immunoassays. *Journal of Electroanalytical Chemistry* **2017**, *786*, 69–76. <https://doi.org/10.1016/j.jelechem.2016.12.051>.
- (115) Lesch, A.; Cortés-Salazar, F.; Amstutz, V.; Tacchini, P.; Girault, H. H. Inkjet Printed Nanohydrogel Coated Carbon Nanotubes Electrodes For Matrix Independent Sensing. *Anal. Chem.* **2015**, *87* (2), 1026–1033. <https://doi.org/10.1021/ac503748g>.

- (116) Qin, Y.; Kwon, H.-J.; Subrahmanyam, A.; Howlader, M. M. R.; Selvaganapathy, P. R.; Adronov, A.; Deen, M. J. Inkjet-Printed Bifunctional Carbon Nanotubes for PH Sensing. *Materials Letters* **2016**, *176*, 68–70. <https://doi.org/10.1016/j.matlet.2016.04.048>.
- (117) R. Das, S.; Nian, Q.; A. Cargill, A.; A. Hondred, J.; Ding, S.; Saei, M.; J. Cheng, G.; C. Claussen, J. 3D Nanostructured Inkjet Printed Graphene via UV-Pulsed Laser Irradiation Enables Paper-Based Electronics and Electrochemical Devices. *Nanoscale* **2016**, *8* (35), 15870–15879. <https://doi.org/10.1039/C6NR04310K>.
- (118) Pu, Z.; Wang, R.; Wu, J.; Yu, H.; Xu, K.; Li, D. A Flexible Electrochemical Glucose Sensor with Composite Nanostructured Surface of the Working Electrode. *Sensors and Actuators B: Chemical* **2016**, *230*, 801–809. <https://doi.org/10.1016/j.snb.2016.02.115>.
- (119) Ihalainen, P.; Määttänen, A.; Pesonen, M.; Sjöberg, P.; Sarfraz, J.; Österbacka, R.; Peltonen, J. Paper-Supported Nanostructured Ultrathin Gold Film Electrodes – Characterization and Functionalization. *Applied Surface Science* **2015**, *329*, 321–329. <https://doi.org/10.1016/j.apsusc.2014.12.156>.
- (120) Bardpho, C.; Rattanarat, P.; Siangproh, W.; Chailapakul, O. Ultra-High Performance Liquid Chromatographic Determination of Antioxidants in Teas Using Inkjet-Printed Graphene–Polyaniline Electrode. *Talanta* **2016**, *148*, 673–679. <https://doi.org/10.1016/j.talanta.2015.05.020>.
- (121) Brannelly, N. T.; Killard, A. J. A Printed and Microfabricated Sensor Device for the Sensitive Low Volume Measurement of Aqueous Ammonia. *Electroanalysis* **2017**, *29* (1), 162–171. <https://doi.org/10.1002/elan.201600556>.
- (122) Teengam, P.; Siangproh, W.; Tuantranont, A.; Henry, C. S.; Vilaivan, T.; Chailapakul, O. Electrochemical Paper-Based Peptide Nucleic Acid Biosensor for Detecting Human Papillomavirus. *Analytica Chimica Acta* **2017**, *952*, 32–40. <https://doi.org/10.1016/j.aca.2016.11.071>.
- (123) Qin, Y.; Alam, A. U.; Howlader, M. M. R.; Hu, N.-X.; Deen, M. J. Inkjet Printing of a Highly Loaded Palladium Ink for Integrated, Low-Cost PH Sensors. *Advanced Functional Materials* **2016**, *26* (27), 4923–4933. <https://doi.org/10.1002/adfm.201600657>.
- (124) Jović, M.; Cortés-Salazar, F.; Lesch, A.; Amstutz, V.; Bi, H.; Girault, H. H. Electrochemical Detection of Free Chlorine at Inkjet Printed Silver Electrodes. *Journal of Electroanalytical Chemistry* **2015**, *756*, 171–178. <https://doi.org/10.1016/j.jelechem.2015.08.024>.
- (125) Hu, C.; Bai, X.; Wang, Y.; Jin, W.; Zhang, X.; Hu, S. Inkjet Printing of Nanoporous Gold Electrode Arrays on Cellulose Membranes for High-Sensitive Paper-Like Electrochemical Oxygen Sensors Using Ionic Liquid Electrolytes. *Anal. Chem.* **2012**, *84* (8), 3745–3750. <https://doi.org/10.1021/ac3003243>.

- (126) Khan, M. S.; Fon, D.; Li, X.; Tian, J.; Forsythe, J.; Garnier, G.; Shen, W. Biosurface Engineering through Ink Jet Printing. *Colloids and Surfaces B: Biointerfaces* **2010**, *75* (2), 441–447. <https://doi.org/10.1016/j.colsurfb.2009.09.032>.
- (127) Haque, R. I.; Ogam, E.; Loussert, C.; Benaben, P.; Boddaert, X. Fabrication of Capacitive Acoustic Resonators Combining 3D Printing and 2D Inkjet Printing Techniques. *Sensors* **2015**, *15* (10), 26018–26038. <https://doi.org/10.3390/s151026018>.
- (128) Rahim, M. A. and M. K. A. Triple-Band Printed Dipole Antenna for RFID. *Progress In Electromagnetics Research C* **2009**, *9*, 145–153. <https://doi.org/10.2528/PIERC09070703>.
- (129) Trommnau, J.; Kühnle, J.; Siegert, J.; Inderka, R.; Bauernhansl, T. Overview of the State of the Art in the Production Process of Automotive Wire Harnesses, Current Research and Future Trends. *Procedia CIRP* **2019**, *81*, 387–392.
- (130) Rajan, K.; Roppolo, I.; Chiappone, A.; Bocchini, S.; Perrone, D.; Chiolerio, A. Silver Nanoparticle Ink Technology: State of the Art. *Nanotechnol Sci Appl* **2016**, *9*, 1–13. <https://doi.org/10.2147/NSA.S68080>.
- (131) Roberts, T.; Graaf, J. B. D.; Nicol, C.; Hervé, T.; Fiocchi, M.; Sanaur, S. Flexible Inkjet-Printed Multielectrode Arrays for Neuromuscular Cartography. *Advanced Healthcare Materials* **2016**, *5* (12), 1462–1470. <https://doi.org/10.1002/adhm.201600108>.
- (132) Lim, T.; Han, S.; Chung, J.; Chung, J. T.; Ko, S.; Grigoropoulos, C. P. Experimental Study on Spreading and Evaporation of Inkjet Printed Pico-Liter Droplet on a Heated Substrate. *International Journal of Heat and Mass Transfer* **2009**, *52* (1), 431–441. <https://doi.org/10.1016/j.ijheatmasstransfer.2008.05.028>.
- (133) Castrejón-Pita, J. R.; Martin, G. D.; Hoath, S. D.; Hutchings, I. M. A Simple Large-Scale Droplet Generator for Studies of Inkjet Printing. *Review of Scientific Instruments* **2008**, *79* (7), 075108. <https://doi.org/10.1063/1.2957744>.
- (134) Zhang, Y.; Chen, X.; Liu, F.; Li, L.; Dai, J.; Liu, T. Enhanced Coffee-Ring Effect via Substrate Roughness in Evaporation of Colloidal Droplets. *Advances in Condensed Matter Physics* **2018**, *2018*, e9795654. <https://doi.org/10.1155/2018/9795654>.
- (135) Jeong, S.; Song, H. C.; Lee, W. W.; Lee, S. S.; Choi, Y.; Son, W.; Kim, E. D.; Paik, C. H.; Oh, S. H.; Ryu, B.-H. Stable Aqueous Based Cu Nanoparticle Ink for Printing Well-Defined Highly Conductive Features on a Plastic Substrate. *Langmuir* **2011**, *27* (6), 3144–3149. <https://doi.org/10.1021/la104136w>.
- (136) Tai, Y.-L.; Yang, Z.-G. Fabrication of Paper-Based Conductive Patterns for Flexible Electronics by Direct-Writing. *J. Mater. Chem.* **2011**, *21* (16), 5938–5943. <https://doi.org/10.1039/C0JM03065A>.

- (137) Tan, H. W.; An, J.; Chua, C. K.; Tran, T. Metallic Nanoparticle Inks for 3D Printing of Electronics. *Advanced Electronic Materials* **2019**, *5* (5), 1800831. <https://doi.org/10.1002/aelm.201800831>.
- (138) Hrehorova, E.; Wood, L. K.; Pekarovic, J.; Pekarovicova, A.; Fleming, P. D.; Bliznyuk, V. The Properties of Conducting Polymers and Substrates for Printed Electronics. *NIP & Digital Fabrication Conference* **2005**, *2005* (3), 197–202.
- (139) Tortorich, R. P.; Choi, J.-W. Inkjet Printing of Carbon Nanotubes. *Nanomaterials* **2013**, *3* (3), 453–468. <https://doi.org/10.3390/nano3030453>.
- (140) Salomoni, R.; Léo, P.; Montemor, A. F.; Rinaldi, B. G.; Rodrigues, M. F. A. Antibacterial Effect of Silver Nanoparticles in *Pseudomonas Aeruginosa*. *NSA* **2017**, *10*, 115–121. <https://doi.org/10.2147/NSA.S133415>.
- (141) Marinho, B.; Ghislandi, M.; Tkalya, E.; Koning, C. E.; de With, G. Electrical Conductivity of Compacts of Graphene, Multi-Wall Carbon Nanotubes, Carbon Black, and Graphite Powder. *Powder Technology* **2012**, *221*, 351–358. <https://doi.org/10.1016/j.powtec.2012.01.024>.
- (142) Falkovsky, L. A. Optical Properties of Graphene. *J. Phys.: Conf. Ser.* **2008**, *129*, 012004. <https://doi.org/10.1088/1742-6596/129/1/012004>.
- (143) Xu, Y.; Cao, H.; Xue, Y.; Li, B.; Cai, W. Liquid-Phase Exfoliation of Graphene: An Overview on Exfoliation Media, Techniques, and Challenges. *Nanomaterials* **2018**, *8* (11), 942. <https://doi.org/10.3390/nano8110942>.
- (144) Rossouw, D.; Botton, G. A.; Najafi, E.; Lee, V.; Hitchcock, A. P. Metallic and Semiconducting Single-Walled Carbon Nanotubes: Differentiating Individual SWCNTs by Their Carbon 1s Spectra. *ACS Nano* **2012**, *6* (12), 10965–10972. <https://doi.org/10.1021/nn3045227>.
- (145) Nayak, L.; Mohanty, S.; Nayak, S. K.; Ramadoss, A. A Review on Inkjet Printing of Nanoparticle Inks for Flexible Electronics. *J. Mater. Chem. C* **2019**, *7* (29), 8771–8795. <https://doi.org/10.1039/C9TC01630A>.
- (146) Gleiter, H. Nanostructured Materials: Basic Concepts and Microstructure. *Acta Materialia* **2000**, *48* (1), 1–29. [https://doi.org/10.1016/S1359-6454\(99\)00285-2](https://doi.org/10.1016/S1359-6454(99)00285-2).
- (147) Luo, W.; Hu, W.; Xiao, S. Size Effect on the Thermodynamic Properties of Silver Nanoparticles. *J. Phys. Chem. C* **2008**, *112* (7), 2359–2369. <https://doi.org/10.1021/jp0770155>.
- (148) Pawlow, P. Über die Abhängigkeit des Schmelzpunktes von der Oberflächenenergie eines festen Körpers. *Zeitschrift für Physikalische Chemie* **1909**, *65U* (1), 1–35. <https://doi.org/10.1515/zpch-1909-6502>.

- (149) Takagi, M. Electron-Diffraction Study of Liquid-Solid Transition of Thin Metal Films. *Journal of the Physical Society of Japan* **1954**, *9* (3), 359–363. <https://doi.org/10.1143/JPSJ.9.359>.
- (150) Ding, F.; Bolton, K.; Rosén, A. Iron-Carbide Cluster Thermal Dynamics for Catalyzed Carbon Nanotube Growth. *Journal of Vacuum Science & Technology A* **2004**, *22* (4), 1471–1476. <https://doi.org/10.1116/1.1752895>.
- (151) Buffat, Ph.; Borel, J.-P. Size Effect on the Melting Temperature of Gold Particles. *Phys. Rev. A* **1976**, *13* (6), 2287–2298. <https://doi.org/10.1103/PhysRevA.13.2287>.
- (152) Gülseren, O.; Ercolessi, F.; Tosatti, E. Premelting of Thin Wires. *Phys. Rev. B* **1995**, *51* (11), 7377–7380. <https://doi.org/10.1103/PhysRevB.51.7377>.
- (153) Safaei, A.; Shandiz, M. A.; Sanjabi, S.; Barber, Z. H. Modelling the Size Effect on the Melting Temperature of Nanoparticles, Nanowires and Nanofilms. *J. Phys.: Condens. Matter* **2007**, *19* (21), 216216. <https://doi.org/10.1088/0953-8984/19/21/216216>.
- (154) Nogueira, A. L.; Machado, R. A. F.; de Souza, A. Z.; Martinello, F.; Franco, C. V.; Dutra, G. B. Synthesis and Characterization of Silver Nanoparticles Produced with a Bifunctional Stabilizing Agent. *Ind. Eng. Chem. Res.* **2014**, *53* (9), 3426–3434. <https://doi.org/10.1021/ie4030903>.
- (155) Denneulin, A.; Bras, J.; Blayo, A.; Khelifi, B.; Roussel-Dherbey, F.; Neuman, C. The Influence of Carbon Nanotubes in Inkjet Printing of Conductive Polymer Suspensions. *Nanotechnology* **2009**, *20* (38), 385701. <https://doi.org/10.1088/0957-4484/20/38/385701>.
- (156) Kirchmeyer, S.; Reuter, K. Scientific Importance, Properties and Growing Applications of Poly(3,4-Ethylenedioxythiophene). *J. Mater. Chem.* **2005**, *15* (21), 2077–2088. <https://doi.org/10.1039/B417803N>.
- (157) Groenendaal, L.; Jonas, F.; Freitag, D.; Pielartzik, H.; Reynolds, J. R. Poly(3,4-Ethylenedioxythiophene) and Its Derivatives: Past, Present, and Future. *Advanced Materials* **2000**, *12* (7), 481–494. [https://doi.org/10.1002/\(SICI\)1521-4095\(200004\)12:7<481::AID-ADMA481>3.0.CO;2-C](https://doi.org/10.1002/(SICI)1521-4095(200004)12:7<481::AID-ADMA481>3.0.CO;2-C).
- (158) Dietrich, M.; Heinze, J.; Heywang, G.; Jonas, F. Electrochemical and Spectroscopic Characterization of Polyalkylenedioxythiophenes. *Journal of Electroanalytical Chemistry* **1994**, *369* (1), 87–92. [https://doi.org/10.1016/0022-0728\(94\)87085-3](https://doi.org/10.1016/0022-0728(94)87085-3).
- (159) Yoshioka, Y.; Jabbour, G. E. Desktop Inkjet Printer as a Tool to Print Conducting Polymers. *Synthetic Metals* **2006**, *156* (11), 779–783. <https://doi.org/10.1016/j.synthmet.2006.03.013>.
- (160) Jonas, F.; Krafft, W.; Muys, B. Poly(3, 4-Ethylenedioxythiophene): Conductive Coatings, Technical Applications and Properties. *Macromolecular Symposia* **1995**, *100* (1), 169–173. <https://doi.org/10.1002/masy.19951000128>.

- (161) Lanzani, G. Materials for Bioelectronics: Organic Electronics Meets Biology. *Nature materials* **2014**, *13* (8), 775–776. <https://doi.org/10.1038/nmat4021>.
- (162) Ryu, H.; Cho, S. J.; Kim, B.; Lim, G. A Stretchable Humidity Sensor Based on a Wrinkled Polyaniline Nanostructure. *RSC Adv.* **2014**, *4* (75), 39767. <https://doi.org/10.1039/C4RA04938A>.
- (163) Li, P.; Sun, K.; Ouyang, J. Stretchable and Conductive Polymer Films Prepared by Solution Blending. *ACS Applied Materials and Interfaces* **2015**, *7* (33), 18415–18423. <https://doi.org/10.1021/acsami.5b04492>.
- (164) Ouyang, J.; Li, Y. Great Improvement of Polypyrrole Films Prepared Electrochemically from Aqueous Solutions by Adding Nonaphenol Polyethyleneoxy (10) Ether. *Polymer* **1997**, *38* (15), 3997–3999.
- (165) Ouyang, J. “secondary Doping” Methods to Significantly Enhance the Conductivity of PEDOT:PSS for Its Application as Transparent Electrode of Optoelectronic Devices. *Displays* **2013**, *34* (5), 423–436. <https://doi.org/10.1016/j.displa.2013.08.007>.
- (166) Rikukawa, M.; Sanui, K. Proton-Conducting Polymer Electrolyte Membranes Based on Hydrocarbon Polymers. *Progress in Polymer Science (Oxford)* **2000**, *25* (10), 1463–1502. [https://doi.org/10.1016/S0079-6700\(00\)00032-0](https://doi.org/10.1016/S0079-6700(00)00032-0).
- (167) Guo, L.; Ma, M.; Zhang, N.; Langer, R.; Anderson, D. G. Stretchable Polymeric Multielectrode Array for Conformal Neural Interfacing. *Advanced Materials* **2014**, *26* (9), 1427–1433. <https://doi.org/10.1002/adma.201304140>.
- (168) Yoshikawa, H.; Hino, T.; Kuramoto, N. Effect of Temperature and Moisture on Electrical Conductivity in Polyaniline/Polyurethane (PANI/PU) Blends. *Synthetic Metals* **2006**, *156* (18–20), 1187–1193. <https://doi.org/10.1016/j.synthmet.2006.08.007>.
- (169) Stoyanov, H.; Kollosche, M.; Risse, S.; Waché, R.; Kofod, G. Soft Conductive Elastomer Materials for Stretchable Electronics and Voltage Controlled Artificial Muscles. *Advanced Materials* **2013**, *25* (4), 578–583. <https://doi.org/10.1002/adma.201202728>.
- (170) Roberts, M. E.; Sokolov, A. N.; Bao, Z. Material and Device Considerations for Organic Thin-Film Transistor Sensors. *Journal of Materials Chemistry* **2009**, *19* (21), 3351. <https://doi.org/10.1039/b816386c>.
- (171) Sokolov, A. N.; Roberts, M. E.; Bao, Z. Fabrication of Low-Cost Electronic Biosensors. *Materials Today* **2009**, *12* (9), 12–20. [https://doi.org/10.1016/S1369-7021\(09\)70247-0](https://doi.org/10.1016/S1369-7021(09)70247-0).
- (172) Aher, S. S.; Malsane, S. T.; Saudagar, R. Nanosuspension: An Overview. *Asian Journal of Research in Pharmaceutical Sciences* **2017**, *7* (2), 81–86.

- (173) Lenhardt, T.; Vergnault, G.; Grenier, P.; Scherer, D.; Langguth, P. Evaluation of Nanosuspensions for Absorption Enhancement of Poorly Soluble Drugs: In Vitro Transport Studies Across Intestinal Epithelial Monolayers. *AAPS J* **2008**, *10* (3), 435–438. <https://doi.org/10.1208/s12248-008-9050-7>.
- (174) Arunkumar, N.; Deecaraman, M.; Rani, C. Nanosuspension Technology and Its Applications in Drug Delivery. *Asian Journal of Pharmaceutics (AJP): Free full text articles from Asian J Pharm* **2014**, *3* (3).
- (175) Pu, X.; Sun, J.; Li, M.; He, Z. Formulation of Nanosuspensions as a New Approach for the Delivery of Poorly Soluble Drugs. *Current Nanoscience* **2009**, *5* (4), 417–427. <https://doi.org/10.2174/157341309789378177>.
- (176) Liversidge, G. G.; Cundy, K. C. Particle Size Reduction for Improvement of Oral Bioavailability of Hydrophobic Drugs: I. Absolute Oral Bioavailability of Nanocrystalline Danazol in Beagle Dogs. *International journal of pharmaceutics* **1995**, *125* (1), 91–97.
- (177) Senthil Kumar, C.; Vedha Hari, B.; Sharavanan, S.; Subramanian, N.; Punitha, S.; Senthil Kumar, V. Novel Metronidazole Nanosuspension as a Controlled Drug Delivery System for Anthelmintic Activity. *Journal of Pharmacy Research* **2010**, *3* (10), 2404–2407.
- (178) Li, L.; Ferng, L.; Wei, Y.; Yang, C.; Ji, H. F. Effects of Acidity on the Size of Polyaniline-Poly(Sodium 4-Styrenesulfonate) Composite Particles and the Stability of Corresponding Colloids in Water. *Journal of Colloid and Interface Science* **2012**, *381* (1), 11–16. <https://doi.org/10.1016/j.jcis.2012.05.004>.
- (179) Nagarajan, R.; Tripathy, S.; Kumar, J.; Bruno, F. F.; Samuelson, L. Enzymatically Synthesized Conducting Molecular Complex of Polyaniline and Poly(Vinylphosphonic Acid). *Macromolecules* **2000**, *33* (26), 9542–9547. <https://doi.org/10.1021/ma000954+>.
- (180) Cruz-Silva, R.; Romero-García, J.; Angulo-Sánchez, J. L.; Ledezma-Pérez, A.; Arias-Marín, E.; Moggio, I.; Flores-Loyola, E. Template-Free Enzymatic Synthesis of Electrically Conducting Polyaniline Using Soybean Peroxidase. *European Polymer Journal* **2005**, *41* (5), 1129–1135. <https://doi.org/10.1016/j.eurpolymj.2004.11.012>.
- (181) Kuo, C. W.; Wen, T. C. Dispersible Polyaniline Nanoparticles in Aqueous Poly(Styrenesulfonic Acid) via the Interfacial Polymerization Route. *European Polymer Journal* **2008**, *44* (11), 3393–3401. <https://doi.org/10.1016/j.eurpolymj.2008.07.018>.
- (182) Ngamna, O.; Morrin, A.; Killard, A. J.; Moulton, S. E.; Smyth, M. R.; Wallace, G. G. Inkjet Printable Polyaniline Nanoformulations. *Langmuir* **2007**, *23* (16), 8569–8574. <https://doi.org/10.1021/la700540g>.
- (183) Jang, J.; Ha, J.; Cho, J. Fabrication of Water-Dispersible Polyaniline-Poly(4-Styrenesulfonate) Nanoparticles For Inkjet-Printed Chemical-Sensor Applications. *Advanced Materials* **2007**, *19* (13), 1772–1775. <https://doi.org/10.1002/adma.200602127>.

- (184) Teixidó Bartes, R. Novel Electronic Stretchable Materials for Future Medical Devices. PhD Thesis, Universitat Ramon Llull, 2017.
- (185) Aleeva, Y.; Pignataro, B. Recent Advances in Upscalable Wet Methods and Ink Formulations for Printed Electronics. *J. Mater. Chem. C* **2014**, *2* (32), 6436–6453. <https://doi.org/10.1039/C4TC00618F>.
- (186) Calvert, P. Inkjet Printing for Materials and Devices. *Chem. Mater.* **2001**, *13* (10), 3299–3305. <https://doi.org/10.1021/cm0101632>.
- (187) MacDiarmid, A. G. “Synthetic Metals”: A Novel Role for Organic Polymers (Nobel Lecture). *Angewandte Chemie International Edition* **2001**, *40* (14), 2581–2590. [https://doi.org/10.1002/1521-3773\(20010716\)40:14<2581::AID-ANIE2581>3.0.CO;2-2](https://doi.org/10.1002/1521-3773(20010716)40:14<2581::AID-ANIE2581>3.0.CO;2-2).
- (188) McCulloch, I.; Heeney, M.; Bailey, C.; Genevicius, K.; MacDonald, I.; Shkunov, M.; Sparrowe, D.; Tierney, S.; Wagner, R.; Zhang, W.; Chabiny, M. L.; Kline, R. J.; McGehee, M. D.; Toney, M. F. Liquid-Crystalline Semiconducting Polymers with High Charge-Carrier Mobility. *Nature Mater* **2006**, *5* (4), 328–333. <https://doi.org/10.1038/nmat1612>.
- (189) Subramanian, V.; Chang, J. B.; de la Fuente Vornbrock, A.; Huang, D. C.; Jagannathan, L.; Liao, F.; Mattis, B.; Molesa, S.; Redinger, D. R.; Soltman, D.; Volkman, S. K.; Zhang, Q. Printed Electronics for Low-Cost Electronic Systems: Technology Status and Application Development. In *ESSCIRC 2008 - 34th European Solid-State Circuits Conference*; 2008; pp 17–24. <https://doi.org/10.1109/ESSCIRC.2008.4681785>.
- (190) Männl, U.; Berg, C. van den; Magunje, B.; Härting, M.; Britton, D. T.; Jones, S.; Staden, M. J. van; Scriba, M. R. Nanoparticle Composites for Printed Electronics. *Nanotechnology* **2014**, *25* (9), 094004. <https://doi.org/10.1088/0957-4484/25/9/094004>.
- (191) Nam, J.-G.; Lee, E.-S.; Jung, W.-C.; Park, Y.-J.; Sohn, B.-H.; Park, S.-C.; Kim, J. S.; Bae, J.-Y. Photovoltaic Enhancement of Dye-Sensitized Solar Cell Prepared from [TiO₂/Ethyl Cellulose/Terpineol] Paste Employing TRITON™ X-Based Surfactant with Carboxylic Acid Group in the Oxyethylene Chain End. *Materials Chemistry and Physics* **2009**, *116* (1), 46–51. <https://doi.org/10.1016/j.matchemphys.2009.02.037>.
- (192) Li, H.; Xie, Z.; Zhang, Y.; Wang, J. The Effects of Ethyl Cellulose on PV Performance of DSSC Made of Nanostructured ZnO Pastes. *Thin Solid Films* **2010**, *518* (24, Supplement), e68–e71. <https://doi.org/10.1016/j.tsf.2010.03.125>.
- (193) Britton, D. T.; Härting, M. Printed nanoparticulate composites for silicon thick-film electronics. *Pure and Applied Chemistry* **2006**, *78* (9), 1723–1739. <https://doi.org/10.1351/pac200678091723>.
- (194) Mattana, G.; Loi, A.; Woytasik, M.; Barbaro, M.; Noël, V.; Piro, B. Inkjet-Printing: A New Fabrication Technology for Organic Transistors. *Advanced Materials Technologies* **2017**, *2* (10), 1700063. <https://doi.org/10.1002/admt.201700063>.

- (195) Flexible AM OLED panel driven by bottom-contact OTFTs http://ieeexplore.ieee.org/abstract/document/1610776/?casa_token=KFUdFanr3UgAAAAA:sNkZtpH-dp-9RsG-JmCzGrjvPoLrhdHIViAFr6RLSEVBqhgVucGo0X7kUCuVFN-_yJWNVMOjGjA (accessed 2021 -06 -23).
- (196) Haas, U.; Haase, A.; Satzinger, V.; Pichler, H.; Leising, G.; Jakopic, G.; Stadlober, B.; Houbertz, R.; Domann, G.; Schmitt, A. Hybrid Polymers as Tunable and Directly-Patternable Gate Dielectrics in Organic Thin-Film Transistors. *Phys. Rev. B* **2006**, *73* (23), 235339. <https://doi.org/10.1103/PhysRevB.73.235339>.
- (197) Rao, Y.; Wong, C. P. Material Characterization of a High-Dielectric-Constant Polymer–Ceramic Composite for Embedded Capacitor for RF Applications. *Journal of Applied Polymer Science* **2004**, *92* (4), 2228–2231. <https://doi.org/10.1002/app.13690>.
- (198) Shen, Y.; Lin, Y.; Li, M.; Nan, C.-W. High Dielectric Performance of Polymer Composite Films Induced by a Percolating Interparticle Barrier Layer. *Advanced Materials* **2007**, *19* (10), 1418–1422. <https://doi.org/10.1002/adma.200602097>.
- (199) Fix, W.; Ullmann, A.; Ficker, J.; Clemens, W. Fast Polymer Integrated Circuits. *Appl. Phys. Lett.* **2002**, *81* (9), 1735–1737. <https://doi.org/10.1063/1.1501450>.
- (200) Elger, D. F.; LeBret, B. A.; Crowe, C. T.; Roberson, J. A. *Engineering Fluid Mechanics*; John Wiley & Sons, 2020.
- (201) Seeton, C. J. Viscosity-Temperature Correlation for Liquids; American Society of Mechanical Engineers Digital Collection, 2008; pp 131–142. <https://doi.org/10.1115/IJTC2006-12139>.
- (202) Furlani, E. P. Fluid Mechanics for Inkjet Printing. *Fundamentals of Inkjet Printing* **2016**, 34–56.
- (203) Blevins, R. Applied Fluid Dynamics Handbook Van Nostrand Reinhold Co. *New York, NY* **1984**.
- (204) Sullivan, D. E. Surface Tension and Contact Angle of a Liquid–Solid Interface. *J. Chem. Phys.* **1981**, *74* (4), 2604–2615. <https://doi.org/10.1063/1.441333>.
- (205) Jung, S.; Hwang, H. J.; Hong, S. H. Drops on Substrates. *Fundamentals of Inkjet Printing* **2016**, 199–218.
- (206) Lim, J. A.; Lee, W. H.; Lee, H. S.; Lee, J. H.; Park, Y. D.; Cho, K. Self-Organization of Ink-Jet-Printed Triisopropylsilylethynyl Pentacene via Evaporation-Induced Flows in a Drying Droplet. *Advanced Functional Materials* **2008**, *18* (2), 229–234. <https://doi.org/10.1002/adfm.200700859>.

- (207) Good, R. J. A Thermodynamic Derivation of Wenzel's Modification of Young's Equation for Contact Angles; Together with a Theory of Hysteresis¹. *Journal of the American Chemical Society* **1952**, *74* (20), 5041–5042.
- (208) Deegan, R. D.; Bakajin, O.; Dupont, T. F.; Huber, G.; Nagel, S. R.; Witten, T. A. Capillary Flow as the Cause of Ring Stains from Dried Liquid Drops. *Nature* **1997**, *389* (6653), 827–829. <https://doi.org/10.1038/39827>.
- (209) Kim, D.; Jeong, S.; Park, B. K.; Moon, J. Direct Writing of Silver Conductive Patterns: Improvement of Film Morphology and Conductance by Controlling Solvent Compositions. *Appl. Phys. Lett.* **2006**, *89* (26), 264101. <https://doi.org/10.1063/1.2424671>.
- (210) Hu, H.; Larson, R. G. Marangoni Effect Reverses Coffee-Ring Depositions. *J. Phys. Chem. B* **2006**, *110* (14), 7090–7094. <https://doi.org/10.1021/jp0609232>.
- (211) de Gans, B.-J.; Schubert, U. S. Inkjet Printing of Well-Defined Polymer Dots and Arrays. *Langmuir* **2004**, *20* (18), 7789–7793. <https://doi.org/10.1021/la049469o>.
- (212) Sliz, R.; Lejay, M.; Fan, J. Z.; Choi, M.-J.; Kinge, S.; Hoogland, S.; Fabritius, T.; García de Arquer, F. P.; Sargent, E. H. Stable Colloidal Quantum Dot Inks Enable Inkjet-Printed High-Sensitivity Infrared Photodetectors. *ACS Nano* **2019**, *13* (10), 11988–11995. <https://doi.org/10.1021/acsnano.9b06125>.
- (213) Salonikidou, B.; Yasunori, T.; Le Borgne, B.; England, J.; Shizuo, T.; Sporea, R. A. Toward Fully Printed Memristive Elements: A-TiO₂ Electronic Synapse from Functionalized Nanoparticle Ink. *ACS Appl. Electron. Mater.* **2019**, *1* (12), 2692–2700. <https://doi.org/10.1021/acsaelm.9b00701>.
- (214) Han, G. D.; Bae, K.; Kang, E. H.; Choi, H. J.; Shim, J. H. Inkjet Printing for Manufacturing Solid Oxide Fuel Cells. *ACS Energy Lett.* **2020**, *5* (5), 1586–1592. <https://doi.org/10.1021/acsenerylett.0c00721>.
- (215) Kang, T.-H.; Lee, S.-W.; Hwang, K.; Shim, W.; Lee, K.-Y.; Lim, J.-A.; Yu, W.-R.; Choi, I.-S.; Yi, H. All-Inkjet-Printed Flexible Nanobio-Devices with Efficient Electrochemical Coupling Using Amphiphilic Biomaterials. *ACS Appl. Mater. Interfaces* **2020**, *12* (21), 24231–24241. <https://doi.org/10.1021/acсами.0c02596>.
- (216) Kuang, M.; Wu, L.; Huang, Z.; Wang, J.; Zhang, X.; Song, Y. Inkjet Printing of a Micro/Nanopatterned Surface to Serve as Microreactor Arrays. *ACS Appl. Mater. Interfaces* **2020**, *12* (27), 30962–30971. <https://doi.org/10.1021/acсами.0c07066>.
- (217) Zhu, Z.; Zhang, J.; Guo, D.; Ning, H.; Zhou, S.; Liang, Z.; Yao, R.; Wang, Y.; Lu, X.; Peng, J. Functional Metal Oxide Ink Systems for Drop-on-Demand Printed Thin-Film Transistors. *Langmuir* **2020**, *36* (30), 8655–8667. <https://doi.org/10.1021/acs.langmuir.0c00835>.

- (218) Fromm, J. E. Numerical Calculation of the Fluid Dynamics of Drop-on-Demand Jets. *IBM Journal of Research and Development* **1984**, 28 (3), 322–333. <https://doi.org/10.1147/rd.283.0322>.
- (219) Wilts, E. M.; Ma, D.; Bai, Y.; Williams, C. B.; Long, T. E. Comparison of Linear and 4-Arm Star Poly(Vinyl Pyrrolidone) for Aqueous Binder Jetting Additive Manufacturing of Personalized Dosage Tablets. *ACS Appl. Mater. Interfaces* **2019**, 11 (27), 23938–23947. <https://doi.org/10.1021/acsami.9b08116>.
- (220) Cook, B.; Gong, M.; Ewing, D.; Casper, M.; Stramel, A.; Elliot, A.; Wu, J. Inkjet Printing Multicolor Pixelated Quantum Dots on Graphene for Broadband Photodetection. *ACS Appl. Nano Mater.* **2019**, 2 (5), 3246–3252. <https://doi.org/10.1021/acsanm.9b00539>.
- (221) Jang, D.; Kim, D.; Moon, J. Influence of Fluid Physical Properties on Ink-Jet Printability. *Langmuir* **2009**, 25 (5), 2629–2635. <https://doi.org/10.1021/la900059m>.
- (222) Liu, Y.; Derby, B. Experimental Study of the Parameters for Stable Drop-on-Demand Inkjet Performance. *Physics of Fluids* **2019**, 31 (3), 032004. <https://doi.org/10.1063/1.5085868>.
- (223) Manjakkal, L.; Dervin, S.; Dahiya, R. Flexible Potentiometric PH Sensors for Wearable Systems. *RSC Adv.* **2020**, 10 (15), 8594–8617. <https://doi.org/10.1039/D0RA00016G>.
- (224) Bandodkar, A. J.; Jeerapan, I.; Wang, J. Wearable Chemical Sensors: Present Challenges and Future Prospects. *ACS Sens.* **2016**, 1 (5), 464–482. <https://doi.org/10.1021/acssensors.6b00250>.
- (225) Jin, W.; Wu, L.; Song, Y.; Jiang, J.; Zhu, X.; Yang, D.; Bai, C. Continuous Intra-Arterial Blood PH Monitoring by a Fiber-Optic Fluorosensor. *IEEE Transactions on Biomedical Engineering* **2011**, 58 (5), 1232–1238. <https://doi.org/10.1109/TBME.2011.2107514>.
- (226) Chaisiwamongkhol, K.; Batchelor-McAuley, C.; Compton, R. G. Optimising Amperometric PH Sensing in Blood Samples: An Iridium Oxide Electrode for Blood PH Sensing. *Analyst* **2019**, 144 (4), 1386–1393. <https://doi.org/10.1039/C8AN02238K>.
- (227) Dang, W.; Manjakkal, L.; Navaraj, W. T.; Lorenzelli, L.; Vinciguerra, V.; Dahiya, R. Stretchable Wireless System for Sweat PH Monitoring. *Biosensors and Bioelectronics* **2018**, 107, 192–202. <https://doi.org/10.1016/j.bios.2018.02.025>.
- (228) Nakata, S.; Shiomi, M.; Fujita, Y.; Arie, T.; Akita, S.; Takei, K. A Wearable PH Sensor with High Sensitivity Based on a Flexible Charge-Coupled Device. *Nature Electronics* **2018**, 1 (11), 596–603. <https://doi.org/10.1038/s41928-018-0162-5>.
- (229) Zhao, P.; Tang, Z.; Chen, X.; He, Z.; He, X.; Zhang, M.; Liu, Y.; Ren, D.; Zhao, K.; Bu, W. Ferrous-Cysteine-Phosphotungstate Nanoagent with Neutral PH Fenton Reaction Activity for Enhanced Cancer Chemodynamic Therapy. *Mater. Horiz.* **2019**, 6 (2), 369–374. <https://doi.org/10.1039/C8MH01176A>.

- (230) Ray, T. R.; Choi, J.; Bhandodkar, A. J.; Krishnan, S.; Gutruf, P.; Tian, L.; Ghaffari, R.; Rogers, J. A. Bio-Integrated Wearable Systems: A Comprehensive Review. *Chem. Rev.* **2019**, *119* (8), 5461–5533. <https://doi.org/10.1021/acs.chemrev.8b00573>.
- (231) Manjakkal, L.; Szwagierczak, D.; Dahiya, R. Metal Oxides Based Electrochemical PH Sensors: Current Progress and Future Perspectives. *Progress in Materials Science* **2019**, 100635. <https://doi.org/10.1016/j.pmatsci.2019.100635>.
- (232) Yuqing, M.; Jianrong, C.; Keming, F. New Technology for the Detection of PH. *Journal of Biochemical and Biophysical Methods* **2005**, *63* (1), 1–9. <https://doi.org/10.1016/j.jbbm.2005.02.001>.
- (233) Manjakkal, L.; Zaraska, K.; Cvejic, K.; Kulawik, J.; Szwagierczak, D. Potentiometric RuO₂-Ta₂O₅ PH Sensors Fabricated Using Thick Film and LTCC Technologies. *Talanta* **2016**, *147*, 233–240. <https://doi.org/10.1016/j.talanta.2015.09.069>.
- (234) Stojanović, G.; Kojić, T.; Radovanović, M.; Vasiljević, D.; Panić, S.; Srdić, V.; Cvejić, J. Flexible Sensors Based on Two Conductive Electrodes and MWCNTs Coating for Efficient PH Value Measurement. *Journal of Alloys and Compounds* **2019**, *794*, 76–83. <https://doi.org/10.1016/j.jallcom.2019.04.243>.
- (235) Manjakkal, L.; Cvejic, K.; Kulawik, J.; Zaraska, K.; Socha, R. P.; Szwagierczak, D. X-Ray Photoelectron Spectroscopic and Electrochemical Impedance Spectroscopic Analysis of RuO₂-Ta₂O₅ Thick Film PH Sensors. *Analytica Chimica Acta* **2016**, *931*, 47–56. <https://doi.org/10.1016/j.aca.2016.05.012>.
- (236) Manjakkal, L.; Djurdjic, E.; Cvejic, K.; Kulawik, J.; Zaraska, K.; Szwagierczak, D. Electrochemical Impedance Spectroscopic Analysis of RuO₂ Based Thick Film PH Sensors. *Electrochimica Acta* **2015**, *168*, 246–255. <https://doi.org/10.1016/j.electacta.2015.04.048>.
- (237) Arshak, K.; Gill, E.; Arshak, A.; Korostynska, O. Investigation of Tin Oxides as Sensing Layers in Conductimetric Interdigitated PH Sensors. *Sensors and Actuators B: Chemical* **2007**, *127* (1), 42–53. <https://doi.org/10.1016/j.snb.2007.07.014>.
- (238) Sinha, S.; Mukhiya, R.; Sharma, R.; Khanna, P. K.; Khanna, V. K. Fabrication, Characterization and Electrochemical Simulation of AlN-Gate ISFET PH Sensor. *J Mater Sci: Mater Electron* **2019**, *30* (7), 7163–7174. <https://doi.org/10.1007/s10854-019-01033-5>.
- (239) Hsu, W.-E.; Chang, Y.-H.; Huang, Y.-J.; Huang, J.-C.; Lin, C.-T. A PH/Light Dual-Modal Sensing ISFET Assisted by Artificial Neural Networks. *ECS Trans.* **2019**, *89* (6), 31. <https://doi.org/10.1149/08906.0031ecst>.
- (240) Parizi, K. B.; Xu, X.; Pal, A.; Hu, X.; Wong, H. S. P. ISFET PH Sensitivity: Counter-Ions Play a Key Role. *Sci Rep* **2017**, *7* (1), 41305. <https://doi.org/10.1038/srep41305>.

- (241) Qin, Y.; Kwon, H.-J.; Howlader, M. M. R.; Deen, M. J. Microfabricated Electrochemical PH and Free Chlorine Sensors for Water Quality Monitoring: Recent Advances and Research Challenges. *RSC Adv.* **2015**, *5* (85), 69086–69109. <https://doi.org/10.1039/C5RA11291E>.
- (242) Määttänen, A.; Vanamo, U.; Ihalainen, P.; Pulkkinen, P.; Tenhu, H.; Bobacka, J.; Peltonen, J. A Low-Cost Paper-Based Inkjet-Printed Platform for Electrochemical Analyses. *Sensors and Actuators B: Chemical* **2013**, *177*, 153–162. <https://doi.org/10.1016/j.snb.2012.10.113>.
- (243) Kamyshny, A.; Magdassi, S. Aqueous Dispersions of Metallic Nanoparticles: Preparation, Stabilization and Application. *Nanoscience: Colloidal and Interfacial Aspects* **2010**, 747–778.
- (244) Cummins, G.; Desmulliez, M. P. Inkjet Printing of Conductive Materials: A Review. *Circuit World* **2012**, *38* (4), 193–213.
- (245) Lesch, A. Print-Light-Synthesis of Platinum Nanostructured Indium-Tin-Oxide Electrodes for Energy Research. *Advanced Materials Technologies* **2017**.
- (246) Özkan, M.; Hashmi, S. G.; Halme, J.; Karakoç, A.; Sarikka, T.; Paltakari, J.; Lund, P. D. Inkjet-Printed Platinum Counter Electrodes for Dye-Sensitized Solar Cells. *Organic Electronics* **2017**, *44*, 159–167.
- (247) Chatziiona, V. K.; Constantinou, B. K.; Savva, P. G.; Olympiou, G. G.; Kapnisis, K.; Anayiotos, A.; Costa, C. N. Regulating the Catalytic Properties of Pt/Al₂O₃ through Nanoscale Inkjet Printing. *Catalysis Communications* **2018**, *103*, 69–73.
- (248) Wang, M.; Yao, S.; Madou, M. A Long-Term Stable Iridium Oxide PH Electrode. *Sensors and Actuators B: Chemical* **2002**, *81* (2), 313–315.
- (249) Lu, Y.; Wang, T.; Cai, Z.; Cao, Y.; Yang, H.; Duan, Y. Y. Anodically Electrodeposited Iridium Oxide Films Microelectrodes for Neural Microstimulation and Recording. *Sensors and Actuators B: Chemical* **2009**, *137* (1), 334–339.
- (250) Kim, T. Y.; Yang, S. Fabrication Method and Characterization of Electrodeposited and Heat-Treated Iridium Oxide Films for PH Sensing. *Sensors and Actuators B: Chemical* **2014**, *196*, 31–38.
- (251) Yao, S.; Wang, M.; Madou, M. A PH Electrode Based on Melt-Oxidized Iridium Oxide. *Journal of the electrochemical society* **2001**, *148* (4), H29–H36.
- (252) Tarlov, M. J.; Semancik, S.; Kreider, K. G. Mechanistic and Response Studies of Iridium Oxide PH Sensors. *Sensors and Actuators B: Chemical* **1990**, *1* (1), 293–297.

- (253) Ardizzone, S.; Carugati, A.; Trasatti, S. Properties of Thermally Prepared Iridium Dioxide Electrodes. *Journal of Electroanalytical Chemistry and Interfacial Electrochemistry* **1981**, *126* (1), 287–292.
- (254) Casella, I. G.; Contursi, M.; Toniolo, R. Anodic Electrodeposition of Iridium Oxide Particles on Glassy Carbon Surfaces and Their Electrochemical/SEM/XPS Characterization. *Journal of Electroanalytical Chemistry* **2015**, *736*, 147–152.
- (255) Baur, J. E.; Spaine, T. W. Electrochemical Deposition of Iridium (IV) Oxide from Alkaline Solutions of Iridium(III) Oxide. *Journal of Electroanalytical Chemistry* **1998**, *443* (2), 208–216.
- (256) Bezbaruah, A. N.; Zhang, T. C. Fabrication of Anodically Electrodeposited Iridium Oxide Film PH Microelectrodes for Microenvironmental Studies. *Anal. Chem.* **2002**, *74* (22), 5726–5733. <https://doi.org/10.1021/ac020326l>.
- (257) Olthuis, W.; Robben, M. A. M.; Bergveld, P.; Bos, M.; Linden, W. E. van der. PH Sensor Properties of Electrochemically Grown Iridium Oxide. *Sensors and Actuators B: Chemical* **1990**, *2* (4), 247–256.
- (258) Jin, X.; Lu, J.; Liu, P.; Tong, H. The Electrochemical Formation and Reduction of a Thick AgCl Deposition Layer on a Silver Substrate. *Journal of Electroanalytical Chemistry* **2003**, *542*, 85–96. [https://doi.org/10.1016/S0022-0728\(02\)01474-2](https://doi.org/10.1016/S0022-0728(02)01474-2).
- (259) Yamanaka, K. The Electrochemical Behavior of Anodically Electrodeposited Iridium Oxide Films and the Reliability of Transmittance Variable Cells. *Japanese journal of applied physics* **1991**, *30* (6R), 1285.
- (260) Prats-Alfonso, E.; Abad, L.; Casañ-Pastor, N.; Gonzalo-Ruiz, J.; Baldrich, E. Iridium Oxide PH Sensor for Biomedical Applications. Case Urea–Urease in Real Urine Samples. *Biosensors and Bioelectronics* **2013**, *39* (1), 163–169.
- (261) Zhou, B.; Bian, C.; Tong, J.; Xia, S. Fabrication of a Miniature Multi-Parameter Sensor Chip for Water Quality Assessment. *Sensors* **2017**, *17* (1), 157.
- (262) Cruz, A. M.; Abad, L.; Carretero, N. M.; Moral-Vico, J.; Fraxedas, J.; Lozano, P.; Subías, G.; Padial, V.; Carballo, M.; Collazos-Castro, J. E.; Casañ-Pastor, N. Iridium Oxohydroxide, a Significant Member in the Family of Iridium Oxides. Stoichiometry, Characterization, and Implications in Bioelectrodes. *The Journal of Physical Chemistry C* **2012**, *116* (8), 5155–5168.
- (263) Jurk, R.; Mosch, S.; Fritsch, M.; Ihle, M. Synthesis of Nano Metal Particles for Low Sintering Conductive Inks. *DDMC* **2014**.
- (264) Soltman, D.; Subramanian, V. Inkjet-Printed Line Morphologies and Temperature Control of the Coffee Ring Effect. *Langmuir* **2008**, *24* (5), 2224–2231.

- (265) Van der Pauw, L. A Method of Measuring Specific Resistivity and Hall Effect of Discs of Arbitrary Shape. *Philips Res. Rep* **1958**, *13*, 1–9.
- (266) Gabriel, G.; Erill, I.; Caro, J.; Gómez, R.; Riera, D.; Villa, R.; Godignon, P. Manufacturing and Full Characterization of Silicon Carbide-Based Multi-Sensor Micro-Probes for Biomedical Applications. *Microelectronics Journal* **2007**, *38* (3), 406–415.
- (267) Cogan, S. F. Neural Stimulation and Recording Electrodes. *Annual Review of Biomedical Engineering* **2008**, *10* (1), 275–309.
- (268) Burke, L. D.; Whelan, D. P. A Voltammetric Investigation of the Charge Storage Reactions of Hydrrous Iridium Oxide Layers. *Journal of Electroanalytical Chemistry and Interfacial Electrochemistry* **1984**, *162* (1), 121–141.
- (269) Steegstra, P.; Ahlberg, E. Influence of Oxidation State on the PH Dependence of Hydrrous Iridium Oxide Films. *Electrochimica Acta* **2012**, *76*, 26–33.
- (270) McLauchlan, G.; Rawlings, J.; Lucas, M.; McCloy, R.; Crean, G.; McColl, K. Electrodes for 24 Hours PH Monitoring—a Comparative Study. *Gut* **1987**, *28* (8), 935–939.
- (271) Ges, I. A.; Ivanov, B. L.; Schaffer, D. K.; Lima, E. A.; Werdich, A. A.; Baudenbacher, F. J. Thin-Film IrO_x PH Microelectrode for Microfluidic-Based Microsystems. *Biosensors and Bioelectronics* **2005**, *21* (2), 248–256.
- (272) Pasztor, K.; Sekiguchi, A.; Shimo, N.; Kitamura, N.; Masuhara, H. Iridium Oxide-Based Microelectrochemical Transistors for PH Sensing. *Sensors and Actuators B: Chemical* **1993**, *12* (3), 225–230.
- (273) Marzouk, S. A. M.; Ufer, S.; Buck, R. P.; Johnson, T. A.; Dunlap, L. A.; Cascio, W. E. Electrodeposited Iridium Oxide PH Electrode for Measurement of Extracellular Myocardial Acidosis during Acute Ischemia. *Analytical Chemistry* **1998**, *70* (23), 5054–5061.
- (274) Guinovart, T.; Crespo, G. A.; Rius, F. X.; Andrade, F. J. A Reference Electrode Based on Polyvinyl Butyral (PVB) Polymer for Decentralized Chemical Measurements. *Analytica Chimica Acta* **2014**, *821*, 72–80. <https://doi.org/10.1016/j.aca.2014.02.028>.
- (275) Huang, W.-D.; Cao, H.; Deb, S.; Chiao, M.; Chiao, J.-C. A Flexible PH Sensor Based on the Iridium Oxide Sensing Film. *Sensors and Actuators A: Physical* **2011**, *169* (1), 1–11.
- (276) Liao, Y.-H.; Chou, J.-C. Preparation and Characteristics of Ruthenium Dioxide for PH Array Sensors with Real-Time Measurement System. *Sensors and Actuators B: Chemical* **2008**, *128* (2), 603–612.
- (277) Meyer, R. D.; Cogan, S. F.; Nguyen, T. H.; Rauh, R. D. Electrodeposited Iridium Oxide for Neural Stimulation and Recording Electrodes. *IEEE Transactions on Neural Systems and Rehabilitation Engineering* **2001**, *9* (1), 2–11.

- (278) Marzouk, S. A. M. Improved Electrodeposited Iridium Oxide PH Sensor Fabricated on Etched Titanium Substrates. *Analytical Chemistry* **2003**, *75* (6), 1258–1266.
- (279) Boehler, C.; Oberueber, F.; Schlabach, S.; Stieglitz, T.; Asplund, M. Long-Term Stable Adhesion for Conducting Polymers in Biomedical Applications: IrO_x and Nanostructured Platinum Solve the Chronic Challenge. *ACS Appl. Mater. Interfaces* **2017**, *9* (1), 189–197. <https://doi.org/10.1021/acsami.6b13468>.
- (280) Green, R. A.; Hassarati, R. T.; Bouchinet, L.; Lee, C. S.; Cheong, G. L. M.; Yu, J. F.; Dodds, C. W.; Suaning, G. J.; Poole-Warren, L. A.; Lovell, N. H. Substrate Dependent Stability of Conducting Polymer Coatings on Medical Electrodes. *Biomaterials* **2012**, *33* (25), 5875–5886.
- (281) Bobacka, J.; Ivaska, A.; Lewenstam, A. Potentiometric Ion Sensors. *Chemical Reviews* **2008**, *108* (2), 329–351.
- (282) Roy, S.; David-Pur, M.; Hanein, Y. Carbon Nanotube-Based Ion Selective Sensors for Wearable Applications. *ACS Applied Materials & Interfaces* **2017**, *9* (40), 35169–35177.
- (283) Cui, X.; Martin, D. C. Fuzzy Gold Electrodes for Lowering Impedance and Improving Adhesion with Electrodeposited Conducting Polymer Films. *Sensors and Actuators A: Physical* **2003**, *103* (3), 384–394.
- (284) Gabriel, G.; Gomez, R.; Bongard, M.; Benito, N.; Fernandez, E.; Villa, R. Easily Made Single-Walled Carbon Nanotube Surface Microelectrodes for Neuronal Applications. *Biosensors and Bioelectronics* **2009**.
- (285) Flexible Electronics Market Size Growth | Industry Forecast Report 2024 <https://www.grandviewresearch.com/industry-analysis/flexible-electronics-market/toc> (accessed 2020 -06 -04).
- (286) Yin, Z.; Huang, Y.; Bu, N.; Wang, X.; Xiong, Y. Inkjet Printing for Flexible Electronics: Materials, Processes and Equipments. *Chin. Sci. Bull.* **2010**, *55* (30), 3383–3407. <https://doi.org/10.1007/s11434-010-3251-y>.
- (287) Sui, Y.; Zorman, C. A. Review—Inkjet Printing of Metal Structures for Electrochemical Sensor Applications. *J. Electrochem. Soc.* **2020**, *167* (3), 037571. <https://doi.org/10.1149/1945-7111/ab721f>.
- (288) Sundriyal, P.; Bhattacharya, S. Inkjet-Printed Sensors on Flexible Substrates. In *Environmental, Chemical and Medical Sensors*; Bhattacharya, S., Agarwal, A. K., Chanda, N., Pandey, A., Sen, A. K., Eds.; Energy, Environment, and Sustainability; Springer: Singapore, 2018; pp 89–113. https://doi.org/10.1007/978-981-10-7751-7_5.

- (289) Zea, M.; Moya, A.; Fritsch, M.; Ramon, E.; Villa, R.; Gabriel, G. Enhanced Performance Stability of Iridium Oxide Based PH Sensors Fabricated on Rough Inkjet-Printed Platinum. *ACS Applied Materials & Interfaces* **2019**. <https://doi.org/10.1021/acsami.9b03085>.
- (290) Alam, A. U.; Qin, Y.; Nambiar, S.; Yeow, J. T. W.; Howlader, M. M. R.; Hu, N. X.; Deen, M. J. Polymers and Organic Materials-Based PH Sensors for Healthcare Applications. *Progress in Materials Science* **2018**, *96* (March), 174–216. <https://doi.org/10.1016/j.pmatsci.2018.03.008>.
- (291) Korostynska, O.; Arshak, K.; Gill, E.; Arshak, A. Review on State-of-the-Art in Polymer Based PH Sensors. *Sensors* **2007**, *7* (12), 3027–3042.
- (292) Binag, C. A.; Bartolome, A. J.; Tongol, B.; Santiago, K. S. Electronically Synthesized Polymer-Based PH Sensors. *Philippine Journal of Science* **1999**, *128* (3), 247–252.
- (293) Kocak, G.; Tuncer, C.; Bütün, V. PH-Responsive Polymers. *Polym. Chem.* **2016**, *8* (1), 144–176. <https://doi.org/10.1039/C6PY01872F>.
- (294) Fanzio, P.; Chang, C.-T.; Skolimowski, M.; Tanzi, S.; Sasso, L. Fully-Polymeric PH Sensor Realized by Means of a Single-Step Soft Embossing Technique. *Sensors* **2017**, *17* (5), 1169. <https://doi.org/10.3390/s17051169>.
- (295) Guinovart, T.; Valdés-Ramírez, G.; Windmiller, J. R.; Andrade, F. J.; Wang, J. Bandage-Based Wearable Potentiometric Sensor for Monitoring Wound PH. *Electroanalysis* **2014**, *26* (6), 1345–1353. <https://doi.org/10.1002/elan.201300558>.
- (296) Zea, M.; Moya, A.; Abrao-Nemeir, I.; Gallardo-Gonzalez, J.; Zine, N.; Errachid, A.; Villa, R.; Gabriel, G. All Inkjet Printing Sensor Device on Paper: For Immunosensors Applications. In *2019 20th International Conference on Solid-State Sensors, Actuators and Microsystems Eurosensors XXXIII (TRANSDUCERS EUROSENSORS XXXIII)*; 2019; pp 2472–2475. <https://doi.org/10.1109/TRANSDUCERS.2019.8808473>.
- (297) Park, Y. R.; Doh, J. H.; Shin, K.; Seo, Y. S.; Kim, Y. S.; Kim, S. Y.; Choi, W. K.; Hong, Y. J. Solution-Processed Quantum Dot Light-Emitting Diodes with PANI:PSS Hole-Transport Interlayers. *Organic Electronics* **2015**, *19*, 131–139. <https://doi.org/10.1016/j.orgel.2014.12.030>.
- (298) Han, H.; Lee, J. S.; Cho, S. Comparative Studies on Two-Electrode Symmetric Supercapacitors Based on Polypyrrole: Poly(4-Styrenesulfonate) with Different Molecular Weights of Poly(4-Styrenesulfonate). *Polymers* **2019**, *11* (2), 3–6. <https://doi.org/10.3390/polym11020232>.
- (299) Texidó, R.; Borrós, S. Allylamine PECVD Modification of PDMS as Simple Method to Obtain Conductive Flexible Polypyrrole Thin Films. *Polymers* **2019**, *11* (12), 2108. <https://doi.org/10.3390/POLYM11122108>.

- (300) Texidó, R.; Orgaz, A.; Ramos, V.; Borrós, S. Stretchable Conductive Polypyrrole Films Modified with Dopaminated Hyaluronic Acid. *Materials Science and Engineering: C* **2017**. <https://doi.org/10.1016/j.msec.2017.03.072>.
- (301) Nardes, A. M.; Kemerink, M.; Janssen, R. A. J.; Bastiaansen, J. A. M.; Kiggen, N. M. M.; Langeveld, B. M. W.; Van Breemen, A. J. J. M.; De Kok, M. M. Microscopic Understanding of the Anisotropic Conductivity of PEDOT:PSS Thin Films. *Advanced Materials* **2007**, *19* (9), 1196–1200. <https://doi.org/10.1002/adma.200602575>.
- (302) Lang, U.; Muller, E.; Naujoks, N.; Dual, J. Microscopical Investigations of PEDOT:PSS Thin Films. *Advanced Functional Materials* **2009**, *19* (8), 1215–1220. <https://doi.org/10.1002/adfm.200801258>.
- (303) Yan, W.; Han, J. Synthesis and Formation Mechanism Study of Rectangular-Sectioned Polypyrrole Micro/Nanotubules. *Polymer* **2007**, *48* (23), 6782–6790. <https://doi.org/10.1016/j.polymer.2007.09.026>.
- (304) Zhang, J.; Gao, L.; Sun, J.; Liu, Y.; Wang, Y.; Wang, J. Incorporation of Single-Walled Carbon Nanotubes with PEDOT/PSS in DMSO for the Production of Transparent Conducting Films. *Diamond and Related Materials* **2012**, *22*, 82–87. <https://doi.org/10.1016/j.diamond.2011.12.008>.
- (305) Eom, S. H.; Senthilarasu, S.; Uthirakumar, P.; Yoon, S. C.; Lim, J.; Lee, C.; Lim, H. S.; Lee, J.; Lee, S. H. Polymer Solar Cells Based on Inkjet-Printed PEDOT:PSS Layer. *Organic Electronics* **2009**, *10* (3), 536–542. <https://doi.org/10.1016/j.orgel.2009.01.015>.
- (306) Savagatrup, S.; Chan, E.; Renteria-Garcia, S. M.; Printz, A. D.; Zaretski, A. V.; O'Connor, T. F.; Rodriguez, D.; Valle, E.; Lipomi, D. J. Plasticization of PEDOT:PSS by Common Additives for Mechanically Robust Organic Solar Cells and Wearable Sensors. *Advanced Functional Materials* **2015**, *25* (3), 427–436. <https://doi.org/10.1002/adfm.201401758>.
- (307) Latonen, R. M.; Määttä, A.; Ihalainen, P.; Xu, W.; Pesonen, M.; Nurmi, M.; Xu, C. Conducting Ink Based on Cellulose Nanocrystals and Polyaniline for Flexographical Printing. *Journal of Materials Chemistry C* **2017**, *5* (46), 12172–12181. <https://doi.org/10.1039/c7tc03729e>.
- (308) Ghamouss, F.; Brugère, A.; Anbalagan, A. C.; Schmaltz, B.; Luais, E.; Tran-Van, F. Novel Glycerol Assisted Synthesis of Polypyrrole Nanospheres and Its Electrochemical Properties. *Synthetic Metals* **2013**, *168* (1), 9–15. <https://doi.org/10.1016/j.synthmet.2013.02.005>.
- (309) Lee, M. W.; Lee, M. Y.; Choi, J. C.; Park, J. S.; Song, C. K. Fine Patterning of Glycerol-Doped PEDOT:PSS on Hydrophobic PVP Dielectric with Ink Jet for Source and Drain Electrode of OTFTs. *Organic Electronics* **2010**, *11* (5), 854–859. <https://doi.org/10.1016/j.orgel.2010.01.028>.

- (310) Oh, Y.; Kim, J.; Yoon, Y. J.; Kim, H.; Yoon, H. G.; Lee, S.-N.; Kim, J. Inkjet Printing of Al₂O₃ Dots, Lines, and Films: From Uniform Dots to Uniform Films. *Current Applied Physics* **2011**, *11* (3), S359–S363.
- (311) Lopez Aldaba, A.; González-Vila, Á.; Debliquy, M.; Lopez-Amo, M.; Caucheteur, C.; Lahem, D. Polyaniline-Coated Tilted Fiber Bragg Gratings for PH Sensing. *Sensors and Actuators B: Chemical* **2018**, *254*, 1087–1093. <https://doi.org/10.1016/j.snb.2017.07.167>.
- (312) Rahimi, R.; Ochoa, M.; Parupudi, T.; Zhao, X.; Yazdi, I. K.; Dokmeci, M. R.; Tamayol, A.; Khademhosseini, A.; Ziaie, B. A Low-Cost Flexible PH Sensor Array for Wound Assessment. *Sensors and Actuators B: Chemical* **2016**, *229*, 609–617. <https://doi.org/10.1016/j.snb.2015.12.082>.
- (313) Lindfors, T.; Ivaska, A. PH Sensitivity of Polyaniline and Its Substituted Derivatives. *Journal of Electroanalytical Chemistry* **2002**, *531* (1), 43–52. [https://doi.org/10.1016/S0022-0728\(02\)01005-7](https://doi.org/10.1016/S0022-0728(02)01005-7).
- (314) Lakard, B.; Segut, O.; Lakard, S.; Herlem, G.; Gharbi, T. Potentiometric Miniaturized PH Sensors Based on Polypyrrole Films. *Sensors and Actuators B: Chemical* **2007**, *122* (1), 101–108. <https://doi.org/10.1016/j.snb.2006.04.112>.
- (315) Gao, W.; Song, J. Polyaniline Film Based Amperometric PH Sensor Using a Novel Electrochemical Measurement System. *Electroanalysis* **2009**, *21* (8), 973–978. <https://doi.org/10.1002/elan.200804500>.
- (316) Lakard, B.; Segut, O.; Lakard, S.; Herlem, G.; Gharbi, T. Potentiometric Miniaturized PH Sensors Based on Polypyrrole Films. *Sensors and Actuators, B: Chemical* **2007**, *122* (1), 101–108. <https://doi.org/10.1016/j.snb.2006.04.112>.
- (317) Lindfors, T.; Ivaska, A. PH Sensitivity of Polyaniline and Its Substituted Derivatives. *Journal of Electroanalytical Chemistry* **2002**, *531* (1), 43–52. [https://doi.org/10.1016/S0022-0728\(02\)01005-7](https://doi.org/10.1016/S0022-0728(02)01005-7).
- (318) Lakard, B.; Segut, O.; Lakard, S.; Herlem, G.; Gharbi, T. Potentiometric Miniaturized PH Sensors Based on Polypyrrole Films. *Sensors and Actuators, B: Chemical* **2007**, *122* (1), 101–108. <https://doi.org/10.1016/j.snb.2006.04.112>.
- (319) Masalles, C.; Borrós, S.; Viñas, C.; Teixidor, F. Simple PVC-PPy Electrode for PH Measurement and Titrations. *Analytical and Bioanalytical Chemistry* **2002**, *372*, 513–518. <https://doi.org/10.1007/s00216-001-1221-7>.
- (320) Dang, W.; Manjakkal, L.; Navaraj, W. T.; Lorenzelli, L.; Vinciguerra, V.; Dahiya, R. Stretchable Wireless System for Sweat PH Monitoring. *Biosensors and Bioelectronics* **2018**, *107*, 192–202. <https://doi.org/10.1016/j.bios.2018.02.025>.

- (321) Minari, T.; Kanehara, Y.; Liu, C.; Sakamoto, K.; Yasuda, T.; Yaguchi, A.; Tsukada, S.; Kashizaki, K.; Kanehara, M. Room-Temperature Printing of Organic Thin-Film Transistors with π -Junction Gold Nanoparticles. *Advanced Functional Materials* **2014**, *24* (31), 4886–4892. <https://doi.org/10.1002/adfm.201400169>.
- (322) Radhakrishnan, S.; Deshpande, S. D. Electrical Properties of Conducting Polypyrrole Films Functionalized with Phthalocyanine. *Materials Letters* **2001**, *48* (3–4), 144–150. [https://doi.org/10.1016/S0167-577X\(00\)00294-9](https://doi.org/10.1016/S0167-577X(00)00294-9).
- (323) Panwar, V.; Kumar, P.; Ray, S. S.; Jain, S. L. Organic Inorganic Hybrid Cobalt Phthalocyanine/Polyaniline as Efficient Catalyst for Aerobic Oxidation of Alcohols in Liquid Phase. *Tetrahedron Letters* **2015**, *56* (25), 3948–3953. <https://doi.org/10.1016/j.tetlet.2015.05.003>.
- (324) Prissanaroon-Ouajai, W.; Pigram, P. J.; Jones, R.; Sirivat, A. A Sensitive and Highly Stable Polypyrrole-Based PH Sensor with Hydroquinone Monosulfonate and Oxalate Co-Doping. *Sensors and Actuators B: Chemical* **2009**, *138* (2), 504–511. <https://doi.org/10.1016/j.snb.2009.01.037>.
- (325) Park, H. J.; Yoon, J. H.; Lee, K. G.; Choi, B. G. Potentiometric Performance of Flexible PH Sensor Based on Polyaniline Nanofiber Arrays. *Nano Convergence* **2019**, *6* (1), 9. <https://doi.org/10.1186/s40580-019-0179-0>.
- (326) Yoon, J. H.; Hong, S. B.; Yun, S.-O.; Lee, S. J.; Lee, T. J.; Lee, K. G.; Choi, B. G. High Performance Flexible PH Sensor Based on Polyaniline Nanopillar Array Electrode. *Journal of Colloid and Interface Science* **2017**, *490*, 53–58. <https://doi.org/10.1016/j.jcis.2016.11.033>.
- (327) Ferrer-Anglada, N.; Kaempgen, M.; Roth, S. Transparent and Flexible Carbon Nanotube/Polypyrrole and Carbon Nanotube/Polyaniline PH Sensors. *physica status solidi (b)* **2006**, *243* (13), 3519–3523. <https://doi.org/10.1002/pssb.200669220>.
- (328) Rahimi, R.; Ochoa, M.; Yu, W.; Ziaie, B. A Highly Stretchable PH Sensor Array Using Elastomer-Embedded Laser Carbonized Patterns. In *2015 Transducers - 2015 18th International Conference on Solid-State Sensors, Actuators and Microsystems (TRANSDUCERS)*; 2015; pp 1897–1900. <https://doi.org/10.1109/TRANSDUCERS.2015.7181321>.
- (329) Punjiya, M.; Rezaei, H.; Zeeshan, M. A.; Sonkusale, S. A Flexible PH Sensing Smart Bandage with Wireless CMOS Readout for Chronic Wound Monitoring. In *2017 19th International Conference on Solid-State Sensors, Actuators and Microsystems (TRANSDUCERS)*; 2017; pp 1700–1702. <https://doi.org/10.1109/TRANSDUCERS.2017.7994393>.

- (330) Kaempgen, M.; Roth, S. Transparent and Flexible Carbon Nanotube/Polyaniline PH Sensors. *Journal of Electroanalytical Chemistry* **2006**, *586* (1), 72–76. <https://doi.org/10.1016/j.jelechem.2005.09.009>.
- (331) Aquino-Binag, C. N.; Kumar, N.; Lamb, R. N.; Pigram, P. J. Fabrication and Characterization of a Hydroquinone-Functionalized Polypyrrole Thin-Film PH Sensor. *Chem. Mater.* **1996**, *8* (11), 2579–2585. <https://doi.org/10.1021/cm9506114>.
- (332) Bao, Q.; Yang, Z.; Song, Y.; Fan, M.; Pan, P.; Liu, J.; Liao, Z.; Wei, J. Printed Flexible Bifunctional Electrochemical Urea-PH Sensor Based on Multiwalled Carbon Nanotube/Polyaniline Electronic Ink. *J Mater Sci: Mater Electron* **2019**, *30* (2), 1751–1759. <https://doi.org/10.1007/s10854-018-0447-5>.
- (333) Wang, R.; Zhai, Q.; Zhao, Y.; An, T.; Gong, S.; Guo, Z.; Shi, Q.; Yong, Z.; Cheng, W. Stretchable Gold Fiber-Based Wearable Electrochemical Sensor toward PH Monitoring. *Journal of Materials Chemistry B* **2020**, *8* (16), 3655–3660. <https://doi.org/10.1039/C9TB02477H>.
- (334) Yu, K.; He, N.; Kumar, N.; Wang, N.; Bobacka, J.; Ivaska, A. Electrosynthesized Polypyrrole/Zeolite Composites as Solid Contact in Potassium Ion-Selective Electrode. *Electrochimica Acta* **2017**, *228*, 66–75. <https://doi.org/10.1016/j.electacta.2017.01.009>.
- (335) Hart, R. W.; Mauk, M. G.; Liu, C.; Qiu, X.; Thompson, J. A.; Chen, D.; Malamud, D.; Abrams, W. R.; Bau, H. H. Point-of-Care Oral-Based Diagnostics. *Oral Diseases* **2011**, *17* (8), 745–752. <https://doi.org/10.1111/j.1601-0825.2011.01808.x>.
- (336) Tabak, L. A. Point-of-Care Diagnostics Enter the Mouth. *Annals of the New York Academy of Sciences* **2007**, *1098* (1), 7–14. <https://doi.org/10.1196/annals.1384.043>.
- (337) Hauck, T. S.; Giri, S.; Gao, Y.; Chan, W. C. W. Nanotechnology Diagnostics for Infectious Diseases Prevalent in Developing Countries. *Advanced Drug Delivery Reviews* **2010**, *62* (4), 438–448. <https://doi.org/10.1016/j.addr.2009.11.015>.
- (338) Lee, W. G.; Kim, Y.-G.; Chung, B. G.; Demirci, U.; Khademhosseini, A. Nano/Microfluidics for Diagnosis of Infectious Diseases in Developing Countries. *Advanced Drug Delivery Reviews* **2010**, *62* (4), 449–457. <https://doi.org/10.1016/j.addr.2009.11.016>.
- (339) Wang, S.; Inci, F.; De Libero, G.; Singhal, A.; Demirci, U. Point-of-Care Assays for Tuberculosis: Role of Nanotechnology/Microfluidics. *Biotechnology Advances* **2013**, *31* (4), 438–449. <https://doi.org/10.1016/j.biotechadv.2013.01.006>.
- (340) Wang, S.; Xu, F.; Demirci, U. Advances in Developing HIV-1 Viral Load Assays for Resource-Limited Settings. *Biotechnology Advances* **2010**, *28* (6), 770–781. <https://doi.org/10.1016/j.biotechadv.2010.06.004>.

- (341) Ruiz Vega, G. One-Step Electrochemical Magneto Assays for the Development of Point-of-Care (POC) Diagnostic Devices. Ph.D. Thesis, Universitat Autònoma de Barcelona, 2019.
- (342) Vashist, S. K. Point-of-Care Diagnostics: Recent Advances and Trends. *Biosensors* **2017**, *7* (4), 62. <https://doi.org/10.3390/bios7040062>.
- (343) Gous, N.; Boeras, D. I.; Cheng, B.; Takle, J.; Cunningham, B.; Peeling, R. W. The Impact of Digital Technologies on Point-of-Care Diagnostics in Resource-Limited Settings. *Expert Review of Molecular Diagnostics* **2018**, *18* (4), 385–397. <https://doi.org/10.1080/14737159.2018.1460205>.
- (344) Wang, S.; Chinnasamy, T.; Lifson, M. A.; Inci, F.; Demirci, U. Flexible Substrate-Based Devices for Point-of-Care Diagnostics. *Trends in Biotechnology* **2016**, *34* (11), 909–921. <https://doi.org/10.1016/j.tibtech.2016.05.009>.
- (345) Zarei, M. Advances in Point-of-Care Technologies for Molecular Diagnostics. *Biosensors and Bioelectronics* **2017**, *98*, 494–506. <https://doi.org/10.1016/j.bios.2017.07.024>.
- (346) Wang, P.; Kricka, L. J. Current and Emerging Trends in Point-of-Care Technology and Strategies for Clinical Validation and Implementation. *Clinical Chemistry* **2018**, *64* (10), 1439–1452. <https://doi.org/10.1373/clinchem.2018.287052>.
- (347) Koumantakis, G.; Watkinson, L. Contribution of Industry to PoCT Implementation. *Clin Biochem Rev* **2010**, *31* (3), 89–91.
- (348) Quesada-González, D.; Merkoçi, A. Mobile Phone-Based Biosensing: An Emerging “Diagnostic and Communication” Technology. *Biosensors and Bioelectronics* **2017**, *92*, 549–562. <https://doi.org/10.1016/j.bios.2016.10.062>.
- (349) Privett, B. J.; Shin, J. H.; Schoenfisch, M. H. Electrochemical Sensors. *Anal. Chem.* **2010**, *82* (12), 4723–4741. <https://doi.org/10.1021/ac101075n>.
- (350) Lesch, A.; Jović, M.; Baudoz, M.; Zhu, Y.; Tacchini, P.; Gummy, F.; Girault, H. H. Point-of-Care Diagnostics with Inkjet-Printed Microchips. *ECS Trans.* **2017**, *77* (7), 73. <https://doi.org/10.1149/07707.0073ecst>.
- (351) Lesch, A.; Cortés-Salazar, F.; Bassetto, V. C.; Amstutz, V.; Girault, H. H. Inkjet Printing Meets Electrochemical Energy Conversion. *CHIMIA International Journal for Chemistry* **2015**, *69* (5), 284–289. <https://doi.org/10.2533/chimia.2015.284>.
- (352) Gao, M.; Li, L.; Song, Y. Inkjet Printing Wearable Electronic Devices. *J. Mater. Chem. C* **2017**, *5* (12), 2971–2993. <https://doi.org/10.1039/C7TC00038C>.
- (353) Moonen, P. F.; Yakimets, I.; Huskens, J. Fabrication of Transistors on Flexible Substrates: From Mass-Printing to High-Resolution Alternative Lithography Strategies. *Advanced Materials* **2012**, *24* (41), 5526–5541. <https://doi.org/10.1002/adma.201202949>.

- (354) Hu, B.; Li, D.; Ala, O.; Manandhar, P.; Fan, Q.; Kasilingam, D.; Calvert, P. D. Textile-Based Flexible Electroluminescent Devices. *Advanced Functional Materials* **2011**, *21* (2), 305–311. <https://doi.org/10.1002/adfm.201001110>.
- (355) Chen, P.; Chen, H.; Qiu, J.; Zhou, C. Inkjet Printing of Single-Walled Carbon Nanotube/RuO₂ Nanowire Supercapacitors on Cloth Fabrics and Flexible Substrates. *Nano Res.* **2010**, *3* (8), 594–603. <https://doi.org/10.1007/s12274-010-0020-x>.
- (356) Chauraya, A.; Whittow, W. G.; Vardaxoglou, J. Y. C.; Li, Y.; Torah, R.; Yang, K.; Beeby, S.; Tudor, J. Inkjet Printed Dipole Antennas on Textiles for Wearable Communications. *IET Microwaves, Antennas & Propagation* **2013**, *7* (9), 760–767.
- (357) Karim, N.; Afroj, S.; Malandraki, A.; Butterworth, S.; Beach, C.; Rigout, M.; S. Novoselov, K.; J. Casson, A.; G. Yeates, S. All Inkjet-Printed Graphene-Based Conductive Patterns for Wearable e-Textile Applications. *Journal of Materials Chemistry C* **2017**, *5* (44), 11640–11648. <https://doi.org/10.1039/C7TC03669H>.
- (358) Nechyporchuk, O.; Yu, J.; Nierstrasz, V. A.; Bordes, R. Cellulose Nanofibril-Based Coatings of Woven Cotton Fabrics for Improved Inkjet Printing with a Potential in E-Textile Manufacturing. *ACS Sustainable Chem. Eng.* **2017**, *5* (6), 4793–4801. <https://doi.org/10.1021/acssuschemeng.7b00200>.
- (359) Tobjörk, D.; Österbacka, R. Paper Electronics. *Advanced Materials* **2011**, *23* (17), 1935–1961. <https://doi.org/10.1002/adma.201004692>.
- (360) Grau, G.; Kitsomboonloha, R.; Swisher, S. L.; Kang, H.; Subramanian, V. Printed Transistors on Paper: Towards Smart Consumer Product Packaging. *Advanced Functional Materials* **2014**, *24* (32), 5067–5074. <https://doi.org/10.1002/adfm.201400129>.
- (361) Lien, D.-H.; Kao, Z.-K.; Huang, T.-H.; Liao, Y.-C.; Lee, S.-C.; He, J.-H. All-Printed Paper Memory. *ACS Nano* **2014**, *8* (8), 7613–7619. <https://doi.org/10.1021/nn501231z>.
- (362) Zhang, T.; Wang, X.; Li, T.; Guo, Q.; Yang, J. Fabrication of Flexible Copper-Based Electronics with High-Resolution and High-Conductivity on Paper via Inkjet Printing. *J. Mater. Chem. C* **2013**, *2* (2), 286–294. <https://doi.org/10.1039/C3TC31740D>.
- (363) Lessing, J.; Glavan, A. C.; Walker, S. B.; Keplinger, C.; Lewis, J. A.; Whitesides, G. M. Inkjet Printing of Conductive Inks with High Lateral Resolution on Omniphobic “RF Paper” for Paper-Based Electronics and MEMS. *Advanced Materials* **2014**, *26* (27), 4677–4682. <https://doi.org/10.1002/adma.201401053>.
- (364) Ko, H.; Lee, J.; Kim, Y.; Lee, B.; Jung, C.-H.; Choi, J.-H.; Kwon, O.-S.; Shin, K. Active Digital Microfluidic Paper Chips with Inkjet-Printed Patterned Electrodes. *Advanced Materials* **2014**, *26* (15), 2335–2340. <https://doi.org/10.1002/adma.201305014>.

- (365) Ballerini, D. R.; Li, X.; Shen, W. Patterned Paper and Alternative Materials as Substrates for Low-Cost Microfluidic Diagnostics. *Microfluid Nanofluid* **2012**, *13* (5), 769–787. <https://doi.org/10.1007/s10404-012-0999-2>.
- (366) Kemal Yetisen, A.; Safwan Akram, M.; R. Lowe, C. Paper-Based Microfluidic Point-of-Care Diagnostic Devices. *Lab on a Chip* **2013**, *13* (12), 2210–2251. <https://doi.org/10.1039/C3LC50169H>.
- (367) Wong, R.; Tse, H. *Lateral Flow Immunoassay*; Springer Science & Business Media, 2008.
- (368) Pelton, R. Bioactive Paper Provides a Low-Cost Platform for Diagnostics. *TrAC Trends in Analytical Chemistry* **2009**, *28* (8), 925–942. <https://doi.org/10.1016/j.trac.2009.05.005>.
- (369) Hubbe, M. A.; Rojas, O. J.; Sulic, N.; Sezaki, T. Unique Behaviour of Polyampholytes as Drystrength Additives. *Appita : Technology, Innovation, Manufacturing, Environment* **2007**.
- (370) Sampson, W. W. *Modelling Stochastic Fibrous Materials with Mathematica®*; Springer Science & Business Media, 2008.
- (371) Niskanen, K. Book 16: Paper Physics. *Helsinki: Fapet Oy* **1998**.
- (372) Gong, M. M.; Sinton, D. Turning the Page: Advancing Paper-Based Microfluidics for Broad Diagnostic Application. *Chem. Rev.* **2017**, *117* (12), 8447–8480. <https://doi.org/10.1021/acs.chemrev.7b00024>.
- (373) Thompson, M.; Willis, J. R. A Reformation of the Equations of Anisotropic Poroelasticity. *Journal of Applied Mechanics* **1991**, *58* (3), 612–616. <https://doi.org/10.1115/1.2897239>.
- (374) Bruzewicz, D. A.; Reches, M.; Whitesides, G. M. Low-Cost Printing of Poly(Dimethylsiloxane) Barriers To Define Microchannels in Paper. *Anal. Chem.* **2008**, *80* (9), 3387–3392. <https://doi.org/10.1021/ac702605a>.
- (375) Hu, L.; Chen, W.; Xie, X.; Liu, N.; Yang, Y.; Wu, H.; Yao, Y.; Pasta, M.; Alshareef, H. N.; Cui, Y. Symmetrical MnO₂–Carbon Nanotube–Textile Nanostructures for Wearable Pseudocapacitors with High Mass Loading. *ACS Nano* **2011**, *5* (11), 8904–8913. <https://doi.org/10.1021/nn203085j>.
- (376) Ko, Y.; Kwon, M.; Bae, W. K.; Lee, B.; Lee, S. W.; Cho, J. Flexible Supercapacitor Electrodes Based on Real Metal-like Cellulose Papers. *Nat Commun* **2017**, *8* (1), 536. <https://doi.org/10.1038/s41467-017-00550-3>.
- (377) Gui, Z.; Zhu, H.; Gillette, E.; Han, X.; Rubloff, G. W.; Hu, L.; Lee, S. B. Natural Cellulose Fiber as Substrate for Supercapacitor. *ACS Nano* **2013**, *7* (7), 6037–6046. <https://doi.org/10.1021/nn401818t>.

- (378) Kaneta, T.; Alahmad, W.; Varanusupakul, P. Microfluidic Paper-Based Analytical Devices with Instrument-Free Detection and Miniaturized Portable Detectors. *Applied Spectroscopy Reviews* **2019**, *54* (2), 117–141. <https://doi.org/10.1080/05704928.2018.1457045>.
- (379) Singh, A. T.; Lantigua, D.; Meka, A.; Taing, S.; Pandher, M.; Camci-Unal, G. Paper-Based Sensors: Emerging Themes and Applications. *Sensors (Basel)* **2018**, *18* (9). <https://doi.org/10.3390/s18092838>.
- (380) Mazzu-Nascimento, T.; Gianini Morbioli, G.; Aparecido Milan, L.; Furtado Silva, D.; Cristina Donofrio, F.; Alberto Mestriner, C.; Carrilho, E. Improved Assessment of Accuracy and Performance Indicators in Paper-Based ELISA. *Analytical Methods* **2017**, *9* (18), 2644–2653. <https://doi.org/10.1039/C7AY00505A>.
- (381) Mazzu-Nascimento, T.; Morbioli, G. G.; Milan, L. A.; Donofrio, F. C.; Mestriner, C. A.; Carrilho, E. Development and Statistical Assessment of a Paper-Based Immunoassay for Detection of Tumor Markers. *Analytica Chimica Acta* **2017**, *950*, 156–161. <https://doi.org/10.1016/j.aca.2016.11.011>.
- (382) Lee, V. B. C.; Mohd-Naim, N. F.; Tamiya, E.; Ahmed, M. U. Trends in Paper-Based Electrochemical Biosensors: From Design to Application. *Analytical Sciences* **2018**, *34* (1), 7–18. <https://doi.org/10.2116/analsci.34.7>.
- (383) Meredith, N. A.; Quinn, C.; Cate, D. M.; Reilly, T. H.; Volckens, J.; Henry, C. S. Paper-Based Analytical Devices for Environmental Analysis. *Analyst* **2016**, *141* (6), 1874–1887. <https://doi.org/10.1039/C5AN02572A>.
- (384) Tang, R. H.; Yang, H.; Choi, J. R.; Gong, Y.; Feng, S. S.; Pingguan-Murphy, B.; Huang, Q. S.; Shi, J. L.; Mei, Q. B.; Xu, F. Advances in Paper-Based Sample Pretreatment for Point-of-Care Testing. *Critical Reviews in Biotechnology* **2017**, *37* (4), 411–428. <https://doi.org/10.3109/07388551.2016.1164664>.
- (385) Silveira, C. M.; Monteiro, T.; Almeida, M. G. Biosensing with Paper-Based Miniaturized Printed Electrodes—A Modern Trend. *Biosensors* **2016**, *6* (4), 51. <https://doi.org/10.3390/bios6040051>.
- (386) Gao, C.; Xue, J.; Zhang, L.; Cui, K.; Li, H.; Yu, J. Paper-Based Origami Photoelectrochemical Sensing Platform with TiO₂/Bi₄NbO₈Cl/Co-Pi Cascade Structure Enabling of Bidirectional Modulation of Charge Carrier Separation. *Anal. Chem.* **2018**, *90* (24), 14116–14120. <https://doi.org/10.1021/acs.analchem.8b04662>.
- (387) Fu, X.; Xia, B.; Ji, B.; Lei, S.; Zhou, Y. Flow Controllable Three-Dimensional Paper-Based Microfluidic Analytical Devices Fabricated by 3D Printing Technology. *Analytica Chimica Acta* **2019**, *1065*, 64–70. <https://doi.org/10.1016/j.aca.2019.02.046>.

- (388) Yamada, K.; Shibata, H.; Suzuki, K.; Citterio, D. Toward Practical Application of Paper-Based Microfluidics for Medical Diagnostics: State-of-the-Art and Challenges. *Lab Chip* **2017**, *17* (7), 1206–1249. <https://doi.org/10.1039/C6LC01577H>.
- (389) Lim, S. A.; Ahmed, M. U. Electrochemical Immunosensors and Their Recent Nanomaterial-Based Signal Amplification Strategies: A Review. *RSC Adv.* **2016**, *6* (30), 24995–25014. <https://doi.org/10.1039/C6RA00333H>.
- (390) Shamkhalichenar, H.; Choi, J.-W. An Inkjet-Printed Non-Enzymatic Hydrogen Peroxide Sensor on Paper. *J. Electrochem. Soc.* **2017**, *164* (5), B3101–B3106. <https://doi.org/10.1149/2.0161705jes>.
- (391) Glavan, A. C.; Martinez, R. V.; Subramaniam, A. B.; Yoon, H. J.; Nunes, R. M. D.; Lange, H.; Thuo, M. M.; Whitesides, G. M. Omniphobic “RF Paper” Produced by Silanization of Paper with Fluoroalkyltrichlorosilanes. *Advanced Functional Materials* **2014**, *24* (1), 60–70. <https://doi.org/10.1002/adfm.201300780>.
- (392) Zhang, Y.; Ren, T.; He, J. Inkjet Printing Enabled Controllable Paper Superhydrophobization and Its Applications. *ACS Appl. Mater. Interfaces* **2018**, *10* (13), 11343–11349. <https://doi.org/10.1021/acsami.8b01133>.
- (393) Bihar, E.; Wustoni, S.; Pappa, A. M.; Salama, K. N.; Baran, D.; Inal, S. A Fully Inkjet-Printed Disposable Glucose Sensor on Paper. *npj Flexible Electronics* **2018**, *2* (1), 30. <https://doi.org/10.1038/s41528-018-0044-y>.
- (394) Mettakoonpitak, J.; Boehle, K.; Nantaphol, S.; Teengam, P.; Adkins, J. A.; Srisa-Art, M.; Henry, C. S. Electrochemistry on Paper-Based Analytical Devices: A Review. *Electroanalysis* **2016**, *28* (7), 1420–1436. <https://doi.org/10.1002/elan.201501143>.
- (395) Akyazi, T.; Basabe-Desmots, L.; Benito-Lopez, F. Review on Microfluidic Paper-Based Analytical Devices towards Commercialisation. *Analytica Chimica Acta* **2018**, *1001*, 1–17. <https://doi.org/10.1016/j.aca.2017.11.010>.
- (396) Mahadeva, S. K.; Walus, K.; Stoeber, B. Paper as a Platform for Sensing Applications and Other Devices: A Review. *ACS Appl. Mater. Interfaces* **2015**, *7* (16), 8345–8362. <https://doi.org/10.1021/acsami.5b00373>.
- (397) Cate, D. M.; Adkins, J. A.; Mettakoonpitak, J.; Henry, C. S. Recent Developments in Paper-Based Microfluidic Devices. *Anal. Chem.* **2015**, *87* (1), 19–41. <https://doi.org/10.1021/ac503968p>.
- (398) Noviana, E.; Carrão, D. B.; Pratiwi, R.; Henry, C. S. Emerging Applications of Paper-Based Analytical Devices for Drug Analysis: A Review. *Analytica Chimica Acta* **2020**, *1116*, 70–90. <https://doi.org/10.1016/j.aca.2020.03.013>.

- (399) Nery, E. W.; Kubota, L. T. Sensing Approaches on Paper-Based Devices: A Review. *Anal Bioanal Chem* **2013**, *405* (24), 7573–7595. <https://doi.org/10.1007/s00216-013-6911-4>.
- (400) Ratajczak, K.; Stobiecka, M. High-Performance Modified Cellulose Paper-Based Biosensors for Medical Diagnostics and Early Cancer Screening: A Concise Review. *Carbohydrate Polymers* **2020**, *229*, 115463. <https://doi.org/10.1016/j.carbpol.2019.115463>.
- (401) Martinez, A. W.; Phillips, S. T.; Whitesides, G. M.; Carrilho, E. Diagnostics for the Developing World: Microfluidic Paper-Based Analytical Devices. *Anal. Chem.* **2010**, *82* (1), 3–10. <https://doi.org/10.1021/ac9013989>.
- (402) Fu, L.-M.; Wang, Y.-N. Detection Methods and Applications of Microfluidic Paper-Based Analytical Devices. *TrAC Trends in Analytical Chemistry* **2018**, *107*, 196–211. <https://doi.org/10.1016/j.trac.2018.08.018>.
- (403) Dungchai, W.; Chailapakul, O.; Henry, C. S. Electrochemical Detection for Paper-Based Microfluidics. *Anal. Chem.* **2009**, *81* (14), 5821–5826. <https://doi.org/10.1021/ac9007573>.
- (404) Hogenelst, K.; Soeter, M.; Kallen, V. Ambulatory Measurement of Cortisol: Where Do We Stand, and Which Way to Follow? *Sensing and Bio-Sensing Research* **2019**, *22*, 100249. <https://doi.org/10.1016/j.sbsr.2018.100249>.
- (405) Zhang, L.; Ding, B.; Chen, Q.; Feng, Q.; Lin, L.; Sun, J. Point-of-Care-Testing of Nucleic Acids by Microfluidics. *TrAC Trends in Analytical Chemistry* **2017**, *94*, 106–116. <https://doi.org/10.1016/j.trac.2017.07.013>.
- (406) Sun, L.-J.; Xie, Y.; Yan, Y.-F.; Yang, H.; Gu, H.-Y.; Bao, N. Paper-Based Analytical Devices for Direct Electrochemical Detection of Free IAA and SA in Plant Samples with the Weight of Several Milligrams. *Sensors and Actuators B: Chemical* **2017**, *247*, 336–342. <https://doi.org/10.1016/j.snb.2017.03.025>.
- (407) Santhiago, M.; Nery, E. W.; Santos, G. P.; Kubota, L. T. Microfluidic Paper-Based Devices for Bioanalytical Applications. *Bioanalysis* **2014**, *6* (1), 89–106. <https://doi.org/10.4155/bio.13.296>.
- (408) Santhiago, M.; Kubota, L. T. A New Approach for Paper-Based Analytical Devices with Electrochemical Detection Based on Graphite Pencil Electrodes. *Sensors and Actuators B: Chemical* **2013**, *177*, 224–230. <https://doi.org/10.1016/j.snb.2012.11.002>.
- (409) Nie, Z.; Nijhuis, C. A.; Gong, J.; Chen, X.; Kumachev, A.; Martinez, A. W.; Narovlyansky, M.; Whitesides, G. M. Electrochemical Sensing in Paper-Based Microfluidic Devices. *Lab Chip* **2010**, *10* (4), 477–483. <https://doi.org/10.1039/B917150A>.
- (410) Shiroma, L. Y.; Santhiago, M.; Gobbi, A. L.; Kubota, L. T. Separation and Electrochemical Detection of Paracetamol and 4-Aminophenol in a Paper-Based Microfluidic Device. *Analytica Chimica Acta* **2012**, *725*, 44–50. <https://doi.org/10.1016/j.aca.2012.03.011>.

- (411) Santhiago, M.; Wydallis, J. B.; Kubota, L. T.; Henry, C. S. Construction and Electrochemical Characterization of Microelectrodes for Improved Sensitivity in Paper-Based Analytical Devices. *Anal. Chem.* **2013**, *85* (10), 5233–5239. <https://doi.org/10.1021/ac400728y>.
- (412) Li, W.; Qian, D.; Wang, Q.; Li, Y.; Bao, N.; Gu, H.; Yu, C. Fully-Drawn Origami Paper Analytical Device for Electrochemical Detection of Glucose. *Sensors and Actuators B: Chemical* **2016**, *231*, 230–238. <https://doi.org/10.1016/j.snb.2016.03.031>.
- (413) Krejci, J.; Sajdlova, Z.; Nedela, V.; Flodrova, E.; Sejnohova, R.; Vranova, H.; Plicka, R. Effective Surface Area of Electrochemical Sensors. *J. Electrochem. Soc.* **2014**, *161* (6), B147–B150. <https://doi.org/10.1149/2.091406jes>.
- (414) García-Miranda Ferrari, A.; Foster, C. W.; Kelly, P. J.; Brownson, D. A. C.; Banks, C. E. Determination of the Electrochemical Area of Screen-Printed Electrochemical Sensing Platforms. *Biosensors* **2018**, *8* (2), 53. <https://doi.org/10.3390/bios8020053>.
- (415) Jarzabek, G.; Borkowska, Z. On the Real Surface Area of Smooth Solid Electrodes. *Electrochimica Acta* **1997**, *42* (19), 2915–2918. [https://doi.org/10.1016/S0013-4686\(97\)00112-6](https://doi.org/10.1016/S0013-4686(97)00112-6).
- (416) Lukaszewski, M.; Soszko, M.; Czerwiński, A. Electrochemical Methods of Real Surface Area Determination of Noble Metal Electrodes—an Overview. *Int. J. Electrochem. Sci* **2016**, *11* (6), 4442–4469.
- (417) Zhang, Y.; Ren, T.; Li, T.; He, J.; Fang, D. Paper-Based Hydrophobic/Lipophobic Surface for Sensing Applications Involving Aggressive Liquids. *Advanced Materials Interfaces* **2016**, *3* (22), 1600672. <https://doi.org/10.1002/admi.201600672>.
- (418) Sowade, E.; Göthel, F.; Zichner, R.; Baumann, R. R. Inkjet Printing of UHF Antennas on Corrugated Cardboards for Packaging Applications. *Applied Surface Science* **2015**, *332*, 500–506. <https://doi.org/10.1016/j.apsusc.2015.01.113>.
- (419) da Silva, E. T. S. G.; Miserere, S.; Kubota, L. T.; Merkoçi, A. Simple On-Plastic/Paper Inkjet-Printed Solid-State Ag/AgCl Pseudoreference Electrode. *Anal. Chem.* **2014**, *86* (21), 10531–10534. <https://doi.org/10.1021/ac503029q>.
- (420) Bard, A. J.; Faulkner, L. R.; Leddy, J.; Zoski, C. G. *Electrochemical Methods: Fundamentals and Applications*; Wiley New York, 1980; Vol. 2.
- (421) Compton, R. G.; Banks, C. E. *Understanding Voltammetry*; World Scientific, 2011.
- (422) Aller Pellitero, M.; Kitsara, M.; Eibensteiner, F.; del Campo, F. J. Rapid Prototyping of Electrochemical Lateral Flow Devices: Stencilled Electrodes. *Analyst* **2016**, *141* (8), 2515–2522. <https://doi.org/10.1039/C5AN02424B>.

- (423) Suntornsuk, W.; Suntornsuk, L. Recent Applications of Paper-Based Point-of-Care Devices for Biomarker Detection. *ELECTROPHORESIS* **2020**, *41* (5–6), 287–305. <https://doi.org/10.1002/elps.201900258>.
- (424) Akbulut, Y.; Zengin, A. A Molecularly Imprinted Whatman Paper for Clinical Detection of Propranolol. *Sensors and Actuators B: Chemical* **2020**, *304*, 127276. <https://doi.org/10.1016/j.snb.2019.127276>.
- (425) Wynn, D.; Raut, N.; Joel, S.; Pasini, P.; K. Deo, S.; Daunert, S. Detection of Bacterial Contamination in Food Matrices by Integration of Quorum Sensing in a Paper-Strip Test. *Analyt* **2018**, *143* (19), 4774–4782. <https://doi.org/10.1039/C8AN00878G>.
- (426) Álvarez-Diduk, R.; Orozco, J.; Merkoçi, A. Paper Strip-Embedded Graphene Quantum Dots: A Screening Device with a Smartphone Readout. *Scientific Reports* **2017**, *7* (1), 976. <https://doi.org/10.1038/s41598-017-01134-3>.
- (427) Chen, P.; Gates-Hollingsworth, M.; Pandit, S.; Park, A.; Montgomery, D.; AuCoin, D.; Gu, J.; Zenhausern, F. Paper-Based Vertical Flow Immunoassay (VFI) for Detection of Bio-Threat Pathogens. *Talanta* **2019**, *191*, 81–88. <https://doi.org/10.1016/j.talanta.2018.08.043>.
- (428) Tian, D.; Song, Y.; Jiang, L. Patterning of Controllable Surface Wettability for Printing Techniques. *Chem. Soc. Rev.* **2013**, *42* (12), 5184–5209. <https://doi.org/10.1039/C3CS35501B>.
- (429) Jung, H. C.; Cho, S.-H.; Joung, J. W.; Oh, Y.-S. Studies on Inkjet-Printed Conducting Lines for Electronic Devices. *Journal of Elec Materi* **2007**, *36* (9), 1211–1218. <https://doi.org/10.1007/s11664-007-0194-5>.
- (430) Martinez, A. W.; Phillips, S. T.; Butte, M. J.; Whitesides, G. M. Patterned Paper as a Platform for Inexpensive, Low-Volume, Portable Bioassays. *Angewandte Chemie* **2007**, *119* (8), 1340–1342. <https://doi.org/10.1002/ange.200603817>.
- (431) Pietrikova, A.; Lukacs, P.; Jakubeczyova, D.; Balloková, B.; Potencki, J.; Tomaszewski, G.; Pekarek, J.; Prikrylova, K.; Fides, M. Surface Analysis of Polymeric Substrates Used for Inkjet Printing Technology. *Circuit World* **2016**, *42* (1), 9–16. <https://doi.org/10.1108/CW-10-2015-0047>.
- (432) Denneulin, A.; Bras, J.; Blayo, A.; Neuman, C. Substrate Pre-Treatment of Flexible Material for Printed Electronics with Carbon Nanotube Based Ink. *Applied Surface Science* **2011**, *257* (8), 3645–3651. <https://doi.org/10.1016/j.apsusc.2010.11.097>.
- (433) Sturgess, C.; J. Tuck, C.; A. Ashcroft, I.; D. Wildman, R. 3D Reactive Inkjet Printing of Polydimethylsiloxane. *Journal of Materials Chemistry C* **2017**, *5* (37), 9733–9743. <https://doi.org/10.1039/C7TC02412F>.

- (434) Gotoh, K.; Yasukawa, A.; Kobayashi, Y. Wettability Characteristics of Poly(Ethylene Terephthalate) Films Treated by Atmospheric Pressure Plasma and Ultraviolet Excimer Light. *Polym J* **2011**, *43* (6), 545–551. <https://doi.org/10.1038/pj.2011.20>.
- (435) Zikulnig, J.; Roshanghias, A.; Rauter, L.; Hirschl, C. Evaluation of the Sheet Resistance of Inkjet-Printed Ag-Layers on Flexible, Uncoated Paper Substrates Using Van-Der-Pauw's Method. *Sensors* **2020**, *20* (8), 2398. <https://doi.org/10.3390/s20082398>.
- (436) Kissinger, P. T.; Heineman, W. R. Cyclic Voltammetry. *Journal of Chemical Education* **1983**, *60* (9), 702.
- (437) Fischer, L. M.; Tenje, M.; Heiskanen, A. R.; Masuda, N.; Castillo, J.; Bentien, A.; Émneus, J.; Jakobsen, M. H.; Boisen, A. Gold Cleaning Methods for Electrochemical Detection Applications. *Microelectronic Engineering* **2009**, *86* (4), 1282–1285. <https://doi.org/10.1016/j.mee.2008.11.045>.
- (438) Kadara, R. O.; Jenkinson, N.; Banks, C. E. Characterisation of Commercially Available Electrochemical Sensing Platforms. *Sensors and Actuators B: Chemical* **2009**, *138* (2), 556–562. <https://doi.org/10.1016/j.snb.2009.01.044>.
- (439) Fragkou, V.; Ge, Y.; Steiner, G.; Freeman, D.; Bartetzko, N.; Turner, A. P. Determination of the Real Surface Area of a Screen-Printed Electrode by Chronocoulometry. *Int. J. Electrochem. Sci* **2012**, *7*, 6214–6220.
- (440) Matsuda, H.; Ayabe, Y. Theoretical Analysis of Polarographic Waves. I. Reduction of Simple Metal Ions. *BCSJ* **1955**, *28* (6), 422–428. <https://doi.org/10.1246/bcsj.28.422>.
- (441) Levine, A.; Zagoory-Sharon, O.; Feldman, R.; Lewis, J. G.; Weller, A. Measuring Cortisol in Human Psychobiological Studies. *Physiology & Behavior* **2007**, *90* (1), 43–53. <https://doi.org/10.1016/j.physbeh.2006.08.025>.
- (442) Gatti, R.; Antonelli, G.; Prearo, M.; Spinella, P.; Cappellin, E.; De Palo, E. F. Cortisol Assays and Diagnostic Laboratory Procedures in Human Biological Fluids. *Clinical Biochemistry* **2009**, *42* (12), 1205–1217. <https://doi.org/10.1016/j.clinbiochem.2009.04.011>.
- (443) de Kloet, E. R.; Joëls, M.; Holsboer, F. Stress and the Brain: From Adaptation to Disease. *Nat Rev Neurosci* **2005**, *6* (6), 463–475. <https://doi.org/10.1038/nrn1683>.
- (444) Kaushik, A.; Vasudev, A.; Arya, S. K.; Pasha, S. K.; Bhansali, S. Recent Advances in Cortisol Sensing Technologies for Point-of-Care Application. *Biosensors and Bioelectronics* **2014**, *53*, 499–512. <https://doi.org/10.1016/j.bios.2013.09.060>.
- (445) Gallagher, T. F.; Yoshida, K.; Roffwarg, H. D.; Fukushima, D. K.; Weitzman, E. D.; Hellman, L. ACTH and Cortisol Secretory Patterns in Man. *None* **1973**, *36* (6), 1058–1068. <https://doi.org/10.1210/jcem-36-6-1058>.

- (446) Taves, M. D.; Gomez-Sanchez, C. E.; Soma, K. K. Extra-Adrenal Glucocorticoids and Mineralocorticoids: Evidence for Local Synthesis, Regulation, and Function. *American Journal of Physiology-Endocrinology and Metabolism* **2011**, *301* (1), E11–E24. <https://doi.org/10.1152/ajpendo.00100.2011>.
- (447) Stachowicz, M.; Lebidzińska, A. The Effect of Diet Components on the Level of Cortisol. *European Food Research and Technology* **2016**, *242* (12), 2001–2009. <https://doi.org/10.1007/s00217-016-2772-3>.
- (448) Tomiyama, A. J.; Mann, T.; Vinas, D.; Hunger, J. M.; DeJager, J.; Taylor, S. E. Low Calorie Dieting Increases Cortisol. *Psychosom Med* **2010**, *72* (4), 357–364. <https://doi.org/10.1097/PSY.0b013e3181d9523c>.
- (449) Coderre, L.; Srivastava, A. K.; Chiasson, J. L. Role of Glucocorticoid in the Regulation of Glycogen Metabolism in Skeletal Muscle. *American Journal of Physiology-Endocrinology and Metabolism* **1991**, *260* (6), E927–E932. <https://doi.org/10.1152/ajpendo.1991.260.6.E927>.
- (450) Kirschbaum, C.; Bono, E. G.; Rohleder, N.; Gessner, C.; Pirke, K. M.; Salvador, A.; Hellhammer, D. H. Effects of Fasting and Glucose Load on Free Cortisol Responses to Stress and Nicotine. *J Clin Endocrinol Metab* **1997**, *82* (4), 1101–1105. <https://doi.org/10.1210/jcem.82.4.3882>.
- (451) Simmons, P. S.; Miles, J. M.; Gerich, J. E.; Haymond, M. W. Increased Proteolysis. An Effect of Increases in Plasma Cortisol within the Physiologic Range. *J Clin Invest* **1984**, *73* (2), 412–420. <https://doi.org/10.1172/JCI111227>.
- (452) Yaribeygi, H.; Panahi, Y.; Sahraei, H.; Johnston, T. P.; Sahebkar, A. The Impact of Stress on Body Function: A Review. *EXCLI J* **2017**, *16*, 1057–1072. <https://doi.org/10.17179/excli2017-480>.
- (453) Palacios, R.; Sugawara, I. Hydrocortisone Abrogates Proliferation of T Cells in Autologous Mixed Lymphocyte Reaction by Rendering the Interleukin-2 Producer T Cells Unresponsive to Interleukin-1 and Unable to Synthesize the T-Cell Growth Factor. *Scandinavian Journal of Immunology* **1982**, *15* (1), 25–31. <https://doi.org/10.1111/j.1365-3083.1982.tb00618.x>.
- (454) Canalis, E.; Mazziotti, G.; Giustina, A.; Bilezikian, J. P. Glucocorticoid-Induced Osteoporosis: Pathophysiology and Therapy. *Osteoporos Int* **2007**, *18* (10), 1319–1328. <https://doi.org/10.1007/s00198-007-0394-0>.
- (455) Seller, M. J. The Effect of Cortisol on the Haematocrit Values and Serum Electrolytes of the Adult and Foetal Rat. *The Journal of Physiology* **1966**, *184* (3), 657–662. <https://doi.org/10.1113/jphysiol.1966.sp007938>.

- (456) Chan, S.; Debono, M. Replication of Cortisol Circadian Rhythm: New Advances in Hydrocortisone Replacement Therapy. *Therapeutic advances in endocrinology and metabolism* **2010**, *1* (3), 129–138. <https://doi.org/10.1177/2042018810380214>.
- (457) Clow, A.; Hucklebridge, F.; Stalder, T.; Evans, P.; Thorn, L. The Cortisol Awakening Response: More than a Measure of HPA Axis Function. *Neuroscience & Biobehavioral Reviews* **2010**, *35* (1), 97–103. <https://doi.org/10.1016/j.neubiorev.2009.12.011>.
- (458) Sephton, S. E.; Lush, E.; Dedert, E. A.; Floyd, A. R.; Rebholz, W. N.; Dhabhar, F. S.; Spiegel, D.; Salmon, P. Diurnal Cortisol Rhythm as a Predictor of Lung Cancer Survival. *Brain, behavior, and immunity* **2013**, *30*, S163–S170. <https://doi.org/10.1016/j.bbi.2012.07.019>.
- (459) Fraser, R.; Ingram, M. C.; Anderson, N. H.; Morrison, C.; Davies, E.; Connell, J. M. Cortisol Effects on Body Mass, Blood Pressure, and Cholesterol in the General Population. *Hypertension* **1999**, *33* (6), 1364–1368. <https://doi.org/10.1161/01.HYP.33.6.1364>.
- (460) Sharpley, C. F.; McFarlane, J. R.; Slominski, A. Stress-Linked Cortisol Concentrations in Hair: What We Know and What We Need to Know. *Reviews in the Neurosciences* **2012**, *23* (1), 111–121. <https://doi.org/10.1515/rns.2011.058>.
- (461) Joseph, D. N.; Whirledge, S. Stress and the HPA Axis: Balancing Homeostasis and Fertility. *International journal of molecular sciences* **2017**, *18* (10), 2224. <https://doi.org/10.3390/ijms18102224>.
- (462) Lause, M.; Kamboj, A.; Faith, E. F. Dermatologic Manifestations of Endocrine Disorders. *Translational pediatrics* **2017**, *6* (4), 300. <https://doi.org/10.21037/tp.2017.09.08>.
- (463) Fries, E.; Hesse, J.; Hellhammer, J.; Hellhammer, D. A New View on Hypocortisolism. *Psychoneuroendocrinology* **2005**, *30* (10), 1010–1016. <https://doi.org/10.1016/j.psyneuen.2005.04.006>.
- (464) Heim, C.; Ehlert, U.; Hellhammer, D. H. The Potential Role of Hypocortisolism in the Pathophysiology of Stress-Related Bodily Disorders. *Psychoneuroendocrinology* **2000**, *25* (1), 1–35. [https://doi.org/10.1016/S0306-4530\(99\)00035-9](https://doi.org/10.1016/S0306-4530(99)00035-9).
- (465) Ljubijankić, N.; Popović-Javorić, R.; Šćeta, S.; Šapčanin, A.; Tahirović, I.; Sofić, E. Daily Fluctuation of Cortisol in the Saliva and Serum of Healthy Persons. *Bosn J Basic Med Sci* **2008**, *8* (2), 110–115. <https://doi.org/10.17305/bjbms.2008.2962>.
- (466) Fraser, L.-A.; Uum, S. V. Work-up for Cushing Syndrome. *CMAJ* **2010**, *182* (6), 584–587. <https://doi.org/10.1503/cmaj.090250>.
- (467) Bellagambi, F. G.; Degano, I.; Ghimenti, S.; Lomonaco, T.; Dini, V.; Romanelli, M.; Mastorci, F.; Gemignani, A.; Salvo, P.; Fuoco, R.; Di Francesco, F. Determination of Salivary α -Amylase and Cortisol in Psoriatic Subjects Undergoing the Trier Social Stress

Test. *Microchemical Journal* **2018**, *136*, 177–184.
<https://doi.org/10.1016/j.microc.2017.04.033>.

- (468) Russell, E.; Koren, G.; Reider, M.; Van Uum, S. The Detection of Cortisol in Human Sweat: Implications for Measurement of Cortisol in Hair. *Endocr. Rev.* **2012**, *33*, 03. <https://doi.org/10.1097/FTD.0b013e31829daa0a>.
- (469) Sauv e, B.; Koren, G.; Walsh, G.; Tokmakejian, S.; Uum, S. H. V. Measurement of Cortisol in Human Hair as a Biomarker of Systemic Exposure. *Clinical and Investigative Medicine* **2007**, E183–E191. <https://doi.org/10.25011/cim.v30i5.2894>.
- (470) Gonzalez, D.; Jacobsen, D.; Ibar, C.; Pavan, C.; Monti, J.; Machulsky, N. F.; Balbi, A.; Fritzler, A.; Jamardo, J.; Repetto, E. M.; Berg, G.; Fabre, B. Hair Cortisol Measurement by an Automated Method. *Sci Rep* **2019**, *9* (1), 1–6. <https://doi.org/10.1038/s41598-019-44693-3>.
- (471) Venugopal, M.; Arya, S. K.; Chornokur, G.; Bhansali, S. A Realtime and Continuous Assessment of Cortisol in ISF Using Electrochemical Impedance Spectroscopy. *Sensors and Actuators A: Physical* **2011**, *172* (1), 154–160. <https://doi.org/10.1016/j.sna.2011.04.028>.
- (472) McEwen, B. S. Mood Disorders and Allostatic Load. *Biological Psychiatry* **2003**, *54* (3), 200–207. [https://doi.org/10.1016/S0006-3223\(03\)00177-X](https://doi.org/10.1016/S0006-3223(03)00177-X).
- (473) Andrews, R. C.; Walker, B. R. Glucocorticoids and Insulin Resistance: Old Hormones, New Targets. *Clinical Science* **1999**, *96* (5), 513–523. <https://doi.org/10.1042/cs0960513>.
- (474) Obel, C.; Hedegaard, M.; Henriksen, T. B.; Secher, N. J.; Olsen, J.; Levine, S. Stress and Salivary Cortisol during Pregnancy. *Psychoneuroendocrinology* **2005**, *30* (7), 647–656. <https://doi.org/10.1016/j.psyneuen.2004.11.006>.
- (475) Golf, S. W.; Happel, O.; Graef, V.; Seim, K. E. Plasma Aldosterone, Cortisol and Electrolyte Concentrations in Physical Exercise after Magnesium Supplementation. *Clinical Chemistry and Laboratory Medicine (CCLM)* **1984**, *22* (11), 717–722. <https://doi.org/10.1515/cclm.1984.22.11.717>.
- (476) Thesing, C. S.; Bot, M.; Milaneschi, Y.; Giltay, E. J.; Penninx, B. W. J. H. Omega-3 and Omega-6 Fatty Acid Levels in Depressive and Anxiety Disorders. *Psychoneuroendocrinology* **2018**, *87*, 53–62. <https://doi.org/10.1016/j.psyneuen.2017.10.005>.
- (477) Field, T.; Hernandez-Reif, M.; Diego, M.; Schanberg, S.; Kuhn, C. Cortisol Decreases and Serotonin and Dopamine Increase Following Massage Therapy. *International Journal of Neuroscience* **2005**, *115* (10), 1397–1413. <https://doi.org/10.1080/00207450590956459>.

- (478) Savage, B. M.; Lujan, H. L.; Thipparthi, R. R.; DiCarlo, S. E. Humor, Laughter, Learning, and Health! A Brief Review. *Advances in Physiology Education* **2017**, *41* (3), 341–347. <https://doi.org/10.1152/advan.00030.2017>.
- (479) Kirschbaum, C.; Hellhammer, D. H. Salivary Cortisol in Psychoneuroendocrine Research: Recent Developments and Applications. *Psychoneuroendocrinology* **1994**, *19* (4), 313–333. [https://doi.org/10.1016/0306-4530\(94\)90013-2](https://doi.org/10.1016/0306-4530(94)90013-2).
- (480) Laudat, M. H.; Cerdas, S.; Fournier, C.; Guiban, D.; Guilhaume, B.; Luton, J. P. Salivary Cortisol Measurement: A Practical Approach to Assess Pituitary-Adrenal Function. *J Clin Endocrinol Metab* **1988**, *66* (2), 343–348. <https://doi.org/10.1210/jcem-66-2-343>.
- (481) Estrada-Y-Martin, R. M.; Orlander, P. R. Salivary Cortisol Can Replace Free Serum Cortisol Measurements in Patients With Septic Shock. *Chest* **2011**, *140* (5), 1216–1222. <https://doi.org/10.1378/chest.11-0448>.
- (482) Kaufman, E.; Lamster, I. B. The Diagnostic Applications of Saliva— A Review. *Critical Reviews in Oral Biology & Medicine* **2002**, *13* (2), 197–212. <https://doi.org/10.1177/154411130201300209>.
- (483) Teruhisa, U.; Ryoji, H.; Taisuke, I.; Tatsuya, S.; Fumihiro, M.; Tatsuo, S. Use of Saliva for Monitoring Unbound Free Cortisol Levels in Serum. *Clinica Chimica Acta* **1981**, *110* (2), 245–253. [https://doi.org/10.1016/0009-8981\(81\)90353-3](https://doi.org/10.1016/0009-8981(81)90353-3).
- (484) Vining, R. F.; McGinley, R. A. The Measurement of Hormones in Saliva: Possibilities and Pitfalls. *Journal of Steroid Biochemistry* **1987**, *27* (1), 81–94. [https://doi.org/10.1016/0022-4731\(87\)90297-4](https://doi.org/10.1016/0022-4731(87)90297-4).
- (485) Kudielka, B. M.; Hellhammer, D. H.; Wüst, S. Why Do We Respond so Differently? Reviewing Determinants of Human Salivary Cortisol Responses to Challenge. *Psychoneuroendocrinology* **2009**, *34* (1), 2–18. <https://doi.org/10.1016/j.psyneuen.2008.10.004>.
- (486) Baraket, A.; Lee, M.; Zine, N.; Sigaud, M.; Yaakoubi, N.; Trivella, M. G.; Zabala, M.; Bausells, J.; Jaffrezic-Renault, N.; Errachid, A. Diazonium Modified Gold Microelectrodes onto Polyimide Substrates for Impedimetric Cytokine Detection with an Integrated Ag/AgCl Reference Electrode. *Sensors and Actuators B: Chemical* **2013**, *189*, 165–172. <https://doi.org/10.1016/j.snb.2013.02.088>.
- (487) Stefana, R. I.; Van, J. S.; Aboul-Enein, H. Y. Design and Use of Electrochemical Sensors in Enantioselective High Throughput Screening of Drugs. A Minireview. *Comb Chem High Throughput Screen* **2000**, *3* (6), 445–454. <https://doi.org/10.2174/1386207003331382>.
- (488) Shimada, M.; Takahashi, K.; Sasajima, M.; Segawa, M.; Higurashi, M. Assessment of Circadian Rhythm of Salivary Cortisol in the Childhood of Preterm Infants by Enzyme-

- Linked Immunosorbent Assay (ELISA). *Clinical Pediatric Endocrinology* **1994**, 3 (1), 63–67. <https://doi.org/10.1297/cpe.3.63>.
- (489) Baid, S. K.; Sinaii, N.; Wade, M.; Rubino, D.; Nieman, L. K. Radioimmunoassay and Tandem Mass Spectrometry Measurement of Bedtime Salivary Cortisol Levels: A Comparison of Assays to Establish Hypercortisolism. *None* **2007**, 92 (8), 3102–3107. <https://doi.org/10.1210/jc.2006-2861>.
- (490) Posthuma-Trumpie, G. A.; Korf, J.; van Amerongen, A. Lateral Flow (Immuno)Assay: Its Strengths, Weaknesses, Opportunities and Threats. A Literature Survey. *Anal Bioanal Chem* **2009**, 393 (2), 569–582. <https://doi.org/10.1007/s00216-008-2287-2>.
- (491) Parlak, O.; Keene, S. T.; Marais, A.; Curto, V. F.; Salleo, A. Molecularly Selective Nanoporous Membrane-Based Wearable Organic Electrochemical Device for Noninvasive Cortisol Sensing. *Science Advances* **2018**, 4 (7), eaar2904. <https://doi.org/10.1126/sciadv.aar2904>.
- (492) Qin, Z.; Chan, W. C. W.; Boulware, D. R.; Akkin, T.; Butler, E. K.; Bischof, J. C. Significantly Improved Analytical Sensitivity of Lateral Flow Immunoassays by Using Thermal Contrast. *Angewandte Chemie International Edition* **2012**, 51 (18), 4358–4361. <https://doi.org/10.1002/anie.201200997>.
- (493) Zangheri, M.; Cevenini, L.; Anfossi, L.; Baggiani, C.; Simoni, P.; Di Nardo, F.; Roda, A. A Simple and Compact Smartphone Accessory for Quantitative Chemiluminescence-Based Lateral Flow Immunoassay for Salivary Cortisol Detection. *Biosensors and Bioelectronics* **2015**, 64, 63–68. <https://doi.org/10.1016/j.bios.2014.08.048>.
- (494) Shetty, V.; Yamaguchi, M. Salivary Biosensors for Screening Trauma-Related Psychopathology. *Oral and Maxillofacial Surgery Clinics* **2010**, 22 (2), 269–278. <https://doi.org/10.1016/j.coms.2010.01.004>.
- (495) Pourfarzaneh, M.; White, G. W.; Landon, J.; Smith, D. S. Cortisol Directly Determined in Serum by Fluoroimmunoassay with Magnetizable Solid Phase. *Clinical Chemistry* **1980**, 26 (6), 730–733. <https://doi.org/10.1093/clinchem/26.6.730>.
- (496) Martin, J. A.; Chávez, J. L.; Chushak, Y.; Chapleau, R. R.; Hagen, J.; Kelley-Loughnane, N. Tunable Stringency Aptamer Selection and Gold Nanoparticle Assay for Detection of Cortisol. *Anal Bioanal Chem* **2014**, 406 (19), 4637–4647. <https://doi.org/10.1007/s00216-014-7883-8>.
- (497) Khan, M. S.; Rosner, W. Investigation of the Binding Site of Human Corticosteroid-Binding Globulin by Affinity Labeling. Demonstration of a Cysteinyll Residue in the Binding Site. *J. Biol. Chem.* **1977**, 252 (6), 1895–1900. <https://doi.org/doi:10.1074/jbc.274.21.15046>.

- (498) Brody, J. P.; Yager, P. Diffusion-Based Extraction in a Microfabricated Device. *Sensors and Actuators A: Physical* **1997**, *58* (1), 13–18. [https://doi.org/10.1016/S0924-4247\(97\)80219-1](https://doi.org/10.1016/S0924-4247(97)80219-1).
- (499) Gascoyne, P.; Mahidol, C.; Ruchirawat, M.; Satayavivad, J.; Watcharasit, P.; Becker, F. F. Microsample Preparation by Dielectrophoresis: Isolation of Malaria. *Lab Chip* **2002**, *2* (2), 70–75. <https://doi.org/10.1039/B110990C>.
- (500) Yahya, N. N.; Aziz, N. A.; Buyong, M. R.; Majlis, B. Y. Size-Based Particles Separation Utilizing Dielectrophoresis Technique. In *2017 IEEE Regional Symposium on Micro and Nanoelectronics (RSM)*; 2017; pp 10–13. <https://doi.org/10.1109/RSM.2017.8069123>.
- (501) Murphy, B. E. P.; Jachan, C. Clinical Evaluation of Urinary Cortisol Determinations by Competitive Protein-Binding Radioassay. *The Journal of Clinical Endocrinology & Metabolism* **1968**, *28* (3), 343–348. <https://doi.org/10.1210/jcem-28-3-343>.
- (502) El-Farhan, N.; Rees, D. A.; Evans, C. Measuring Cortisol in Serum, Urine and Saliva—Are Our Assays Good Enough? *Annals of clinical biochemistry* **2017**, *54* (3), 308–322. <https://doi.org/10.1177/0004563216687335>.
- (503) Turpeinen, U.; Hämäläinen, E. Determination of Cortisol in Serum, Saliva and Urine. *Best Practice & Research Clinical Endocrinology & Metabolism* **2013**, *27* (6), 795–801. <https://doi.org/10.1016/j.beem.2013.10.008>.
- (504) Krasowski, M. D.; Drees, D.; Morris, C. S.; Maakestad, J.; Blau, J. L.; Ekins, S. Cross-Reactivity of Steroid Hormone Immunoassays: Clinical Significance and Two-Dimensional Molecular Similarity Prediction. *BMC Clinical Pathology* **2014**, *14* (1), 33. <https://doi.org/10.1186/1472-6890-14-33>.
- (505) Monaghan, P. J.; Owen, L. J.; Trainer, P. J.; Brabant, G.; Keevil, B. G.; Darby, D. Comparison of Serum Cortisol Measurement by Immunoassay and Liquid Chromatography-Tandem Mass Spectrometry in Patients Receiving the 11 β -Hydroxylase Inhibitor Metyrapone. *Ann Clin Biochem* **2011**, *48* (5), 441–446. <https://doi.org/10.1258/acb.2011.011014>.
- (506) Huayllas, M. K. P.; Netzel, B. C.; Singh, R. J.; Kater, C. E. Serum Cortisol Levels via Radioimmunoassay vs Liquid Chromatography Mass Spectrophotometry in Healthy Control Subjects and Patients With Adrenal Incidentalomas. *Lab Med* **2018**, *49* (3), 259–267. <https://doi.org/10.1093/labmed/lmy005>.
- (507) Boumba, V. A.; Ziavrou, K. S.; Vougiouklakis, T. Hair as a Biological Indicator of Drug Use, Drug Abuse or Chronic Exposure to Environmental Toxicants. *Int J Toxicol* **2006**, *25* (3), 143–163. <https://doi.org/10.1080/10915810600683028>.
- (508) Russell, E.; Koren, G.; Rieder, M.; Van Uum, S. Hair Cortisol as a Biological Marker of Chronic Stress: Current Status, Future Directions and Unanswered Questions.

- (509) Koren, L.; Mokady, O.; Karaskov, T.; Klein, J.; Koren, G.; Geffen, E. A Novel Method Using Hair for Determining Hormonal Levels in Wildlife. *Academic Press* **2002**.
<https://doi.org/doi:10.1006/anbe.2001.1907>.
- (510) Uum, S. H. M. V.; Sauv e, B.; Fraser, L. A.; Morley-Forster, P.; Paul, T. L.; Koren, G. Elevated Content of Cortisol in Hair of Patients with Severe Chronic Pain: A Novel Biomarker for Stress. *Stress* **2008**, 11 (6), 483–488.
<https://doi.org/10.1080/10253890801887388>.
- (511) Karl en, J.; Ludvigsson, J.; Frostell, A.; Theodorsson, E.; Faresj o, T. Cortisol in Hair Measured in Young Adults - a Biomarker of Major Life Stressors? *BMC Clinical Pathology* **2011**, 11 (1), 12. <https://doi.org/10.1186/1472-6890-11-12>.
- (512) Jessop, D. S.; Turner-Cobb, J. M. Measurement and Meaning of Salivary Cortisol: A Focus on Health and Disease in Children. *Stress* **2008**, 11 (1), 1–14.
<https://doi.org/10.1080/10253890701365527>.
- (513) Jia, M.; M. Chew, W.; Feinstein, Y.; Skeath, P.; M. Sternberg, E. Quantification of Cortisol in Human Eccrine Sweat by Liquid Chromatography – Tandem Mass Spectrometry. *Analyst* **2016**, 141 (6), 2053–2060. <https://doi.org/10.1039/C5AN02387D>.
- (514) Isaac, A.; Ibrahim, Y.; Andrew, A.; Edward, D. W.; Solomon, A. The Cortisol Steroid Levels as a Determinant of Health Status in Animals; 2017. <https://doi.org/10.4172/jpb.1000452>.
- (515) Kinnamon, D.; Ghanta, R.; Lin, K.-C.; Muthukumar, S.; Prasad, S. Portable Biosensor for Monitoring Cortisol in Low-Volume Perspired Human Sweat. *Sci Rep* **2017**, 7 (1), 1–13.
<https://doi.org/10.1038/s41598-017-13684-7>.
- (516) Ehresman, D. J.; Froehlich, J. W.; Olsen, G. W.; Chang, S.-C.; Butenhoff, J. L. Comparison of Human Whole Blood, Plasma, and Serum Matrices for the Determination of Perfluorooctanesulfonate (PFOS), Perfluorooctanoate (PFOA), and Other Fluorochemicals. *Environmental Research* **2007**, 103 (2), 176–184.
<https://doi.org/10.1016/j.envres.2006.06.008>.
- (517) Hawley, J. M.; Owen, L. J.; Lockhart, S. J.; Monaghan, P. J.; Armston, A.; Chadwick, C. A.; Wilshaw, H.; Freire, M.; Perry, L.; Keevil, B. G. Serum Cortisol: An Up-To-Date Assessment of Routine Assay Performance. *Clinical Chemistry* **2016**, 62 (9), 1220–1229.
<https://doi.org/10.1373/clinchem.2016.255034>.
- (518) Lee, S.; Lim, H.-S.; Shin, H.-J.; Kim, S.-A.; Park, J.; Kim, H.-C.; Kim, H.; Kim, H. J.; Kim, Y.-T.; Lee, K.-R.; Kim, Y.-J. Simultaneous Determination of Cortisol and Cortisone from Human Serum by Liquid Chromatography-Tandem Mass Spectrometry

<https://www.hindawi.com/journals/jamc/2014/787483/abs/> (accessed 2019 -07 -17).
<https://doi.org/10.1155/2014/787483>.

- (519) Bellagambi, F. G.; Lomonaco, T.; Salvo, P.; Vivaldi, F.; Hangouët, M.; Ghimenti, S.; Biagini, D.; Di Francesco, F.; Fuoco, R.; Errachid, A. Saliva Sampling: Methods and Devices. An Overview. *TrAC Trends in Analytical Chemistry* **2019**, 115781. <https://doi.org/10.1016/j.trac.2019.115781>.
- (520) Katz, F. H.; Shannon, I. L. Adrenal Corticosteroids in Submaxillary Fluid. *J Dent Res* **1969**, 48 (3), 448–451. <https://doi.org/10.1177/00220345690480032101>.
- (521) Carr, P. J.; Millar, R. P.; Crowley, H. A Simple Radioimmunoassay for Plasma Cortisol: Comparison with the Fluorimetric Method of Determination. *Ann. Clin. Biochem.* **1977**, 14 (4), 207–211. <https://doi.org/10.1177/000456327701400157>.
- (522) Gozansky, W. S.; Lynn, J. S.; Laudenslager, M. L.; Kohrt, W. M. Salivary Cortisol Determined by Enzyme Immunoassay Is Preferable to Serum Total Cortisol for Assessment of Dynamic Hypothalamic–Pituitary–Adrenal Axis Activity. *Clinical Endocrinology* **2005**, 63 (3), 336–341. <https://doi.org/10.1111/j.1365-2265.2005.02349.x>.
- (523) Morineau, G.; Boudi, A.; Barka, A.; Gourmelen, M.; Degeilh, F.; Hardy, N.; Al-Halnak, A.; Soliman, H.; Gosling, J. P.; Julien, R.; Brerault, J.-L.; Boudou, P.; Aubert, P.; Villette, J.-M.; Pruna, A.; Galons, H.; Fiet, J. Radioimmunoassay of Cortisone in Serum, Urine, and Saliva to Assess the Status of the Cortisol–Cortisone Shuttle. *Clinical Chemistry* **1997**, 43 (8), 1397–1407. <https://doi.org/10.1093/clinchem/43.8.1397>.
- (524) Arya, S. K.; Chornokur, G.; Venugopal, M.; Bhansali, S. Antibody Modified Gold Micro Array Electrode Based Electrochemical Immunosensor for Ultrasensitive Detection of Cortisol in Saliva and ISF. *Procedia Engineering* **2010**, 5, 804–807. <https://doi.org/10.1016/j.proeng.2010.09.230>.
- (525) Barhoumi, L.; Baraket, A.; Bellagambi, F. G.; Karanasiou, G. S.; Ali, M. B.; Fotiadis, D. I.; Bausells, J.; Zine, N.; Sigaud, M.; Errachid, A. A Novel Chronoamperometric Immunosensor for Rapid Detection of TNF- α in Human Saliva. *Sensors and Actuators B: Chemical* **2018**, 266, 477–484. <https://doi.org/10.1016/j.snb.2018.03.135>.
- (526) Singh, A.; Kaushik, A.; Kumar, R.; Nair, M.; Bhansali, S. Electrochemical Sensing of Cortisol: A Recent Update. *Appl Biochem Biotechnol* **2014**, 174 (3), 1115–1126. <https://doi.org/10.1007/s12010-014-0894-2>.
- (527) Yamaguchi, M.; Matsuda, Y.; Sasaki, S.; Sasaki, M.; Kadoma, Y.; Imai, Y.; Niwa, D.; Shetty, V. Immunosensor with Fluid Control Mechanism for Salivary Cortisol Analysis. *Biosensors and Bioelectronics* **2013**, 41, 186–191. <https://doi.org/10.1016/j.bios.2012.08.016>.

- (528) Dalirirad, S.; Steckl, A. J. Aptamer-Based Lateral Flow Assay for Point of Care Cortisol Detection in Sweat. *Sensors and Actuators B: Chemical* **2019**, *283*, 79–86. <https://doi.org/10.1016/j.snb.2018.11.161>.
- (529) Steckl, A. J.; Ray, P. Stress Biomarkers in Biological Fluids and Their Point-of-Use Detection. *ACS Sens.* **2018**, *3* (10), 2025–2044. <https://doi.org/10.1021/acssensors.8b00726>.
- (530) Jiang, L.; Lu, Y.; Dai, Z.; Xie, M.; Lin, B. Mini-Electrochemical Detector for Microchip Electrophoresis. *Lab Chip* **2005**, *5* (9), 930–934. <https://doi.org/10.1039/B505467B>.
- (531) Dhull, N.; Kaur, G.; Gupta, V.; Tomar, M. Highly Sensitive and Non-Invasive Electrochemical Immunosensor for Salivary Cortisol Detection. *Sensors and Actuators B: Chemical* **2019**, *293*, 281–288. <https://doi.org/10.1016/j.snb.2019.05.020>.
- (532) Munje, R. D.; Muthukumar, S.; Panneer Selvam, A.; Prasad, S. Flexible Nanoporous Tunable Electrical Double Layer Biosensors for Sweat Diagnostics. *Scientific Reports* **2015**, *5*, 14586. <https://doi.org/10.1038/srep14586>.
- (533) Tuteja, S. K.; Ormsby, C.; Neethirajan, S. Noninvasive Label-Free Detection of Cortisol and Lactate Using Graphene Embedded Screen-Printed Electrode. *Nano-Micro Lett.* **2018**, *10* (3), 41. <https://doi.org/10.1007/s40820-018-0193-5>.
- (534) Khan, M.; Dighe, K.; Wang, Z.; Srivastava, I.; S. Schwartz-Duval, A.; K. Misra, S.; Pan, D. Electrochemical-Digital Immunosensor with Enhanced Sensitivity for Detecting Human Salivary Glucocorticoid Hormone. *Analyst* **2019**, *144* (4), 1448–1457. <https://doi.org/10.1039/C8AN02085J>.
- (535) Sanghavi, B. J.; Moore, J. A.; Chávez, J. L.; Hagen, J. A.; Kelley-Loughnane, N.; Chou, C.-F.; Swami, N. S. Aptamer-Functionalized Nanoparticles for Surface Immobilization-Free Electrochemical Detection of Cortisol in a Microfluidic Device. *Biosensors and Bioelectronics* **2016**, *78*, 244–252. <https://doi.org/10.1016/j.bios.2015.11.044>.
- (536) Manickam, P.; Pasha, S. K.; Snipes, S. A.; Bhansali, S. A Reusable Electrochemical Biosensor for Monitoring of Small Molecules (Cortisol) Using Molecularly Imprinted Polymers. *J. Electrochem. Soc.* **2017**, *164* (2), B54–B59. <https://doi.org/10.1149/2.0781702jes>.
- (537) Manickam, P.; Fernandez, R. E.; Umasankar, Y.; Gurusamy, M.; Arizaleta, F.; Urizar, G.; Bhansali, S. Salivary Cortisol Analysis Using Metalloporphyrins and Multi-Walled Carbon Nanotubes Nanocomposite Functionalized Electrodes. *Sensors and Actuators B: Chemical* **2018**, *274*, 47–53. <https://doi.org/10.1016/j.snb.2018.07.133>.
- (538) Cruz, A. F. D.; Norena, N.; Kaushik, A.; Bhansali, S. A Low-Cost Miniaturized Potentiostat for Point-of-Care Diagnosis. *Biosensors and Bioelectronics* **2014**, *62*, 249–254. <https://doi.org/10.1016/j.bios.2014.06.053>.

- (539) Vasudev, A.; Kaushik, A.; Tomizawa, Y.; Norena, N.; Bhansali, S. An LTCC-Based Microfluidic System for Label-Free, Electrochemical Detection of Cortisol. *Sensors and Actuators B: Chemical* **2013**, *182*, 139–146. <https://doi.org/10.1016/j.snb.2013.02.096>.
- (540) Madhu, S.; Anthuvan, A. J.; Ramasamy, S.; Manickam, P.; Bhansali, S.; Nagamony, P.; Chinnuswamy, V. ZnO Nanorod Integrated Flexible Carbon Fibers for Sweat Cortisol Detection. *ACS Appl. Electron. Mater.* **2020**, *2* (2), 499–509. <https://doi.org/10.1021/acsaelm.9b00730>.
- (541) Wu, H.; Ohnuki, H.; Ota, S.; Murata, M.; Yoshiura, Y.; Endo, H. New Approach for Monitoring Fish Stress: A Novel Enzyme-Functionalized Label-Free Immunosensor System for Detecting Cortisol Levels in Fish. *Biosensors and Bioelectronics* **2017**, *93*, 57–64. <https://doi.org/10.1016/j.bios.2016.10.001>.
- (542) Rice, P.; Upasham, S.; Jagannath, B.; Manuel, R.; Pali, M.; Prasad, S. CortiWatch: Watch-Based Cortisol Tracker. *Future Science OA* **2019**, *5* (9), FSO416. <https://doi.org/10.2144/foa-2019-0061>.
- (543) Nandhakumar, P.; Haque, A.-M. J.; Lee, N.-S.; Yoon, Y. H.; Yang, H. Washing-Free Displacement Immunosensor for Cortisol in Human Serum Containing Numerous Interfering Species. *Analytical Chemistry* **2018**. <https://doi.org/10.1021/acs.analchem.8b02590>.
- (544) Dhull, N.; Kaur, G.; Gupta, V.; Tomar, M. Development of Nanostructured Nickel Oxide Thin Film Matrix by Rf Sputtering Technique for the Realization of Efficient Bioelectrode. *Vacuum* **2018**, *158*, 68–74. <https://doi.org/10.1016/j.vacuum.2018.09.034>.
- (545) Lee, M.-H.; Thomas, J. L.; Liu, W.-C.; Zhang, Z.-X.; Liu, B.-D.; Yang, C.-H.; Lin, H.-Y. A Multichannel System Integrating Molecularly Imprinted Conductive Polymers for Ultrasensitive Voltammetric Determination of Four Steroid Hormones in Urine. *Microchim Acta* **2019**, *186* (11), 695. <https://doi.org/10.1007/s00604-019-3797-7>.
- (546) Kumar, A.; Aravamudhan, S.; Gordic, M.; Bhansali, S.; Mohapatra, S. S. Ultrasensitive Detection of Cortisol with Enzyme Fragment Complementation Technology Using Functionalized Nanowire. *Biosensors and Bioelectronics* **2007**, *22* (9), 2138–2144. <https://doi.org/10.1016/j.bios.2006.09.035>.
- (547) Kämäräinen, S.; Mäki, M.; Tolonen, T.; Palleschi, G.; Virtanen, V.; Micheli, L.; Sesay, A. M. Disposable Electrochemical Immunosensor for Cortisol Determination in Human Saliva. *Talanta* **2018**, *188*, 50–57. <https://doi.org/10.1016/j.talanta.2018.05.039>.
- (548) Abdulsattar, J. O.; Greenway, G. M.; Wadhawan, J. D. Electrochemical Immunoassay for the Detection of Stress Biomarkers. *Heliyon* **2020**, *6* (3), e03558. <https://doi.org/10.1016/j.heliyon.2020.e03558>.

- (549) Sun, B.; Gou, Y.; Ma, Y.; Zheng, X.; Bai, R.; Ahmed Abdelmoaty, A. A.; Hu, F. Investigate Electrochemical Immunosensor of Cortisol Based on Gold Nanoparticles/Magnetic Functionalized Reduced Graphene Oxide. *Biosensors and Bioelectronics* **2017**, *88*, 55–62. <https://doi.org/10.1016/j.bios.2016.07.047>.
- (550) Liu, J.; Xu, N.; Men, H.; Li, S.; Lu, Y.; Low, S. S.; Li, X.; Zhu, L.; Cheng, C.; Xu, G.; Liu, Q. Salivary Cortisol Determination on Smartphone-Based Differential Pulse Voltammetry System. *Sensors* **2020**, *20* (5), 1422. <https://doi.org/10.3390/s20051422>.
- (551) Liu, X.; Hsu, S. P. C.; Liu, W.-C.; Wang, Y.-M.; Liu, X.; Lo, C.-S.; Lin, Y.-C.; Nabilla, S. C.; Li, Z.; Hong, Y.; Lin, C.; Li, Y.; Zhao, G.; Chung, R.-J. Salivary Electrochemical Cortisol Biosensor Based on Tin Disulfide Nanoflakes. *Nanoscale Research Letters* **2019**, *14* (1), 189. <https://doi.org/10.1186/s11671-019-3012-0>.
- (552) Sekar, M.; Pandiaraj, M.; Bhansali, S.; Ponpandian, N.; Viswanathan, C. Carbon Fiber Based Electrochemical Sensor for Sweat Cortisol Measurement. *Scientific Reports* **2019**, *9* (1), 403. <https://doi.org/10.1038/s41598-018-37243-w>.
- (553) Arya, S. K.; Dey, A.; Bhansali, S. Polyaniline Protected Gold Nanoparticles Based Mediator and Label Free Electrochemical Cortisol Biosensor. *Biosensors and Bioelectronics* **2011**, *28* (1), 166–173. <https://doi.org/10.1016/j.bios.2011.07.015>.
- (554) Vabbina, P. K.; Kaushik, A.; Pokhrel, N.; Bhansali, S.; Pala, N. Electrochemical Cortisol Immunosensors Based on Sonochemically Synthesized Zinc Oxide 1D Nanorods and 2D Nanoflakes. *Biosensors and Bioelectronics* **2015**, *63*, 124–130. <https://doi.org/10.1016/j.bios.2014.07.026>.
- (555) Arya, S. K.; Chornokur, G.; Venugopal, M.; Bhansali, S. Dithiobis(Succinimidyl Propionate) Modified Gold Microarray Electrode Based Electrochemical Immunosensor for Ultrasensitive Detection of Cortisol. *Biosensors and Bioelectronics* **2010**, *25* (10), 2296–2301. <https://doi.org/10.1016/j.bios.2010.03.016>.
- (556) Pali, M.; Garvey, J. E.; Small, B.; Suni, I. I. Detection of Fish Hormones by Electrochemical Impedance Spectroscopy and Quartz Crystal Microbalance. *Sensing and Bio-Sensing Research* **2017**, *13*, 1–8. <https://doi.org/10.1016/j.sbsr.2017.01.001>.
- (557) Kim, K. S.; Lim, S. R.; Kim, S.-E.; Lee, J. Y.; Chung, C.-H.; Choe, W.-S.; Yoo, P. J. Highly Sensitive and Selective Electrochemical Cortisol Sensor Using Bifunctional Protein Interlayer-Modified Graphene Electrodes. *Sensors and Actuators B: Chemical* **2017**, *242*, 1121–1128. <https://doi.org/10.1016/j.snb.2016.09.135>.
- (558) Khan, M. S.; Dighe, K.; Wang, Z.; Schwartz-Duval, A. S.; Misra, S. K.; Pan, D. Ultra-Sensitive Paper-Based Biosensor for Cortisol Sensing in Human Saliva with Electrical Impedance Analyzer. In *2017 IEEE Healthcare Innovations and Point of Care Technologies (HI-POCT)*; 2017; pp 184–187. <https://doi.org/10.1109/HIC.2017.8227615>.

- (559) Sankhala, D.; Muthukumar, S.; Prasad, S. A Four-Channel Electrical Impedance Spectroscopy Module for Cortisol Biosensing in Sweat-Based Wearable Applications. *SLAS TECHNOLOGY: Translating Life Sciences Innovation* **2018**, *23* (6), 529–539. <https://doi.org/10.1177/2472630318759257>.
- (560) Upasham, S.; Tanak, A.; Jagannath, B.; Prasad, S. Development of Ultra-Low Volume, Multi-Bio Fluid, Cortisol Sensing Platform. *Scientific Reports* **2018**, *8* (1), 16745. <https://doi.org/10.1038/s41598-018-35199-5>.
- (561) Cardinell, B. A.; Spano, M. L.; Belle, J. T. L. Toward a Label-Free Electrochemical Impedance Immunosensor Design for Quantifying Cortisol in Tears. *CRB* **2019**, *47* (3). <https://doi.org/10.1615/CritRevBiomedEng.2019026109>.
- (562) Ertuğrul Uygun, H. D.; Uygun, Z. O.; Canbay, E.; Girgin Sağın, F.; Sezer, E. Non-Invasive Cortisol Detection in Saliva by Using Molecularly Cortisol Imprinted Fullerene-Acrylamide Modified Screen Printed Electrodes. *Talanta* **2020**, *206*, 120225. <https://doi.org/10.1016/j.talanta.2019.120225>.
- (563) Solhi, E.; Hasanzadeh, M.; Babaie, P. Electrochemical Paper-Based Analytical Devices (EPADs) toward Biosensing: Recent Advances and Challenges in Bioanalysis. *Anal. Methods* **2020**, *12* (11), 1398–1414. <https://doi.org/10.1039/D0AY00117A>.
- (564) Adkins, J.; Boehle, K.; Henry, C. Electrochemical Paper-Based Microfluidic Devices. *ELECTROPHORESIS* **2015**, *36* (16), 1811–1824. <https://doi.org/10.1002/elps.201500084>.
- (565) Castillo-León, J.; Svendsen, W. E. *Lab-on-a-Chip Devices and Micro-Total Analysis Systems: A Practical Guide*; Springer, 2014.
- (566) Paschoalino, W. J.; Kogikoski Jr., S.; Barragan, J. T. C.; Giarola, J. F.; Cantelli, L.; Rabelo, T. M.; Pessanha, T. M.; Kubota, L. T. Emerging Considerations for the Future Development of Electrochemical Paper-Based Analytical Devices. *ChemElectroChem* **2019**, *6* (1), 10–30. <https://doi.org/10.1002/celec.201800677>.
- (567) e Silva, R. F.; Longo Cesar Paixão, T. R.; Der Torossian Torres, M.; de Araujo, W. R. Simple and Inexpensive Electrochemical Paper-Based Analytical Device for Sensitive Detection of Pseudomonas Aeruginosa. *Sensors and Actuators B: Chemical* **2020**, *308*, 127669. <https://doi.org/10.1016/j.snb.2020.127669>.
- (568) Yamaji Masayuki; Tsutamoto Takayoshi; Kawahara Chiho; Nishiyama Keizo; Yamamoto Takashi; Fujii Masanori; Horie Minoru. Serum Cortisol as a Useful Predictor of Cardiac Events in Patients With Chronic Heart Failure. *Circulation: Heart Failure* **2009**, *2* (6), 608–615. <https://doi.org/10.1161/CIRCHEARTFAILURE.109.868513>.
- (569) Zea, M.; Bellagambi, F. G.; Ben Halima, H.; Zine, N.; Jaffrezic-Renault, N.; Villa, R.; Gabriel, G.; Errachid, A. Electrochemical Sensors for Cortisol Detections: Almost There.

- (570) Sekar, M.; Sriramprabha, R.; Sekhar, P. K.; Bhansali, S.; Ponpandian, N.; Pandiaraj, M.; Viswanathan, C. Review—Towards Wearable Sensor Platforms for the Electrochemical Detection of Cortisol. *J. Electrochem. Soc.* **2020**, *167* (6), 067508. <https://doi.org/10.1149/1945-7111/ab7e24>.
- (571) Bellagambi, F. G.; Baraket, A.; Longo, A.; Vatteroni, M.; Zine, N.; Bausells, J.; Fuoco, R.; Di Francesco, F.; Salvo, P.; Karanasiou, G. S.; Fotiadis, D. I.; Menciassi, A.; Errachid, A. Electrochemical Biosensor Platform for TNF- α Cytokines Detection in Both Artificial and Human Saliva: Heart Failure. *Sensors and Actuators B: Chemical* **2017**, *251*, 1026–1033. <https://doi.org/10.1016/j.snb.2017.05.169>.
- (572) Zea, M.; Moya, A.; Villa, R.; Gabriel, G. Inkjet-Printed Paper-Based Electrochemical Sensors: Tuning Active Area through Surface Modification. *Submitted*.
- (573) Barhoumi, L.; Bellagambi, F. G.; Vivaldi, F. M.; Baraket, A.; Clément, Y.; Zine, N.; Ben Ali, M.; Elaissari, A.; Errachid, A. Ultrasensitive Immunosensor Array for TNF- α Detection in Artificial Saliva Using Polymer-Coated Magnetic Microparticles onto Screen-Printed Gold Electrode. *Sensors* **2019**, *19* (3), 692. <https://doi.org/10.3390/s19030692>.
- (574) Baraket, A.; Lee, M.; Zine, N.; Yaakoubi, N.; Bausells, J.; Errachid, A. A Flexible Electrochemical Micro Lab-on-Chip: Application to the Detection of Interleukin-10. *Microchim Acta* **2016**, *183* (7), 2155–2162. <https://doi.org/10.1007/s00604-016-1847-y>.
- (575) Zhou, W.; Yang, S.; Wang, P. G. Matrix Effects and Application of Matrix Effect Factor. *Bioanalysis* **2017**, *9* (23), 1839–1844. <https://doi.org/10.4155/bio-2017-0214>.
- (576) Gosetti, F.; Mazzucco, E.; Zampieri, D.; Gennaro, M. C. Signal Suppression/Enhancement in High-Performance Liquid Chromatography Tandem Mass Spectrometry. *Journal of Chromatography A* **2010**, *1217* (25), 3929–3937. <https://doi.org/10.1016/j.chroma.2009.11.060>.
- (577) Vozgirdaite, D.; Ben Halima, H.; Bellagambi, F. G.; Alcacer, A.; Palacio, F.; Jaffrezic-Renault, N.; Zine, N.; Bausells, J.; Elaissari, A.; Errachid, A. Development of an ImmunoFET for Analysis of Tumour Necrosis Factor- α in Artificial Saliva: Application for Heart Failure Monitoring. *Chemosensors* **2021**, *9* (2), 26. <https://doi.org/10.3390/chemosensors9020026>.
- (578) Gevaerd, A.; Watanabe, E. Y.; Belli, C.; Marcolino-Junior, L. H.; Bergamini, M. F. A Complete Lab-Made Point of Care Device for Non-Immunological Electrochemical Determination of Cortisol Levels in Salivary Samples. *Sensors and Actuators B: Chemical* **2021**, *332*, 129532. <https://doi.org/10.1016/j.snb.2021.129532>.

- (579) Manzoli, A.; Shimizu, F. M.; Mercante, L. A.; Paris, E. C.; Jr, O. N. O.; Correa, S.; Mattoso, L. H. C. Layer-by-Layer Fabrication of AgCl – PANI Hybrid Nanocomposite Films for Electronic Tongues. *Physical Chemistry Chemical Physics* **2014**, *16*, 24275–24281. <https://doi.org/10.1039/c4cp04150j>.
- (580) Hu, W.; Chen, S.; Yang, Z.; Liu, L.; Wang, H. Flexible Electrically Conductive Nanocomposite Membrane Based on Bacterial Cellulose and Polyaniline. *J. Phys. Chem. B* **2011**, 8453–8457.
- (581) Lee, J. Y.; Lee, J.-W.; Schmidt, C. E. Neuroactive Conducting Scaffolds: Nerve Growth Factor Conjugation on Active Ester-Functionalized Polypyrrole. *Journal of The Royal Society Interface* **2009**, *6* (38), 801–810. <https://doi.org/10.1098/rsif.2008.0403>.
- (582) Dai, T.; Yang, X.; Lu, Y. Conductive Composites of Polypyrrole and Sulfonic-Functionalized Silica Spheres. *Materials Letters* **2007**, *61* (14–15), 3142–3145. <https://doi.org/10.1016/j.matlet.2006.11.012>.